

NSF/CEE-84047

R-8121-5617

PB85-168870

**ANALYTICAL AND EXPERIMENTAL
STUDIES OF SUSPENDED FLOOR
STRUCTURES WITH COULOMB
FRICTION ELEMENTS**

**NATIONAL SCIENCE FOUNDATION
GRANT NO. CEE-8006570**

30 November 1984

**J.A. Malthan
AGBABIAN ASSOCIATES
El Segundo, California**

**S.F. Masri - O.T. Hata
UNIVERSITY OF SOUTHERN CALIFORNIA
Los Angeles, California**

ACKNOWLEDGEMENT

This work was supported by the National Science Foundation through Grant No. CEE-8006570 with Dr. John B. Scalzi as the Program Director. This support is gratefully acknowledged.

Any opinions, findings and conclusions, or recommendations expressed in this report are those of the authors and do not necessarily reflect the views of the National Science Foundation.

TABLE OF CONTENTS

<u>Section</u>		Page
	ACKNOWLEDGEMENT.	ii
1	INTRODUCTION	1-1
2	COMPILATION OF EXISTING DATA	2-1
3	ANALYTICAL STUDIES	3-1
4	EXPERIMENTAL STUDIES	4-1
5	REFERENCES	5-1

SECTION 1

INTRODUCTION

1.1 OBJECTIVE

The objective of this research was to attain a better understanding of the behavior of high-rise buildings with suspended floors in response to earthquake motions. The research was composed of several phases. One phase consisted of an investigation of the range of structures which fall within this classification and the analytical and test procedures previously employed for determination of earthquake behavior. Then the performance of new analyses was initiated to establish a data base of expected behavior. Finally, experimental methods were employed to fully investigate the response mechanism of floor-core interconnect devices.

In general, buildings with suspended floors consist of two types: buildings whose floors are hung on continuous cables as shown in Figure 1-1, or buildings whose floors are hung individually as in Figure 1-2.

From an analytical point of view, these two structure types are virtually identical. However, the relative differences between stiffnesses and masses among the various floor, frame, core, cable, and snubber elements result in different responses. Moreover, both react with the earth at their foundations so that earthquake motions are transmitted to the structures by way of the compliance of the earth; the structure response is also modified by "leakage" of kinetic and strain energy of the structure back into the earth.

1.2 OVERVIEW

The perspective presented below defines the state of the art of suspended floor research prior to embarking on this research:

1. While the suspended floor design is not common, it is also not rare and has been put into use worldwide.

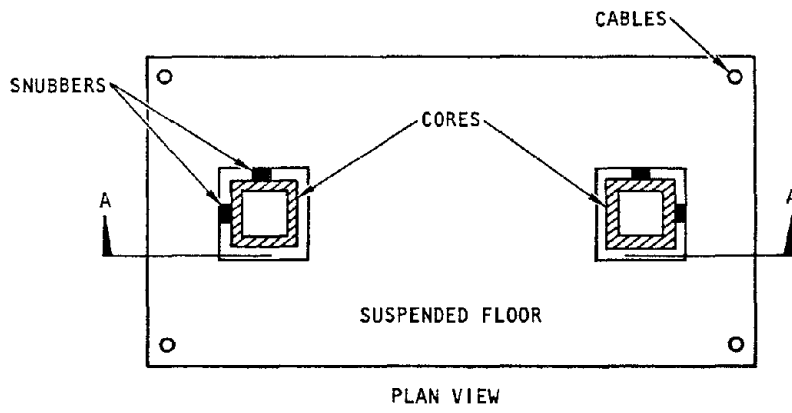
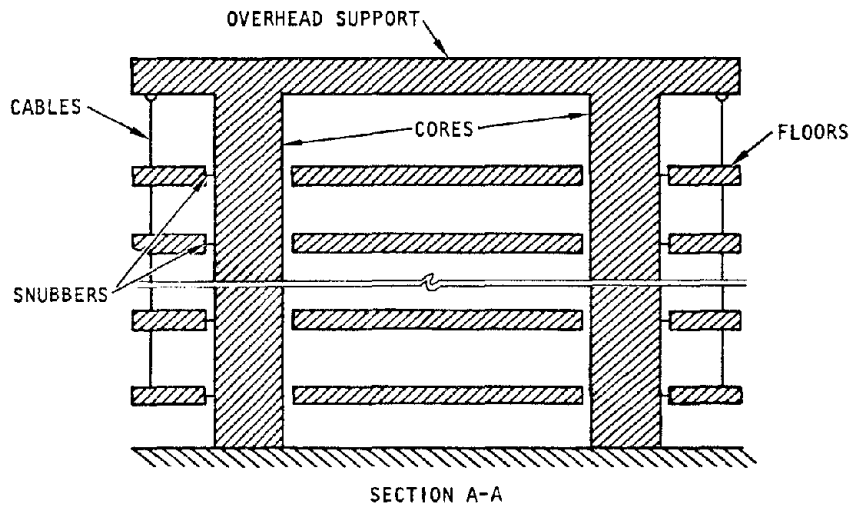
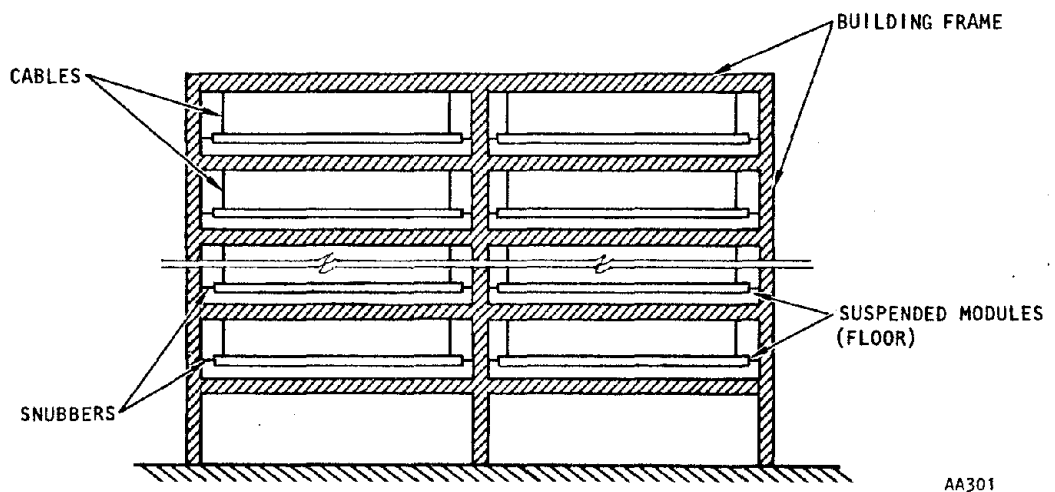


FIGURE 1-1. FLOORS SUSPENDED FROM TOP



AA301

FIGURE 1-2. FLOORS SUSPENDED INDIVIDUALLY

Available existing data on building configurations and pertinent analytical studies are summarized in Section 2, *Compilation of Existing Data*.

2. From the available open literature, neither extensive analytical nor experimental investigations have been performed to fully validate the design concept. Section 2 presents the extent of prior studies.
3. Analyses using various mathematical tools suggest that a number of parameters influence the earthquake response of these buildings:
 - a. Overall arrangement and size of structural elements
 - b. Core design (stiffness and mass)
 - c. Suspension method (cascaded or single-floor suspension)
 - d. Restraint method (sidesway snubbers)
 - e. Foundation design and soil properties
 - f. Floor stiffness and mass
 - g. Earthquake intensity and spectral composition

The suspended floor design can, with one exception, be studied analytically like any high-rise building with conventional floor systems. The exception is in the snubbers or lateral restraints that limit the degree of sidesway that the suspended floors will experience in an earthquake. Most snubbers are frangible, energy absorbent, or otherwise nonlinear devices which can have a significant effect on reducing the lateral response of the building. The suspension systems can serve to shock isolate floor slabs from both vertical and horizontal components of earthquake ground shaking. The behavior of the snubber, especially the Coulomb friction type, thus became the object of intense study in this research.

For the sake of completeness, we present here a discussion of the options for analytically modeling suspended floor

structures as the system of elements previously noted. In general, the models can take two forms: (1) lumped parameter models in which effective masses and stiffnesses are linked together after the method of, say, Biggs (1964); or, (2) explicit modeling using finite element techniques in which actual stiffnesses and masses can be used. Foundation resistances, masses, and dampings can be modeled explicitly in the finite element approach, or foundation properties may be modeled as lumped parameters.

Special attention should be directed to snubber design since this is potentially an excellent, inexpensive mechanism for dissipating energy absorbed by the structure from foundation movement. Otherwise, sizing of primary support structure is governed by contemporary design practice so that the practical range of structural elements occurs within a fairly narrow size distribution.

A typical finite element model of a suspended floor structure with cables supported at the top of the core structure is shown in Figure 1-3. This model is representative of a two-story structure analyzed in two dimensions. The core or tower structures are represented as the T-sections from which cables are hung to support the two floor systems. The floors are connected to the cores by snubber restraints shown on the figure as B . The pendulum restoring force is represented by artificial springs designated P . The cores rest on foundations whose compliance is represented by F . In general, B and F can be assigned any stiffness characteristics including nonlinear behavior with damping. In fact, B usually has a "lock-up" feature to account for impact of the floors against the cores if the floor sway becomes sufficiently large.

In addition to those items mentioned above, some latitude is available in the design of the structure itself. For example, the flexibility of the cores relative to the pendulum action of the floors can result in a structure resistant to or resonant with the spectral content of earthquakes. In turn, postulated

1-5

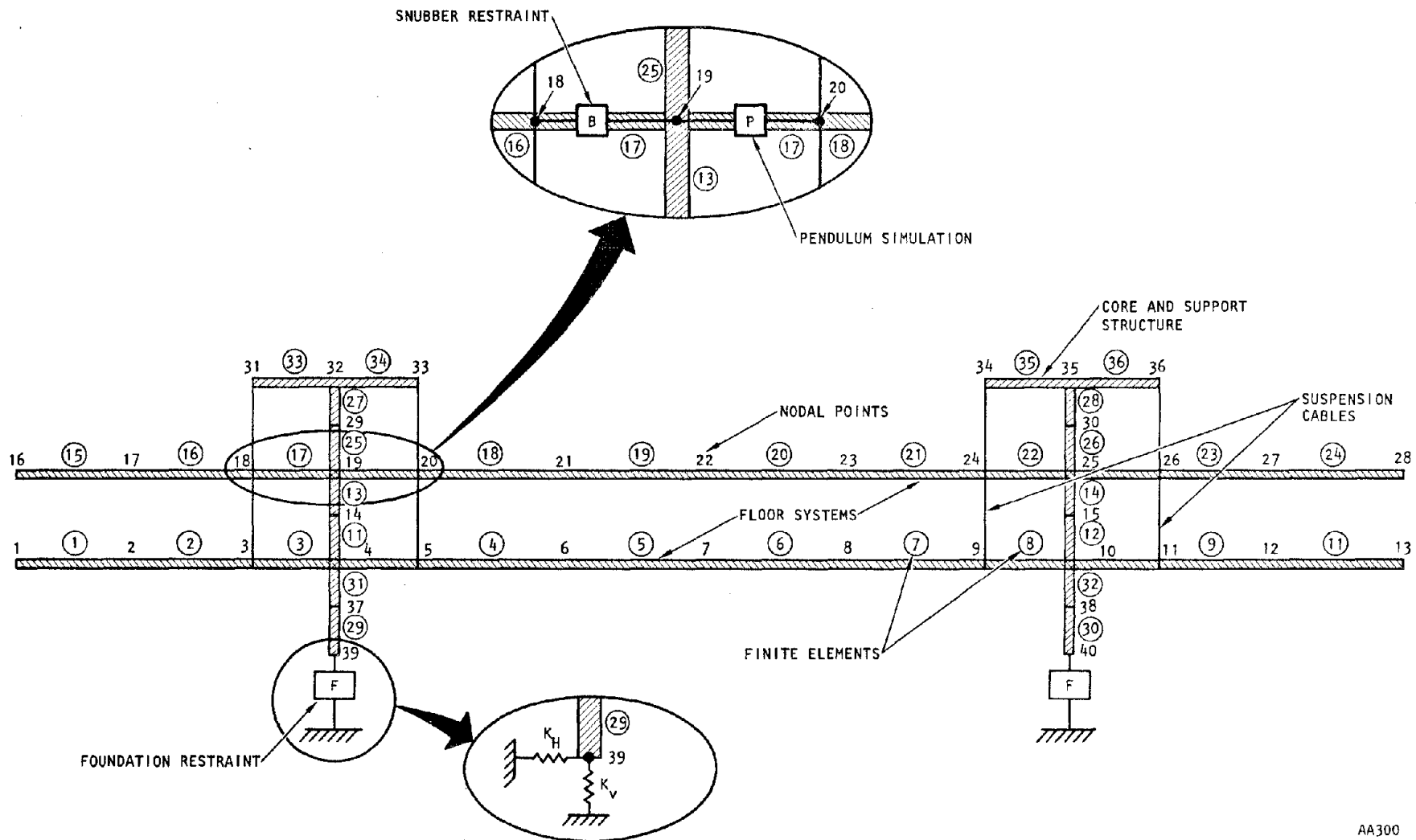


FIGURE 1-3. TYPICAL FINITE ELEMENT MODEL OF A SUSPENDED FLOOR STRUCTURE

earthquakes have different spectral representations as noted in other studies (e.g., ABK, 1981).

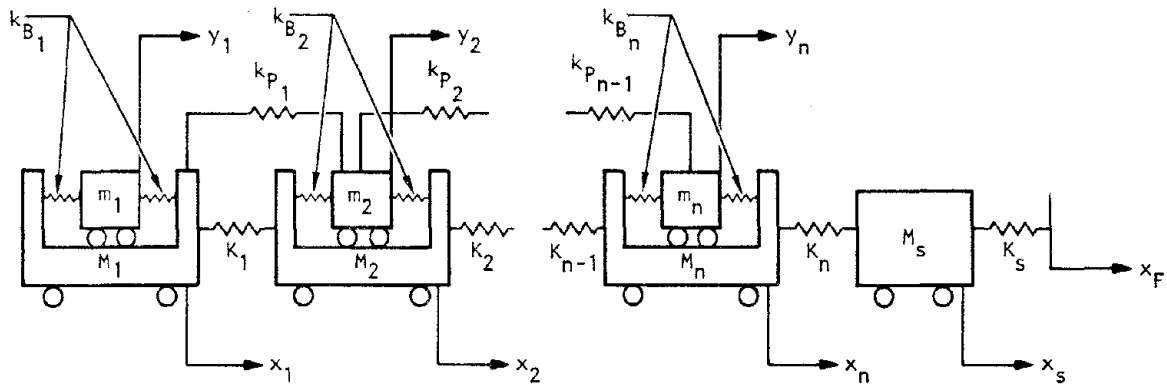
Other factors include site-peculiar soil stiffness and strength, structure size and configuration, and the use for which the structure is designed (e.g., an office building vs. an experimental laboratory).

Although models of the kind shown in Figure 1-3 quite accurately represent a specific structure, they are very detailed in their layout, contain many degrees of freedom, often provide more information than is desired or can be absorbed, and of course are expensive when used as a research tool.

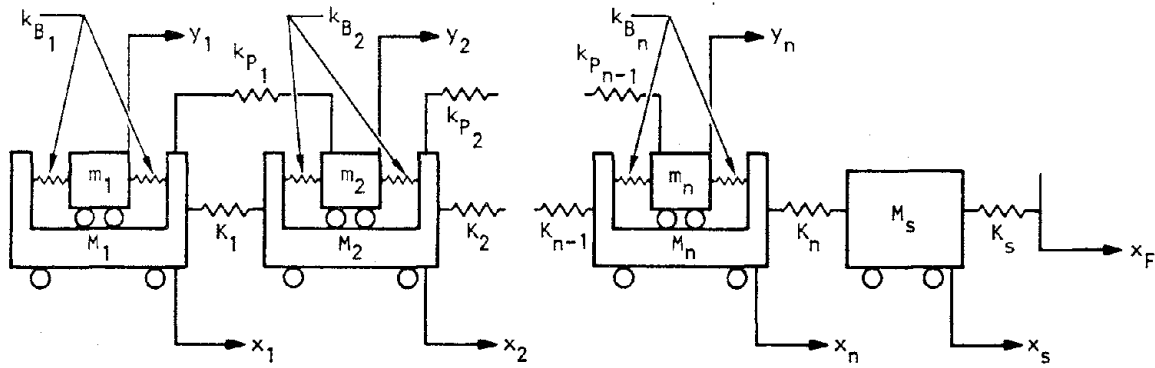
It is preferable that simpler models be devised to investigate the fundamental properties of the structure leading to parametric analyses for a spectrum of realistic configurations, some of which have been detailed above. A typical model is shown in Figure 1-4.

This model considers buildings of n levels where level 1 is at the roof and level n is at the ground. The parameters have the following definitions:

- M_n = effective masses of each story of the cores
- m_n = effective mass of each floor
- M_s = effective mass of soil in foundation
- K_n = effective stiffness and damping of each story of cores
- k_{bn} = stiffness and damping of snubbers
- k_{pn} = effective stiffness of pendulum action
- X_F = horizontal earthquake ground shaking
- X_S = effective horizontal response of mobilized soil
- X_n = horizontal response of cores
- Y_n = horizontal response of floors



(a) Floors suspended from top



(b) Individually-suspended floors

FIGURE 1-4. LUMPED PARAMETER MODELS FOR LATERAL RESPONSE

AA333

It is noted that the difference between the models in Figures 1-3 and 1-4 is solely the way in which the floors couple to each other and to the cores. The model shown in Figure 1-3 is more suitable to vertical shaking because of the bending response of the floors and the elasticity of the suspension system. The model in Figure 1-4 is most useful to the analysis of lateral seismic response since, in sidesway, the floors tend to respond as rigid bodies and lateral in-plane shock waves propagating through the floors are either nonexistent or too benign to be of practical interest to either the designer of these structures or to the ultimate user. For the present research, the lumped parameter method of analysis has been employed.

SECTION 2

COMPILATION OF EXISTING DATA

2.1 BUILDING CONFIGURATIONS

Literature surveys and communications with the engineering community have resulted in a clearer insight into the state of the art of suspended floor high-rise building construction. The concept of suspended floor design in high-rise construction has been put into practical application throughout the world within the past two decades, especially in Europe and the U.S. However, information on the analytical investigations of the seismic behavior of suspended floor buildings is sparse.

In the United States, International Environmental Dynamics (IED) of San Jose, California, progressively developed a concept of suspended floor buildings in the sixties. The primary structural elements of the IED concept are two reinforced concrete cores supporting the suspended steel frame floors and concrete floor slabs. The floor assemblies are erected on the ground level and successively raised to their appropriate elevation. The 11-story Pacific Trade Center (ENR, 1965b) developed by IED was constructed in 1963 in San Pedro, California. This building has two large steel trusses and twenty-four hanger straps suspending the floors from the roof level. In the late 1960's the second building designed by IED was constructed in Berkeley, California (WC, 1970). The 15-story First Savings Building used smaller trusses and sixteen straps to suspend the ten floors, again from roof level.

IED later modified the concept of suspension by replacing the heavy trusses with eight steel hanger straps attached to the concrete saddles on top of the concrete cores. This concept was first applied to the 12-story IED Building in Mountain View, California (ENR, 1971; WC, 1971). Subsequently, the Sherman Building in San Jose and the Marshall Building in San Mateo, California, were constructed with configurations similar to the IED Building. This scheme was also used in the construction of a

Holiday Inn in Huntington, West Virginia, with steel hanger straps supporting the top nine floors of the 13-story building (BSC, 1972).

The advantages claimed for the IED suspended floor concept include cost savings, faster construction, and an increase in usable floor space. Architectural, rather than economical, reasons were, however, the motivation for choosing the suspended floor construction for the 15-story Lincoln Life Insurance Building in Louisville, Kentucky (ENR, 1965b). In this building, a single core shaft, five main roof trusses, and slender hangers accommodated an unbroken curtain wall pattern of lacy precast concrete panels. The hangers also allowed for a dramatic open arcade under the suspended second-floor framing.

A different type of suspended floor construction was demonstrated by the Bacardi Building in Miami, Florida (Bliss et al., 1965). The six upper floors of this building were suspended from the two posttensioned trusses supported by four stilt-like columns. The trusses at the roof level cantilevered over the columns at each end to provide support for the floors below which were suspended by posttensioned concrete walls.

A number of suspended floor buildings were constructed outside of the U.S. within the same time frame as those in the U.S. In Marl, Germany, a 6-story, an 8-story, and an 11-story building, and later a fourth office building were built on the same suspended floor principle in which perimeter prestressed concrete hangers attached at the edges of the roofs picked up the exterior ends of floor beams (ENR, 1965a). The interior ends of the beams were carried by the single core of the building. An 11-story office building in Rotterdam, Netherlands, suspended floors from the prestressed concrete girders on all four sides of the single concrete core (ENR, 1965b). The single-core 13-story office building in Czechoslovakia is another example of suspended floor construction (Kozak, 1972). The floors were suspended from steel beams installed at the top of the reinforced concrete core.

Still another example of suspended floor buildings is the Westcoast Office Building in Vancouver, Canada (Babicki, 1971). The 12 typical steel floors were suspended at the building's perimeter by continuous steel hangers supported directly on the rounded top of the center reinforced concrete core. The floor beams were simply supported at the core in pockets cast into the core walls and were attached to the cables by friction clamps.

2.2 ANALYTICAL STUDIES

Despite the fact that the concept of buildings with suspended floors has long been applied to civil buildings since the 1920's (Nikolaenko et al., 1976), analytical studies for this type of structural system are relatively scarce, especially in the realm of seismic response investigations.

In the late 1960's Larios et al. (1969) developed a simplified lumped mass model with linear springs and dampers, for a typical 10-story building. Various spring and damper combinations were devised in the model to examine the energy absorbing characteristics of the building. The equations of motion were solved by the method of constant velocity numerical integration. Philco-Ford, West performed dynamic analyses of the IED Building by using two levels of earthquake input functions (Irvine, 1980). Subsequently, John Blume and Associates also analyzed the IED Building and a hypothetical building by time history and spectral approaches (Jhaveri, 1980). The energy absorbing characteristics of the bumper bars were investigated by the inclusion of friction and/or viscous dampers in their two-dimensional lumped mass models.

A comprehensive investigation was performed by Goodno on the IED Building and the Sherman Building as discussed in the preceding subsection (Goodno, 1975). A three-dimensional finite element model was used to model the basic components of the building for the linear dynamic analysis. The core structures were modeled by super-elements, floors idealized as laminae having infinite rigidity in their own planes, bumper bars as

axial springs, and hanger straps modeled as axial members. The equations of motion for displacements of the floors were formulated using the stiffness method. These equations were solved by normal mode techniques to obtain the dynamic response of the structure for free vibrations, impulsive lateral loads, and horizontal ground motions.



SECTION 3

ANALYTICAL STUDIES

3.1 CHARACTERISTICS OF COULOMB AND VISCOUS DAMPING

Structures designed and constructed with suspended floors can be mathematically represented as compound pendulum systems coupled to flexible core structures via the suspension system and through floor-core dampers if desired. Without dampers, the swaying of the floors could reach large excursions during an earthquake with the potential for damage to the structure as well as discomfort and danger to occupants. On the other hand, the dampers offer a potential means for restricting floor swaying and core structure distress by dissipating energy in the damper mechanisms.

One of the simplest methods for dissipating energy is with friction damping. Yet, because it is a nonlinear device (and because of the nature of the nonlinearity), computational problems emerge from its use. The purpose of this section is to delineate these problems and to present realistic solutions along with approximate solutions which have been implemented in the past. It is also instructive to compare the behavior of friction (or Coulomb) damping to that of viscous damping to determine whether there is an advantage of one over the other. Either type of damping is fairly easily achieved in actual application, i.e., with hardware.

To the extent that we understand friction, its force characteristics are thought to be represented as shown in Figure 3-1. The relative velocity is the velocity between any two bodies which are sliding against each other. The friction force is the resistance against this sliding which opposes the relative velocity. We understand that for many surfaces and materials, the friction force tends to be larger when the relative velocities are small. In fact, the largest friction force is the "breakaway" force that just initiates sliding. One presumes that as two sliding bodies approach congruency of

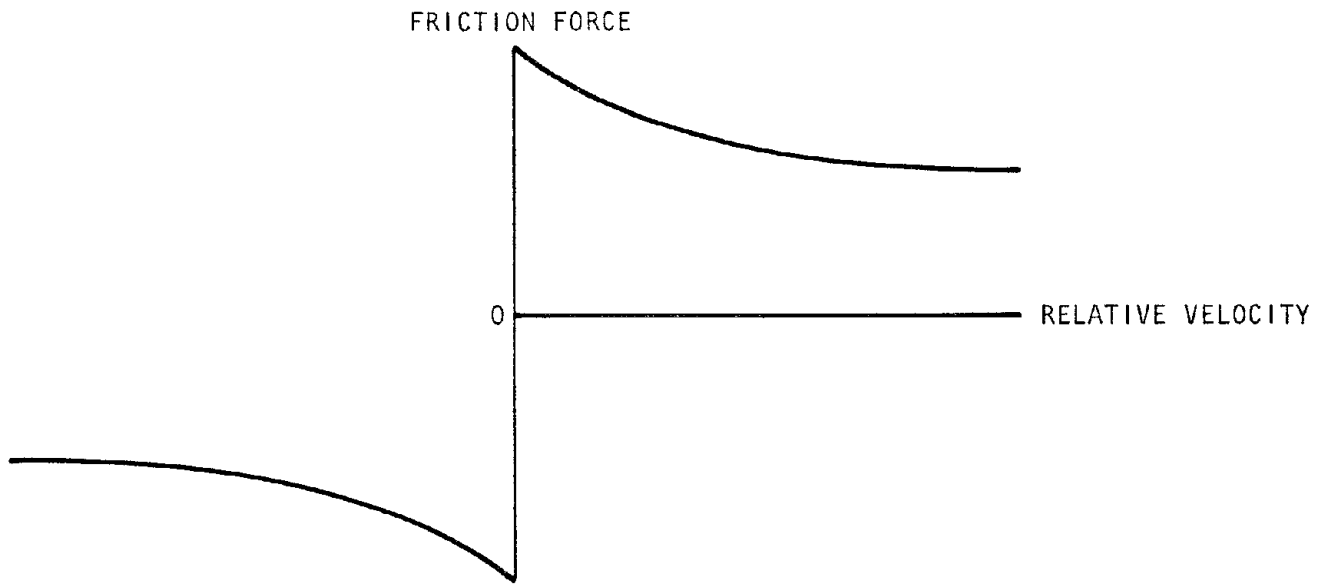


FIGURE 3-1. REPRESENTATIVE BEHAVIOR OF FRICTION

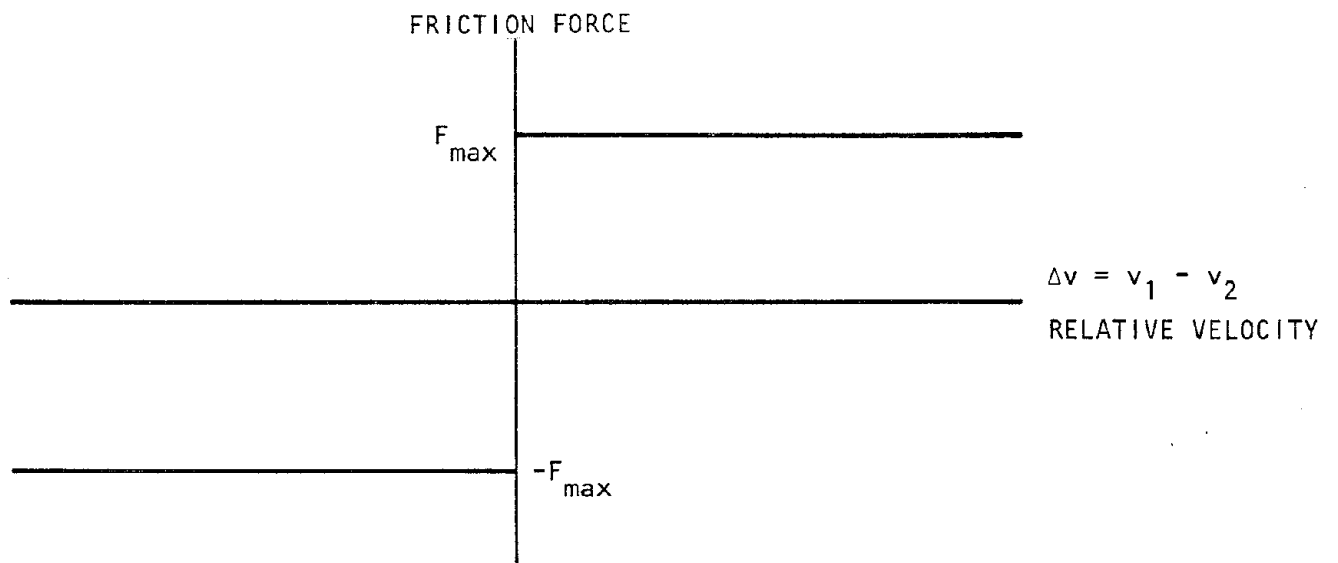


FIGURE 3-2. MATHEMATICAL SIMULATION OF FRICTION

velocity, the force of friction between them increases to a "clutching" force.

In theoretical mechanics, especially in numerical calculations, friction is often simplified as shown in Figure 3-2. Thus, when two bodies move with velocities V_1 and V_2 , respectively, where V_1 is not equal to V_2 , the friction force between them is given by $+ F_{\max}$ or $- F_{\max}$ where the sense of the force depends on whether V_2 is greater than V_1 or vice versa. It should also be clear that when the velocities are equal to each other, then the force that acts between them is just sufficient to keep their velocities equal, or, in other words, the locus of force is on the ordinate in Figure 3-2 but constrained within the limits of $\pm F_{\max}$. For the general case, the friction force is restricted to the $\pm F_{\max}$ envelope or to the vertical line at $\Delta V = 0$ whichever is less.

As a numerical problem, this model can lead to computational difficulties. We demonstrate the problem by examining an exact solution of a simple configuration which is shown in Figure 3-3. The friction force between the two masses is denoted by F_c where F_c is defined in Figure 3-4. The coupled masses are restrained by the spring denoted by constant k .

We may write the equations of motion for the system for three possible regimes:

Case 1, $\dot{x}_2 > \dot{x}_1$

$$m_1 \ddot{x}_1 + kx_1 = F_c$$

$$m_2 \ddot{x}_2 = - F_c$$

Case 2, $\dot{x}_2 = \dot{x}_1$

$$(m_1 + m_2) \ddot{x}_1 + kx_1 = 0 \tag{3-1}$$

$$(m_1 + m_2) \ddot{x}_2 + kx_2 = 0$$

Case 3, $\dot{x}_2 < \dot{x}_1$

$$m_1 \ddot{x}_1 + kx_1 = - F_c$$

$$m_2 \ddot{x}_2 = F_c$$

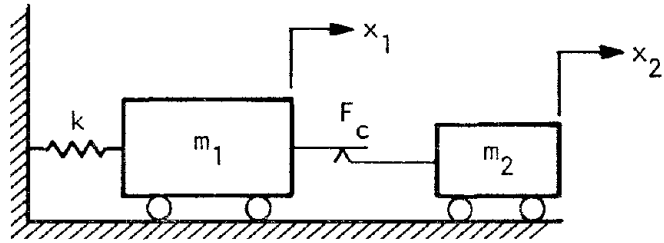


FIGURE 3-3. REPRESENTATIVE FRICTION MODEL

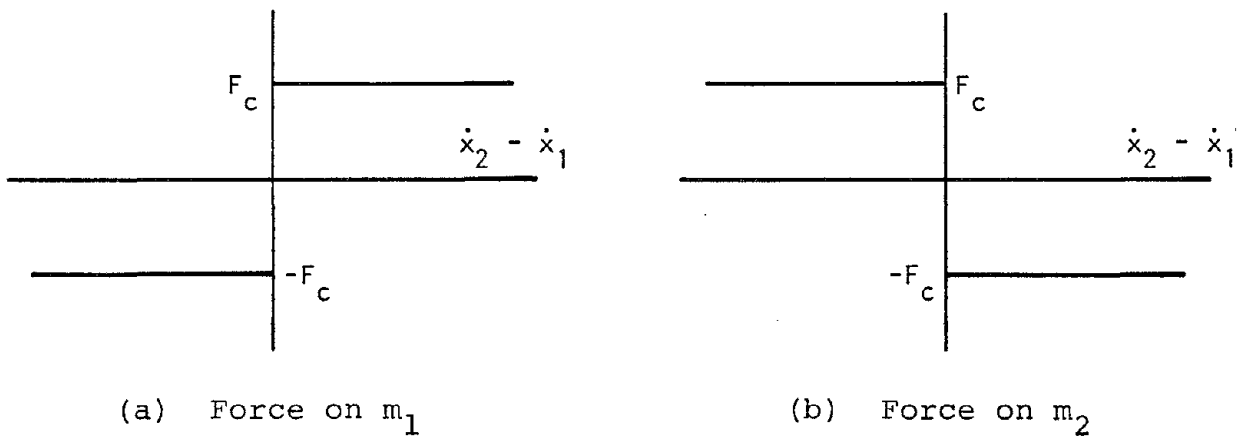


FIGURE 3-4. FRICTION FORCE SIGN CONVENTION

The continuous motion of the masses can be investigated by solving the appropriate equations for the cases defined above. We begin the solution by extending both masses a distance of x_0 and then releasing them at zero time. At that instant of time, Case 1 prevails. Thus:

3.1.1 SOLUTION OF CASE 1: $\dot{x}_2 > \dot{x}_1$

We let

$$F_c = ka \tag{3-2}$$

where a is the static displacement of m_1 that just balances the friction force and the force in the spring assuming that m_2 has not moved. Thus, from Equation 3-1:

$$m_1 \ddot{x}_1 + kx_1 = ka$$

or (3-3)

$$m_1 \ddot{x}_1 + k(x_1 - a) = 0$$

We now introduce a variable $x = x_1 - a$ so that

$$m_1 \ddot{x} + kx = 0 \tag{3-4}$$

whose solution is

$$x = A \cos \omega_1 t + B \sin \omega_1 t \tag{3-5}$$

which transforms to

$$\begin{aligned} x_1 &= A \cos \omega_1 t + B \sin \omega_1 t + a \\ &= A \cos \omega_1 t + B \sin \omega_1 t + \frac{F_c}{k} \end{aligned} \tag{3-6}$$

Equation 3-6 is subject to the initial conditions

$$x_1(0) = x_0, \quad \dot{x}_1(0) = 0 \tag{3-7}$$

provided that

$$x_0 > a = \frac{F_c}{k}$$

The constants in Equation 3-6 are determined from the initial conditions so that the complete response of mass m_1 is given by

$$x_1 = \frac{1}{k} \left[F_c + (x_0 k - F_c) \cos \omega_1 t \right]$$

$$\dot{x}_1 = \frac{F_c - x_0 k}{k} \omega_1 \sin \omega_1 t \quad (3-8)$$

$$\ddot{x}_1 = \frac{F_c - x_0 k}{k} \omega_1^2 \cos \omega_1 t$$

$$\text{where } \omega_1 = \sqrt{\frac{k}{m_1}}$$

The response of Equation 3-8 is valid until such time as the friction force acting on m_2 causes it to reach a velocity that is just equal to that of m_1 . At that time, the conditions of Case 2 will prevail, but we must first determine when that occurs.

The solution to the motion of m_2 during the first regime is:

$$x_2 = \alpha t^2 + \beta t + \gamma \quad (3-9)$$

subject to the initial conditions $x_2(0) = x_0$, $\dot{x}_2(0) = 0$. From this we determine the complete solution

$$x_2 = -\frac{F_c t^2}{2 m_2} + x_0$$

$$\dot{x}_2 = -\frac{F_c t}{m_2} \quad (3-10)$$

$$\ddot{x}_2 = -\frac{F_c}{m_2}$$

We now determine when $\dot{x}_1(t_{01}) = \dot{x}_2(t_{01})$ from Equations 3-8 and 3-10 where t_{01} is the time when equal velocity occurs. Thus,

$$\frac{F_c - x_0 k}{k} \omega_1 \sin \omega_1 t_{01} = -\frac{F_c t_{01}}{m_2} \quad (3-11)$$

Equation 3-11 is satisfied for $t_{01} = 0$ but this solution is trivial; we must search for the first nonzero root of this equation. It can be solved by trial and error, graphical methods, or by iteration.

The motions at $t = t_{01}$ from Equations 3-8 and 3-10 become the initial conditions for the next regime of motion

$$\begin{aligned} x_{01} &= x_1(t_{01}) = \frac{1}{k} \left[F_c + (x_0 k - F_c) \cos \omega_1 t_{01} \right] \\ v_{01} &= \dot{x}_1(t_{01}) = \frac{F_c - x_0 k}{k} \omega_1 \sin \omega_1 t_{01} \end{aligned} \quad (3-12)$$

3.1.2 SOLUTION OF CASE 2: $\dot{x}_1 = \dot{x}_2$

At $t = t_{01}$, from the solution of Equation 3-11, m_1 and m_2 begin moving with the same velocity. In effect, the two masses bond together and their combined motion is given by

$$\begin{aligned} x_1 &= A \cos \omega_2 (t - t_{01}) + B \sin \omega_2 (t - t_{01}) \\ x_2 &= A \cos \omega_2 (t - t_{01}) + B \sin \omega_2 (t - t_{01}) + C \\ \dot{x}_1 &= \dot{x}_2 = -A\omega_2 \sin \omega_2 (t - t_{01}) + B\omega_2 \cos \omega_2 (t - t_{01}) \\ \ddot{x}_1 &= \ddot{x}_2 = -A\omega_2^2 \cos \omega_2 (t - t_{01}) - B\omega_2^2 \sin \omega_2 (t - t_{01}) \end{aligned} \quad (3-13)$$

which are subject to the initial conditions

$$x_1(t_{01}) = x_{01}$$

$$x_2(t_{01}) = x'_{01} = -\frac{F_c t_{01}^2}{2m_2} + x_0$$

and

$$\dot{x}_1(t_{01}) = \dot{x}_2(t_{01}) = v_{01}$$

where

$$\omega_2 = \sqrt{\frac{k}{m_1 + m_2}}$$

Thus,

$$x_1 = x_{01} \cos \omega_2 (t - t_{01}) + \frac{v_{01}}{\omega_2} \sin \omega_2 (t - t_{01})$$

$$x_2 = x_{01} \cos \omega_2 (t - t_{01}) + \frac{v_{01}}{\omega_2} \sin \omega_2 (t - t_{01})$$

$$+ x'_{01} - x_{01}$$

(3-14)

$$\dot{x}_1 = \dot{x}_2 = -x_{01} \omega_2 \sin \omega_2 (t - t_{01}) + v_{01} \cos \omega_2 (t - t_{01})$$

$$\ddot{x}_1 = \ddot{x}_2 = -x_{01} \omega_2^2 \cos \omega_2 (t - t_{01}) - v_{01} \omega_2 \sin \omega_2 (t - t_{01})$$

Equations 3-14 are valid until the acceleration of m_2 causes the maximum allowable friction force to be exceeded at which time m_2 will slide relative to m_1 . We then proceed to the next regime.

3.1.3 SOLUTION OF CASE 3: $\dot{x}_2 < \dot{x}_1$

Sliding of m_2 relative to m_1 occurs exactly when the force between m_1 and m_2 reaches F_c . Thus:

$$m_2 \left[-x_{01} \omega_2^2 \cos \omega_2 (t - t_{01}) - v_{01} \omega_2 \sin \omega_2 (t - t_{01}) \right] = F_c$$

(3-15)

We search for the first root of Equation 3-15 for $t > t_{01}$. We call this root $t = t_{02}$.

The equations of motion for this case are

$$\begin{aligned} m_1 \ddot{x}_1 + kx_1 &= - F_c = - ka \\ m_1 \ddot{x}_1 + k(x_1 - a) &= 0 \end{aligned} \quad (3-16)$$

which has a solution

$$\begin{aligned} x_1 &= A \cos \omega_1 (t - t_{02}) + B \sin \omega_1 (t - t_{02}) - \frac{F_c}{k} \\ \dot{x}_1 &= - A \omega_1 \sin \omega_1 (t - t_{02}) + B \omega_1 \cos \omega_1 (t - t_{02}) \end{aligned} \quad (3-17)$$

The initial conditions for Equation 3-17 are obtained from the final conditions from Equation 3-14 at $t = t_{02}$. Thus:

$$\begin{aligned} x_{02} = x_1(t_{02}) &= x_{01} \cos \omega_2 (t_{02} - t_{01}) \\ &\quad + \frac{v_{01}}{\omega_2} \sin \omega_2 (t_{02} - t_{01}) \end{aligned} \quad (3-18)$$

$$\begin{aligned} v_{02} = \dot{x}_1(t_{02}) &= - x_{01} \omega_2 \sin \omega_2 (t_{02} - t_{01}) \\ &\quad + v_{01} \cos \omega_2 (t_{02} - t_{01}) \end{aligned}$$

The constants in Equation 3-17 are evaluated to obtain

$$\begin{aligned} x_1 &= \left(x_{02} + \frac{F_c}{k} \right) \cos \omega_1 (t - t_{02}) \\ &\quad + \frac{v_{02}}{\omega_1} \sin \omega_1 (t - t_{02}) - \frac{F_c}{k} \\ \dot{x}_1 &= - \left(x_{02} + \frac{F_c}{k} \right) \omega_1 \sin \omega_1 (t - t_{02}) \\ &\quad + v_{02} \cos \omega_1 (t - t_{02}) \\ \ddot{x}_1 &= - \left(x_{02} + \frac{F_c}{k} \right) \omega_1^2 \cos \omega_1 (t - t_{02}) \\ &\quad - v_{02} \omega_1 \sin \omega_1 (t - t_{02}) \end{aligned} \quad (3-19)$$

At the same time, the equations of motion for m_2 are

$$\begin{aligned}x_2 &= \alpha (t - t_{02})^2 + \beta (t - t_{02}) + \gamma \\ \dot{x}_2 &= 2\alpha (t - t_{02}) + \beta\end{aligned}\tag{3-20}$$

which are subject to the final conditions from Equation 3-14 at $t = t_{02}$ i.e.,

$$\begin{aligned}x_2(t_{02}) &= d_2 = x_{01} \cos \omega_2 (t_{02} - t_{01}) \\ &\quad + \frac{v_{01}}{\omega_2} \sin \omega_2 (t_{02} - t_{01}) + x'_{01} - x_{01}\end{aligned}$$

and

$$\begin{aligned}\dot{x}_2(t_{02}) &= v_2 = -x_{01} \omega_2 \sin \omega_2 (t_{02} - t_{01}) \\ &\quad + v_{01} \cos \omega_2 (t_{02} - t_{01})\end{aligned}$$

Thus, Equation 3-20 becomes

$$\begin{aligned}x_2 &= \frac{F_c}{2 m_2} (t - t_{02})^2 + v_2 (t - t_{02}) + d_2 \\ \dot{x}_2 &= \frac{F_c (t - t_{02})}{m_2} + v_2\end{aligned}\tag{3-21}$$

$$\ddot{x}_2 = \frac{F_c}{m_2}$$

The motion of Equations 3-19 and 3-21 will continue until m_1 once again rebounds to m_2 . This occurs when the velocities of m_1 and m_2 are identical. Thus, for $\dot{x}_1 = \dot{x}_2$

$$\begin{aligned}- \left(x_{02} + \frac{F_c}{k} \right) \omega_1 \sin \omega_1 (t - t_{02}) \\ + v_{02} \cos \omega_1 (t - t_{02}) &= \frac{F_c (t - t_{02})}{m_2} + v_2\end{aligned}\tag{3-22}$$

The root to this equation occurs when $t = t_{03}$ where $t > t_{02}$.

When rebonding occurs, masses m_1 and m_2 move together at identical velocities and accelerations. The initial conditions are obtained from Equations 3-19 and 3-21. Thus,

$$x_{03} = x_1(t_{03}) = \left(x_0 + \frac{F_C}{k}\right) \cos \omega_1 (t_{03} - t_{02}) + \frac{v_{02}}{\omega_1} \sin \omega_1 (t_{03} - t_{02}) - \frac{F_C}{k} \quad (3-23)$$

$$v_{03} = \dot{x}_1(t_{03}) = \dot{x}_2(t_{03}) = -\left(x_0 + \frac{F_C}{k}\right) \omega_1 \sin \omega_1 (t_{03} - t_{02}) + v_{02} \cos \omega_1 (t_{03} - t_{02})$$

$$x_2(t_{03}) = \frac{F_C}{2m_2} (t_{03} - t_{02})^2 + v_2 (t_{03} - t_{02}) + d_2$$

We can now proceed to the next regime.

3.1.4 SOLUTION OF CASE 2: $x_1 = x_2$

As before, our equations of motion are given by

$$\begin{aligned} x_1 &= A \cos \omega_2 (t - t_{03}) + B \sin \omega_2 (t - t_{03}) \\ x_2 &= A \cos \omega_2 (t - t_{03}) + B \sin \omega_2 (t - t_{03}) + C \end{aligned} \quad (3-24)$$

subject to the initial conditions from Equation 3-23 above. Thus

$$\begin{aligned} x_1 &= x_{03} \cos \omega_2 (t - t_{03}) + \frac{v_{03}}{\omega_2} \sin \omega_2 (t - t_{03}) \\ \dot{x}_1 &= -x_{03} \omega_2 \sin \omega_2 (t - t_{03}) + v_{03} \cos \omega_2 (t - t_{03}) \\ \ddot{x}_1 &= -x_{03} \omega_2^2 \cos \omega_2 (t - t_{03}) - v_{03} \omega_2 \sin \omega_2 (t - t_{03}) \\ x_2 &= x_{03} \cos \omega_2 (t - t_{03}) + \frac{v_{03}}{\omega_2} \sin \omega_2 (t - t_{03}) + d_3 - x_{03} \\ \dot{x}_2 &= \dot{x}_1 \end{aligned} \quad (3-25)$$

$$\ddot{x}_2 = \ddot{x}_1$$

where $d_3 = x_2 (t_{03})$ from Equation 3-23

These equations are valid until

$$m_2 \ddot{x}_2 = - F_c \tag{3-26}$$

and the process continues until sufficient energy is removed from the system by friction damping that m_1 no longer slides relative to m_2 .

If one examines the dynamic behavior described above, it will be observed that the equations of motion are repetitive i.e., recursive. In fact, qualitatively, the motion can be summarized as shown in Table 3-1. At any point of transition of motion, the final conditions from the previous motion become the starting conditions for the following motion. For the model configuration considered, the motion continues as in Table 3-1 with the bonding time becoming increasingly longer in comparison to the sliding time. Ultimately, no sliding motion will occur and the response will degenerate into a pure sinusoid. The decay of the motion is caused by energy dissipation from damping.

TABLE 3-1. RECURSIVE FRICTION MODEL

<u>Behavior</u>	<u>Transition Condition</u>
Sliding First Direction	Initial Displacement and Velocity
Bonding	Zero Relative Velocity
Sliding Second Direction	Maximum Friction Force Exceeded
Bonding	Zero Relative Velocity
Sliding First Direction	Maximum Friction Force Exceeded
Sequence Repeats	
o	
o	
o	

3.2 EXAMPLE SOLUTIONS

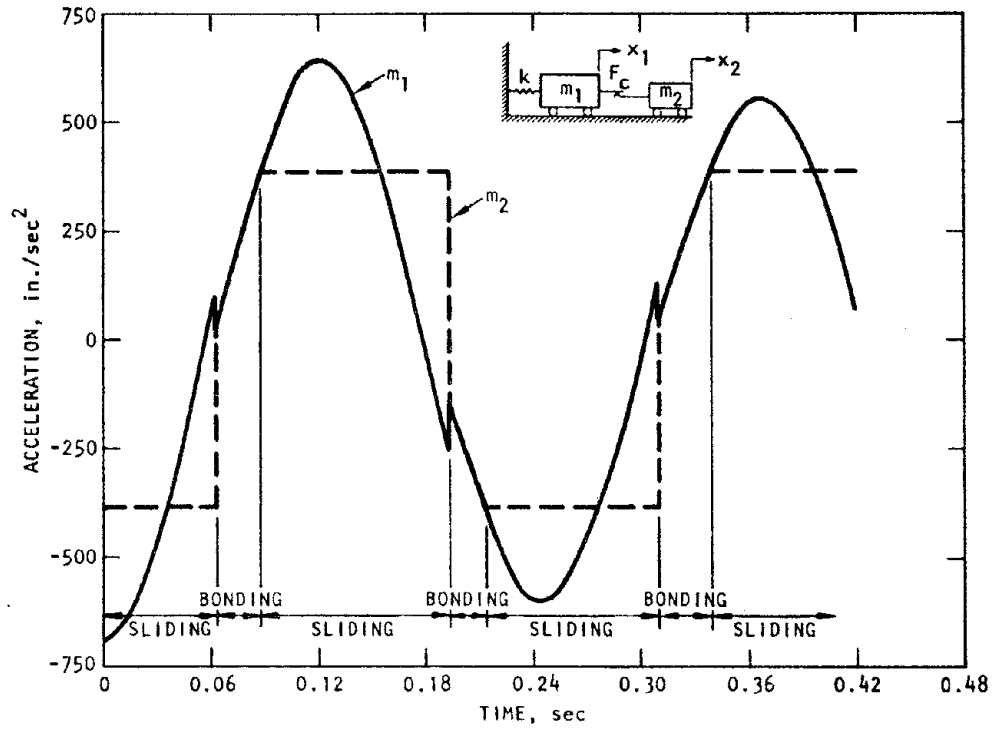
We now examine the consequence of adopting a friction model as simple as that shown in Figure 3-4. In order to do this, we solve the exact equations of motion previously developed above for an example problem in which values of masses, the spring constant, and the friction damping force are chosen. The values are shown in Table 3-2 and they have been chosen to produce a 1 g acceleration of mass m_2 when it is sliding relative to mass m_1 .

TABLE 3-2. PARAMETERS FOR DEMONSTRATION SOLUTION

$m_1 = 5 \text{ lb} = 0.01295335 \text{ lb-sec}^2/\text{in}$
$m_2 = 1 \text{ lb} = 0.00259067 \text{ lb-sec}^2/\text{in}$
$k = 9.815 \text{ lb/in}$
$F_c = \pm 1 \text{ lb}$
$x_0 = 1 \text{ in.}$
$\dot{x}_0 = 0 \text{ in./sec}$

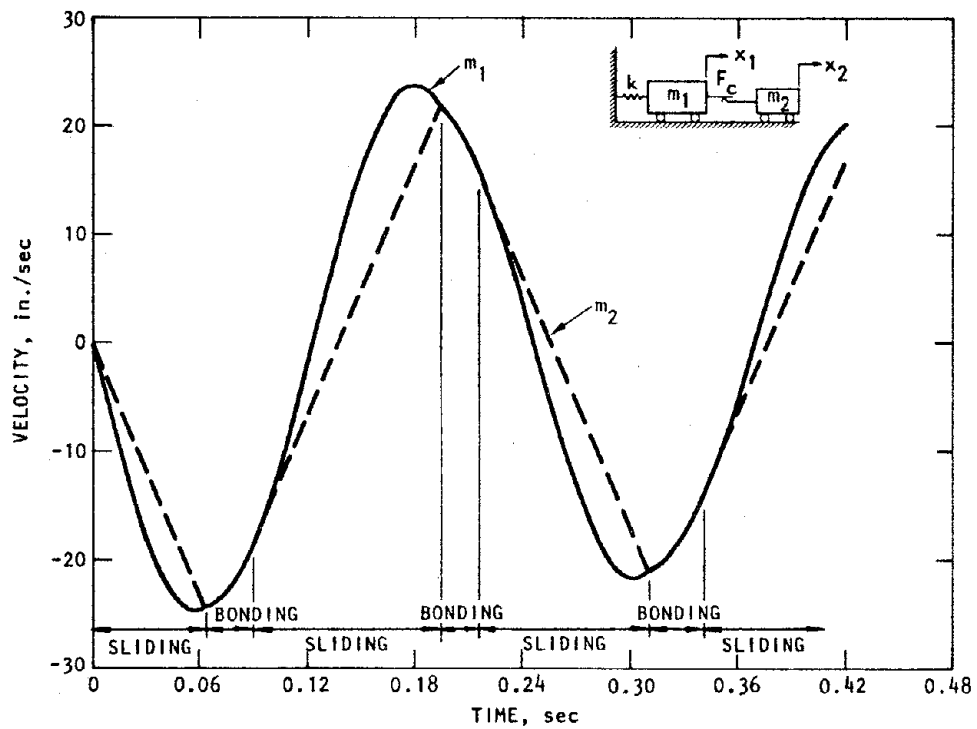
The results of this example are shown in Figures 3-5 through 3-9. It is instructive to discuss these data in some detail. If we examine Figure 3-5 (which shows the acceleration responses of the two masses) we deduce that alternate sliding and bonding between the two masses occurs during the intervals shown on the figure. Note that as the transition between sliding to bonding occurs, discontinuities in the accelerations of both masses occur.

During any sliding phase, the acceleration of mass m_2 is limited by the maximum friction force of $\pm 1 \text{ lb}$ which produces an acceleration of $\pm 1 \text{ g}$ (386 in./sec^2). During this period, the acceleration of mass m_1 is basically sinusoidal under the influence of the deflected spring force. The constant friction force provided by mass m_2 produces a perturbation of this motion with the resultant observed discontinuities.



AA773

FIGURE 3-5. ACCELERATION-TIME HISTORIES OF MASSES m_1 AND m_2



AA774

FIGURE 3-6. VELOCITY-TIME HISTORIES OF MASSES m_1 AND m_2

During the bonded phase, the accelerations of both masses are identical as they must be. The discontinuities in the accelerations reflect the fact that as incipient bonding is approached, i.e., as the velocities of the two masses approach equality, an abrupt adjustment in the velocity rate of change is necessary to maintain the bonded condition.

We also note that as friction consumes energy from the system, the peak accelerations of mass m_1 degrade in amplitude with each succeeding oscillation. We will later use this information as a measure of efficiency of the Coulomb damper in restricting the seismic-induced motion of suspended floor systems.

In Figures 3-6 and 3-7 respectively, the corresponding velocities and displacement of masses m_1 and m_2 are shown. Note that during the period of bonding, the velocities of the two masses are identical. However, the displacement of mass m_2 "floats" as

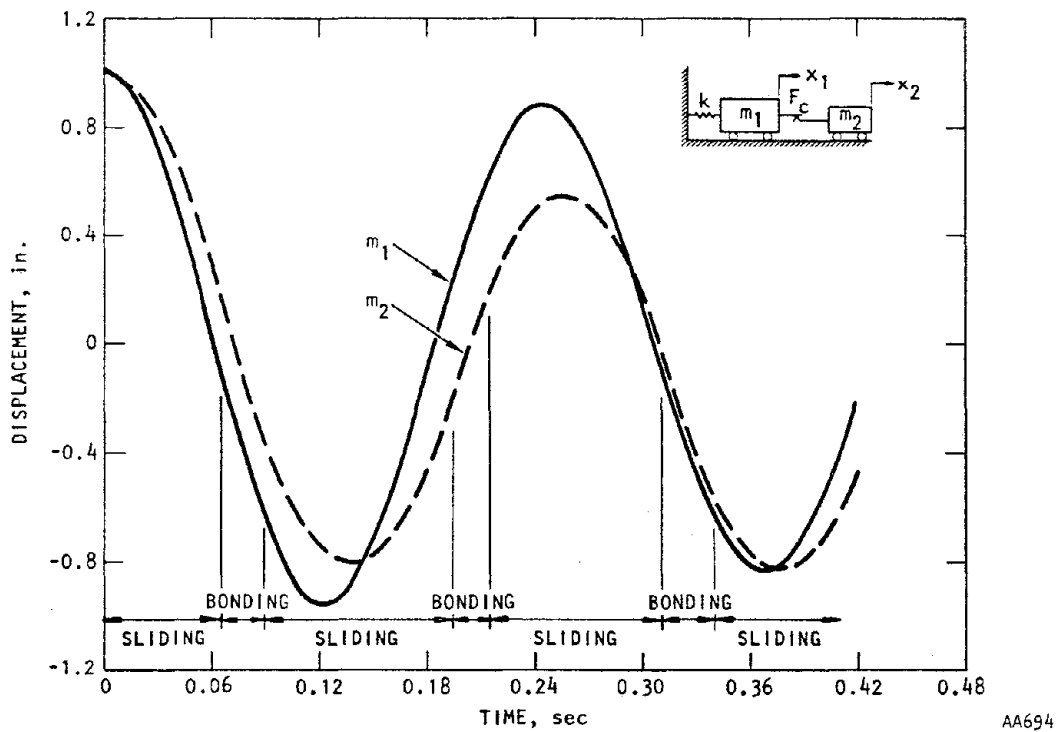


FIGURE 3-7. DISPLACEMENT-TIME HISTORIES OF MASSES m_1 AND m_2

it slides back and forth on the parent mass m_1 . One can observe the character of the relative motions between the masses in Figures 3-8 and 3-9 showing the difference in velocities and displacements respectively.

3.2.1 LIMITATIONS OF THE SIMPLE MODEL

In the simplest numerical solutions of the equations of motion presented in Equation 3-1, the friction model is often patterned from Figure 3-4. In such a model, the friction force which links any two elements which can potentially slide relative to each other is either the maximum positive or the maximum negative friction force depending upon the direction or sense of the relative velocity between the elements. Only in the case where the relative velocity is identically zero can the friction force be anything other than the absolute maximum, and in this case, the force would be set to zero. No intermediate values would be admissible.

In the context of the numerical model discussed previously, we would not expect to see orderly transitions of acceleration occurring at the onset of bonding in Figure 3-5 because only maximum positive or maximum negative values of friction force are possible with the model shown in Figure 3-4. Typically, the force will oscillate between the maximum negative and positive values until stability can be achieved. On the other hand, it might be reasonable to expect that the force oscillation might not be readily apparent in velocity and displacement signatures because the integration process acts to filter out the high frequency switching or oscillation.

To illustrate the point, we now compare the exact solutions of motion in Figures 3-5 through 3-7 with numerical solutions for the same example using the switching model of Figure 3-4. These are shown in Figures 3-10 through 3-12 for the comparisons of acceleration, velocity and displacement, respectively, for masses m_1 and m_2 . Note in Figure 3-10 that the solutions generally agree but that there is considerable "noise" at the

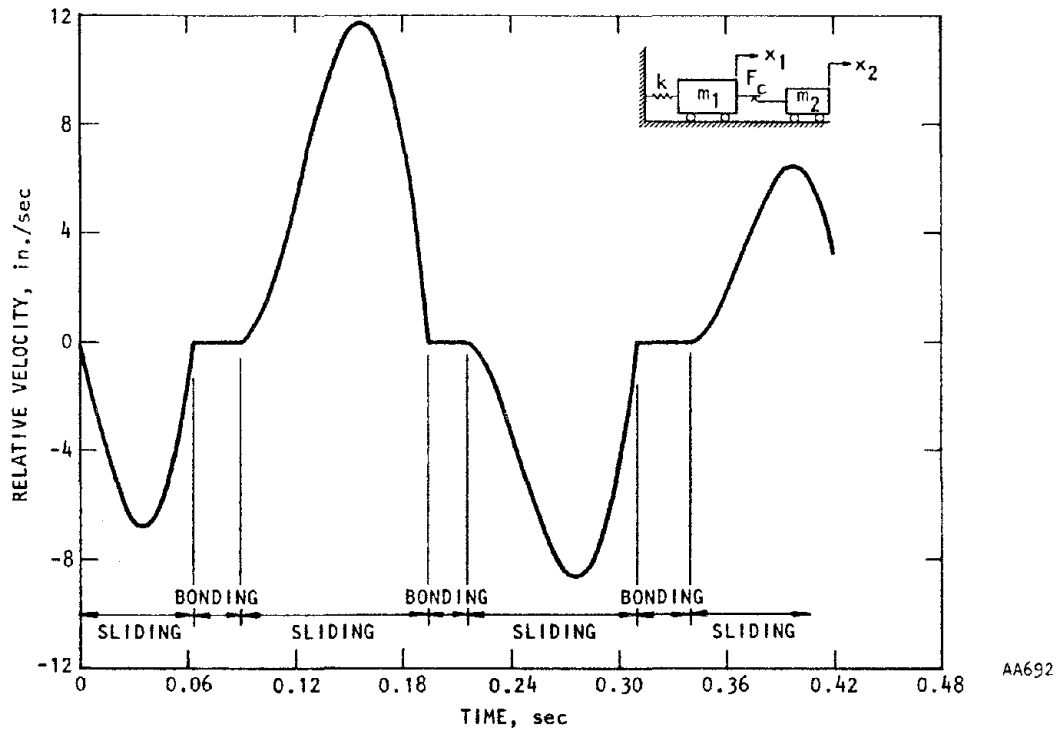


FIGURE 3-8. RELATIVE VELOCITY BETWEEN MASSES m_1 AND m_2

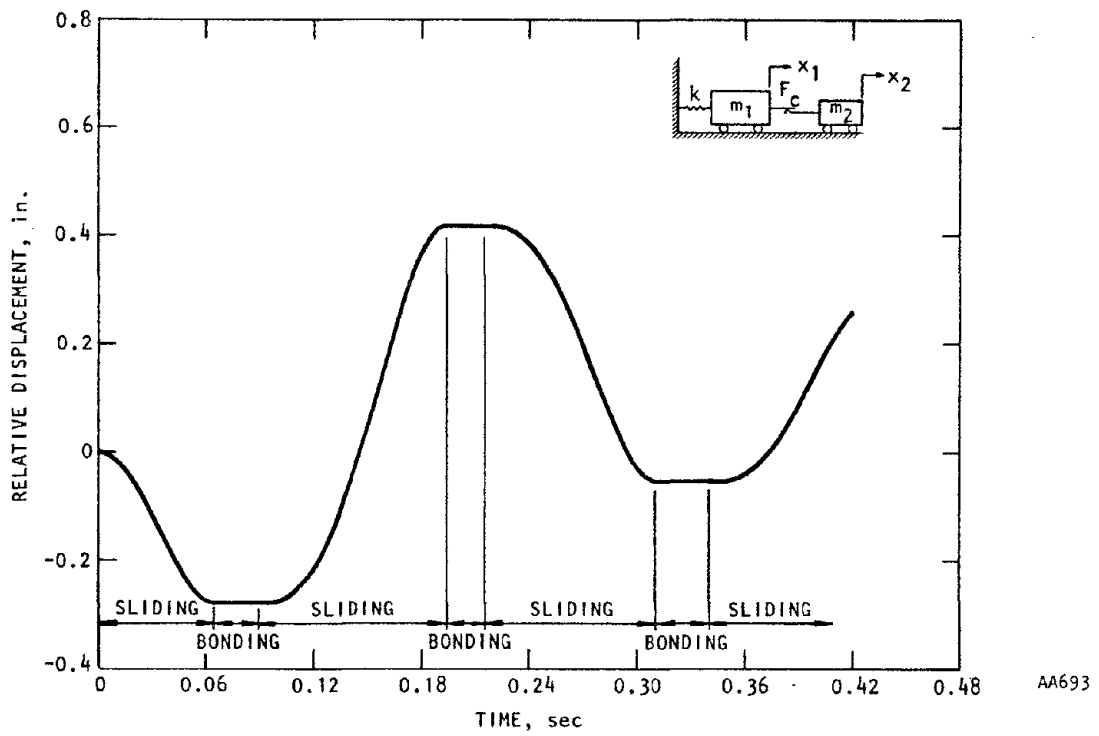
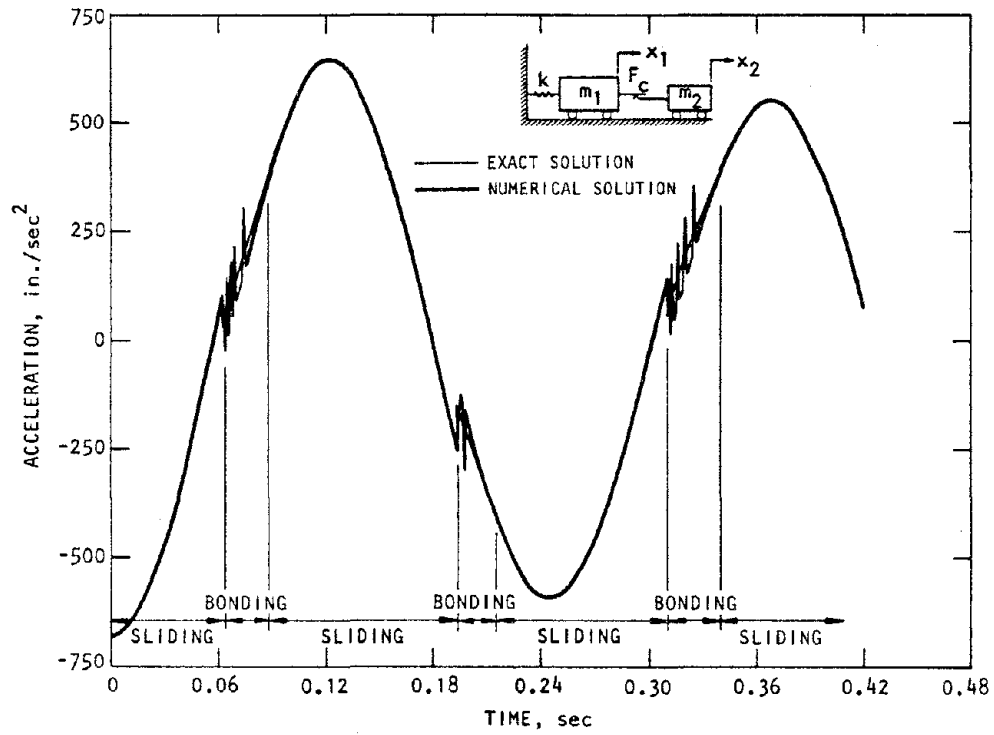
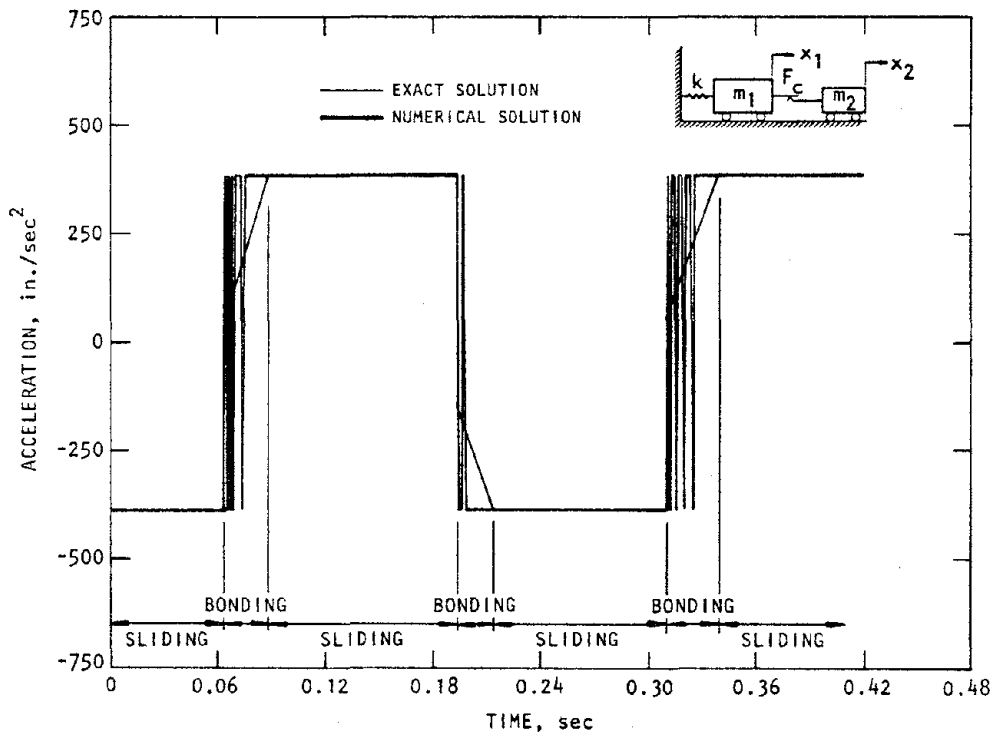


FIGURE 3-9. RELATIVE DISPLACEMENT BETWEEN MASSES m_1 AND m_2



(a) Mass m_1



(b) Mass m_2

FIGURE 3-10. COMPARISON OF ACCELERATION OF EXACT SOLUTION WITH SWITCHING MODEL

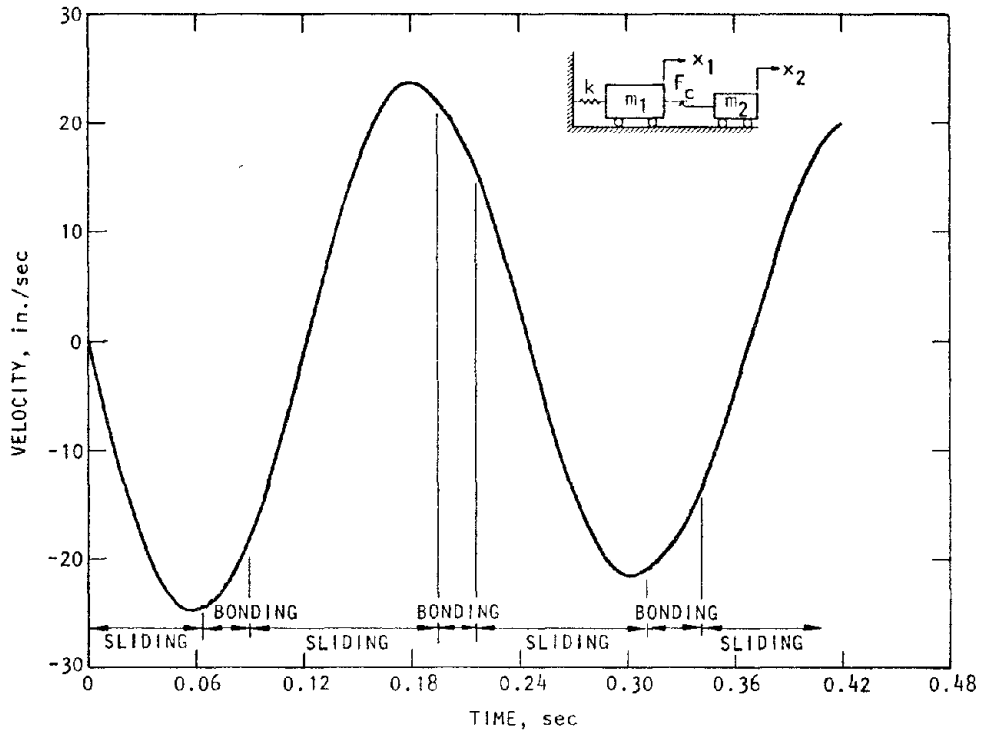
occurrence of real acceleration discontinuities. Note also that as we compare the integrations in Figures 3-11 and 3-12 for the velocities and displacements, respectively, the differences between the exact and numerical solutions for the velocities are quite small and virtually indistinguishable for the displacements.

In many applications, the numerical solutions of friction problems, while "noisy" in acceleration, may be adequate for engineering purposes, especially where the problem concerns mainly structural response. On the other hand, the noise may lead to a problem in many degree-of-freedom systems where one or more elements may be switching virtually throughout the entire period of response. Moreover, such switching may cause a problem in interpretation of the computed data to be used as input into high frequency systems such as equipment. For example, while it may be possible to filter out the high frequency noise (with a low pass filter), the filter may also remove real signal. In that instance, we may have inadvertently distorted the signal in the process of clearing out the noise.

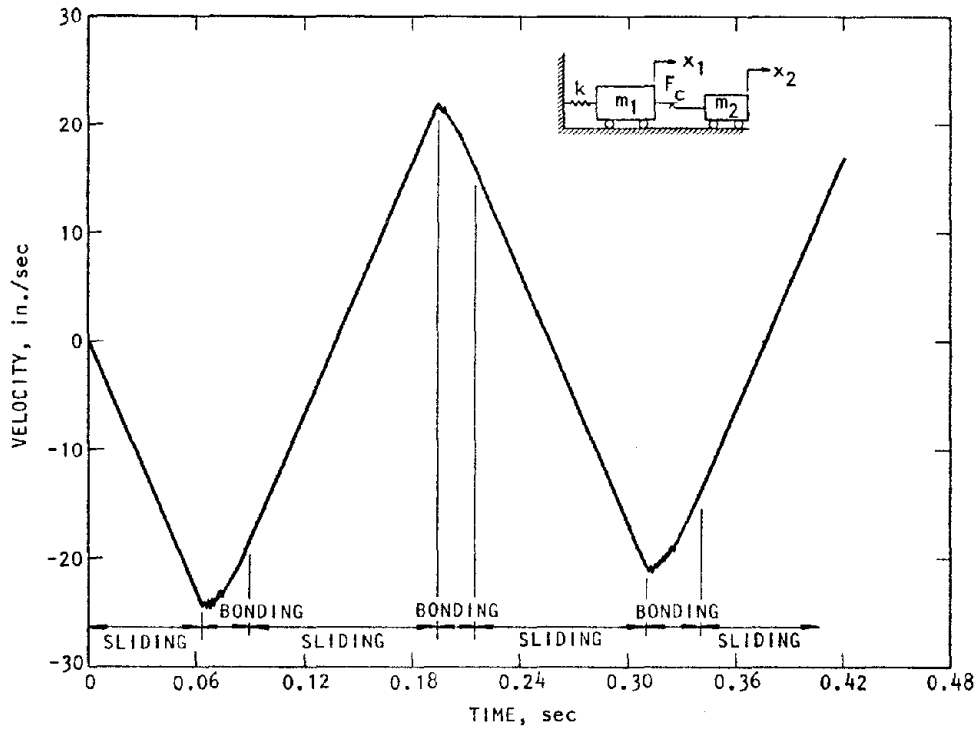
3.2.2 RAMPED COULOMB MODEL

Coulomb friction noise is common and various methods have been used to control it. Frequently, the oscillation in acceleration which occurs in simplified, idealized friction models is damped by modifying the model itself. This is accomplished by an approach which is shown in Figure 3-13. As the velocities between two sliding masses merge, that is, as the relative velocity approaches zero, the friction force is constrained to transition gradually between its maximum force envelope along the ordinate axis. While this approach will damp out the oscillations observed in Figure 3-10, errors in the solution may be introduced because a nonrealistic representation of friction is created.

We normally expect the friction force to increase as the relative velocity approaches zero as shown in Figure 3-1. The

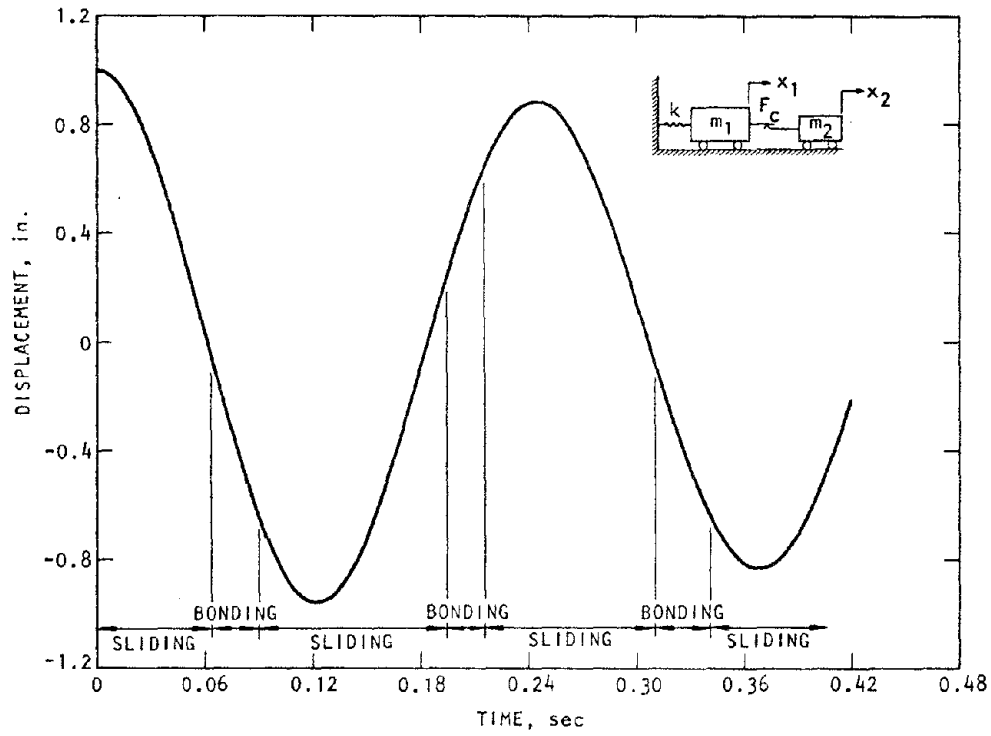


(a) Mass m_1

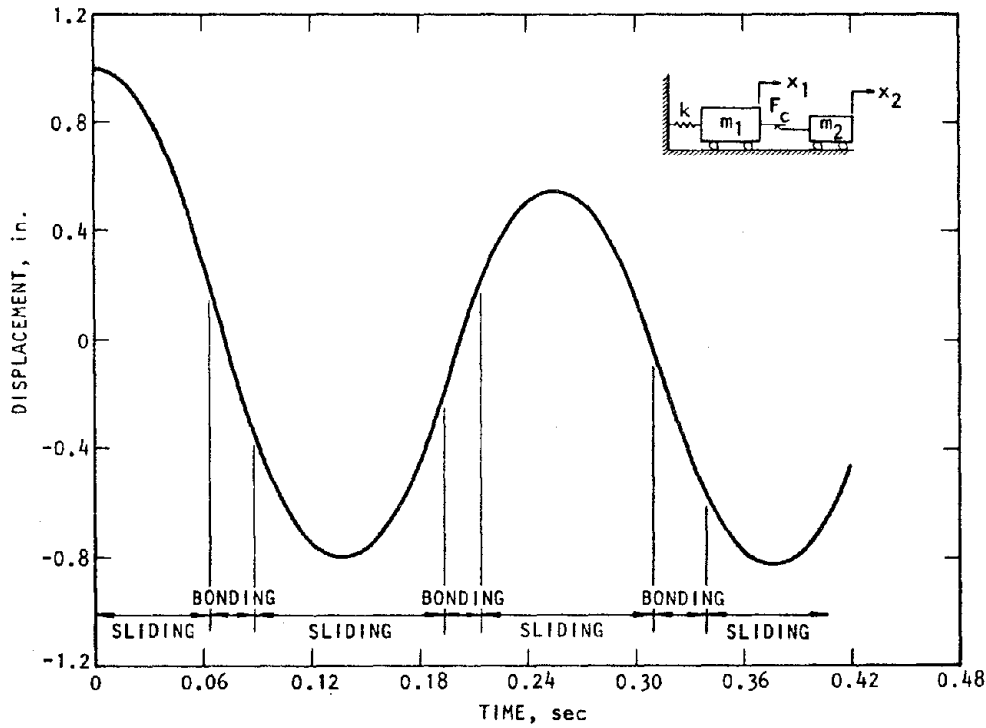


(b) Mass m_2

FIGURE 3-11. COMPARISON OF VELOCITY OF EXACT SOLUTION WITH SWITCHING MODEL



(a) Mass m_1



(b) Mass m_2

FIGURE 3-12. COMPARISON OF DISPLACEMENT OF EXACT SOLUTION WITH SWITCHING MODEL

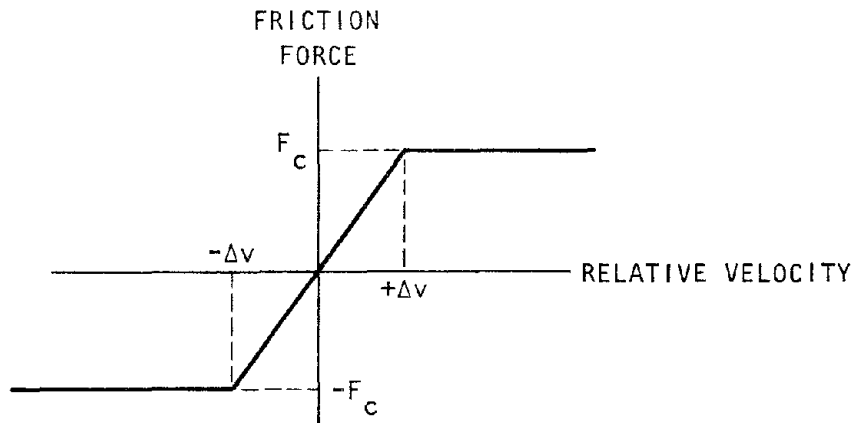
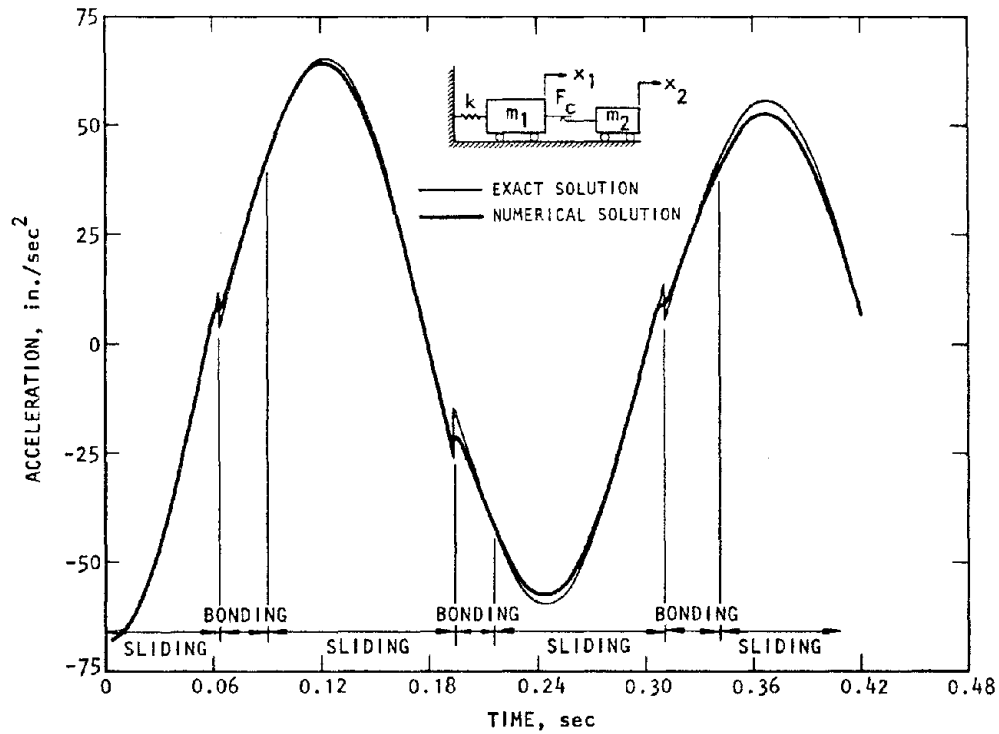


FIGURE 3-13. MODIFIED FRICTION MODEL

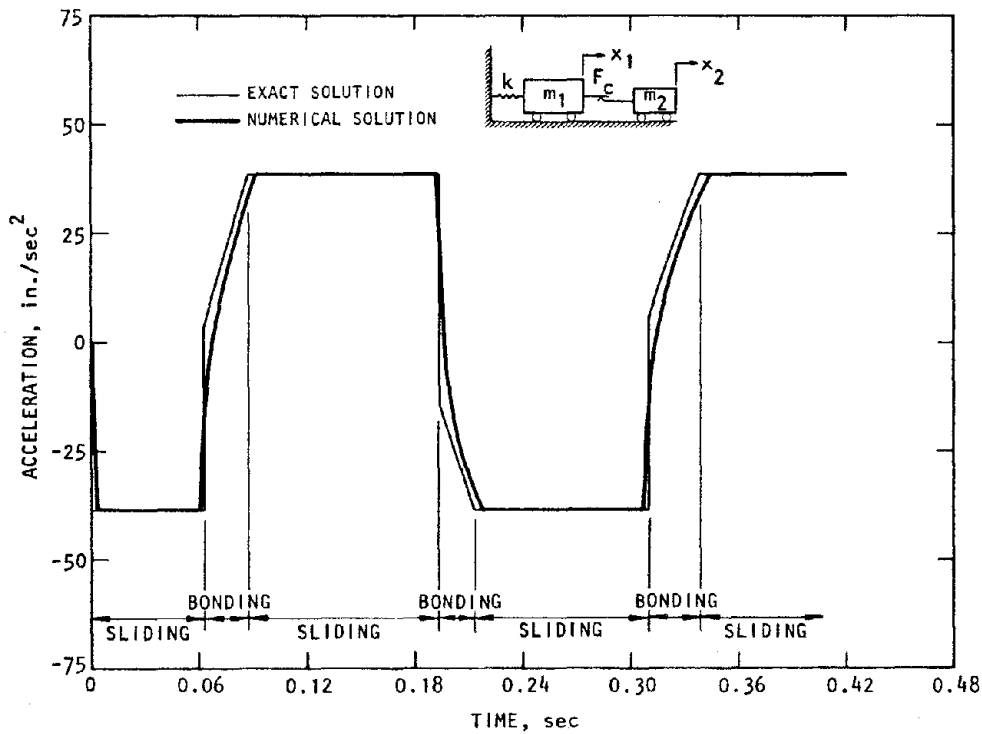
opposite effect occurs with the model in Figure 3-13. Moreover, it is difficult to know beforehand which value of the relative velocity, $\pm\Delta v$, to choose (if $\pm\Delta v$ is too small, the ramp will be stepped over; if too large, the correction will be too crude). Under the best of circumstances, for multiple degree of freedom systems, a rational selection of Δv is probably time and space dependent to guarantee that the beneficial effect will be equally applied throughout the system and for all instances of time (in practice the complexity of implementing any such procedure would exceed the benefit achieved).

An application of the ramped method for constructing the friction model of Figure 3-13 is demonstrated numerically by solving the previous problem summarized in Table 3-2 with a selection of $\Delta v = 2.5$ in./sec. This ramp on the friction force will guarantee a smooth transition between $+F_c$ and $-F_c$ as the relative velocity between m_1 and m_2 changes sign.

The acceleration, velocity, and displacement signatures for the ramped model are compared to the exact solution in Figures 3-14 through 3-16, respectively. One immediately observes that the oscillations seen in Figure 3-10 for the switching model have been brought under control. However, we also note



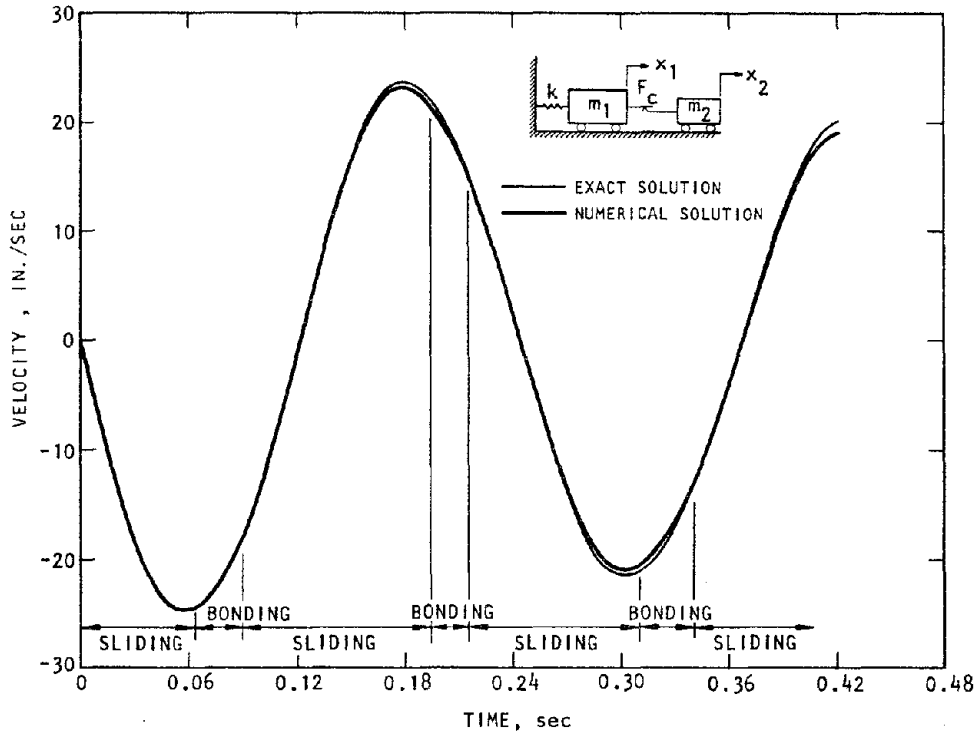
(a) Mass m_1



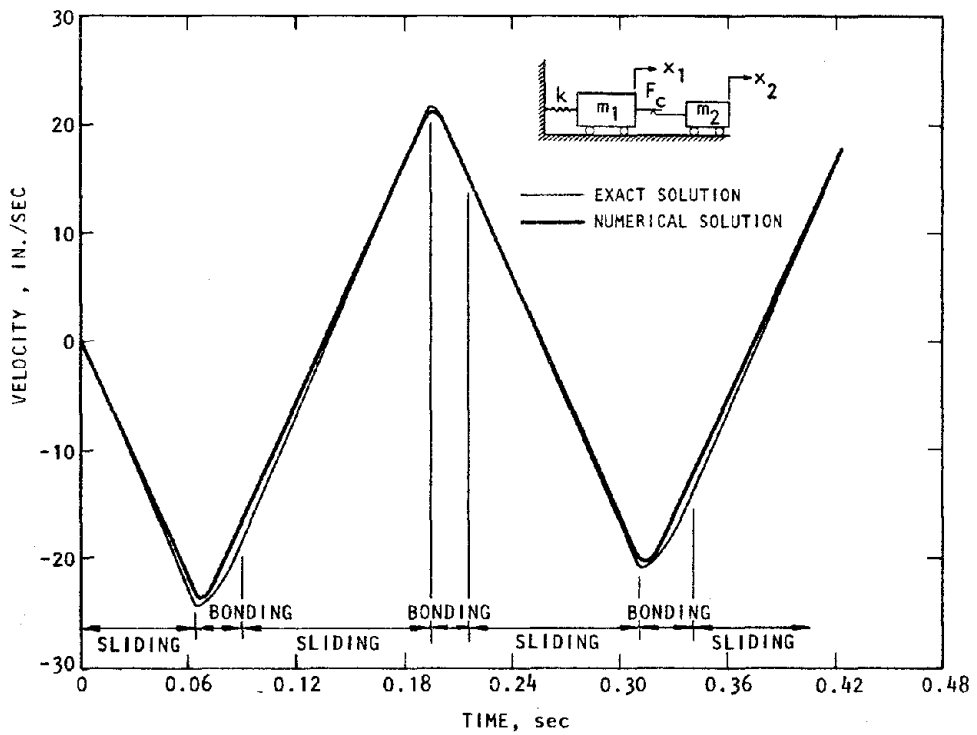
(b) Mass, m_2

AA689

FIGURE 3-14. COMPARISON OF ACCELERATION OF EXACT SOLUTION WITH RAMPED MODEL

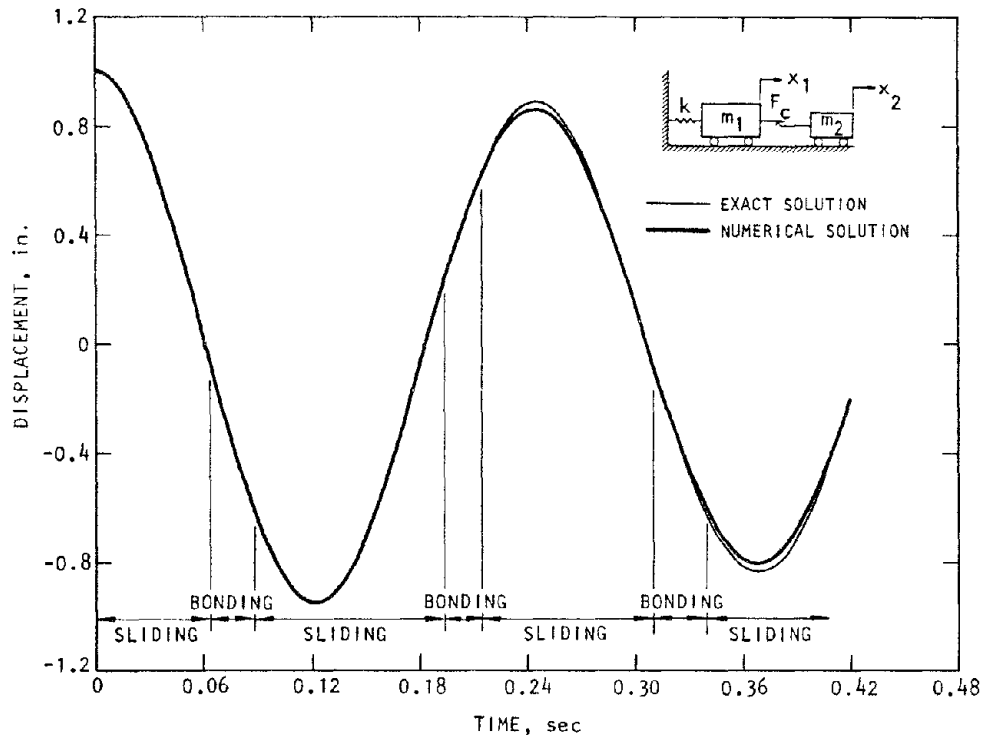


(a) Mass m_1

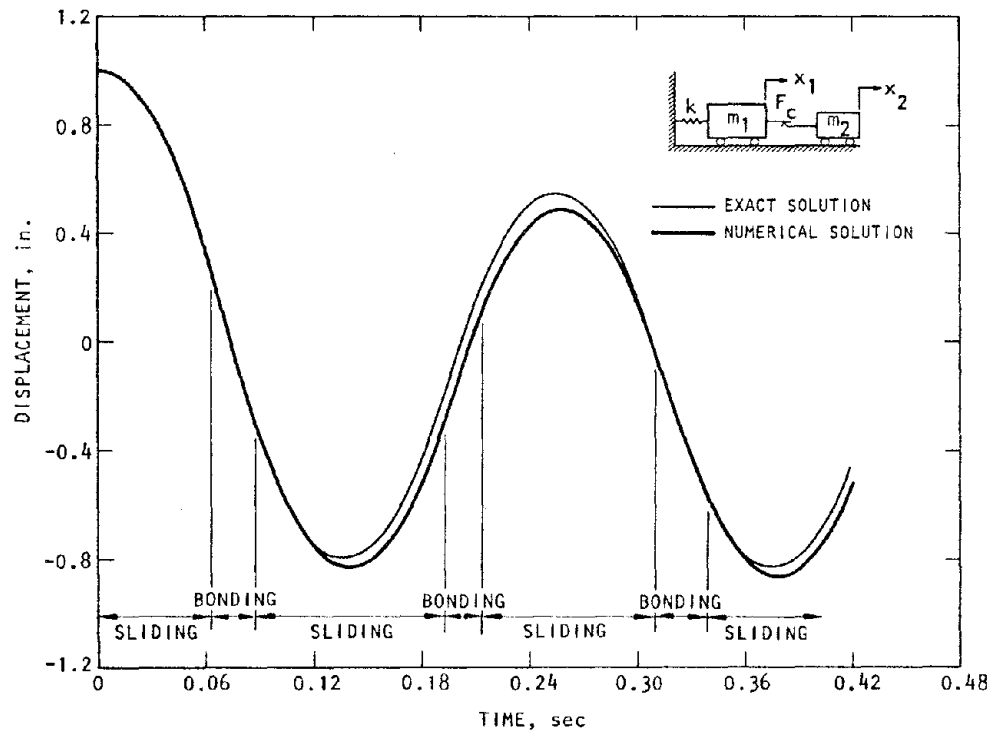


(b) Mass m_2

FIGURE 3-15. COMPARISON OF VELOCITY OF EXACT SOLUTION WITH RAMPED MODEL



(a) Mass m_1



(b) Mass m_2

AA687

FIGURE 3-16. COMPARISON OF DISPLACEMENT OF EXACT SOLUTION WITH RAMPED MODEL

that the true discontinuities in accelerations of Figure 3-14 have been "smeared" and have caused some errors in the subsequent integration as shown in Figures 3-15 and 3-16. Therefore, whereas we have eliminated the "noise" problem observed in the previous solution, we have now introduced an underlying problem in the ramped model which fundamentally alters the solution.

3.2.3 PREDICTOR/CORRECTOR TECHNIQUES

We now develop a numerical procedure which is patterned after the exact solution that we have discussed previously. In Figure 3-17, consider two masses which are directly coupled via a friction damper and which have other generalized forces active upon them.

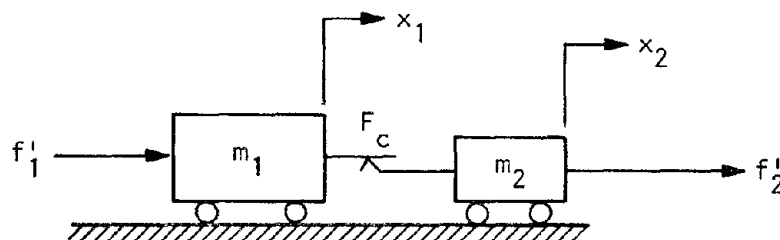


FIGURE 3-17. REPRESENTATION OF A TWO-ELEMENT FRICTION MODEL IMBEDDED IN A MULTIPLE DEGREE-OF-FREEDOM SYSTEM

The total forces on masses m_1 and m_2 are written as

$$f_{i,t} = f'_{i,t} - f_{c,t} \quad i = 1,2 \quad (3-27)$$

where

$f_{i,t}$ = Total force acting on m_i

$f_{c,t}$ = Friction force acting on m_i

$f'_{i,t}$ = Net force acting on m_i exclusive of friction force.

We also note that

$$\ddot{x}_{i,t} = \frac{f_{i,t}}{m_i} \quad (3-28)$$

so that Equation 3-28 becomes

$$\ddot{x}_{i,t} = \frac{f'_{i,t} - f_{c,t}}{m_i} \quad (3-29)$$

An approximation of the acceleration in Equation 3-29 is obtained from

$$\ddot{x}_{i,t} = \frac{\dot{x}_{i,t} - \dot{x}_{i,t-\Delta t}}{\Delta t} \quad (3-30)$$

Combining Equations 3-29 and 3-30, we get

$$\dot{x}_{i,t} = \frac{\Delta t}{m_i} (f'_{i,t} - f_{c,t}) + \dot{x}_{i,t-\Delta t} \quad (3-31)$$

However, we do not know the actual value of $f_{c,t}$ and therefore we estimate it as will be shown shortly and call it $\tilde{f}_{c,t}$. Thus, from Equation 3-27

$$\dot{x}_{i,t} = \frac{\Delta t}{m_1} (f_{i,t} + \tilde{f}_{c,t} - f_{c,t}) + \dot{x}_{i,t-\Delta t} \quad (3-32)$$

At any instant of time, we don't know whether the conditional equality

$$\dot{x}_{1,t} \stackrel{?}{=} \dot{x}_{2,t} \quad (3-33)$$

is true. If it is, the two masses will be bonded together; if it is not, the two masses will be sliding relative to each other. We resolve the question by assuming that Condition 3-33 is true. Thus, from Equation 3-32 using Equation 3-33:

$$f_{c,t} = \tilde{f}_{c,t} + \frac{m_1 f_{2,t} - m_2 f_{1,t} + \frac{m_1 m_2}{\Delta t} \dot{x}_{2,t-\Delta t} - \dot{x}_{1,t-\Delta t}}{m_1 - m_2} \quad (3-34)$$

Equation 3-34 can be evaluated in a computer program which uses predictor-corrector methods of solution. In this arrangement, we simply set $\tilde{f}_{c,t}$ to be whatever it was in the previous time step, i.e.

$$\tilde{f}_{c,t} = f_{c,t-\Delta t} \quad (3-35)$$

and $f_{1,t}$ and $f_{2,t}$ are the predicted total forces acting on masses m_1 and m_2 based on a prediction from their past behavior. Thus, we are able to evaluate $f_{c,t}$ for the current time, t .

Two basic outcomes are expected from the evaluation of Equation 3-34. Either $|f_{c,t}| \geq |F_c|$ or $|f_{c,t}| < |F_c|$. If the first case prevails we let

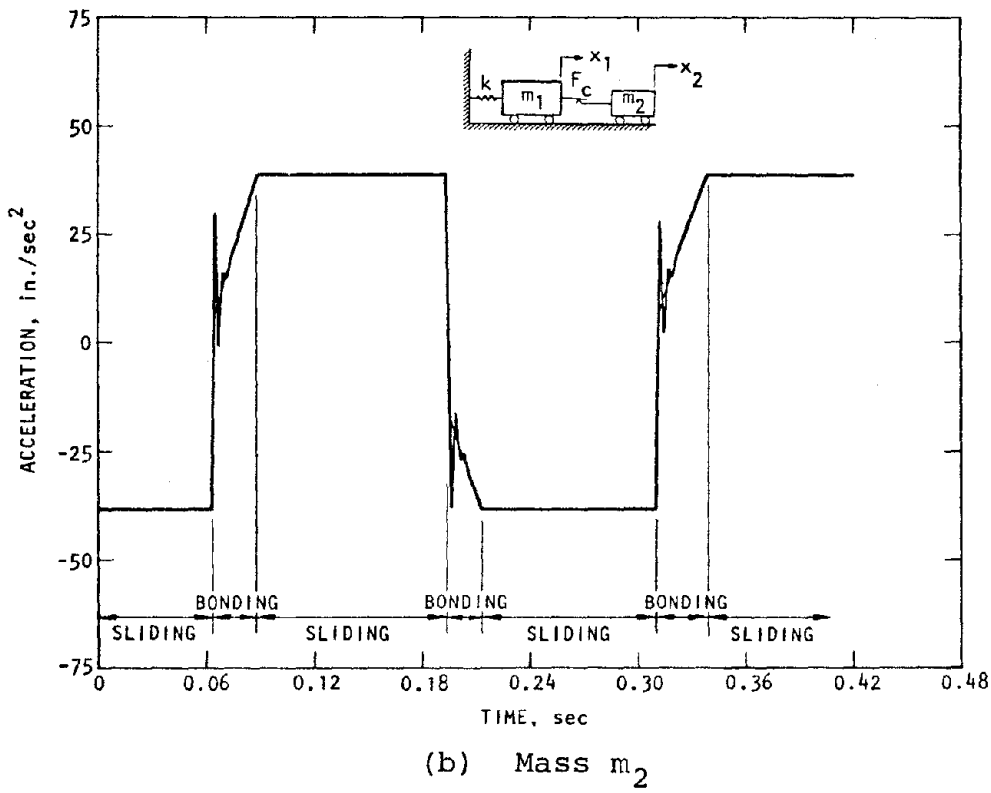
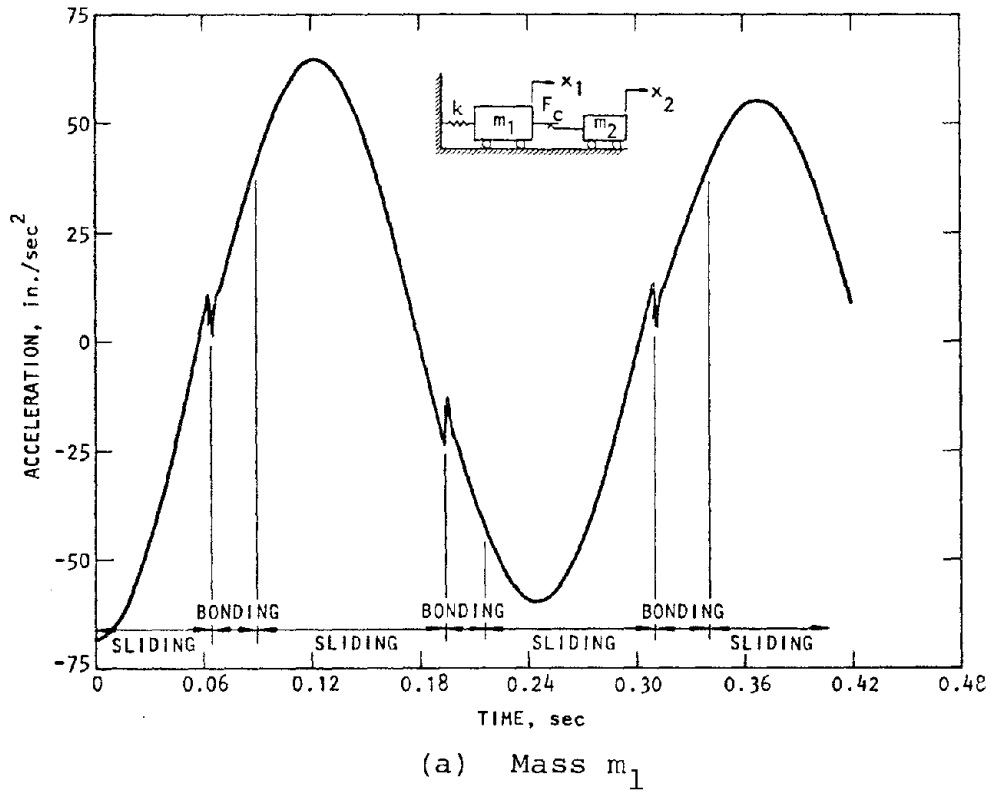
$$f_{c,t} = |F_c| \text{ sign } (\dot{x}_{1,t} - \dot{x}_{2,t}), \quad |f_{c,t}| \geq |F_c| \quad (3-36)$$

or if the second case is applicable

$$f_{c,t} = |f_{c,t}| \text{ sign } (\dot{x}_{1,t} - \dot{x}_{2,t}), \quad |f_{c,t}| < |F_c| \quad (3-37)$$

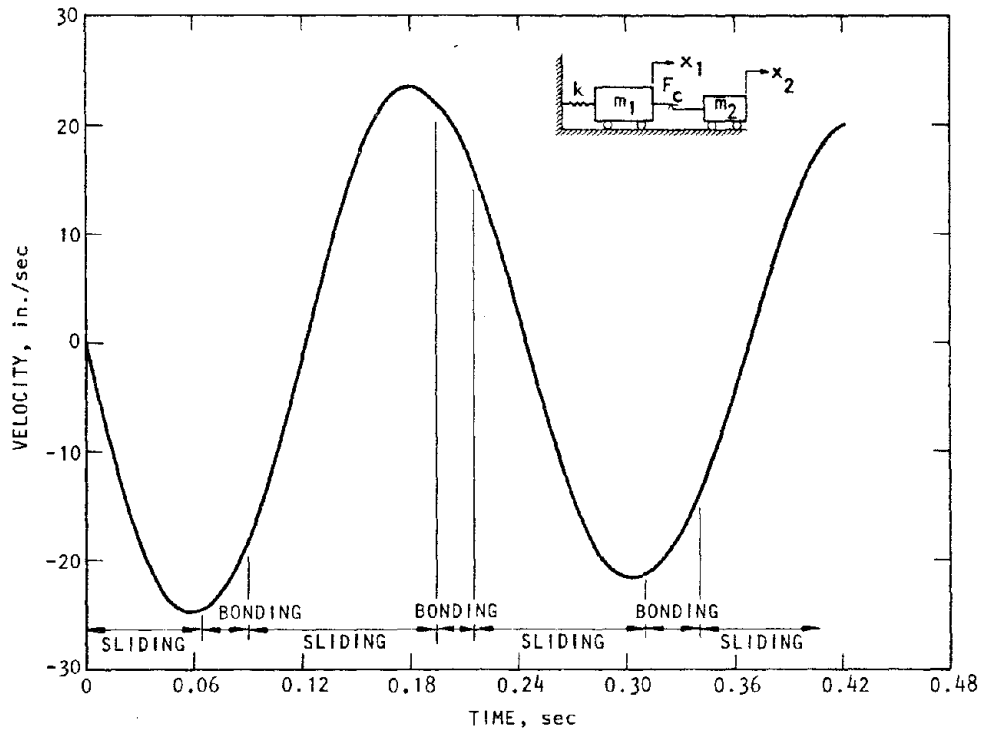
To test the above procedure, we solve the numerical example presented previously and the results are again compared to the exact solution in Figures 3-18 through 3-20 for the acceleration, velocity, and displacement response, respectively. We should recognize that the numerical procedure implemented above is really a refinement of the switching model whose results are shown in Figures 3-10 through 3-12.

For example, if we compare Figure 3-10a with 3-18a and 3-10b with 3-18b, it is clear that the predictor-corrector method allows the numerical solution to stabilize more quickly than the simple switching model. This is especially obvious when comparing the response of mass m_2 . For this reason, the predictor-corrector method is preferable because it introduces less higher-frequency spurious response. Moreover, we can improve the solution further by implementing Equations 3-34 and 3-35 in multiple predictor-corrector passes within any given time step. Thus, at arbitrary time, t , we can predict $\tilde{f}_{c,t}$ from

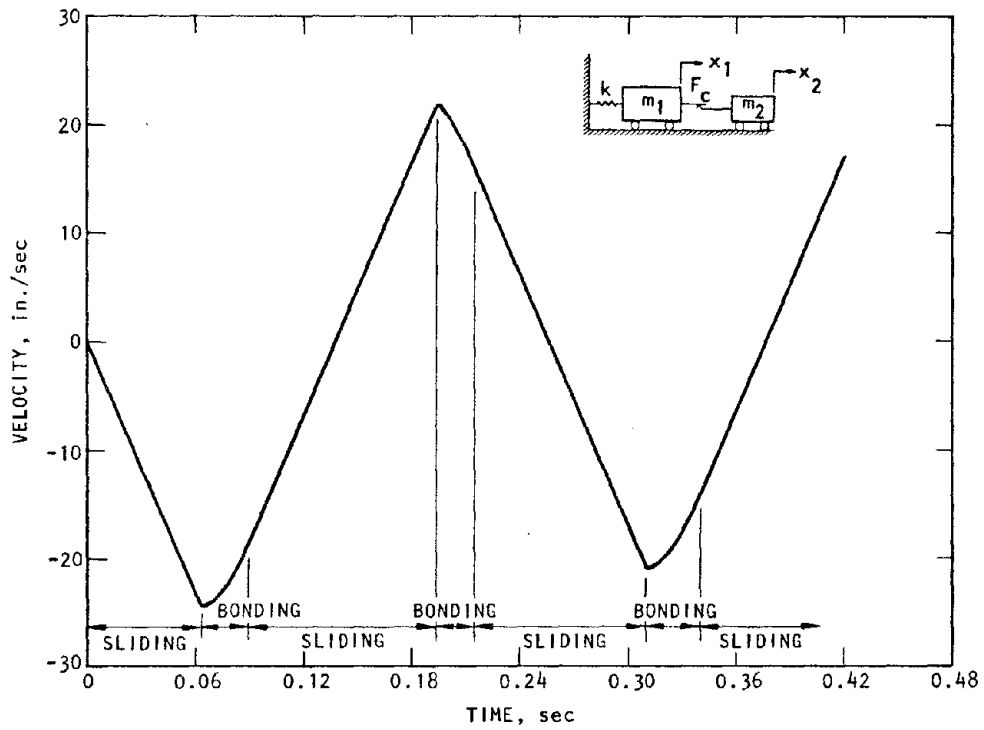


AA686

FIGURE 3-18. COMPARISON OF ACCELERATION OF EXACT SOLUTION WITH PREDICTOR-CORRECTOR NUMERICAL MODEL



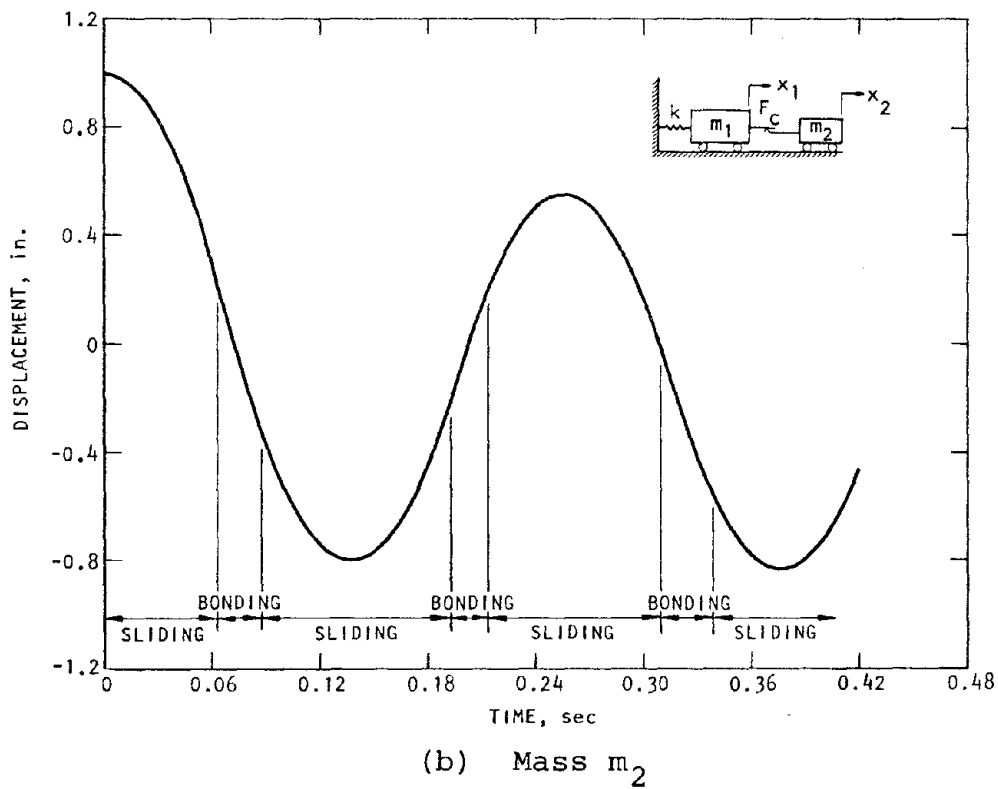
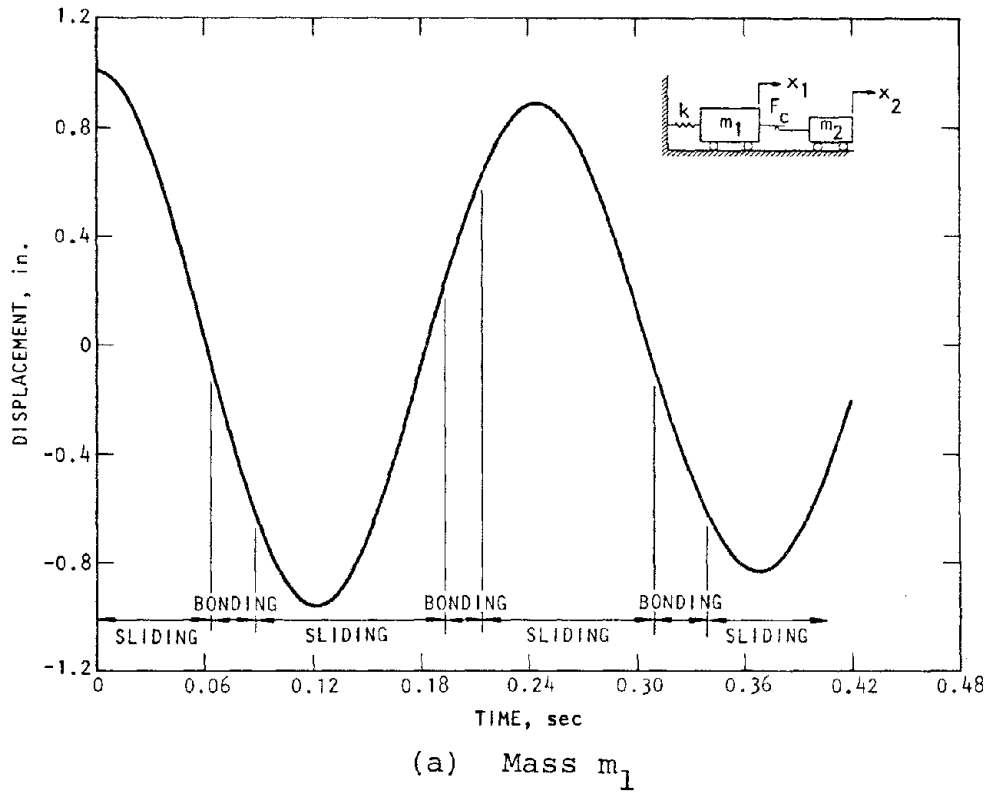
(a) Mass m_1



(b) Mass m_2

AA685

FIGURE 3-19. COMPARISON OF VELOCITY OF EXACT SOLUTION WITH PREDICTOR-CORRECTOR NUMERICAL MODEL



AA684

FIGURE 3-20. COMPARISON OF DISPLACEMENT OF EXACT SOLUTION WITH PREDICTOR-CORRECTOR NUMERICAL MODEL

Equation 3-35 and obtain a correction for $f_{c,t}$ for Equation 3-34. The process can be repeated until an acceptance criterion such as

$$\left| \tilde{f}_{c,t} - f_{c,t} \right| \leq \varepsilon \quad (3-38)$$

is satisfied where ε is an error bound that is preselected as part of the problem setup.

We should also note that the velocities and displacements in Figures 3-11, 3-12, 3-19 and 3-20 are apparently of equal accuracy regardless of the numerical solution method. However, integration of acceleration-time histories essentially suppresses high frequency noise relative to low frequency signal and masks potential high frequency response problems. We need to be at least aware of this as we solve our problems to determine stresses in structural members on the one hand or accelerations imposed on housed equipment on the other.

3.2.4 TENTATIVE CONCLUSIONS

In summary, we may tentatively conclude the following:

1. Switching models to represent friction damping are probably adequate for structural analyses provided that the switching noise does not introduce an unstable condition or otherwise become so severe as to distort the velocity and displacement solutions.
2. The predictor-corrector method is also at least as accurate for structural analysis as the switching method and in addition has better control over spurious noise and therefore reduces the chance for instability or the possibility for spoiling the velocity and displacement response.
3. The ramped method provides an artificial control on spurious noise but it also produces a distortion in the solution which may be especially important to structural calculations (because its effect is especially obvious in displacement). On the other

hand, this method is more beneficial to the calculation of environments for sensitive structure equipments, because no high frequency noise is created.

4. The switching method should not be used for calculations which are to be used for specification of instructure environments for sensitive equipments. To a lesser extent this also applies to the predictor-corrector method.
5. The ramp method is difficult to configure properly in a multi-degree-of-freedom problem since the steepness of the ramp design is a function of the spatial and time meshes and should be optimized while the solution is underway.

3.3 VISCOUS DAMPED SYSTEMS

In conjunction with the friction damped systems considered in previous sections, we now turn our attention to a comparable system damped with a velocity-proportional damper. The model is depicted in Figure 3-21

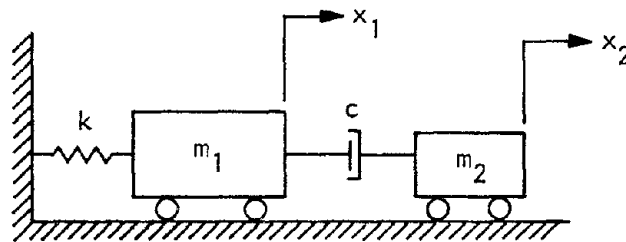


FIGURE 3-21. VISCOUS DAMPED SYSTEMS

The equations of motion are

$$\begin{aligned} m_1 \ddot{x}_1 + kx_1 + c (\dot{x}_1 - \dot{x}_2) &= 0 \\ m_2 \ddot{x}_2 + c (\dot{x}_2 - \dot{x}_1) &= 0 \end{aligned} \tag{3-39}$$

In the usual manner, we assume solutions of the form

$$\begin{aligned}x_1 &= C_1 e^{rt} \\x_2 &= C_2 e^{rt}\end{aligned}\tag{3-40}$$

which are substituted into Equation 3-39 to obtain the equations:

$$\begin{aligned}[m_1 r^2 + cr + k] C_1 - cr C_2 &= 0 \\-cr C_1 + [m_2 r^2 + cr] C_2 &= 0\end{aligned}\tag{3-41}$$

Setting the determinant of Equation 3-41 to zero, we obtain the frequency equation:

$$r^3 + \left(\frac{c}{m_1} + \frac{c}{m_2}\right) r^2 + \left(\frac{k}{m_1}\right) r + \frac{kc}{m_1 m_2} = 0\tag{3-42}$$

Equation 3-42 has three roots we denote by r_i . Therefore, the complete solutions of Equation 3-39 are

$$\begin{aligned}x_1 &= \sum_{i=1}^3 C_{1i} e^{r_i t} \\x_2 &= \sum_{i=1}^3 C_{2i} e^{r_i t}\end{aligned}\tag{3-43}$$

The coefficients C_{1i} are arbitrary and C_{2i} are obtained for Equation 3-41 for values of r_i . Thus,

$$C_{2i} = \frac{c}{m_2 r_i + c} C_{1i} = \lambda_i C_{1i}\tag{3-44}$$

The roots to Equation 3-42 either must be real and negative or complex with negative parts. The first case corresponds to an overdamped system and the second case indicates a damped oscillatory system.

In the first case, Equation 3-43 is solved by noting the following initial conditions:

$$\begin{aligned}x_1(0) &= x_0 \\ \dot{x}_1(0) &= \dot{x}_2(0) = 0\end{aligned}\tag{3-45}$$

From which we determine that

$$\begin{aligned}
 C_{11} &= \frac{x_0 r_2 r_3 (\lambda_3 - \lambda_2)}{\text{DET}} \\
 C_{12} &= \frac{x_0 r_1 r_3 (\lambda_1 - \lambda_3)}{\text{DET}} \\
 C_{13} &= \frac{x_0 r_1 r_2 (\lambda_2 - \lambda_1)}{\text{DET}}
 \end{aligned} \tag{3-46}$$

where

$$\text{DET} = r_2 r_3 (\lambda_3 - \lambda_2) + r_1 r_3 (\lambda_1 - \lambda_3) + r_1 r_2 (\lambda_2 - \lambda_1)$$

In the second case, oscillations will occur and r_1 and r_2 (say) are complex conjugates and r_3 is real and negative. Thus

$$\begin{aligned}
 r_1 &= -a + i\omega_d \\
 r_2 &= -a - i\omega_d
 \end{aligned} \tag{3-47}$$

which when substituted into Equation 3-43 becomes

$$\begin{aligned}
 x_1 &= C_{11} e^{(-a+i\omega_d)t} + C_{12} e^{(-a-i\omega_d)t} + C_{13} e^{r_3 t} \\
 &= e^{-at} \left[(C_{11} + C_{12}) \cos \omega_d t + (C_{11} - C_{12}) i \sin \omega_d t \right] \\
 &\quad + C_{13} e^{r_3 t}
 \end{aligned} \tag{3-48}$$

$$\begin{aligned}
 x_2 &= C_{21} e^{(-a+i\omega_d)t} + C_{22} e^{(-a-i\omega_d)t} + C_{23} e^{r_3 t} \\
 &= e^{-at} \left[(C_{21} + C_{22}) \cos \omega_d t + (C_{21} - C_{22}) i \sin \omega_d t \right] \\
 &\quad + C_{23} e^{r_3 t} \\
 &= e^{-at} \left[(\lambda_1 C_{11} + \lambda_2 C_{12}) \cos \omega_d t \right. \\
 &\quad \left. + (\lambda_1 C_{11} - \lambda_2 C_{12}) i \sin \omega_d t \right] \\
 &\quad + \lambda_3 C_{13} e^{r_3 t}
 \end{aligned}$$

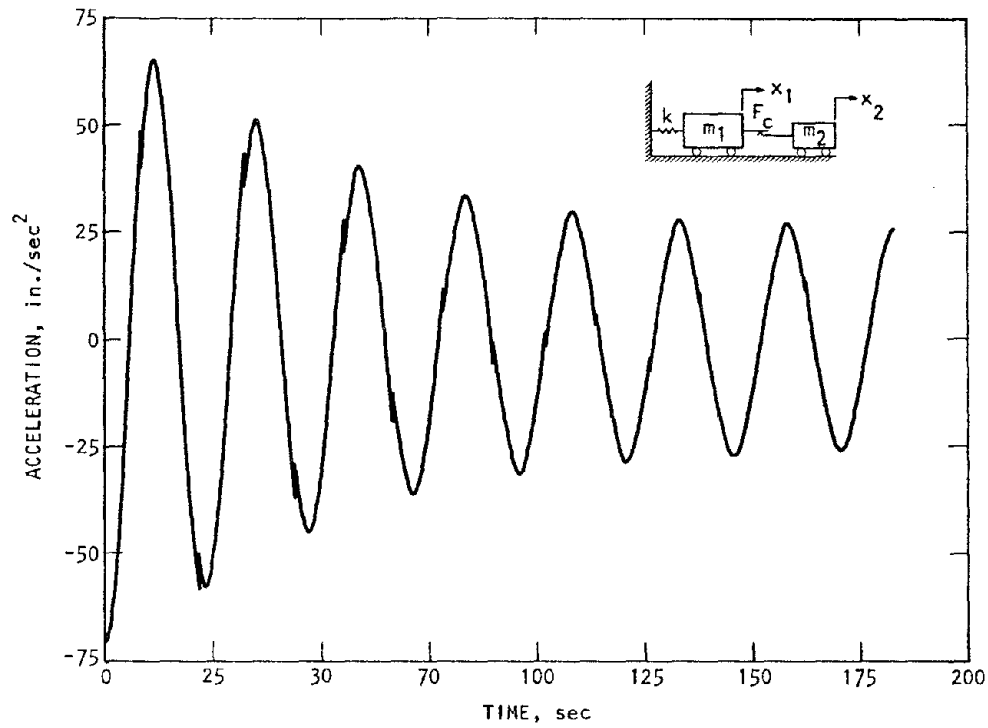
to which the initial conditions from Equation 3-45 apply. The coefficients of Equation 3-46 can be determined leading to the final solution of Equations 3-48.

3.3.1 VISCOUS VS. COULOMB FRICTION

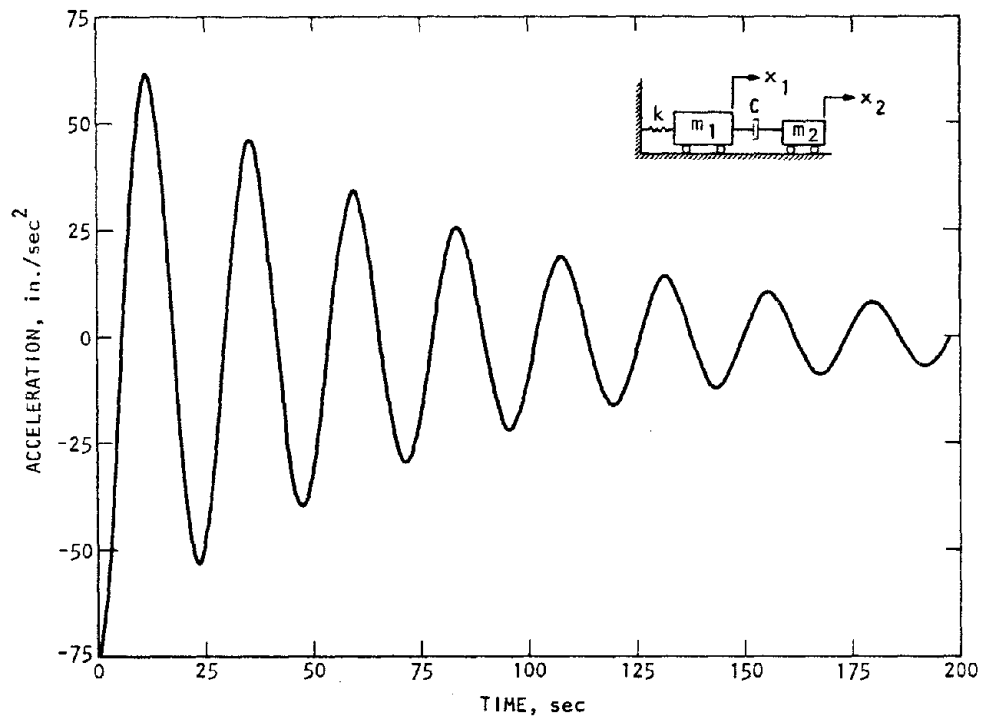
Now, as an example, we show the difference between the response of a friction damped system and a viscous damped system. We take for the friction model, the parameters shown in Table 3-2 except that the maximum friction has been reduced to $F_c = \pm 0.58$ lb. We use the same parameter values to solve the viscous problem except that we have replaced F_c with the viscous damping coefficient $c = 0.07$ lb sec/in. The results are presented in Figures 3-22 through 3-29.

We observe that the viscous damped system attenuates more rapidly than the friction damped system. This is especially true in later time when mass m_2 tends to slide less relative to mass m_1 in the friction model than for the viscous model. This is especially obvious in Figures 3-28 and 3-29 where relative motions are presented. The friction model consumes large amounts of energy in early time but this effect diminishes quickly with passing time. In other words, friction is effective in dissipating energy during periods of strong motion, but the motion tends to the response of a conservative system after the large early energy losses are consummated and the two masses tend to bond together. The data suggests that viscous dampers are more effective energy dissipators than equivalent friction dampers.

The reader's attention is drawn to an interesting observation. As expected, mass m_1 always oscillates about its null position for both systems as seen in Figure 3-24. Obviously, this occurs because the spring k forces mass m_1 to its static equilibrium position. If we examine Figure 3-27a, we note, not unexpectedly, that mass m_2 in the friction model permanently



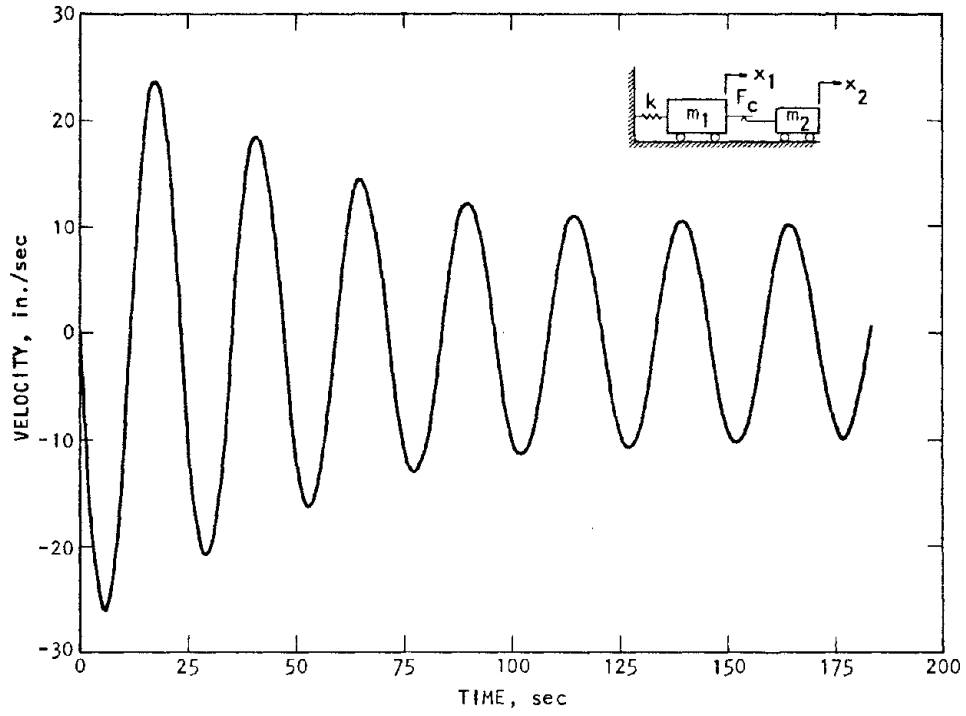
(a) Friction damping



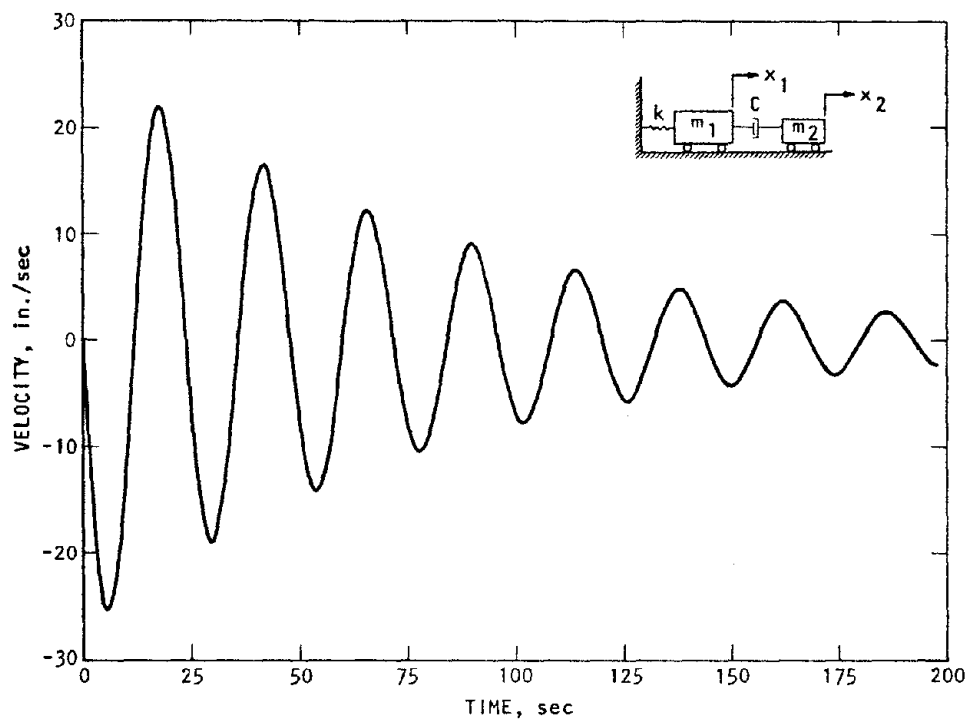
(b) Viscous damping

AA683

FIGURE 3-22. COMPARISON OF ACCELERATION RESPONSE TO MASS m_1



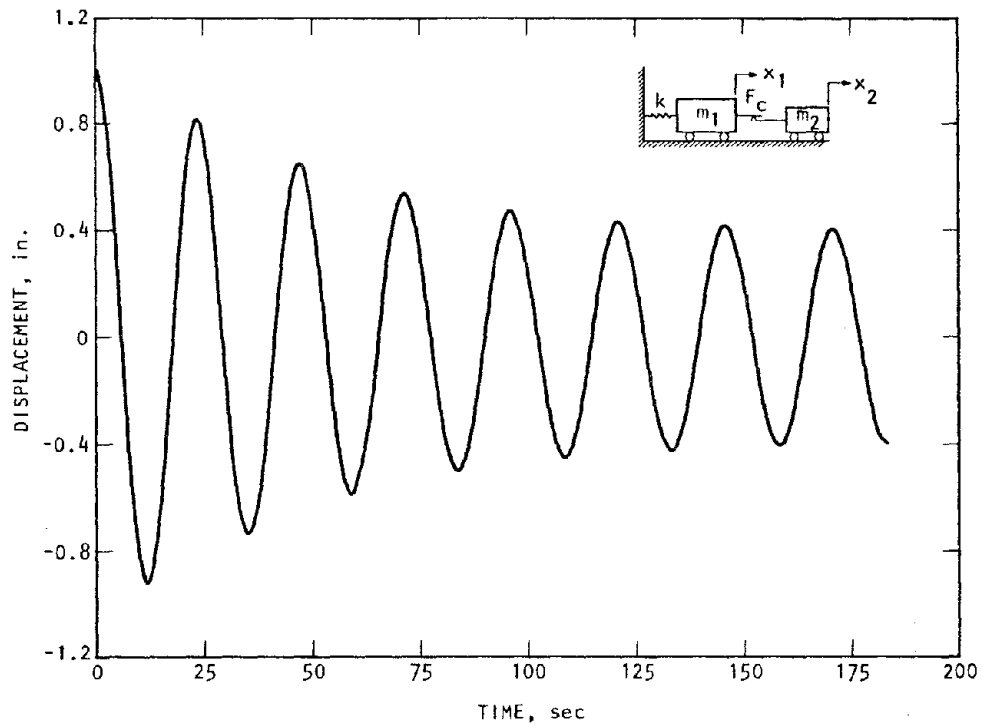
(a) Friction damping



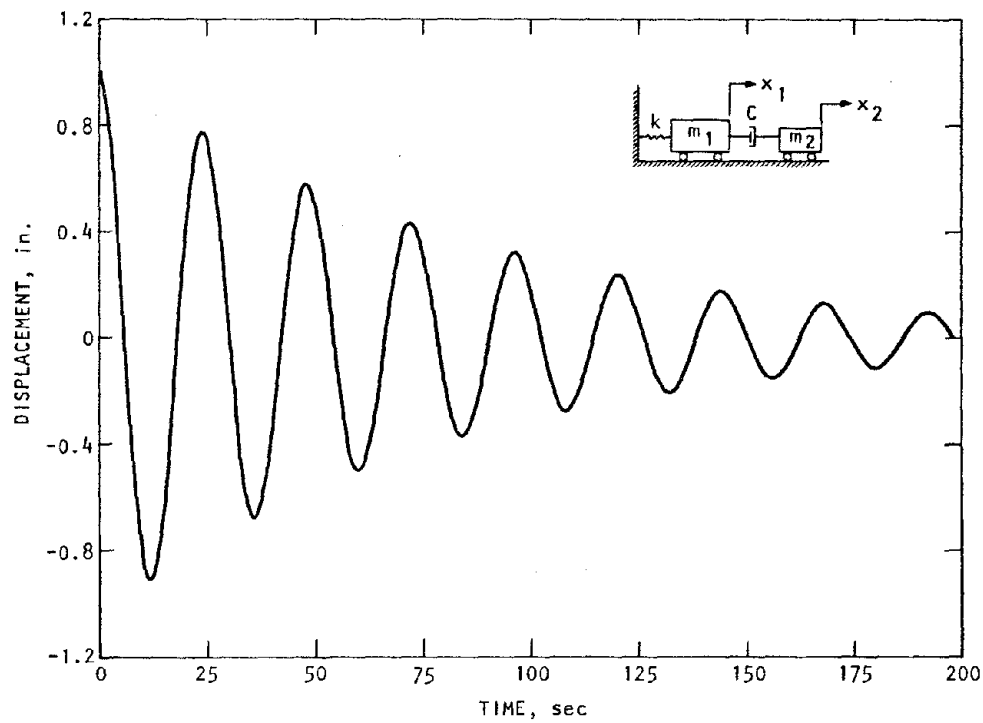
(b) Viscous damping

AA682

FIGURE 3-23. COMPARISON OF VELOCITY RESPONSE OF MASS m_1



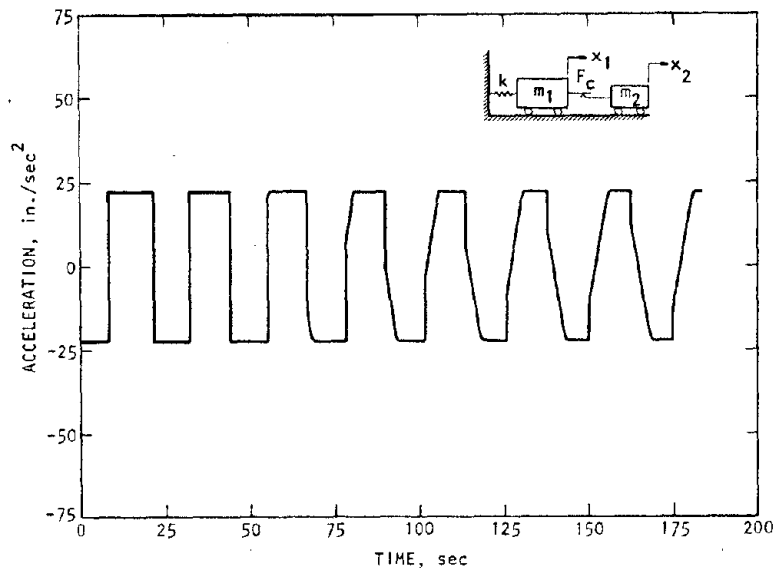
(a) Friction damping



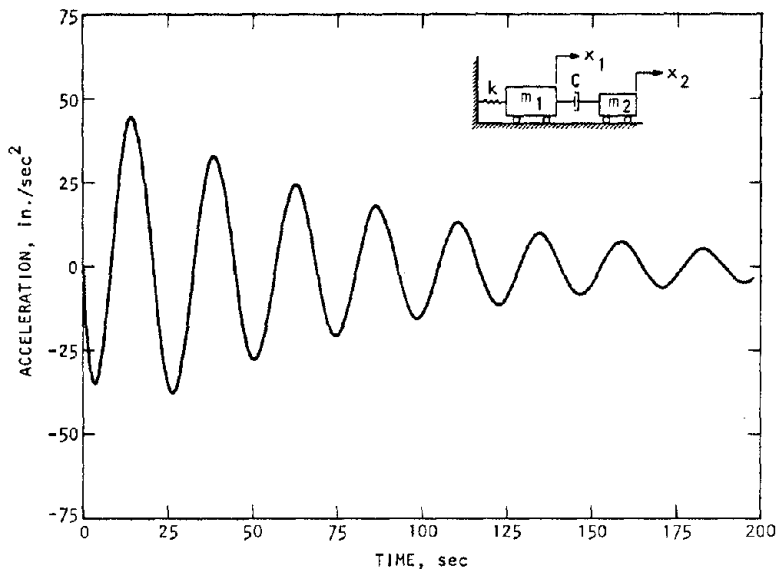
(b) Viscous damping

AA681

FIGURE 3-24. COMPARISON OF DISPLACEMENT RESPONSE OF MASS m_1

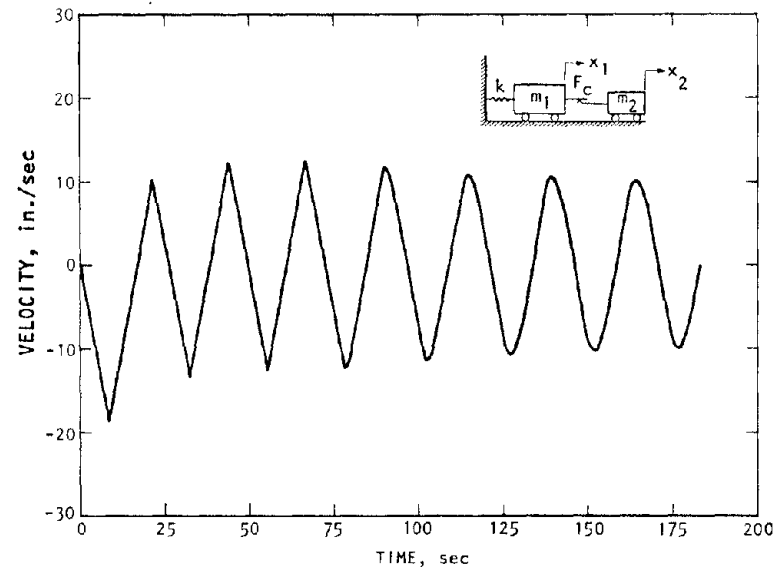


(a) Friction damping

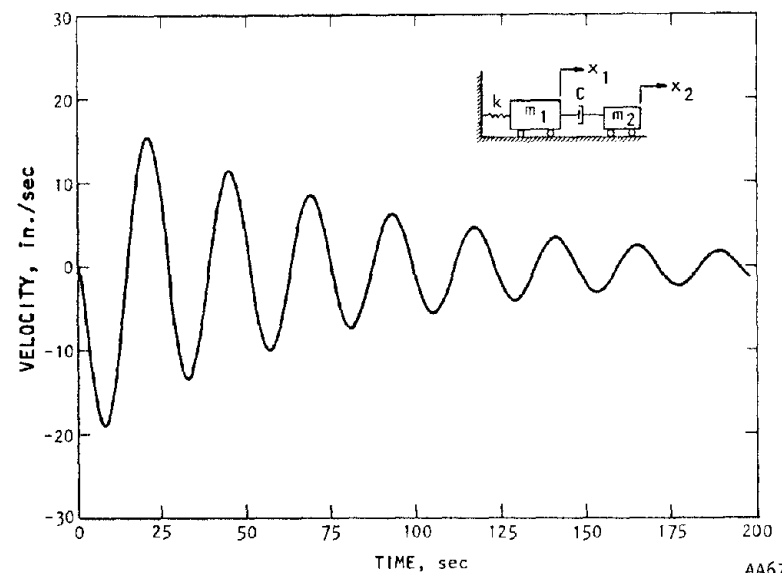


(b) Viscous damping

FIGURE 3-25. COMPARITIVE VELOCITY RESPONSE OF MASS m_2

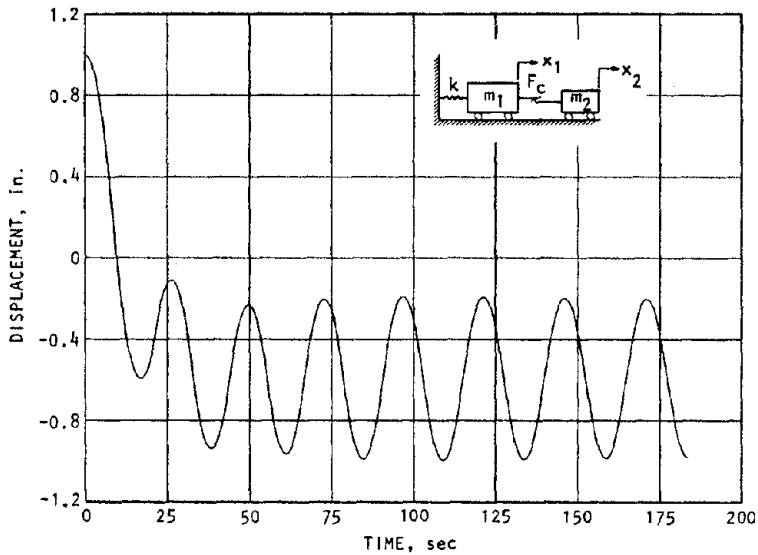


(a) Friction damping

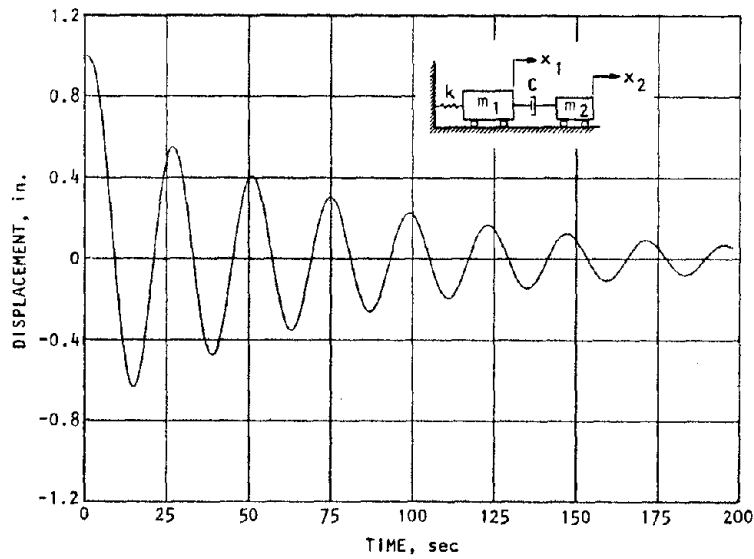


(b) Viscous damping

FIGURE 3-26. COMPARITIVE VELOCITY RESPONSE OF MASS m_2

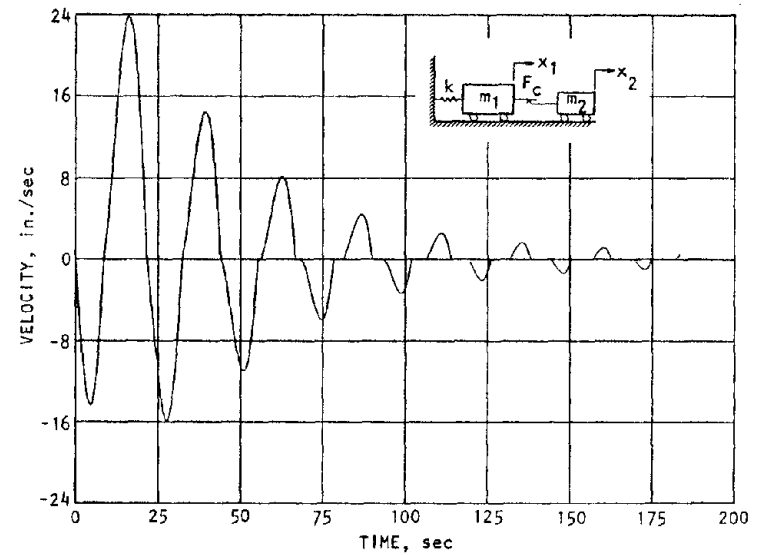


(a) Friction damping

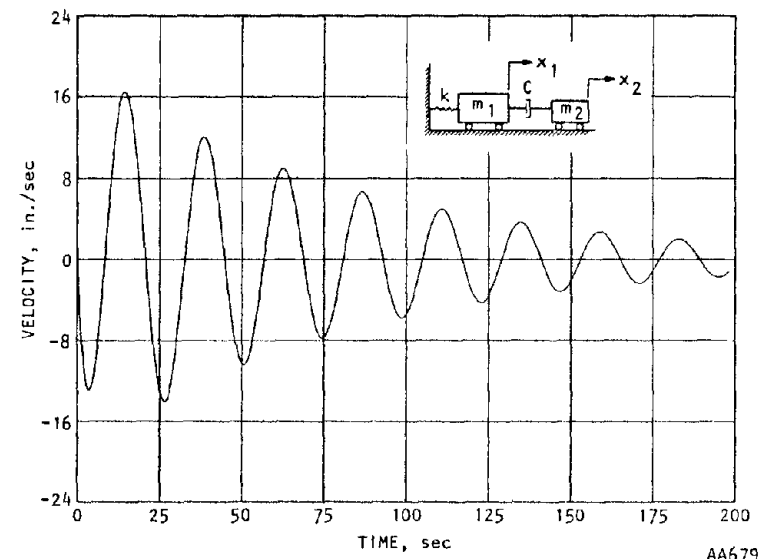


(b) Viscous damping

FIGURE 3-27. COMPARITIVE DISPLACEMENT RESPONSE OF MASS m_2

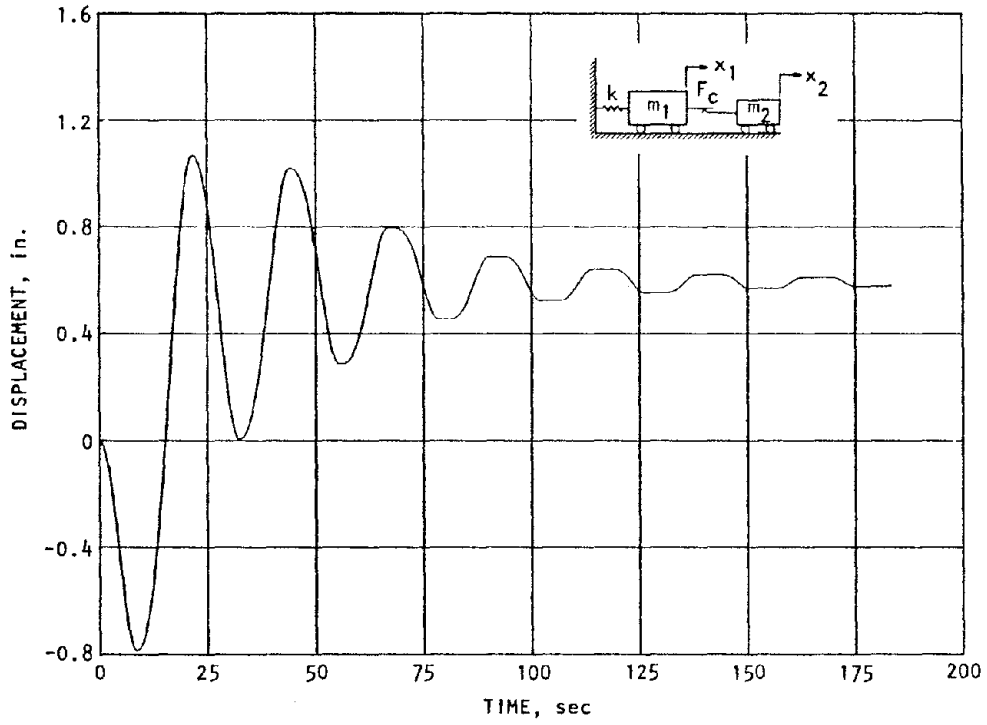


(a) Friction damping

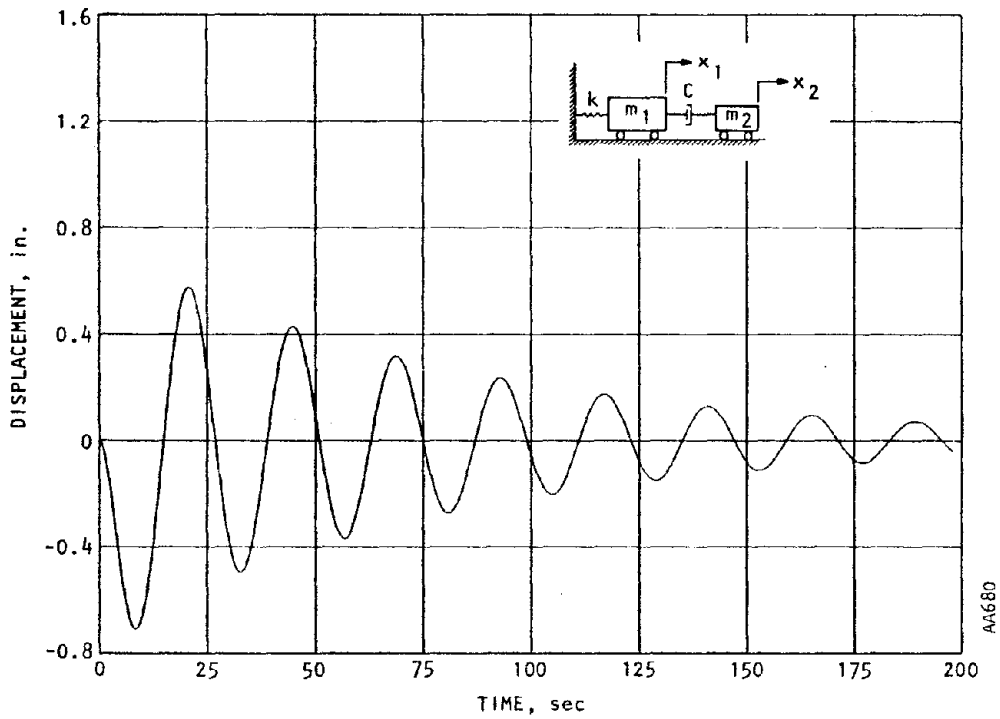


(b) Viscous damping

FIGURE 3-28. RELATIVE VELOCITY RESPONSE BETWEEN MASSES m_1 AND m_2



(a) Friction damping



(b) Viscous damping

FIGURE 3-29. RELATIVE DISPLACEMENT RESPONSE BEHAVIOR
MASSES m_1 AND m_2

displaces with respect to its original position and with respect to mass m_1 (see Fig. 3-29a). However, Figure 3-27b shows that mass m_2 also oscillates about the original null position of the system even though no spring exists between the two masses to establish a displacement related point of static equilibrium.

3.4 ENERGY CONSIDERATIONS WITH DAMPED SYSTEMS

If we examine the energy equations for the system depicted in Figures 3-3 and 3-21, we will obtain the following:

Potential Energy

$$PE = \frac{1}{2} k(x_1)^2 \quad (3-49)$$

Kinetic Energies

$$KE_1 = \frac{1}{2} m_1 (\dot{x}_1)^2 \quad (3-50)$$

$$KE_2 = \frac{1}{2} m_2 (\dot{x}_2)^2 \quad (3-51)$$

The total recoverable energy is given by

$$T = PE + KE_1 + KE_2 \quad (3-52)$$

For the problem set up in Table 3-2, the maximum total energy occurs at time zero for which

$$\begin{aligned} T_{\max} &= PE = \frac{1}{2} kx_1^2 = \frac{1}{2} kx_0^2 = \frac{1}{2} \times 9.816 \times 1 \\ &= 4.908 \text{ in. lb} \end{aligned} \quad (3-53)$$

$$KE_1 = KE_2 = 0$$

for any time $t > 0$, $T \leq T_{\max}$ because the friction damper or the viscous damper will consume energy. At any instant of time, t_0 , the energy lost, E_c , will be given by

$$E_c = T_{\max} - T \quad (3-54)$$

It is this energy loss that is of interest to us.

We now examine Figures 3-30 and 3-31 where characteristics of friction and viscous damped systems are examined respectively. As indices of comparison we consider the strain energy in the spring k and the kinetic energy of the mass m_2 . For purposes of comparison, we establish a "critical damping" for the viscous case given by

$$c_c = \sqrt{4 km_1} = 0.713 \frac{\text{lb-sec}}{\text{in.}} \quad (3-55)$$

Moreover, if we vary F_c for the solution of the friction problem, we find that mass m_1 can be made to bond to mass m_2 for the initial conditions given when the friction force satisfies

$$|F_{c_{\max}}| \geq 1.636 \text{ lb.} \quad (3-56)$$

Clearly, the minimum kinetic energy of mass m_2 is zero and it occurs when

$$c = F_c = 0 \quad (3-57)$$

The maximum kinetic energy of mass m_2 occurs when the masses are bonded, or, because the mass proportions are in the ratio of 1 to 5, the maximum kinetic energy of m_2 will be one-sixth of T_{\max} . That is,

$$KE_{\max} = 0.818 \text{ in.-lb} \quad (3-58)$$

The maximum potential energies of both systems occur at zero time. This computation has already been made in Equation 3-53. The minimum values are most easily determined graphically as we have shown in Figures 3-30 and 3-31. Thus, in Figure 3-30, the friction force, which minimizes strain energy, is seen to be about $F_c \cong 0.60$ lb; by actual investigation, it was found to be $F_c = 0.58$ lb. By the same token, the minimum viscous damping coefficient was found to be $c = 0.07$ lb-sec/in. We also see that these values tend to produce a median response in both the kinetic energy of mass m_2 and the relative displacement between masses m_1 and m_2 .

$KE_{max} = 0.818 \text{ in. lb}$
 $PE_{max} = 4.908 \text{ in. lb}$
 $\Delta x_{max} = 2.000 \text{ in.}$
 $F_{c_{max}} = 1.636 \text{ lb}$

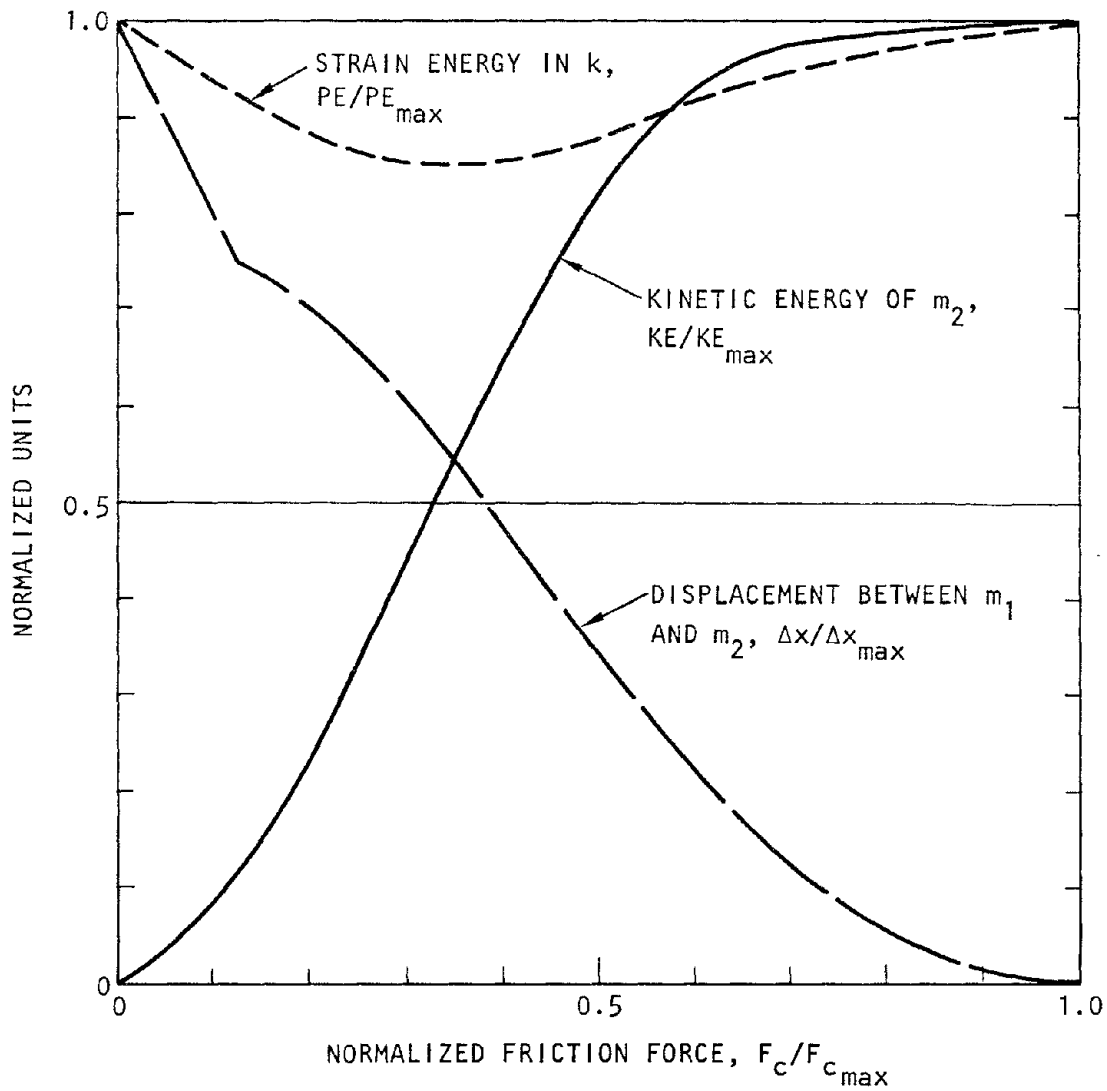


FIGURE 3-30. EFFECT OF FRICTION DAMPING ON RESPONSE OF A 2-DOF SYSTEM

$KE_{max} = 0.818 \text{ in. lb}$
 $PE_{max} = 4.908 \text{ in. lb}$
 $\Delta x_{max} = 2.000 \text{ in.}$
 $c_c = 0.713 \text{ lb-sec/in.}$

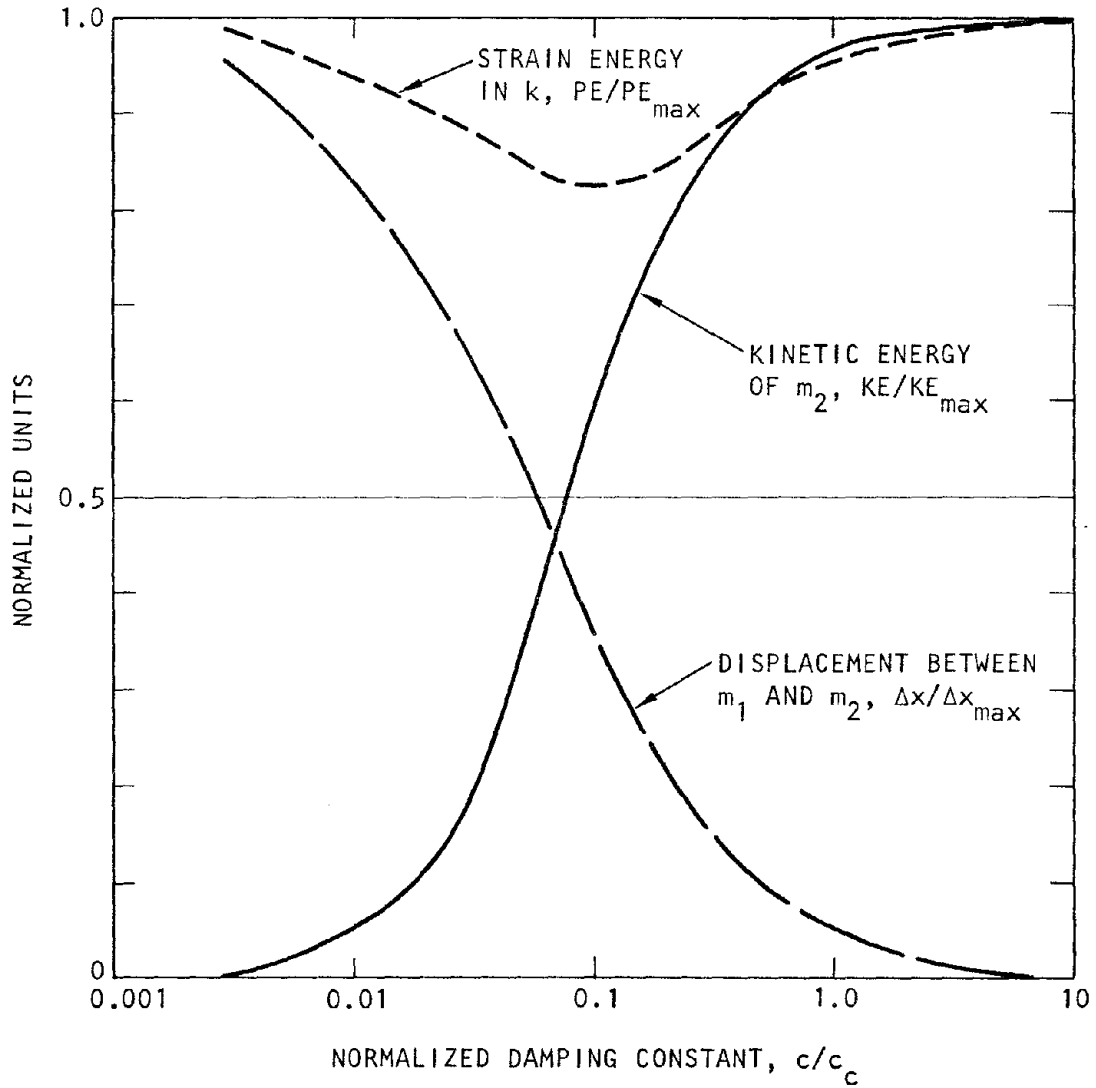


FIGURE 3-31. EFFECT OF VISCOUS DAMPING ON RESPONSE OF A 2-DOF SYSTEM

Figure 3-32 shows the total energy from Equation 3-52 presented as a function of time for both the viscous and friction damper systems. As expected, the viscous damper is most effective in dissipation energy especially at later times because the dashpot is active at all times due to at least some relative velocity between the two masses. On the other hand, the friction damper is effective in early time when the two masses slide relative to each other but less effective at late times when the two masses spend a greater portion of the time bonded together.

3.5 TWO DOF REPRESENTATIONS OF A SUSPENDED FLOOR STRUCTURE

A simple 2 DOF representation of a suspended floor structure can be modeled as shown in Figure 3-33. Here, the stiffness k is the bending resistance of the core structure, m_1 is the mass of the core, m_2 is the mass of the floor system, and F_c is the value of the friction damper between the floors and core. The specific values selected are shown in Table 3-3.

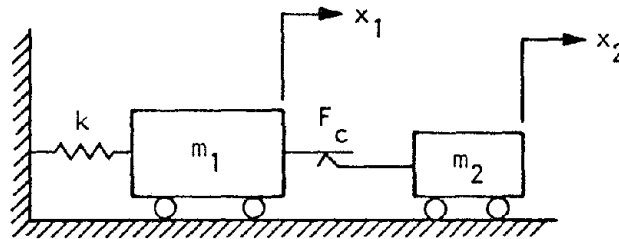


FIGURE 3-33. 2 DOF REPRESENTATIVE OF SUSPENDED FLOOR STRUCTURE

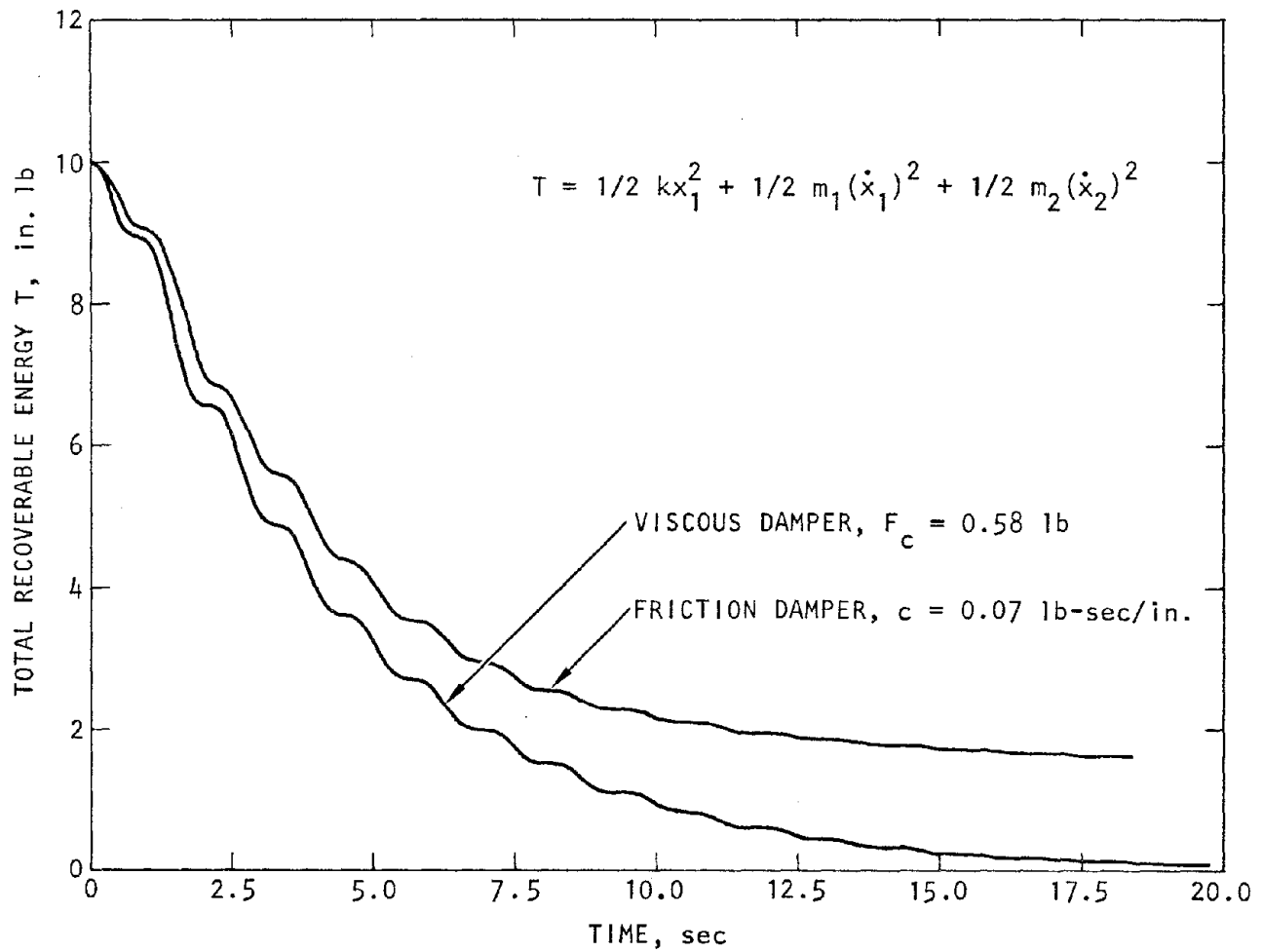


FIGURE 3-32. EFFECT OF VISCOUS AND FRICTION DAMPING ON DISSIPATING ENERGY

TABLE 3-3. PARAMETERS OF MODEL

$m_1 = 2.05 \times 10^6 \text{ lb}$
$m_2 = 3.3 \times 10^6 \text{ lb}$
$f_n = 8.2 \text{ Hz}$
F_c variable

The fundamental natural frequency f_n of the core system was assumed to be 8.2 Hz. From this we obtained the spring stiffness k .

$$f_n = \frac{1}{2\pi} \sqrt{\frac{k}{m_1}} = 8.2 \text{ Hz} \quad (3-59)$$

Thus $k \cong 1.4 \times 10^7 \text{ lb/in.}$

We also give masses m_1 and m_2 the initial condition

$$\begin{aligned} x_0 &= x_1(0) = x_2(0) = 4 \text{ in.} \\ \dot{x}_0 &= \dot{x}_1(0) = \dot{x}_2(0) = 0 \end{aligned} \quad (3-60)$$

so that we can estimate the maximum potential energy in spring k_1 , the maximum kinetic energy in mass m_2 , and the maximum relative displacement between the two masses. Thus

$$PE_{\max} = \frac{1}{2} kx_0 = 1.12 \times 10^8 \text{ in. lb,} \quad F_c = 0 \quad (3-61)$$

Also, the maximum kinetic energy of the entire system is given by

$$V_{\max} = \frac{1}{2} (m_1 + m_2)(\dot{x}_1)^2 = \frac{1}{2} (m_1 + m_2)(\dot{x}_2)^2 = PE_{\max} \quad (3-62)$$

for

$$F_c \geq 3.45 \times 10^7 \text{ lb} \quad (3-63)$$

which is the lock-up friction force. Thus,

$$\dot{x}_1 = \dot{x}_2 \cong 127.194 \text{ in./sec for } F_c \geq 3.45 \times 10^7 \text{ lb} \quad (3-64)$$

from which we calculate the maximum kinetic energy of mass m_2 to be

$$KE_{\max} = \frac{1}{2} m_2 (\dot{x}_2)^2 \cong 6.91 \times 10^7 \text{ in. lb for } F_c \geq 3.45 \times 10^7 \text{ lb} \quad (3-65)$$

Also

$$\Delta x_{\max} = 8 \text{ in. for } F_c = 0 \quad (3-66)$$

Based on the above data, we can now investigate the response of the 2 DOF model by varying the value of the friction force F_c . The results are shown in Figure 3-34. We can compare these results to those shown in Figure 3-30. Qualitatively, the responses are similar. However, the results in Figure 3-30 were based on the mass ratio $m_1/m_2 = 5$ whereas the results in Figure 3-34 were based on the mass ratio $m_1/m_2 \cong 0.62$. Yet the conclusions remain the same: the most effective selection of the damper is $F_c/F_{c_{\max}} \cong 0.35$.

For our simple model, it is easy to estimate $F_{c_{\max}}$. If the masses are bonded together, the natural frequency of the system is given by

$$\omega_n = \sqrt{\frac{k}{m_1 + m_2}} \cong 31.798 \text{ rad/sec} \quad (3-67)$$

Thus, the friction force required to drive mass m_2 at this frequency will be

$$F = 4\omega_n^2 m_2 \cong 3.45 \times 10^7 \text{ lb} \quad (3-68)$$

Any friction force less than this will not be sufficient to produce an acceleration of

$$4 \omega_n^2 \cong 4044 \text{ in./sec}^2 \quad (3-69)$$

which is the peak acceleration of the bonded masses subject to the initial conditions of $x_0 = 4 \text{ in.}$ and $\dot{x}_0 = 0$.

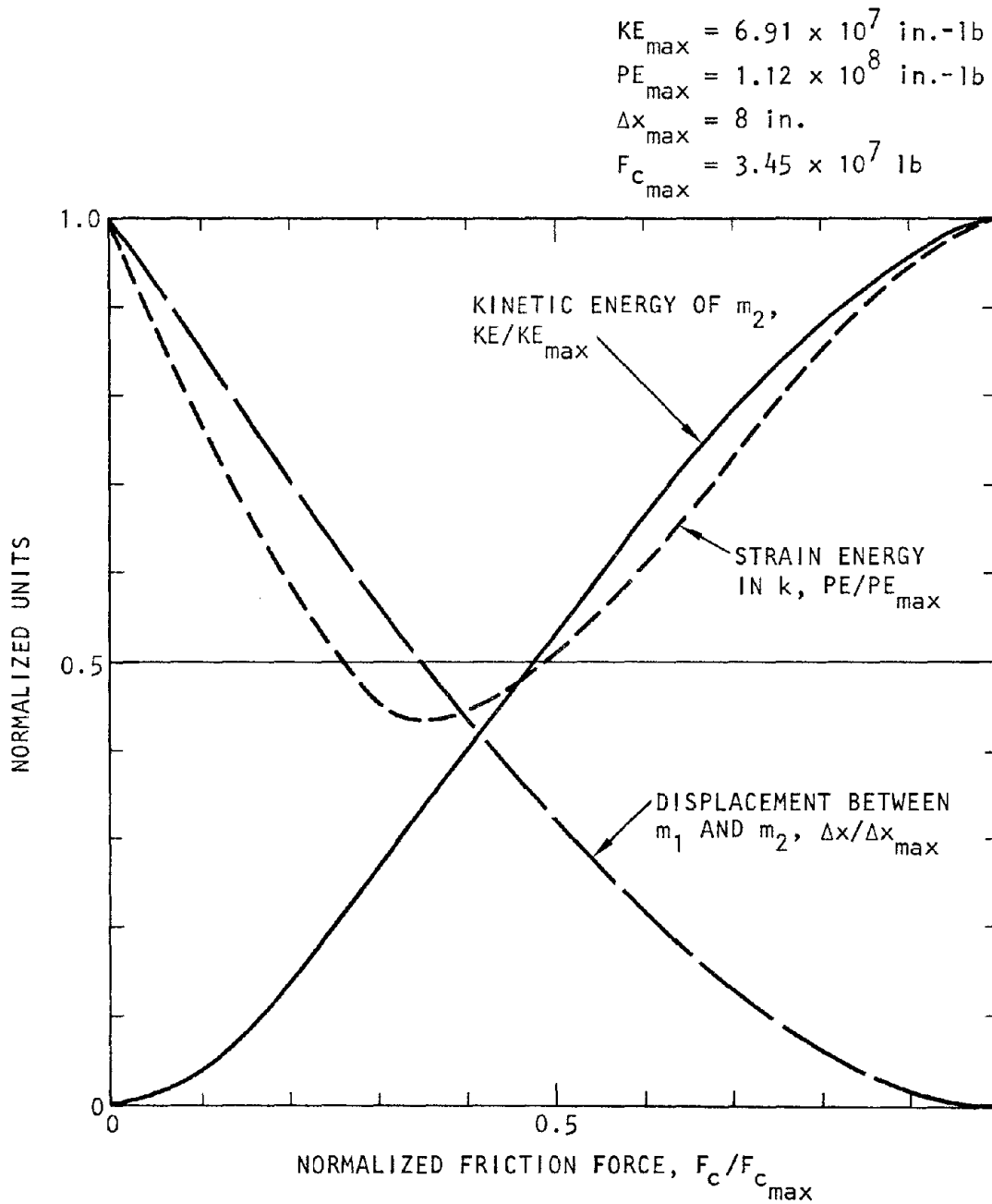


FIGURE 3-34. EFFECT OF FRICTION DAMPING ON A 2-DOF REPRESENTATION OF A SUSPENDED FLOOR STRUCTURE

3.5.1 CONCLUSIONS

Our data seems to suggest the following conclusions with regard to suspended floor structures:

1. Given a choice of damper types, one might be tempted to select a viscous type over a Coulomb type because the former removes more energy from a system in a given period of time (as we have seen in Fig. 3-32). However, if we examine Figures 3-30 and 3-31 we find that either damper is about equally effective in reducing strain energy. From that point of view, either is suitable to decrease the potential for structural distress.
2. Not unexpectantly, the less strongly the slaved mass is tied to the parent mass via the damper, the less severe will be the kinetic energy of the dependent mass. For our structures, this means that the environment for occupancy is likely to be less if the floors are more nearly freely hung. On the other hand, greater sway space is required for this condition.
3. Fortuitously it would seem, as we examine Figures 3-30, 3-31, and 3-34, we conclude that there is an optimum damping that minimizes strain energy and also provides a good compromise between minimizing sway space and minimizing motion. This may well be the design point of departure for damped suspended floor structures.

EXPERIMENTAL STUDIES

1. INTRODUCTION

The experimental phase of this study was performed by means of a simple SDOF system consisting of a rigid mass connected by a linear spring to a supporting base. The mass was provided with a long flexible strip of metal allowed to slide back and forth between two rollers that exert on the strip an adjustable normal force and accompanying friction force.

The mass consisted of a rigid box with dimensions of 6 inches long, 4 inches wide, and 1 inch thick, weighing approximately 16 ounces. The mass can slide freely by means of two rows of ball bearings that attach it to its rigid base. The inherent amount of damping in the sliding mechanism is very small, amounting to about 1.5 percent of critical. In the experimental studies dealing with pseudo-dynamic effects, the base of the mass was held fixed, while in the forced vibration tests the mass was mounted on an oscillating base.

The types of experimental tests conducted consisted of the following:

1.1 Linear Free Vibration Tests (Group F)

The apparatus used to conduct this test is sketched in Figure 1, the details of the test procedure are given in Table 1, and sample results corresponding to the different channels of data measured are given in Appendix

FRICITION

1.

All figure numbers for this group of tests start with the letter F.

1.2 Static Friction Tests (Group S)

The apparatus used to conduct this test is sketched in Figure 2, the details of the test procedure are given in Table 2, and sample results corresponding to the different channels of data measured are given in Appendix 2.

All figure numbers for this group of tests start with the letter S.

1.3 Linear Forced Vibration Tests (Group D)

The apparatus used to conduct this test is sketched in Figure 3, the details of the test procedure are given in Table 3, and sample results corresponding to the different channels of data measured are given in Appendix 3.

All figure numbers for this group of tests start with the letter D.

1.4 Nonlinear Forced Vibration Tests (Group N)

FRICTION

The apparatus used to conduct this test is sketched in Figure 4, the details of the test procedure are given in Table 4, and sample results corresponding to the different channels of data measured are given in Appendix 4.

All figure numbers for this group of tests start with the letter N.

2. INSTRUMENTATION

A complete list of instruments and transducers used in this study is given in Table 5. The main items used were several strain gages, a piezoelectric accelerometer, a force-balance servo accelerometer, a linear variable differential transformer (LVDT), and an optical displacement follower.

In the pseudo-dynamic tests, the exciting force was supplied by an adjustable "static" load consisting of a fluid-filled container, while in the forced vibration tests the driving force was generated by a small electrodynamic shaker.

Figures 5 and 6 show photographs of the overall test apparatus configured for a nonlinear forced vibration test. Details of the oscillating mass with its resilient components and its friction plate, resting on the moving base are shown in the photograph of Figure 7. A detailed front view of the clamping mechanism and the friction plate is shown in the photograph of Figure 8.

3. TEST PROCEDURE

FRICTION

For each one of the four groups of tests discussed above, the corresponding procedure listed in Tables 1 - 4 was followed in order to generate the needed data. The analog measurements were recorded on a 14-channel analog tape recorder in the FM mode at a speed of 30 ips. In the subsequent analog-to-digital (A/D) conversion phase of the experimental study, the analog tape was re-played at a rate of 7.5 ips, thus yielding a 4-fold factor of improved time resolution for analyzing the transient phenomena which was digitized at a very high sampling rate. As a further step in data processing, all the digitized data channels were low-pass filtered in a uniform manner to reduce the extent of noise pollution while maintaining the fidelity of phase information.

4. PRELIMINARY DATA ANALYSIS

As is evident from the sample set of data corresponding to only one (out of many) representative test from each of the four generic groups discussed above, there is a considerable amount of worthwhile information contained within these experimental records which require a significant level of effort to extract the maximum amount of useful information about the behavior of friction dampers.

Data processing of the sample results reveals the following observations:

(1) With reference to Figure F03.1 in Appendix 1 corresponding to the free vibration tests, the natural frequency of the SDOF system is about $f = 5.5$ Hz, and the logarithmic decrement is about 0.11, thus the ratio of critical damping is about 0.015.

FRICTION

(2) With reference to Figure S05.3 and S05.4 in Appendix 2 corresponding to the pseudo-dynamic friction tests, it is clear that the physical processes involved in the sliding mechanism are quite complicated as evidenced by the intricate detail of the observed high frequency acceleration signal. The high frequency components still imbedded in the record after digital noise filtering has been performed indicate that the microscopic details of the sliding surfaces have a major bearing on the nature and extent of the developed friction forces.

(3) Analysis of the response of the dynamic system under swept-sine excitation indicates that the simple model without the friction plate is behaving as a truly linear SDOF system should. Hence, in analyzing the system response when the friction plate is present, all the nonlinear features of the response are completely attributable to the Coulomb friction forces, as opposed to the other elements that constitute the system.

(4) With reference to Figures NN.1, NN.2, and NN.3 corresponding to the motion of SDOF system with the friction plate installed under harmonic excitation, it is seen that even when the excitation is steady-state, the corresponding response is not steady over a time period that is long compared to the system fundamental period. This is due to the nature of the slip-stick behavior of the sliding surfaces. Details of this phenomenon are shown in, e.g., Figure N01.13.2 of Appendix 4. Note that the qualitative behavior of the 2DOF analytical model shown in Figure 10 of Section 2 is similar to the observed response of the nonlinear physical model under discussion. However, due to the lack of sufficient information concerning the details of the "switching" process, the theoretical calculations could not duplicate the details of the observed response.

FRICTION

(5) With reference to the state variable plots included in Appendix 5, it is clear that the linear version of the system has a slight amount of viscous damping (see e.g., Figures F03XY.2 and D33XY.2). On the other hand, the phase plots of the nonlinear system (see, e.g., Figures S05XY.2 and N01XY.5) indicate the presence of a much more complicated damping mechanism.

It is expected that after further sophisticated data processing, a more accurate nonlinear mathematical model will be developed to more accurately represent the details of the Coulomb friction switching process. This model will subsequently be used to perform more accurate computational studies to design optimum friction dampers installed in structures with suspended floors.

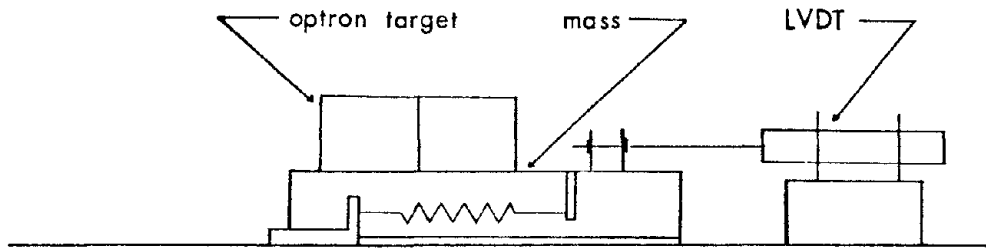


Fig.1 STATIC FREE VIBRATION

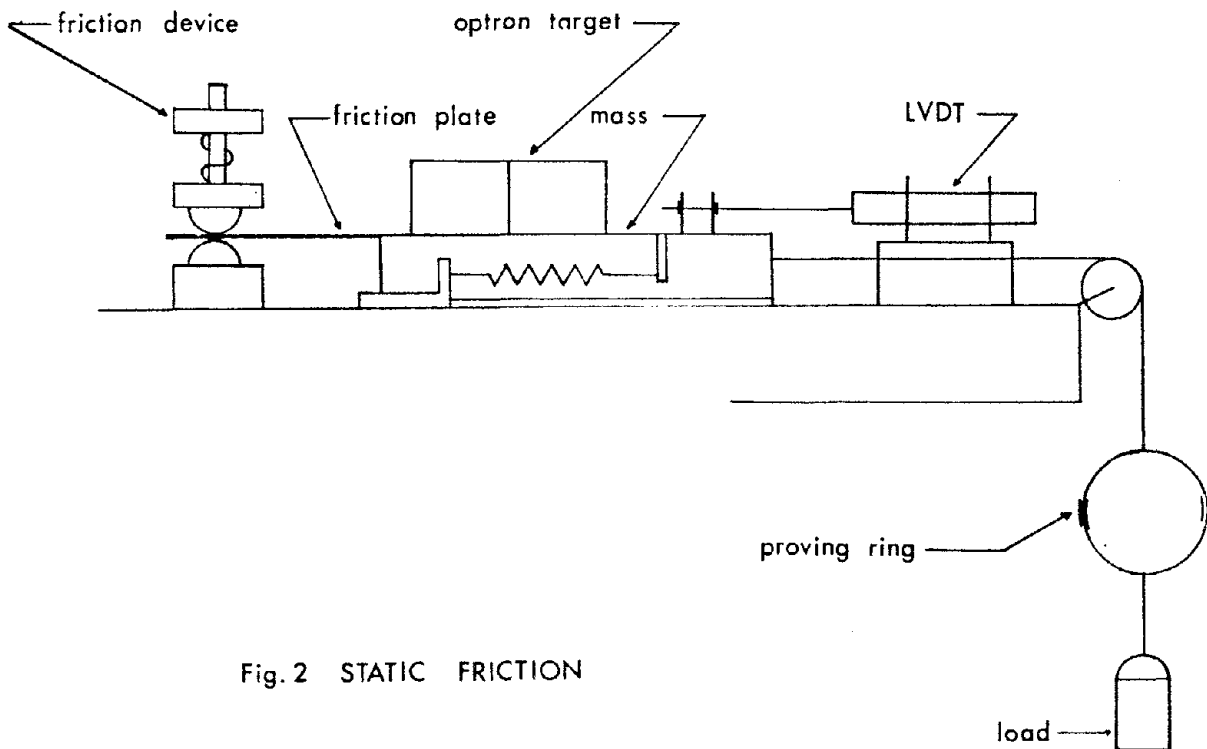


Fig.2 STATIC FRICTION

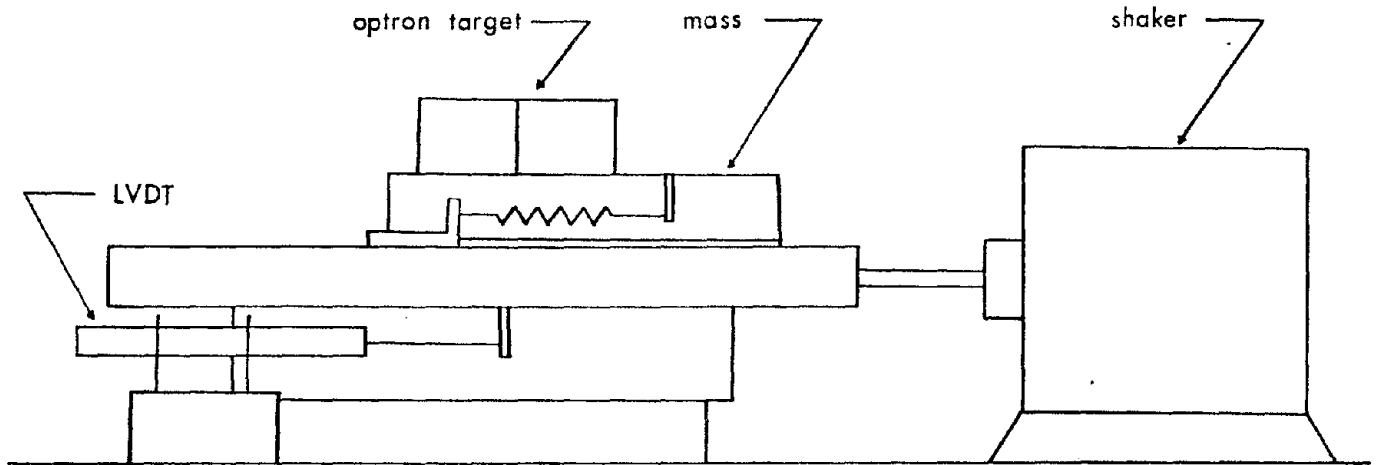


Fig. 3 FORCED VIBRATION

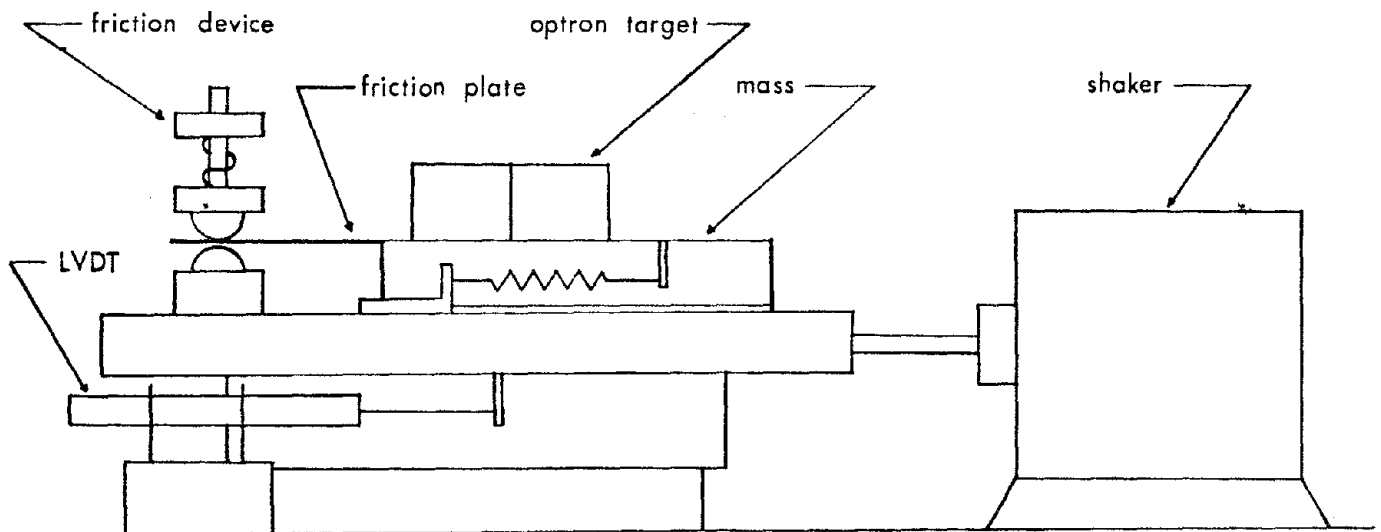


Fig. 4 DYNAMIC NONLINEAR

TABLE 1

Test Summary

Static: Free Vibration 15-July-1984

Set up: Fig.1

Tape Record	Equipment	
Ch 1	Timing	
Ch 2	Optron	Measure displacement of mass
Ch 3	LVDT	
Ch 4	Accel	Measure accel. of mass

Procedure

1. Displace the mass (from equilibrium position, $x(t) = 0$) by an arbitrary amount $x(0) = x_0$
2. "Release" the mass to allow the system to vibrate freely.
3. Record the system response
4. Repeat for various initial displacements.

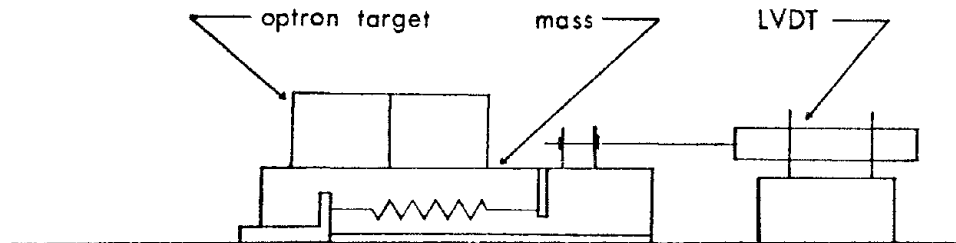


Fig. 1 STATIC FREE VIBRATION

FRICTION

TABLE 2

Test summary

Static: Friction 15-July-1984

Set up: Fig. 2

Tape Record	Equipment	
Ch 1	Timing	
Ch 2	Optron	measure displ. of mass
Ch 3	LVDT	
Ch 4	Accel.	measure accel of mass
Ch 5	proving ring	measure applied load
Ch 6	Friction Device	measure applied normal force

Procedure

1. Apply a normal force (F_n) to the friction plate
 - a. adjust the control screw on the friction device
2. Apply a continuous load to the system
 - a. Fill the burette with water
 - b. Open the stopcock to allow the water to fill the container
3. Stop application of continuous load when static slip is observed.
4. Repeat for various normal forces.

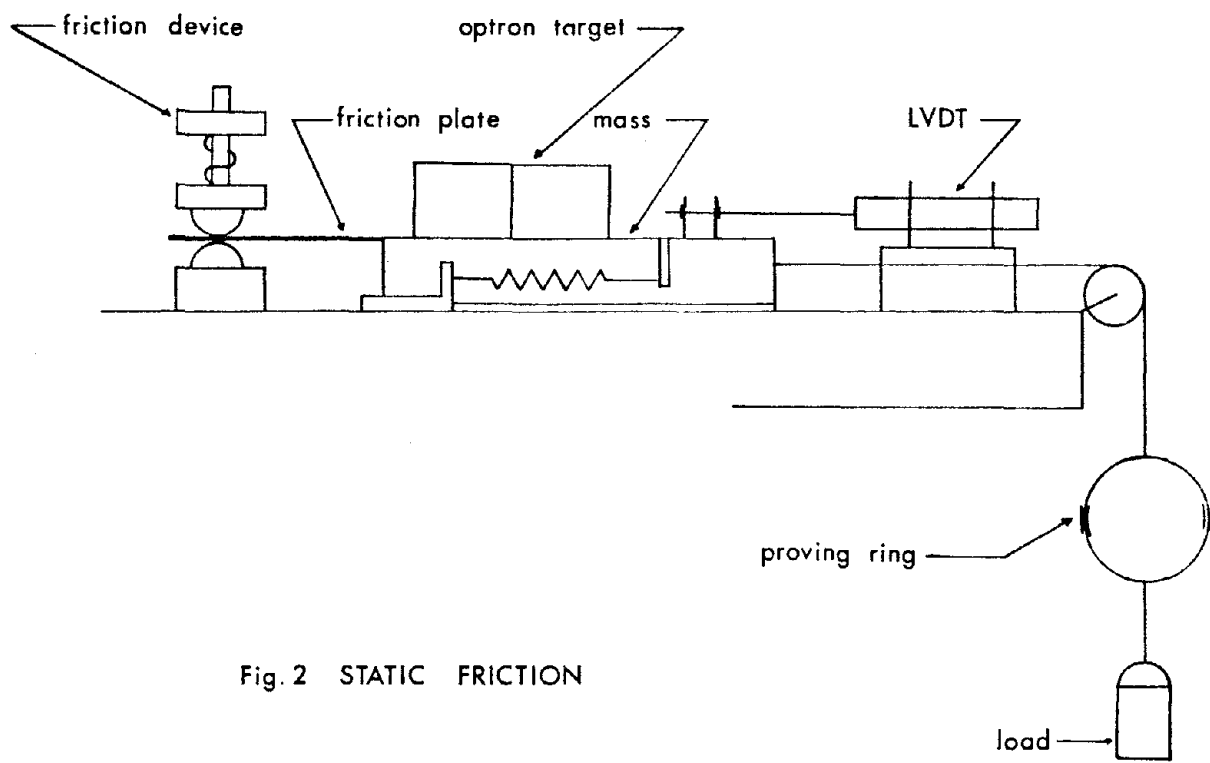


Fig. 2 STATIC FRICTION

TABLE 3

Test Summary

Dynamic: Linear 22-July-1984

Set up : Fig.3

Tape Record Equipment

Ch 1	LVDT	measure displacement of base
Ch 2	accel (3988)	measure accel. of base
Ch 3	Optron	measure displ. of mass
Ch 4	accel (3477)	measure accel. of mass
Ch 5	Function generator	
Ch 6	timing	

Procedure (Harmonic)

I. Steady State

1. Apply a harmonic excitation to the system
 - a. Select an arbitrary frequency (2-6Hz) and amplitude to be used as an excitation, with the function generator.
 - b. Turn on the shaker to excite the system.
2. Allow the system to reach steady state(record the response)

II. Dynamic Free Vibration

1. Allow the system to vibrate freely
 - a. After the system has reached steady state, turn off the shaker and allow the response to damp out.

III. Repeat for various amplitudes and frequencies.

Procedure (Swept Sine)

FRICTION

I. Steady State

1. Apply a swept sine excitation to the system.
 - a. Select an arbitrary frequency range to be swept, sweeping rate and amplitude, to be used as excitation, with the function generator.
 - b. Turn on the shaker.
2. Allow the system to reach steady state (record response)

II. Dynamic Free Vibration

1. Allow the system to vibrate freely
 - a. After the system has reached steady state, turn off the shaker and allow the response to damp out.

III. Repeat for various frequency ranges, sweeping rates and amplitude.

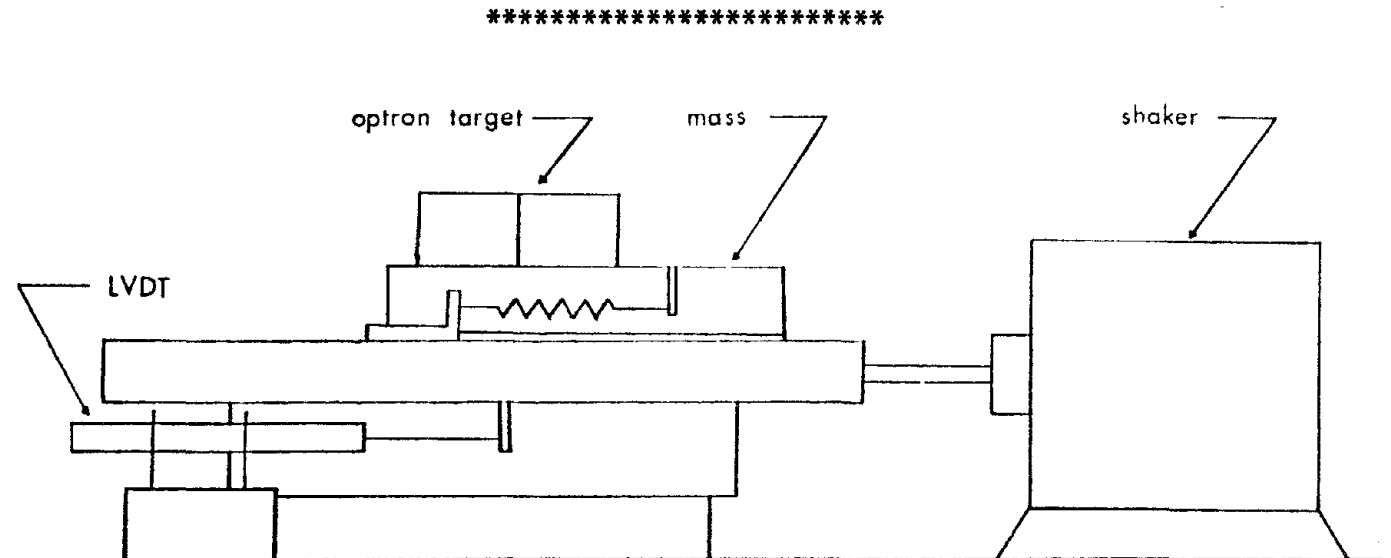


Fig. 3 FORCED VIBRATION

TABLE 4

Test Summary

Dynamic: Nonlinear 25-July-1984

Set up : Fig. 4

Tape Record	Equipment	
Ch 1	LVDT	measure base displ.
Ch 2	accel (3988)	measure base accel.
Ch 3	optron	measure mass displ.
Ch 4	accel (3477)	measure mass accel.
Ch 5	Friction device	measure applied normal force
Ch 6	Function generator	
Ch 7	Timing	

Procedure (Harmonic)

1. Apply a normal force (F_n) to the friction plate
 - a. Adjust the control screw on the friction device
2. Apply a harmonic excitation to the system
 - a. Select an arbitrary frequency (4-6Hz), to be used as an excitation, with the function generator.
 - b. Turn on the shaker to excite the system
3. Vary the amplitude of excitation until dynamic slip occurs.
4. Repeat for various normal forces and frequencies.

Procedure (Swept Sine)

1. Apply a normal force (F_n) to the friction plate
 - a. Adjust the control screw on the friction device

FRICITION

2. Apply a swept sine excitation to the system
 - a. Select an arbitrary frequency range to be swept, sweeping rate and amplitude, to be used as excitation, with the function generator.
 - b. Turn on the shaker
3. Record the response of the system
4. Repeat for various normal forces, frequency ranges, sweeping rates and amplitudes.

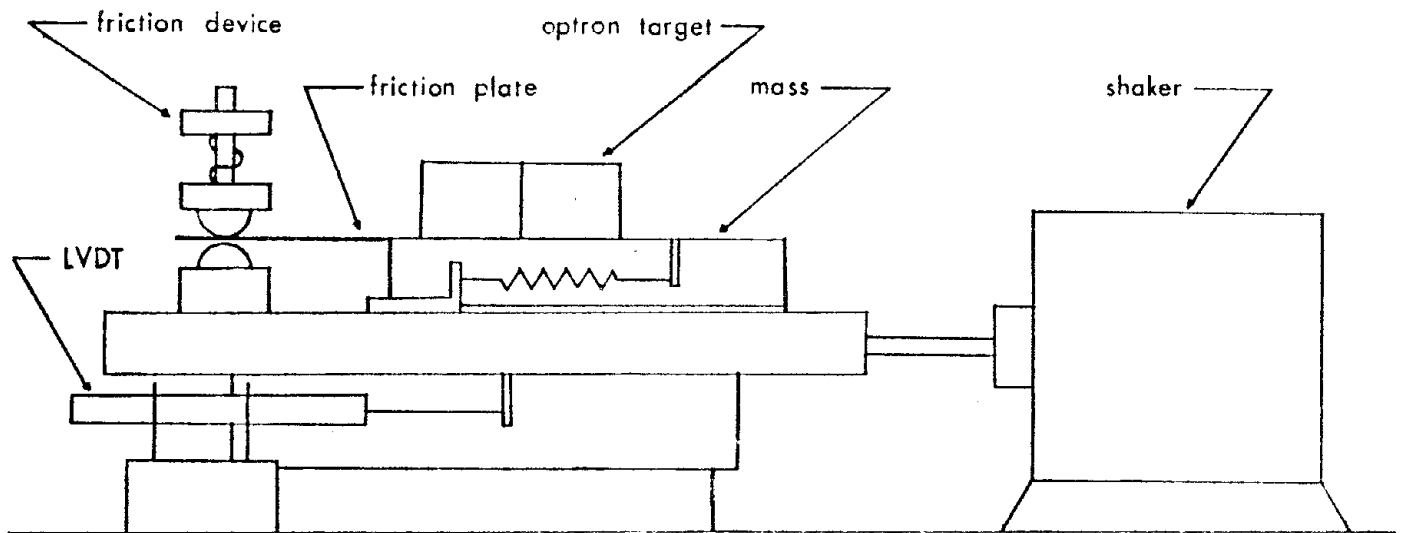


Fig. 4 DYNAMIC NONLINEAR

FRICITION

TABLE 5

Equipment List

Free vibration :::::::::::::::::::::::::::::::::::::::

LVDT Schaevitz 1000HR SN 4512

Optron 806-1-30.5 189

Accelerometer Kistler 303T102 3477

Static Friction :::::::::::::::::::::::::::::::::::::::

LVDT Schaevitz

Optron

Accelerometer Kistler

Friction Device

Proving ring

Dynamic Linear :::::::::::::::::::::::::::::::::::::::

LVDT Kavlico 1113 L602

Optron

Accelerometer Kistler (mass)

Accelerometer Kistler 303T102 3988(base)

Shaker

Dynamic Nonlinear :::::::::::::::::::::::::::::::::::::::

LVDT

Optron

Accelerometer

Accelerometer

Shaker

Friction Device

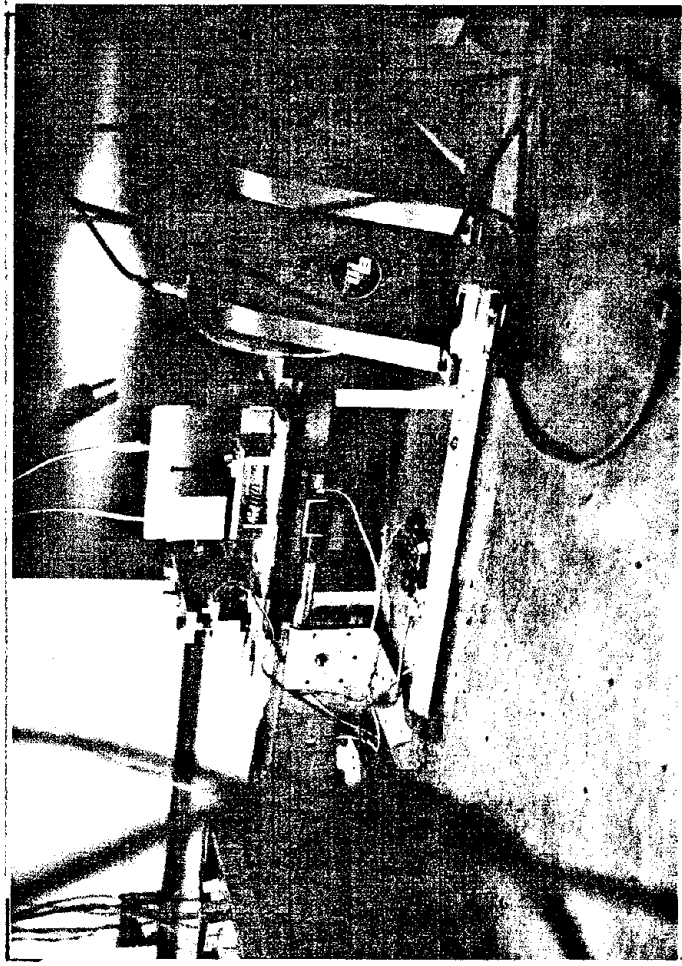


Fig. 5

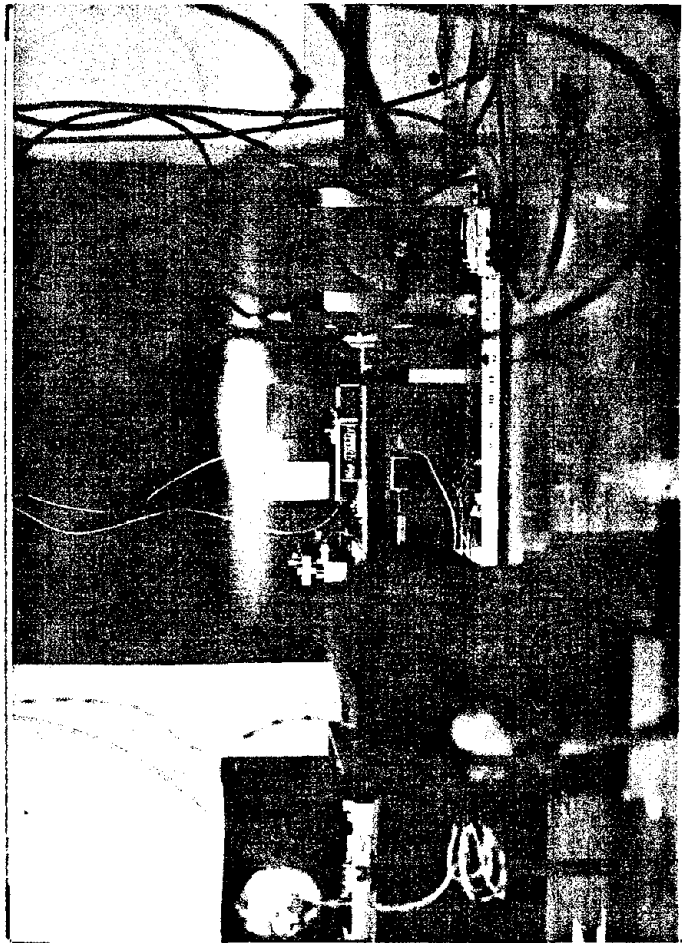


Fig. 6

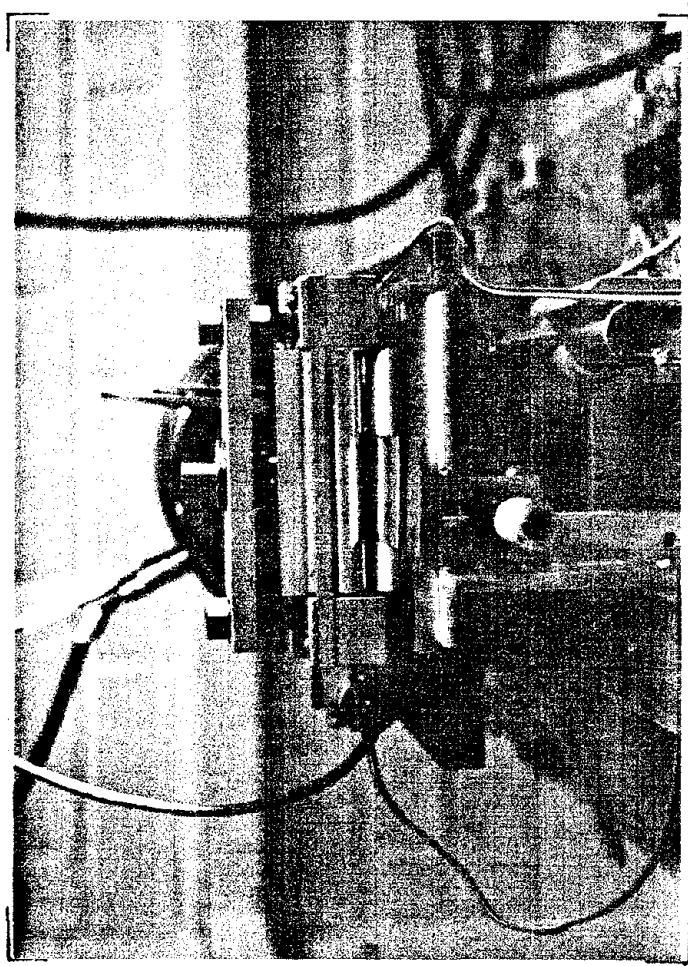


Fig. 7

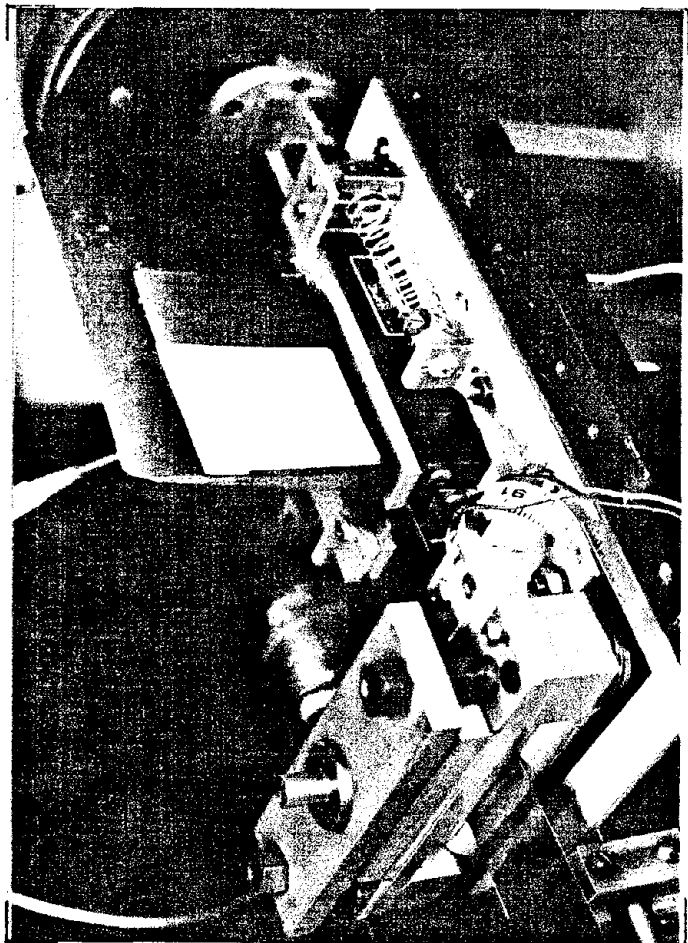


Fig. 8

Reproduced from
best available copy.

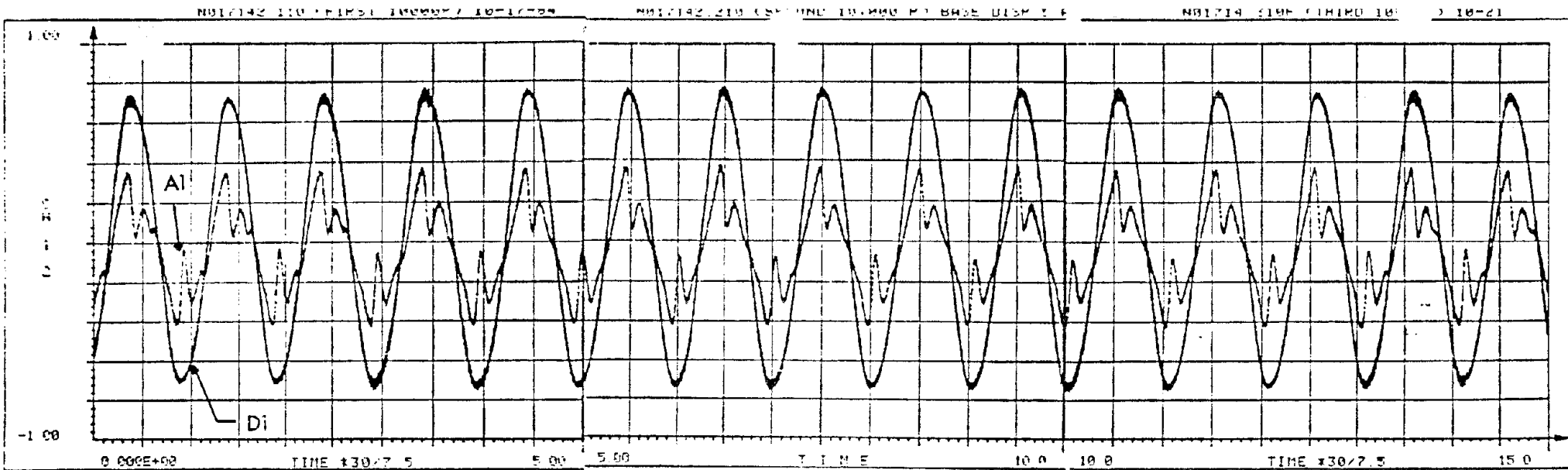


Fig. NN1 Excitation Time History

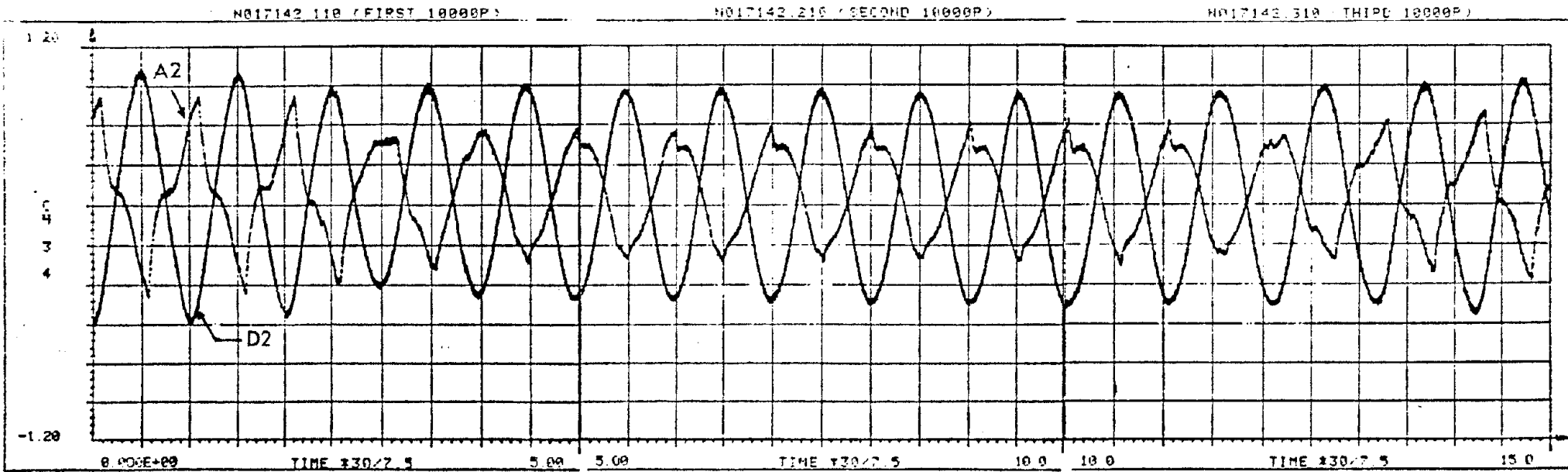


Fig. NN2 Response Time History; of Nonlinear System

418

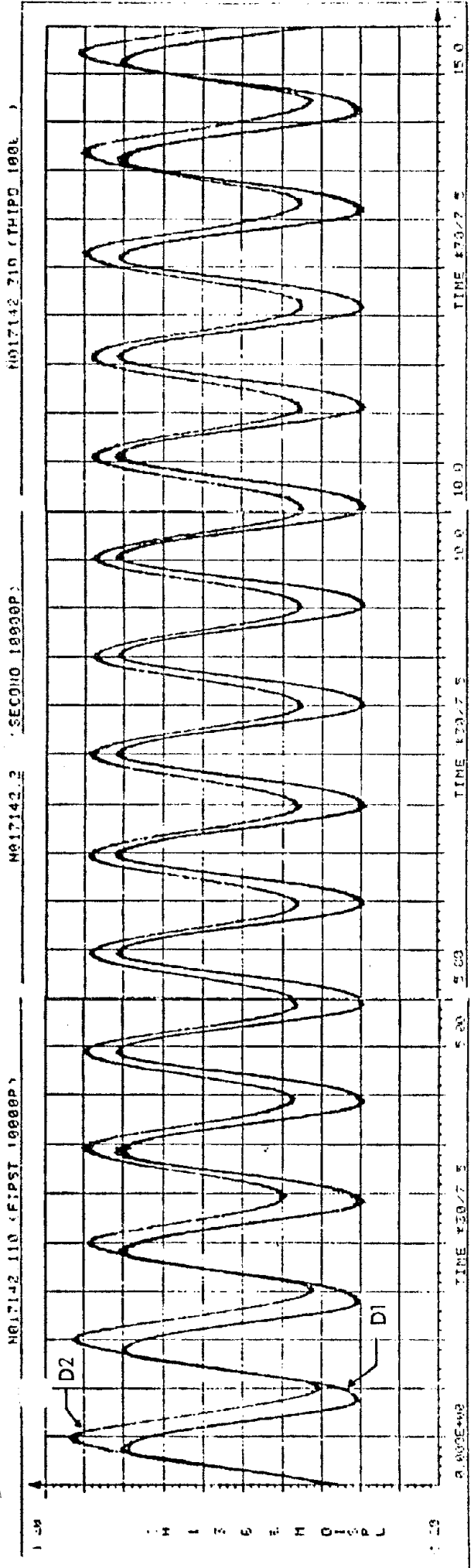


Fig. NN3 Response Time History; of Nonlinear System

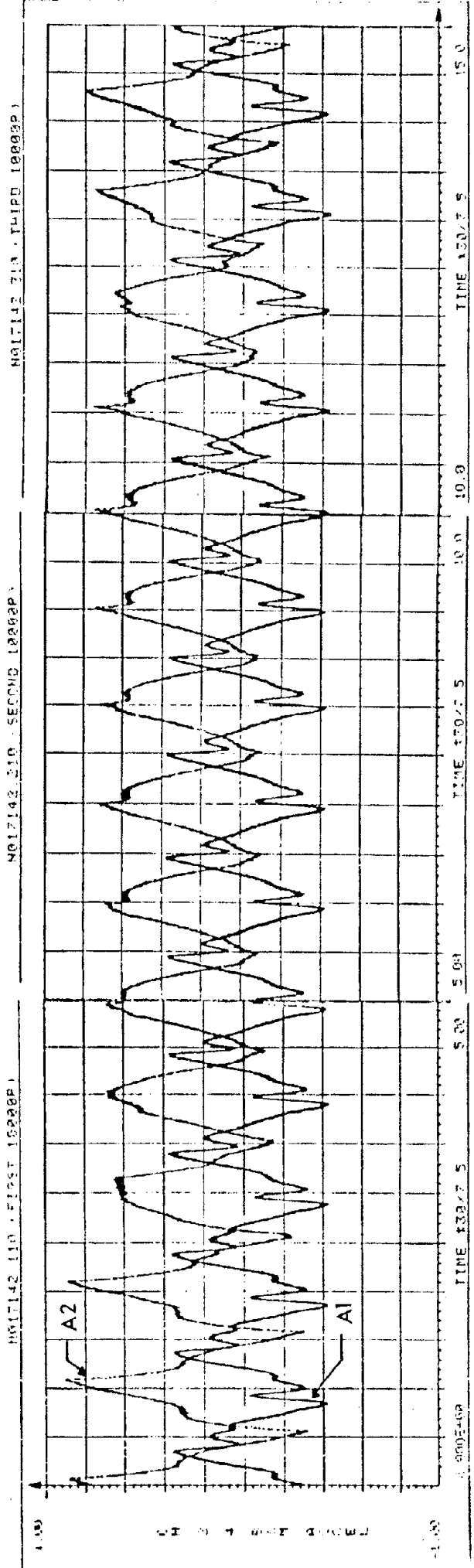


Fig. NN4 Response Time History; of Nonlinear System

SECTION 5

REFERENCES

- ABK, A Joint Venture (1981) Methodology for Mitigation of Seismic Hazards in Existing Unreinforced Masonry Buildings: Seismic Input, ABK-TR-02. El Segundo, CA: Agbabian Assoc., Dec.
- Babicki, B.B. (1971) "Cables Support Office Building," Civil Eng., ASCE, Oct., pp 64-67.
- Barkan, D.D. (1962) Dynamics of Bases and Foundations. New York: McGraw-Hill.
- Bethlehem Steel Corp. (BSC) (1972) Building Case History No. 25: Holiday Inn, Huntington, West Virginia, Folder 2893. Dec.
- Biggs, E.C. et al. (1965) "Bacardi Building - An Unusual Structure for an Unusual Building," Jnl Amer. Conc. Inst., Dec, pp 1521-1532.
- Engineering News-Record (ENR). (1965a) "Germans Hang Floors on Prestressed Members," May, pp 50-51.
- . (1965b) "Hung Framing for Office Tower Gains Ground in

FRICTION

U.S., Europe," Oct., pp 38-45.

----. (1971) "Plastic-Clad Tower Erected from Top Down," Mar,
pp 20-22.

Goodno, B.J. (1975) Dynamic Analysis of Suspended-Floor Highrise
Buildings Using Super-Elements, Report No. 13. Stanford,
CA: John A. Blume Earthq. Eng. Ctr.

Irvine, W. (1980). Personal communication between Mr. W. Irvine
of Irvine Architects, Campbell, CA and Dr. S.J. Hung,
Agbabian Assoc., El Segundo, CA.

Jhaveri, D. (1980). Personal communication between Dr. D. Jhaveri
of John A. Blume, Inc., San Francisco, CA and Dr. S.J. Hung
Agbabian Assoc., El Segundo, CA.

Kozak, J. (1972) "Structural Systems of Tall Buildings with Core
Structures," Proc. Intl. Conf. on Planning and Des. of
Tall Buildings, Aug.

Larios, C.J. et al. (1969) "Study of the Behavior of a Hanging
Building Under the Effect of an Earthquake." Proc.
4th World Conf. on Earthquake Engineering, Santiago,
Chili, Jan.

Nikolaenko, N.A. and Burgman I.N. (1976) "Earthquake Resistance
of Structures with Suspended Masses," Intl. Symp. on

FRICION

Earthq. Struct. Eng., Aug.

Western Construction (WC). (1970) "Berkely Building Features
Floors Suspended from the Top," Mar, pp 39-42.

----. (1971) "Twelve Story Building has Floors Hung in 5-Day
Cycle," Mar, pp 44-45.

Free Vibration (Group F)

F3031P5.5SC F03C1.0AF 1500 SR 3CH 5Sec
 F03C2.0AF
 F03C3.0AF

Group F (Static Free Vibration)

Notation: D1-displacement of mass (Optron)

 D2-displacement of mass (LVDT)

 A1-Acceleration of mass

 (F)-Filtered data

 for figures containing 2 plots

Key: ___ First curve

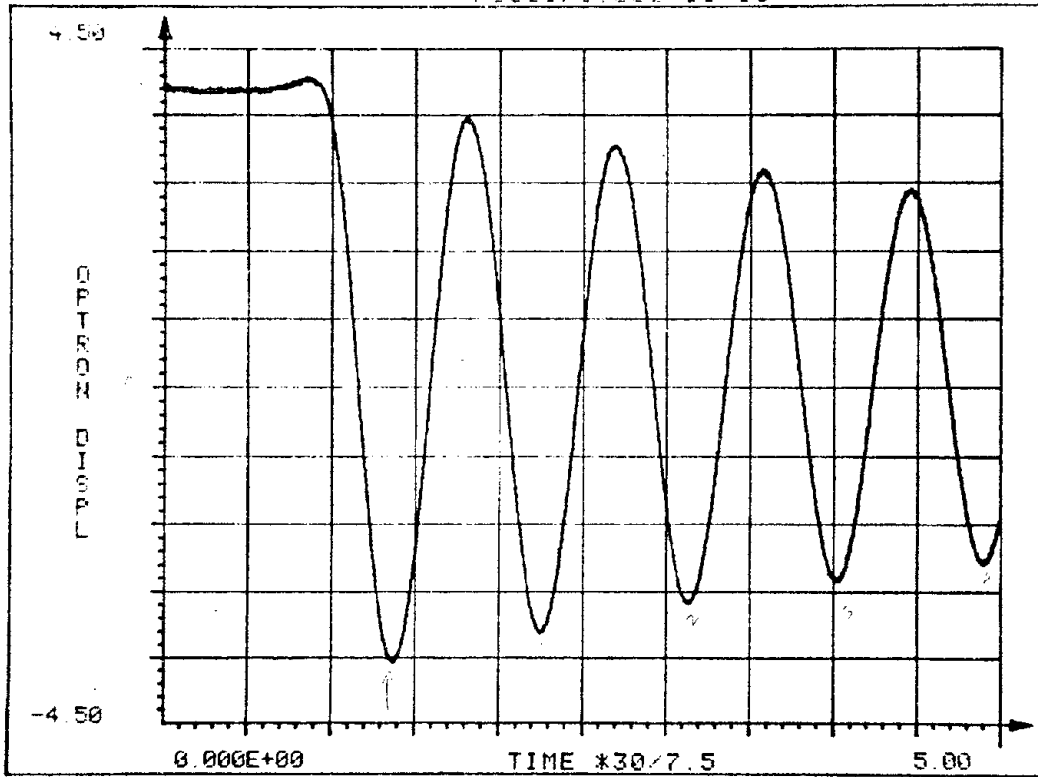
 ---- Second curve

Fig No	Caption
F03.1	D1
F03.2	D2
F03.3	A1
F03.4	1.D1
	2.D2
F03.5	1.D1
	2.A1
F03.6	1.D2
	2.A1

FRICITION

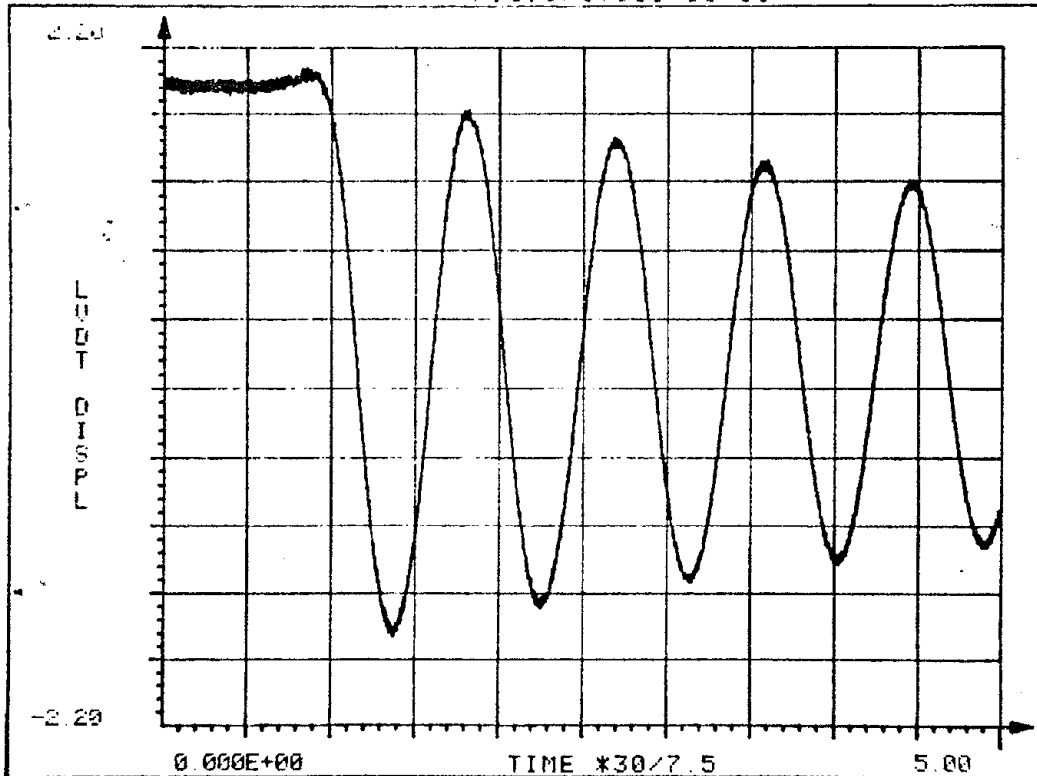
F03.7	D1
F03.8	D1(F)
F03.9	1.D1
	2.D1(F)
F03.10	D2
F03.11	D2(F)
F03.12	1.D2
	2.D2(F)
F03.13	A1
F03.14	A1(F)
F03.15	1.A1
	2.A1(F)

F3031P5.5SC 11-13



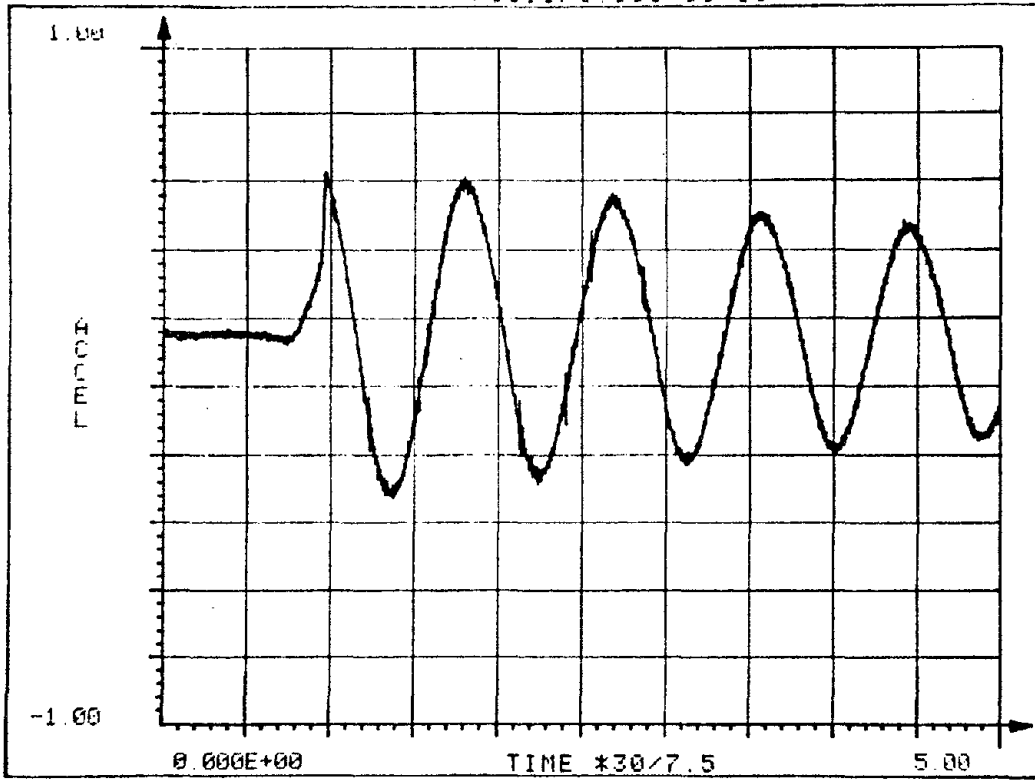
Fφ3.1

F3031P5.5SC 11-13



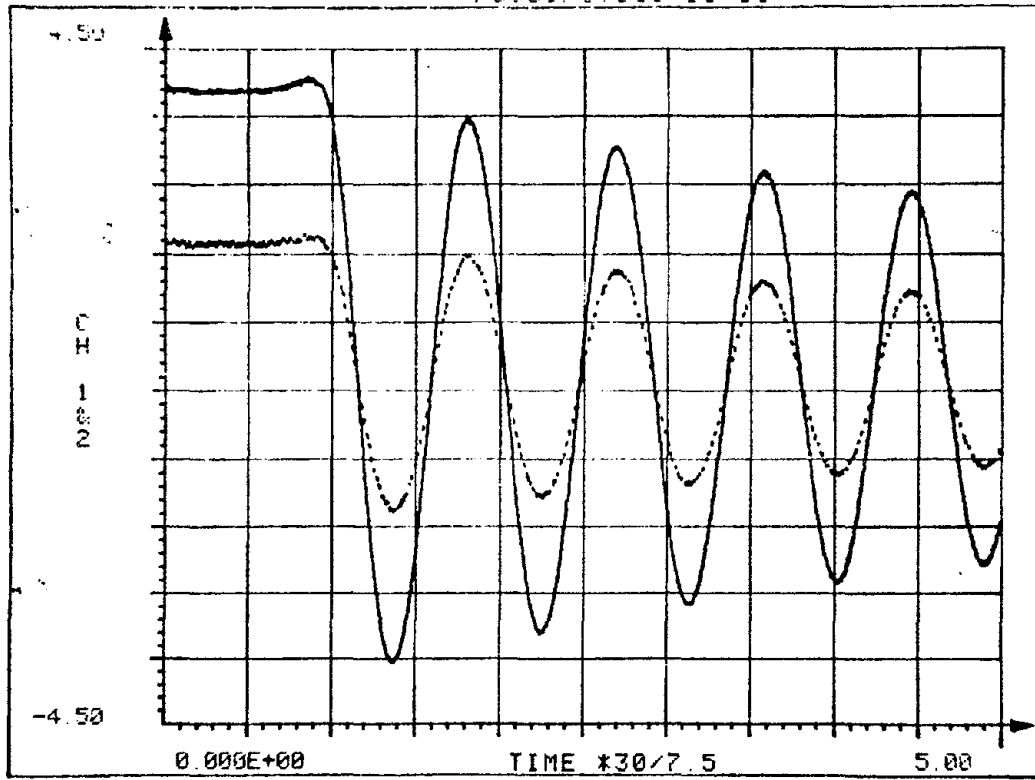
Fφ3.2

F3031P5.5SC 11-13

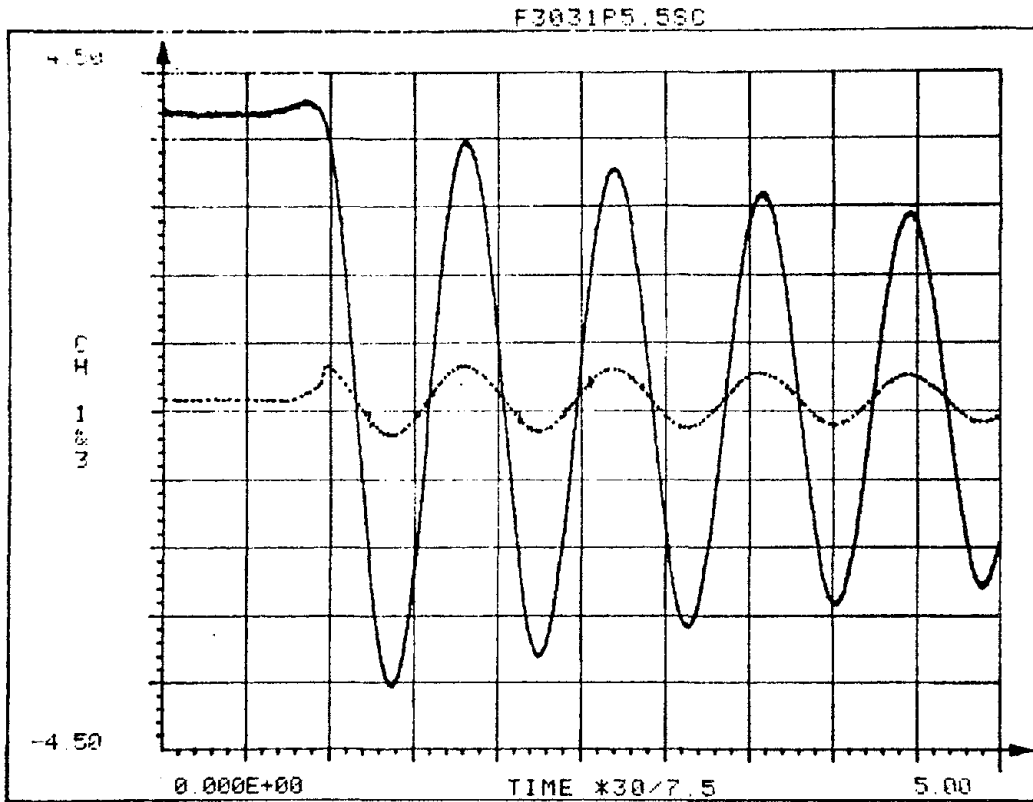


Fφ3.3

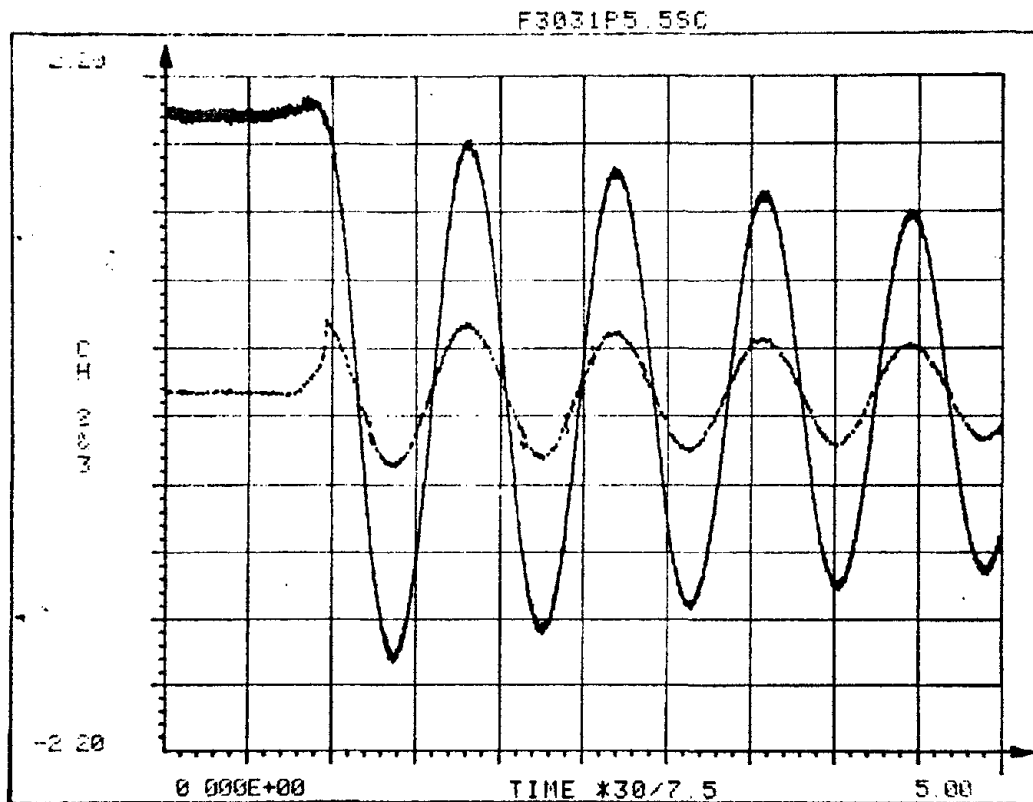
F3031P5.5SC 11-13



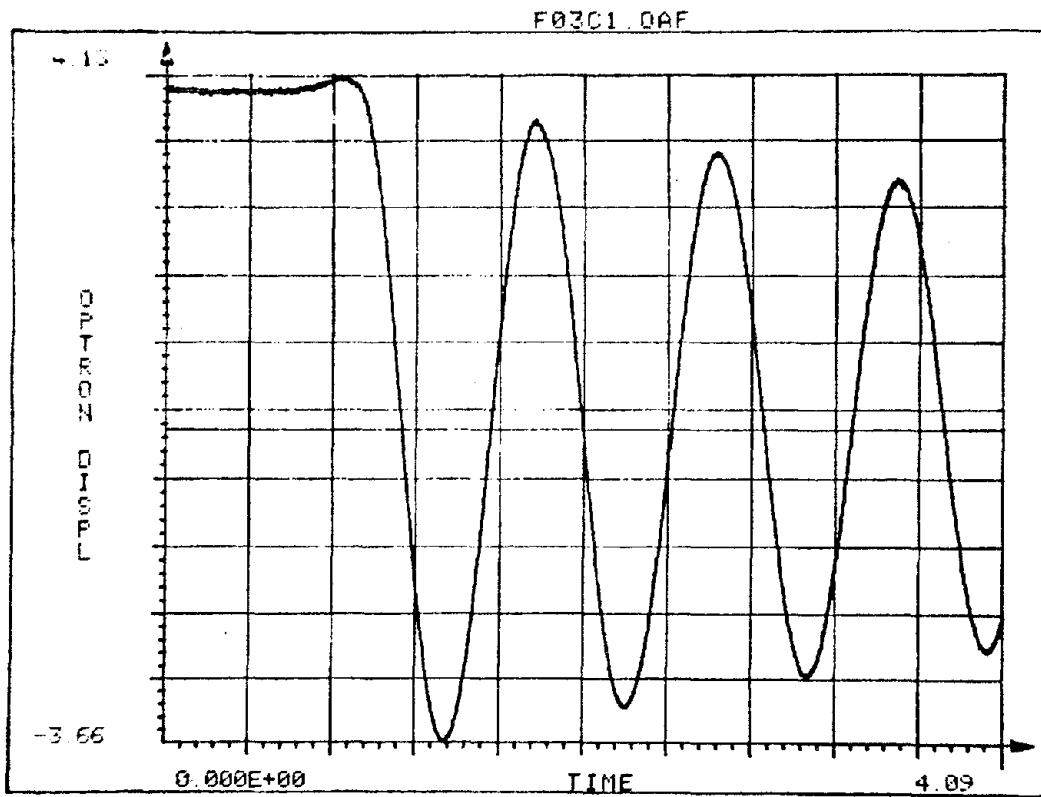
Fφ3.4



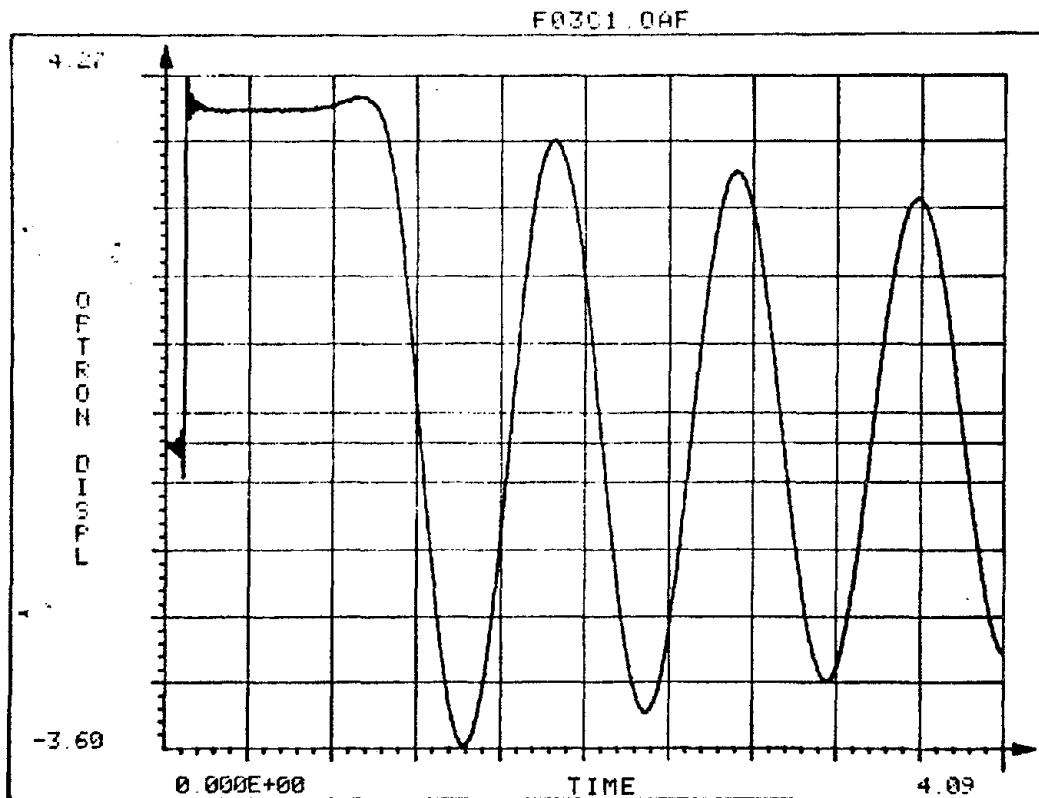
Fφ3.5



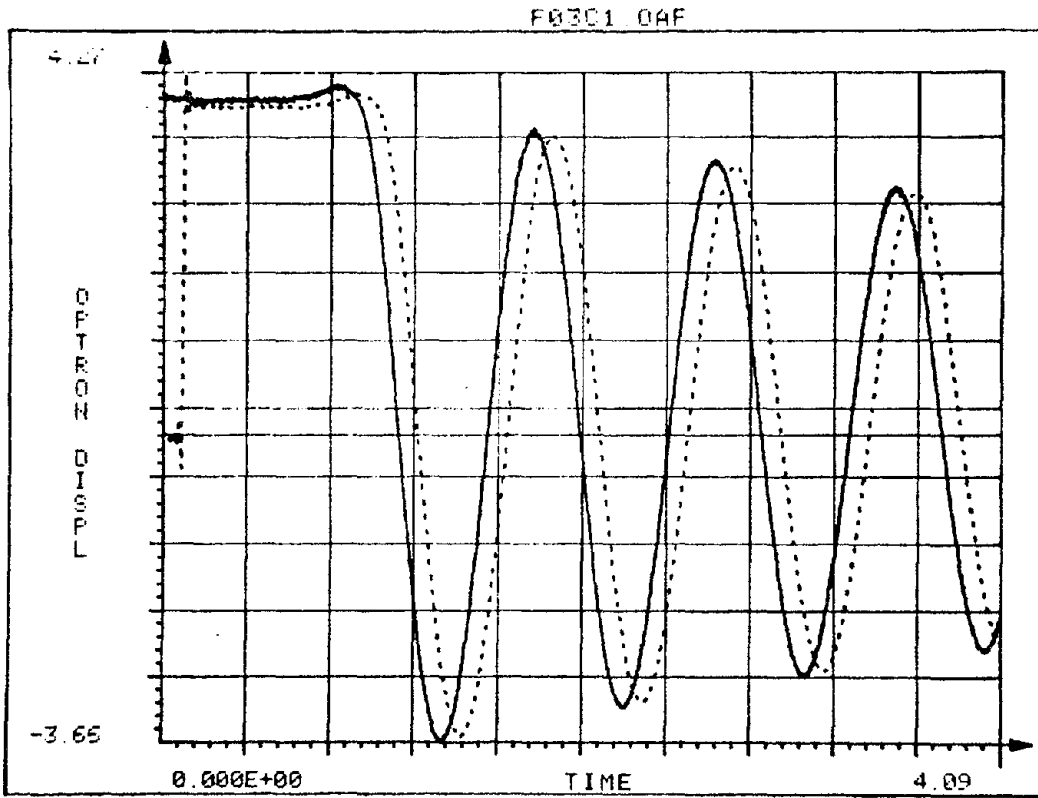
Fφ3.6



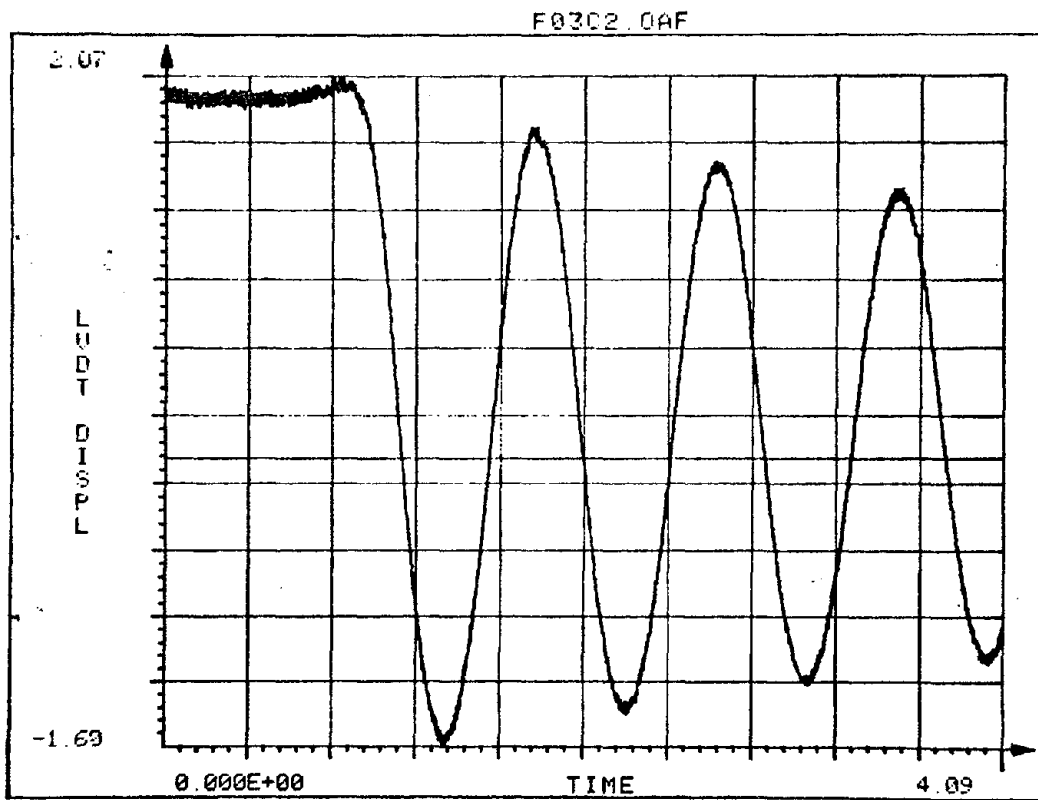
F03.7



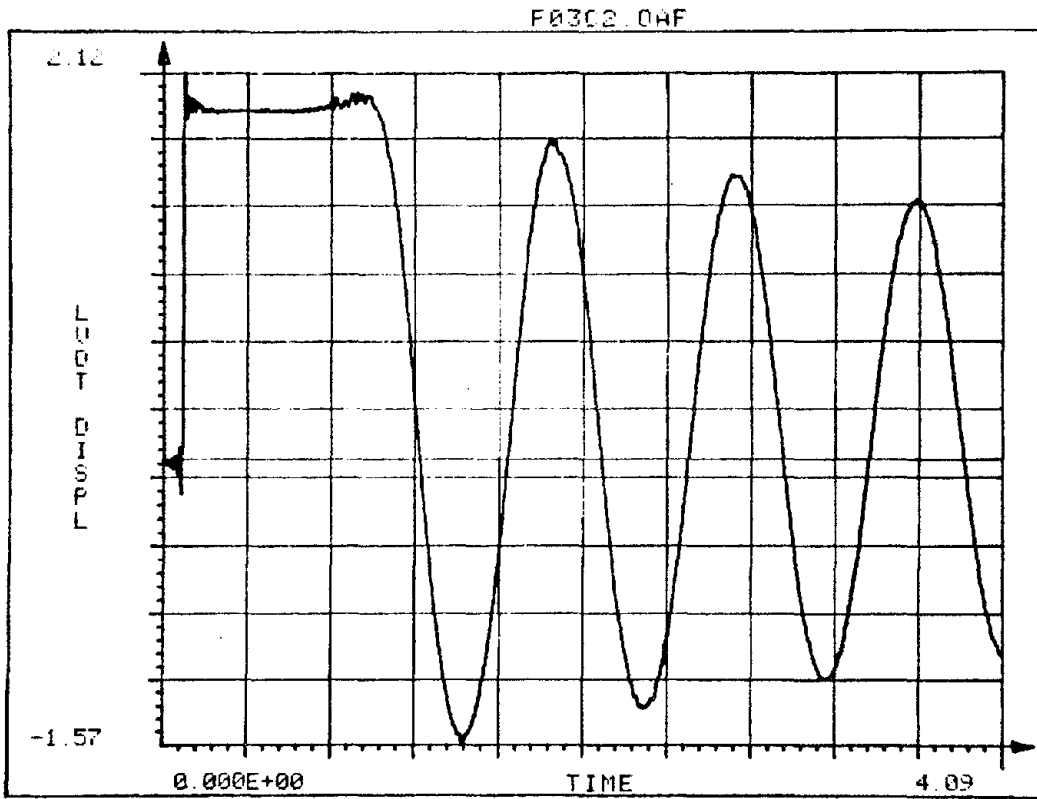
F03.8



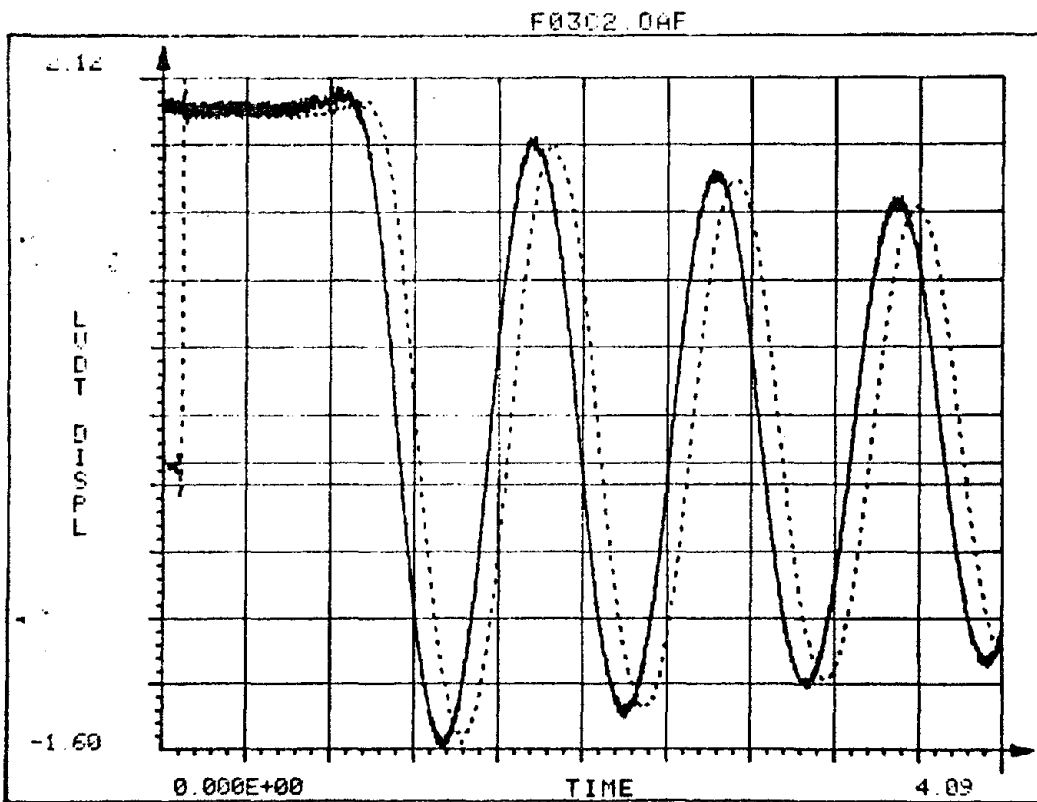
F03.9



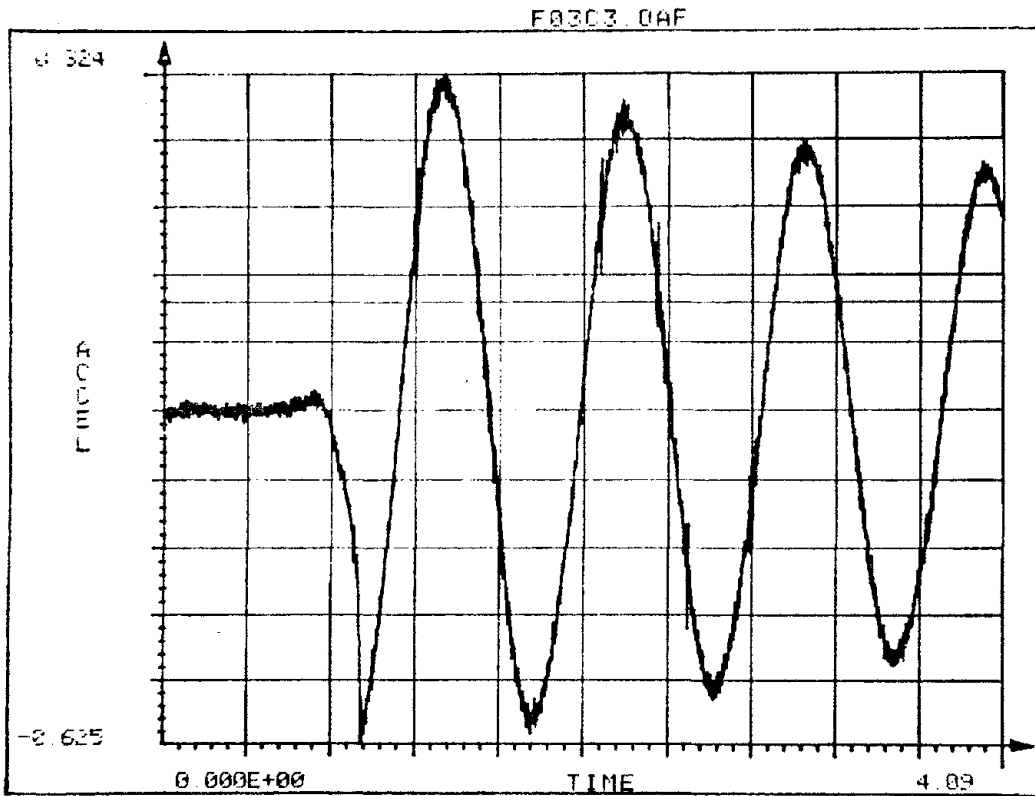
F03.10



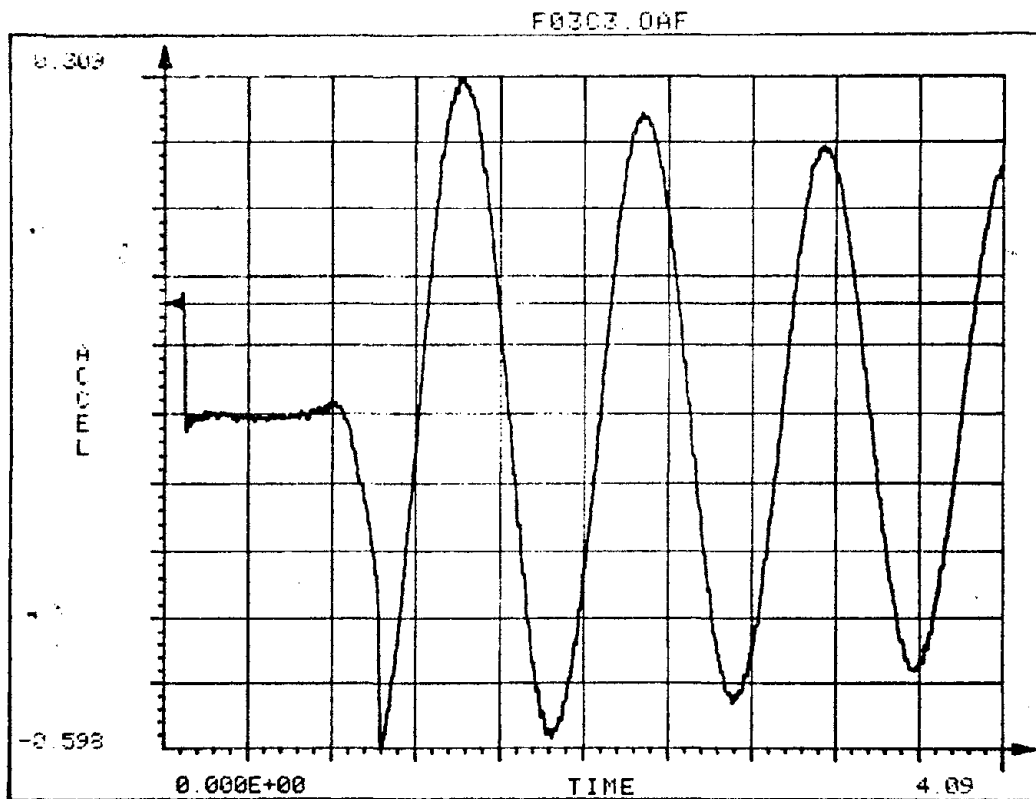
F03.11



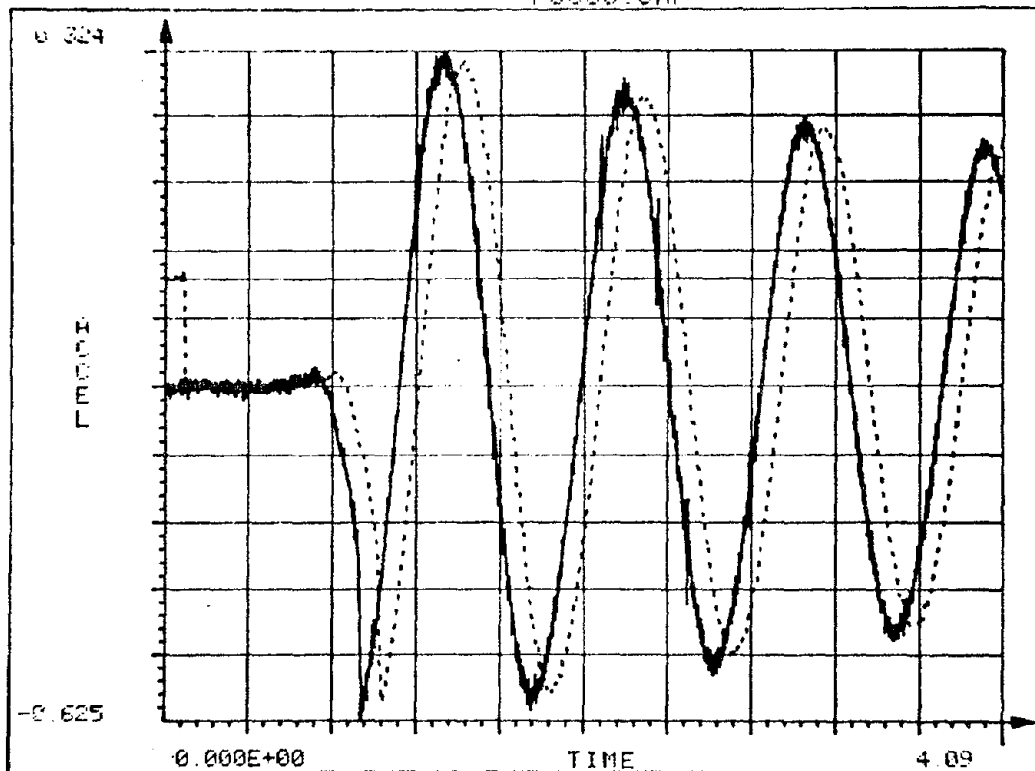
F03.12



F03.13



F03.14



F ϕ 3.15

Group S (Static Friction)

Notation : D1- Mass Displacement (OPTRON)

D2-Mass Displacement (LVDT)

A1-Mass Accceleration

L -Static Load (proving ring)

F -Friction Device

(F) Filtered Data

For figures with 2 curves ___ first curve

----- second curve

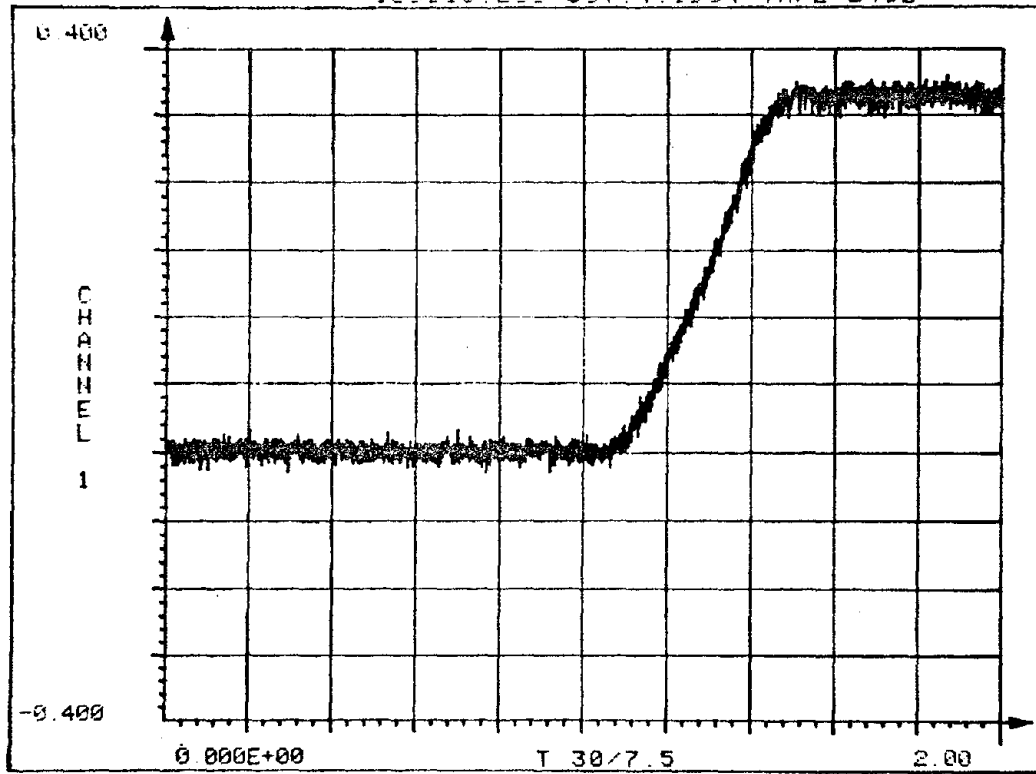
*Figures S05.8-S05.23 correspond to the time segment of 1-2 sec of original (unfiltered) data file.

Fig. No.	Caption
S05.1	D1
S05.2	D2
S05.3	A1 static slip
S05.4	A1 blow-up static slip
S05.5	1.D1
	2.A1
S05.6	L
S05.7	F
S05.8	D1
S05.9	D1(F)

FRICTION

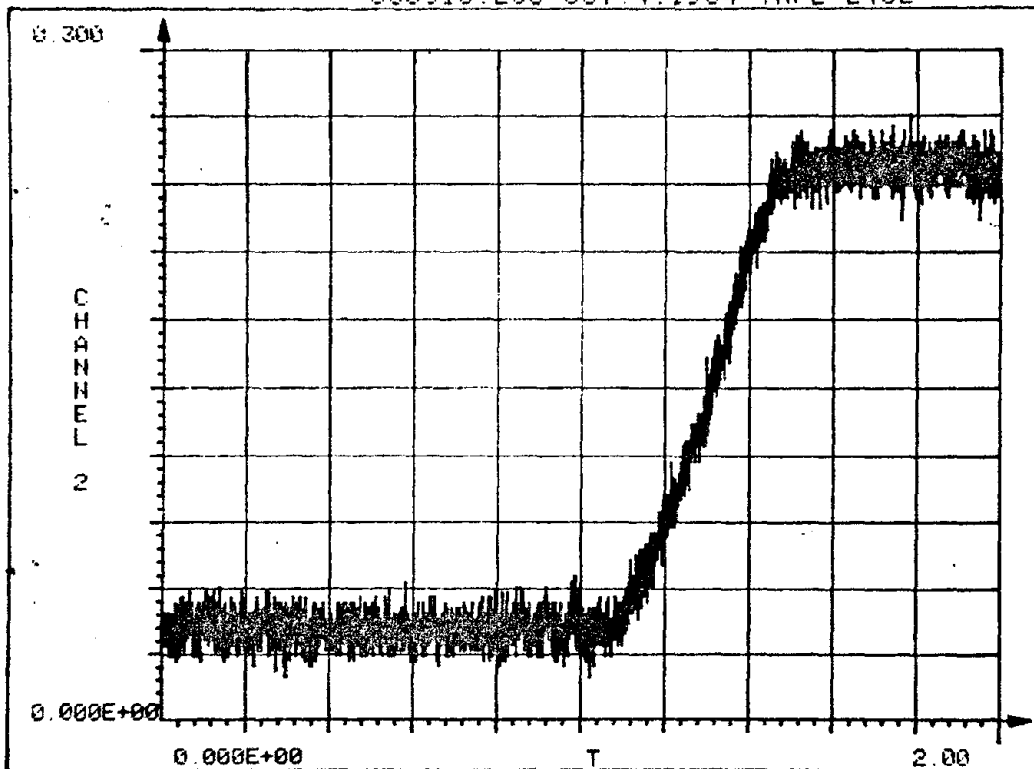
S05.10	1.D1	
	2.D1(F)	
S05.11	D2	
S05.12	D2(F)	
S05.13	1.D2	
	2.D2(F)	
S05.14	A1	static slip
S05.15	A1(F)	
S05.16	1.A1	
	2.A1(F)	
S05.17	A1	blow-up static slip
S05.18	A1(F)	
S05.19	1.A1	
	2.A1(F)	
S05.20	L	
S05.21	L(F)	
S05.22	F	
S05.23	F(F)	

S50510.250 OCT. 4. 1984 TAPE:2402



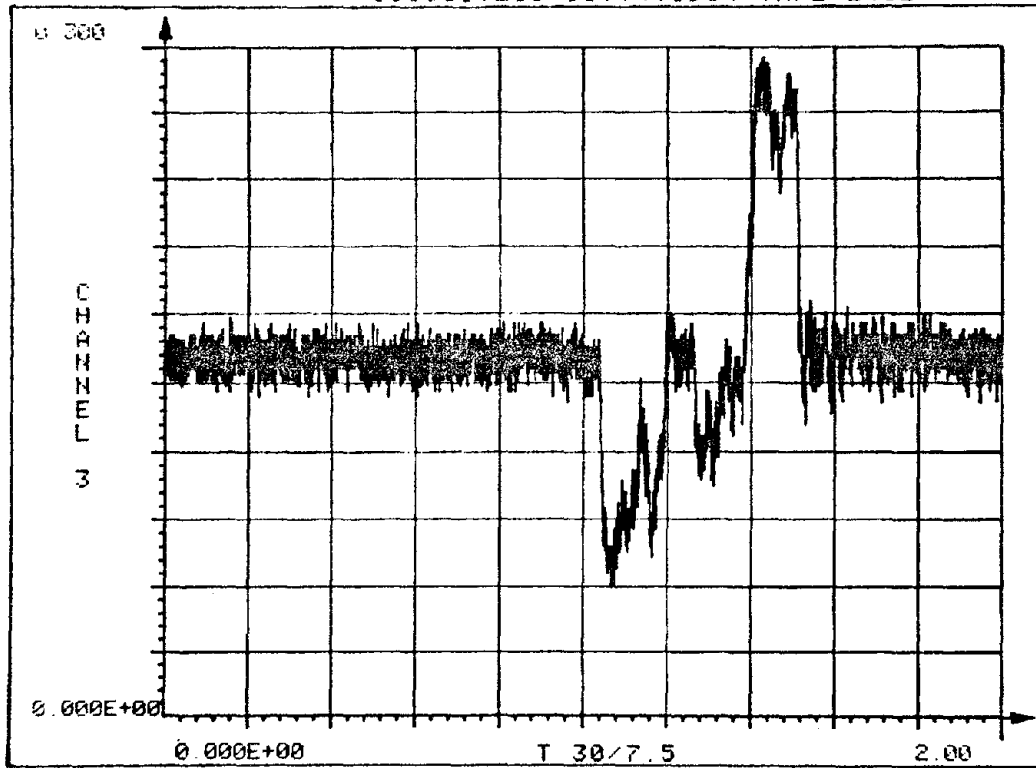
Sφ5.1

S50510.250 OCT. 4. 1984 TAPE:2402



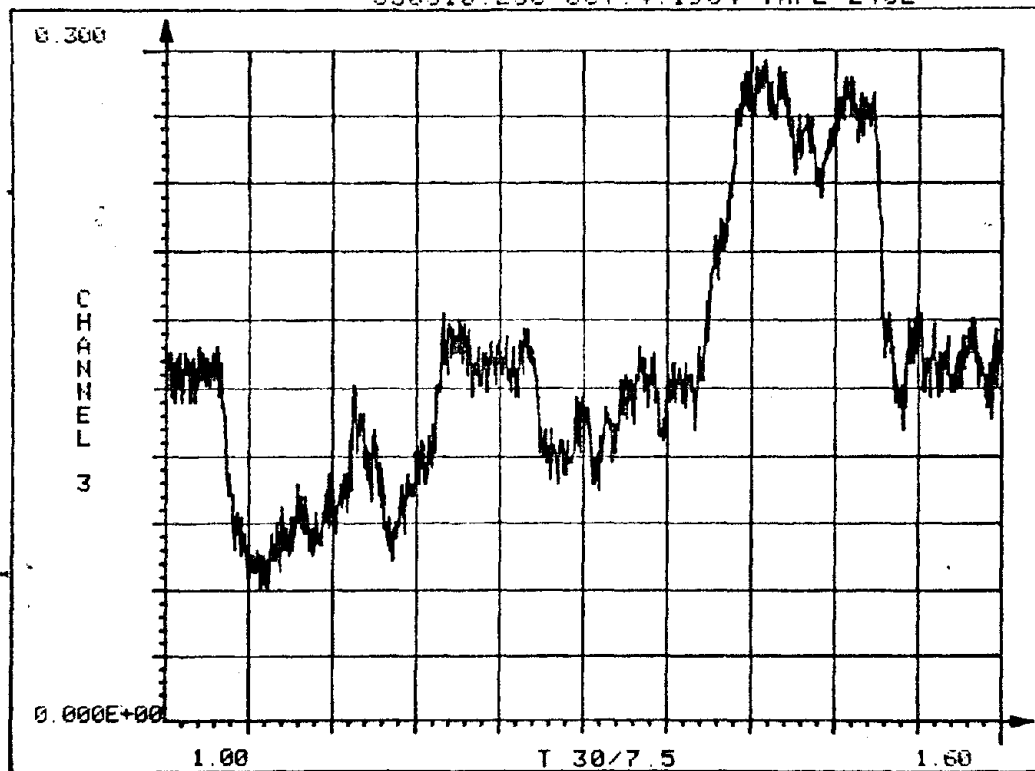
Sφ5.2

S50510.2SC OCT.4.1984 TAPE:2402



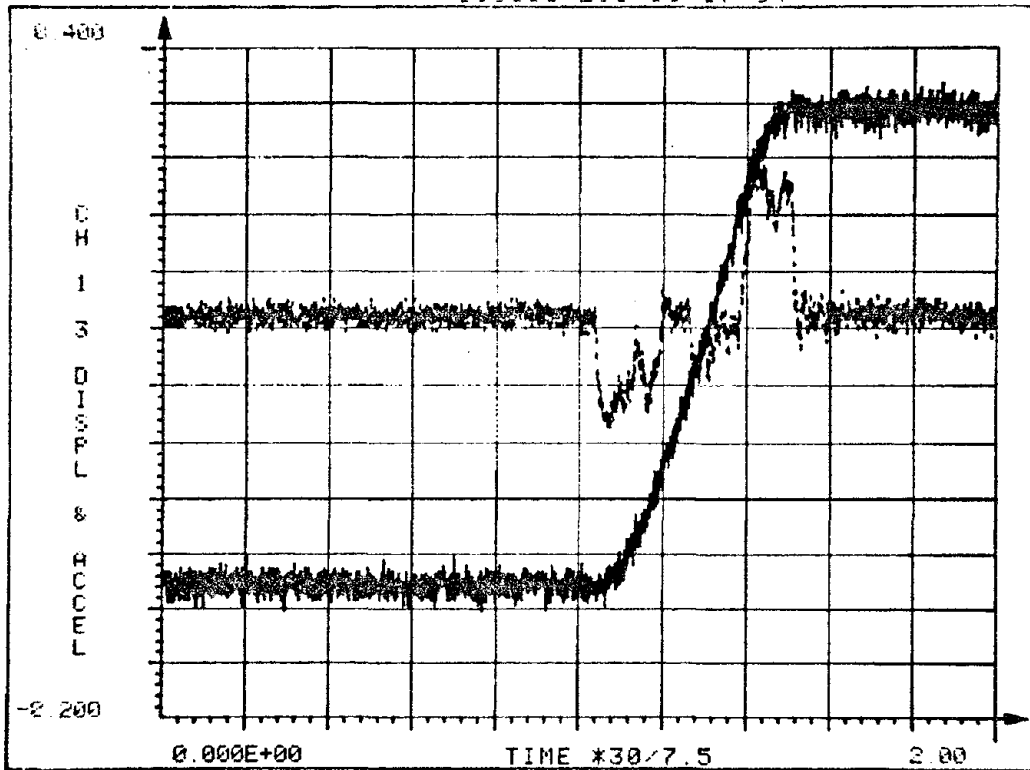
Sφ5.3

S50510.2SC OCT.4.1984 TAPE:2402



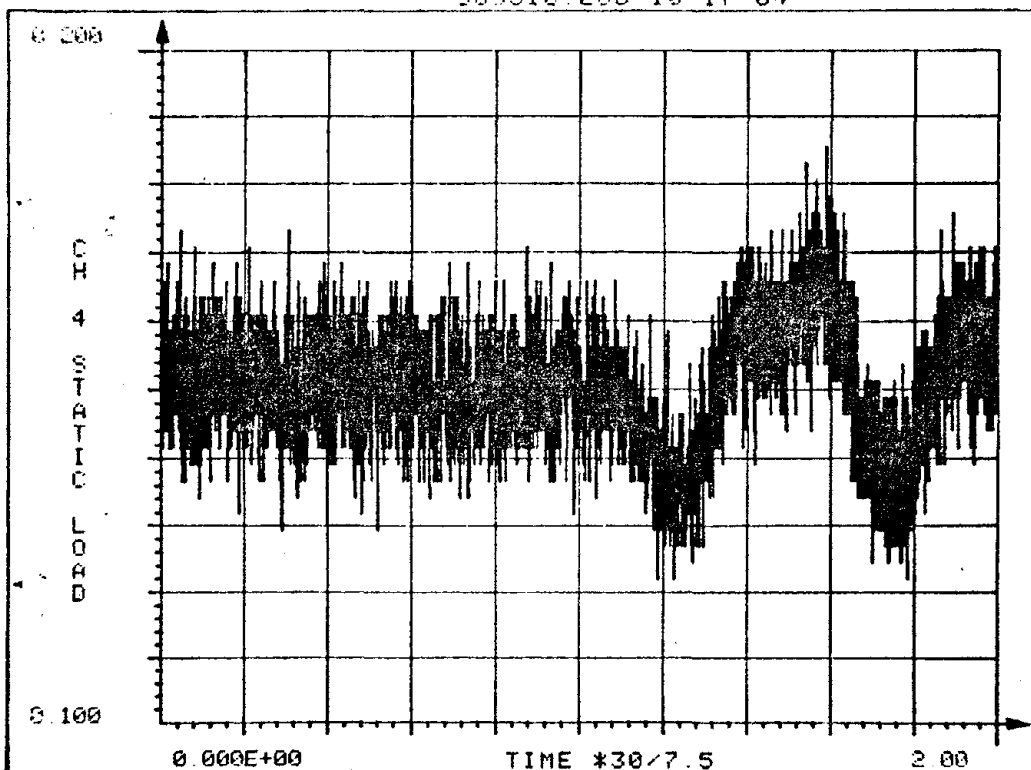
Sφ5.4

550510 290 10-17-84



Sφ5.5

550510 290 10-17-84

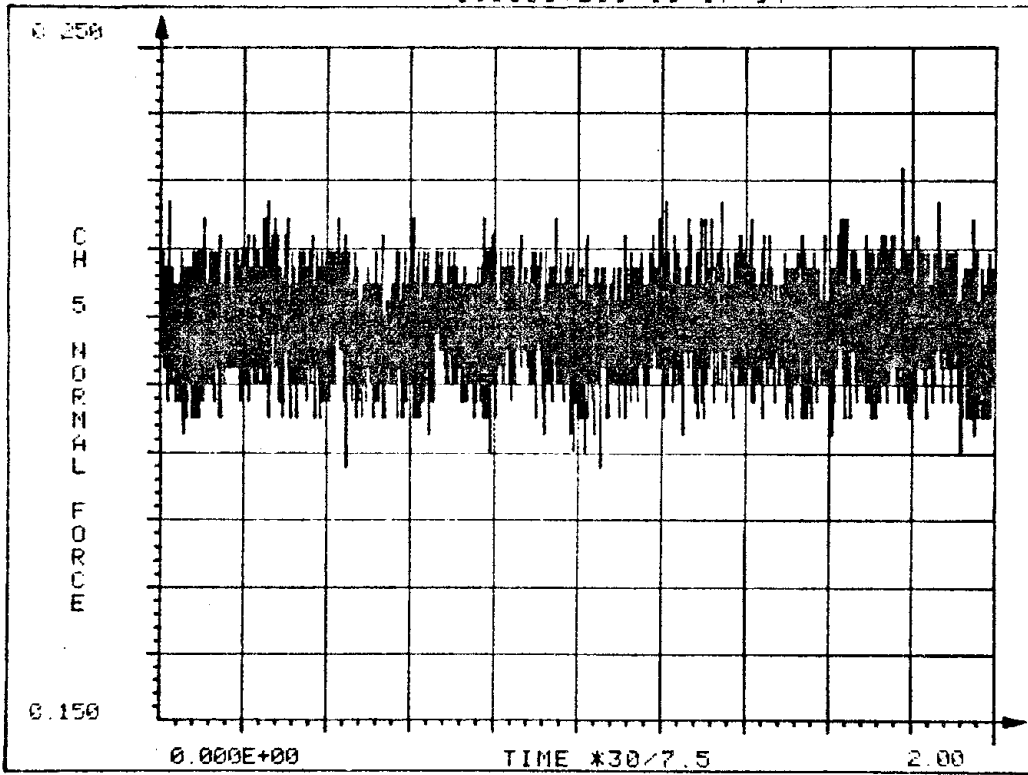


Sφ5.6

Reproduced from
best available copy.

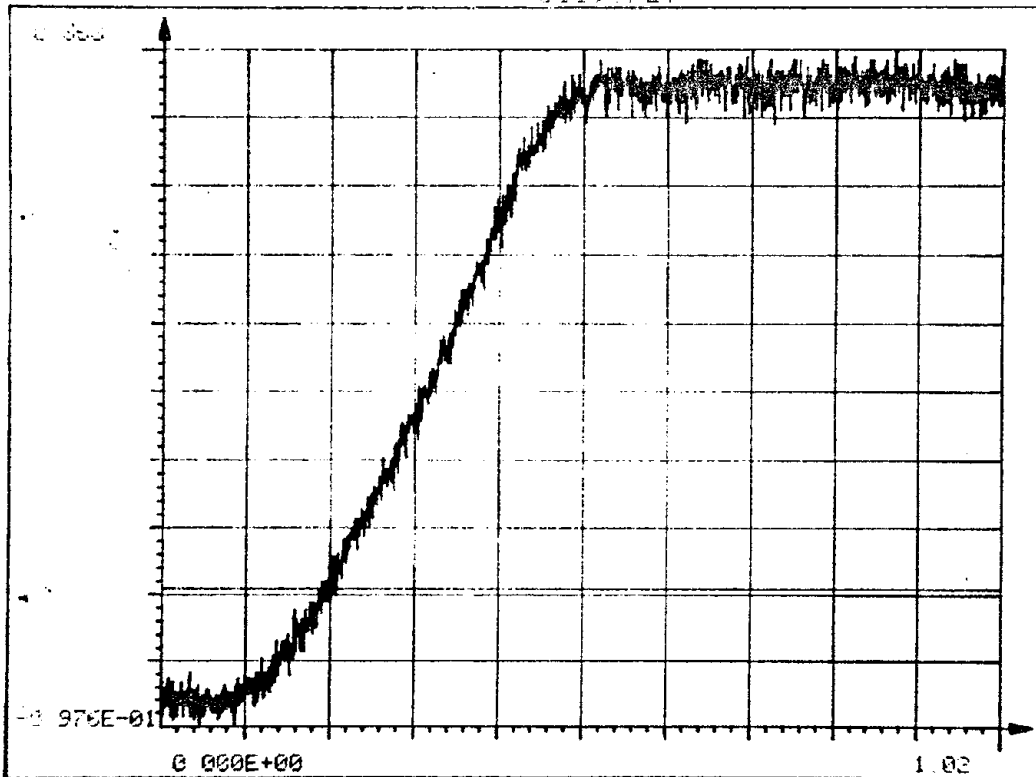


353510 29C 10-17-84



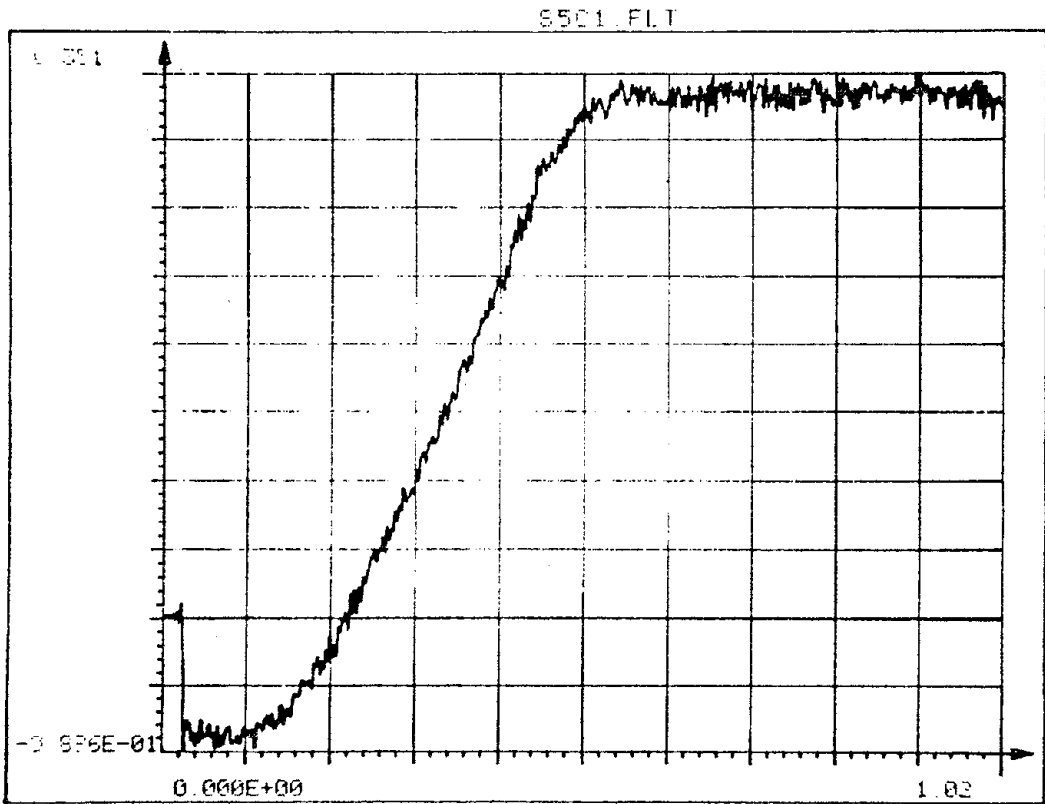
Sφ5.7

8501 FLT

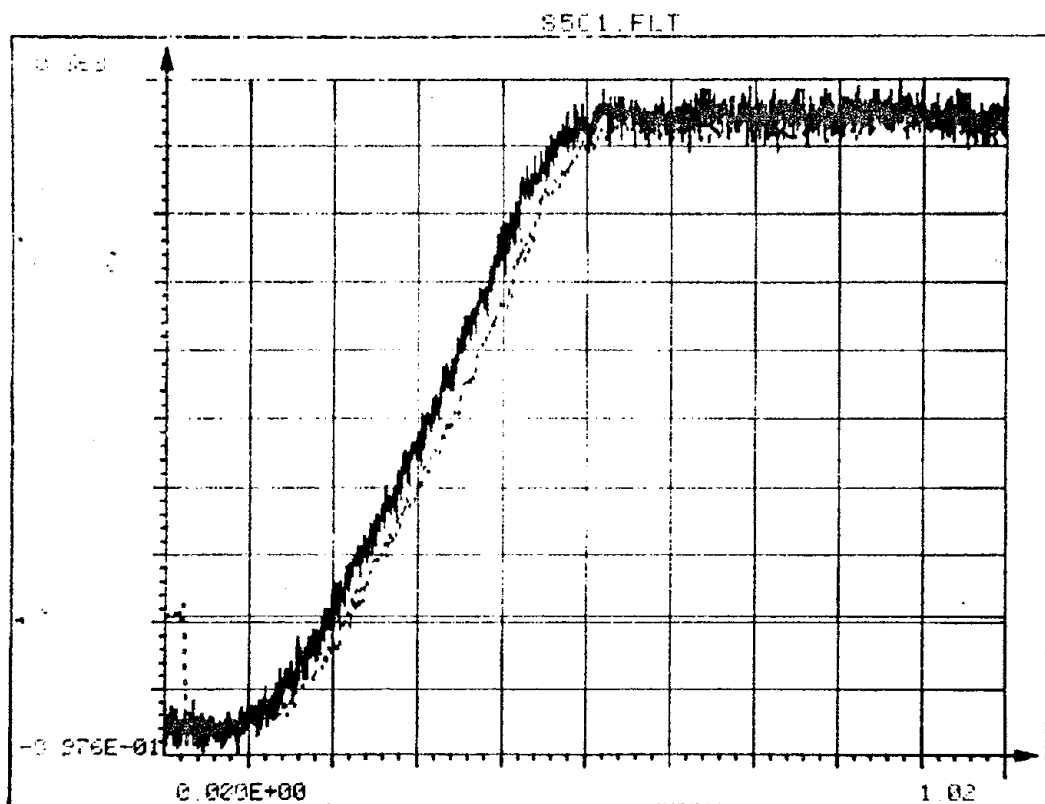


Sφ5.8

B-6

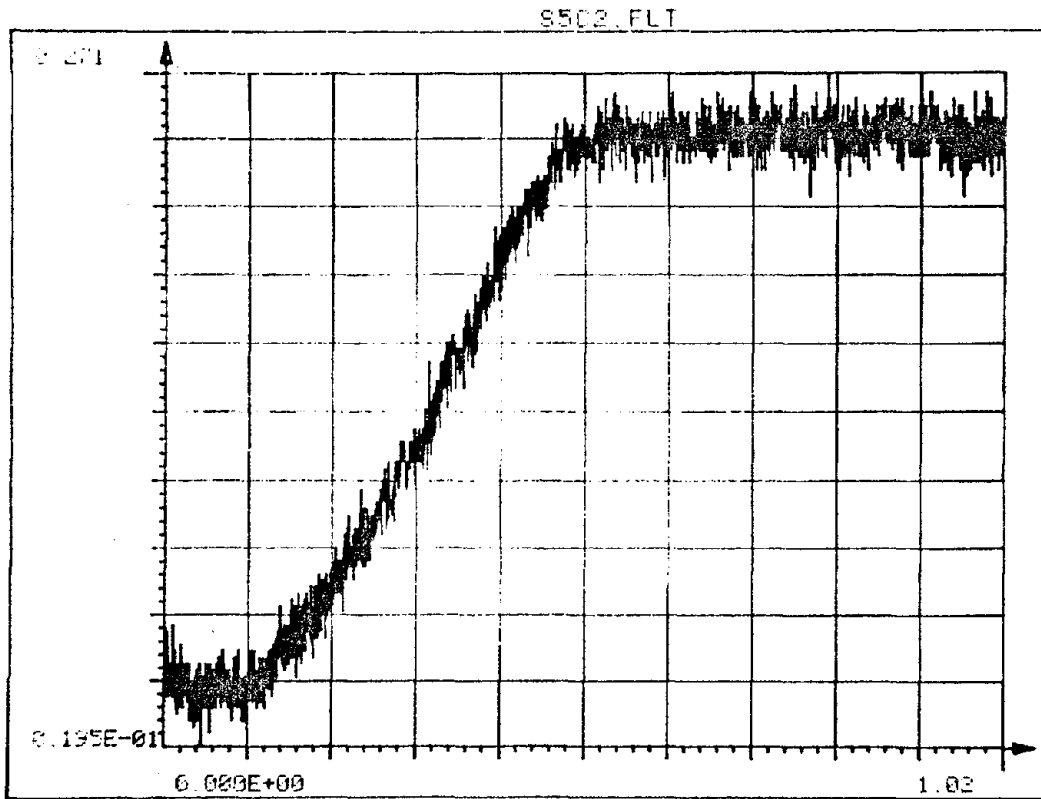


Sφ5.9

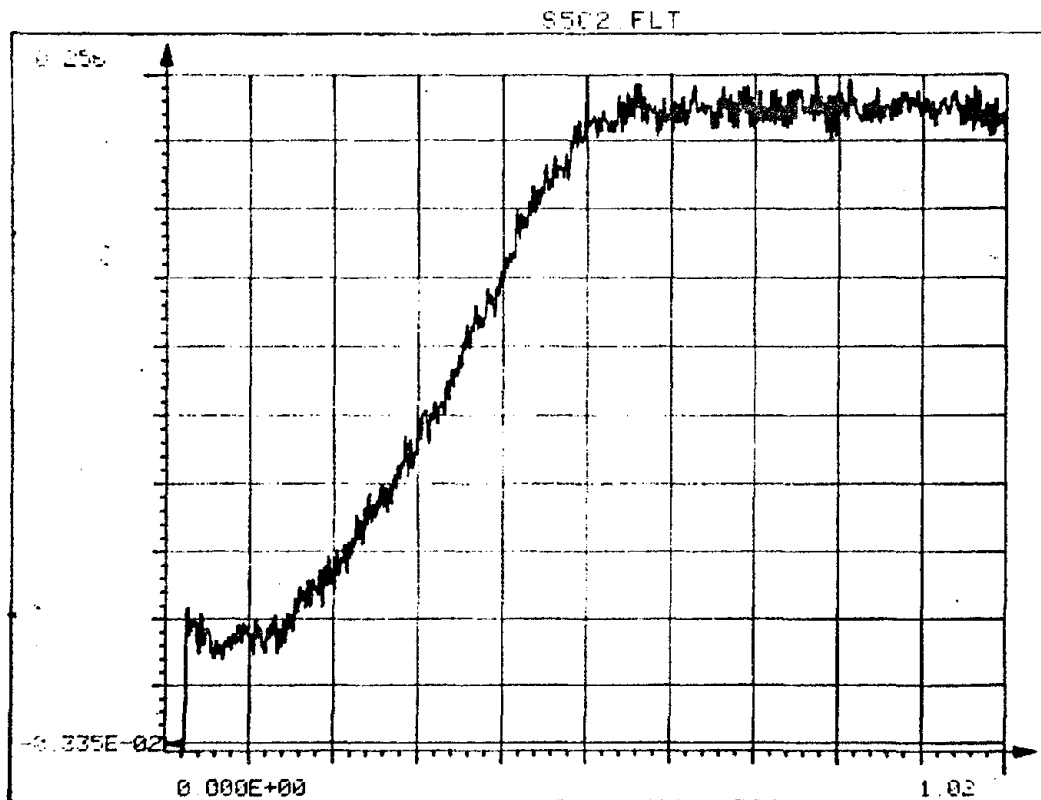


Sφ5.1φ

B-7

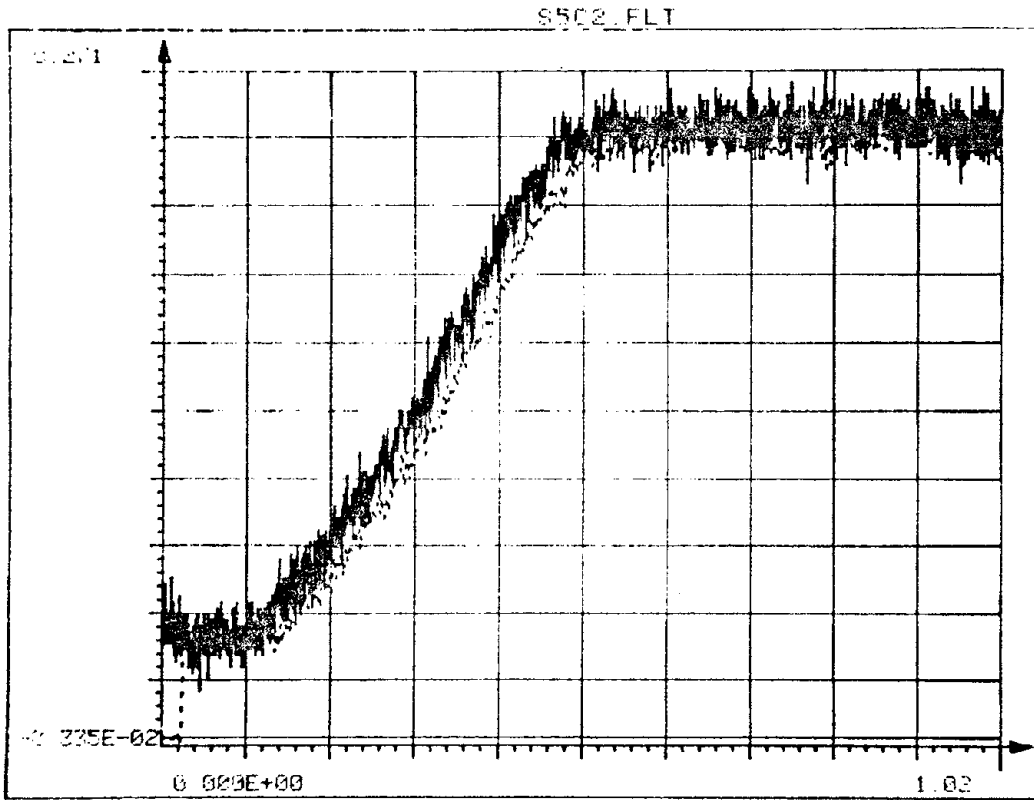


Sφ5.11

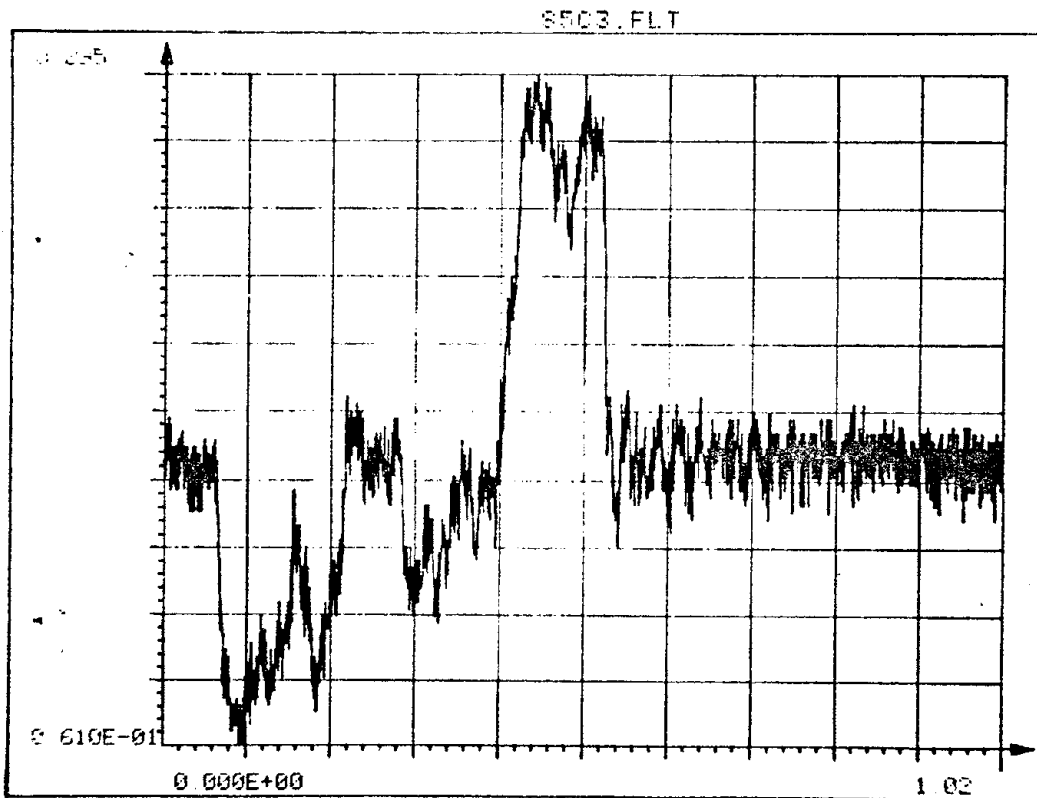


Sφ5.12

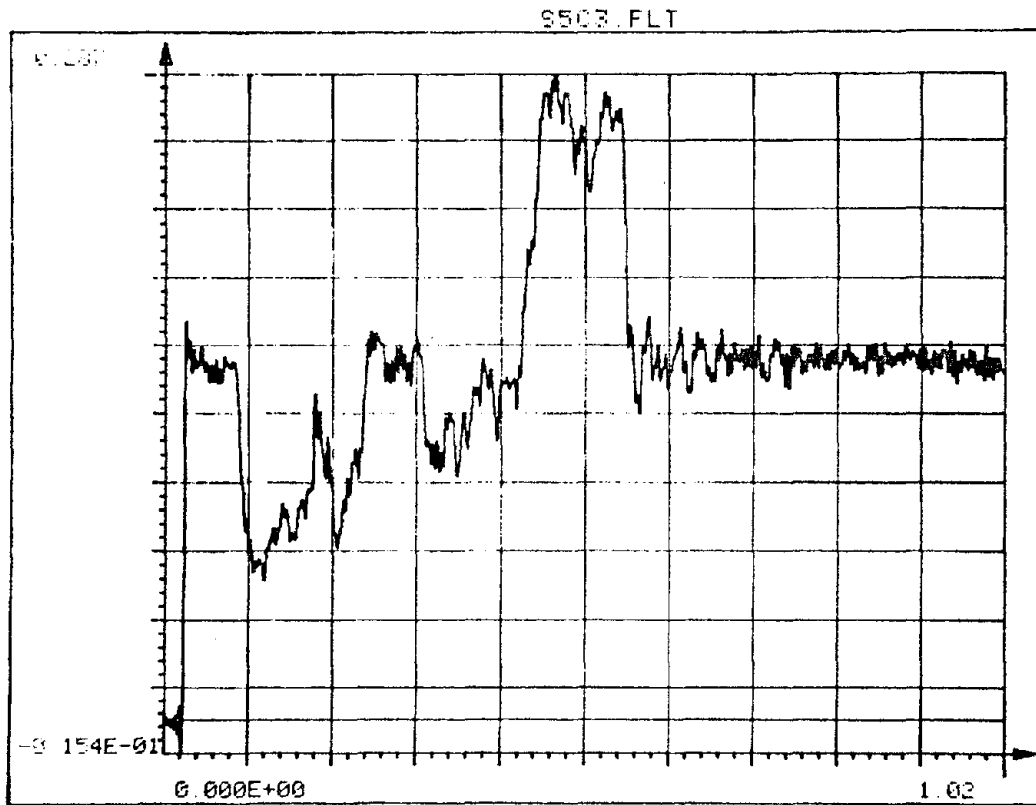
B-8



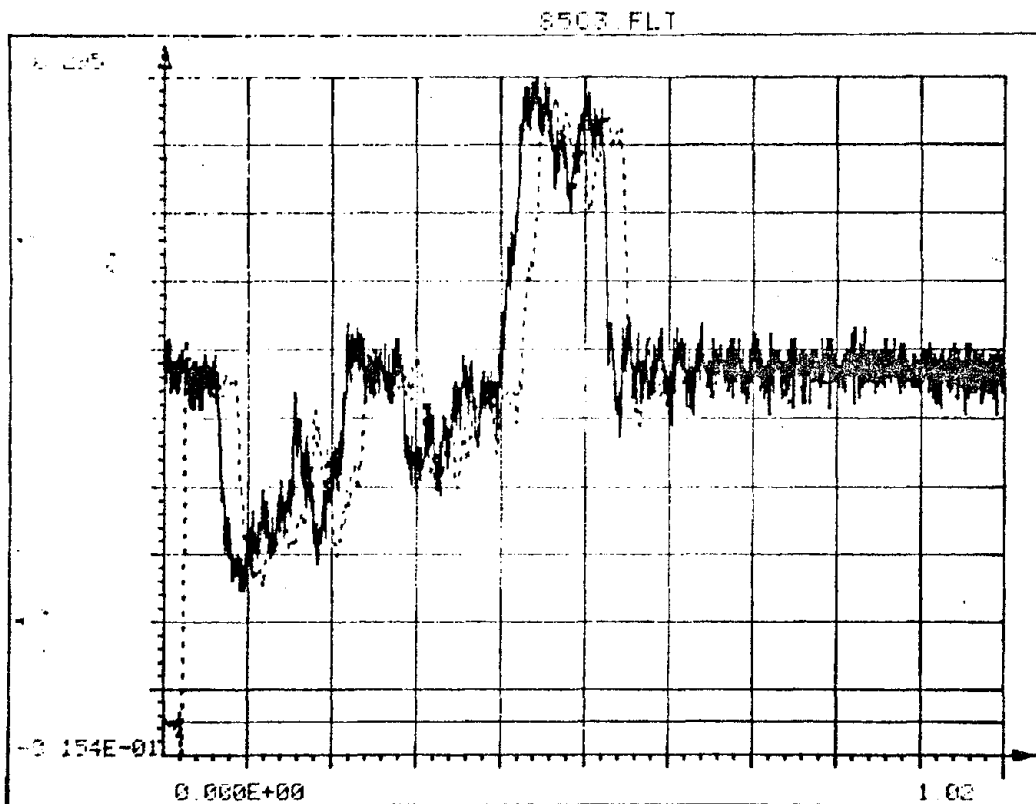
Sφ5.13



Sφ5.14

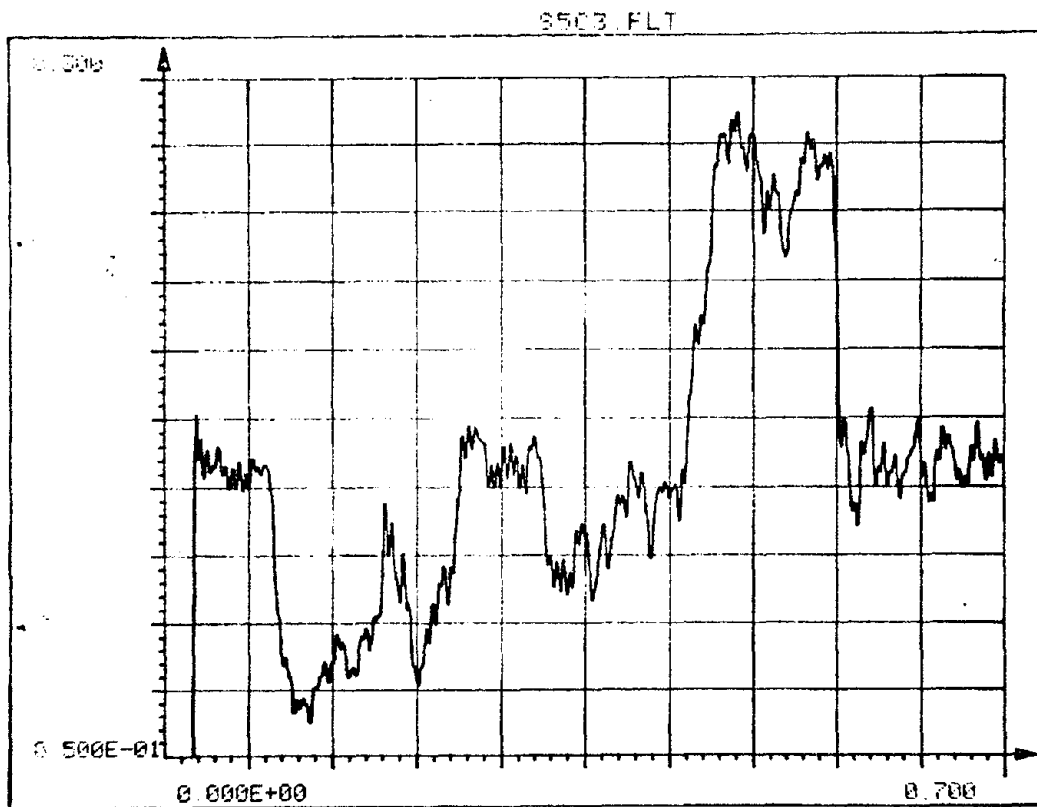
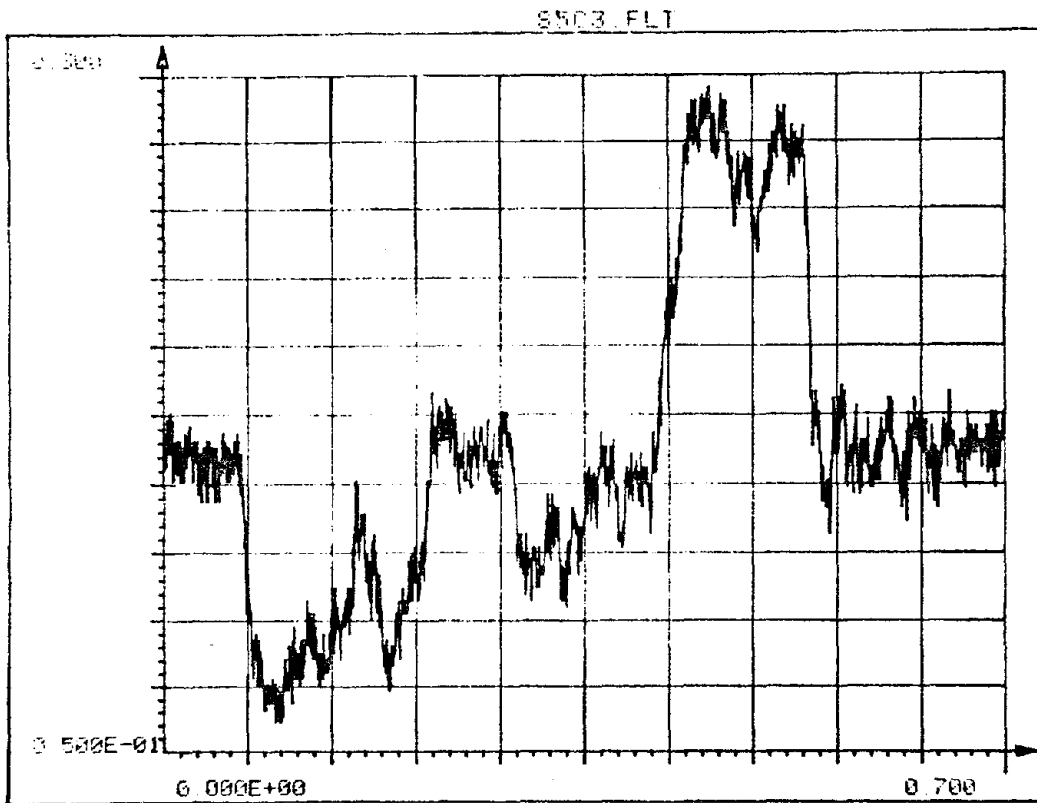


Sφ5.15

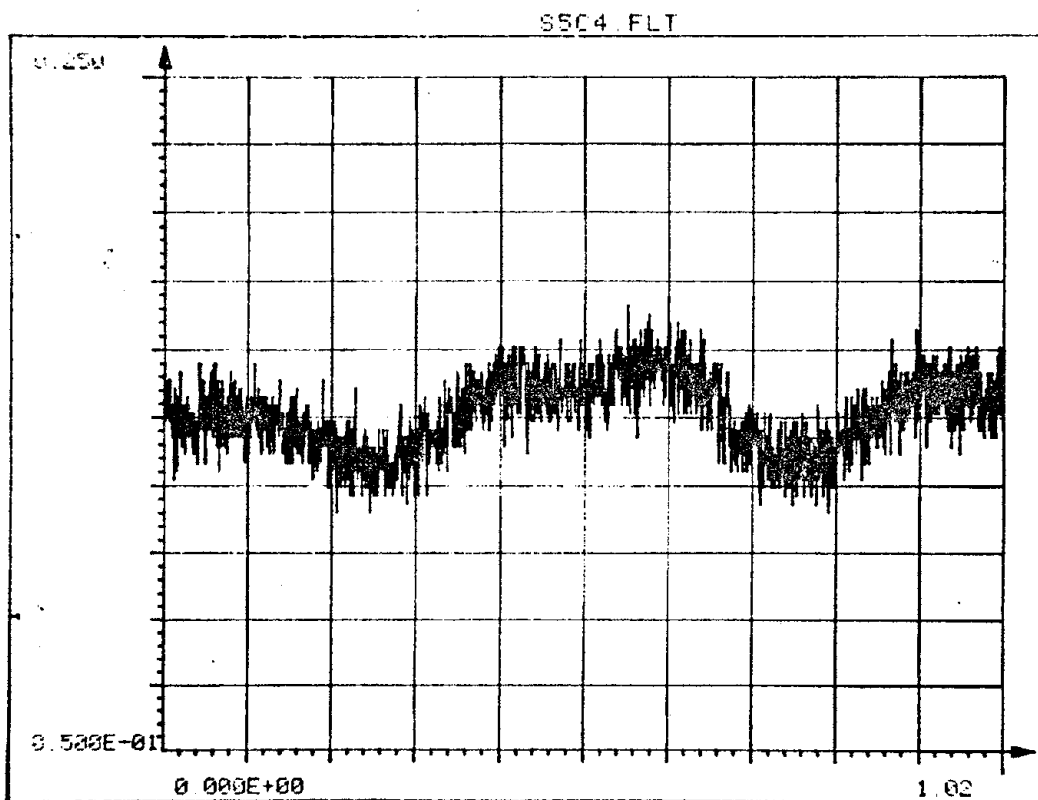
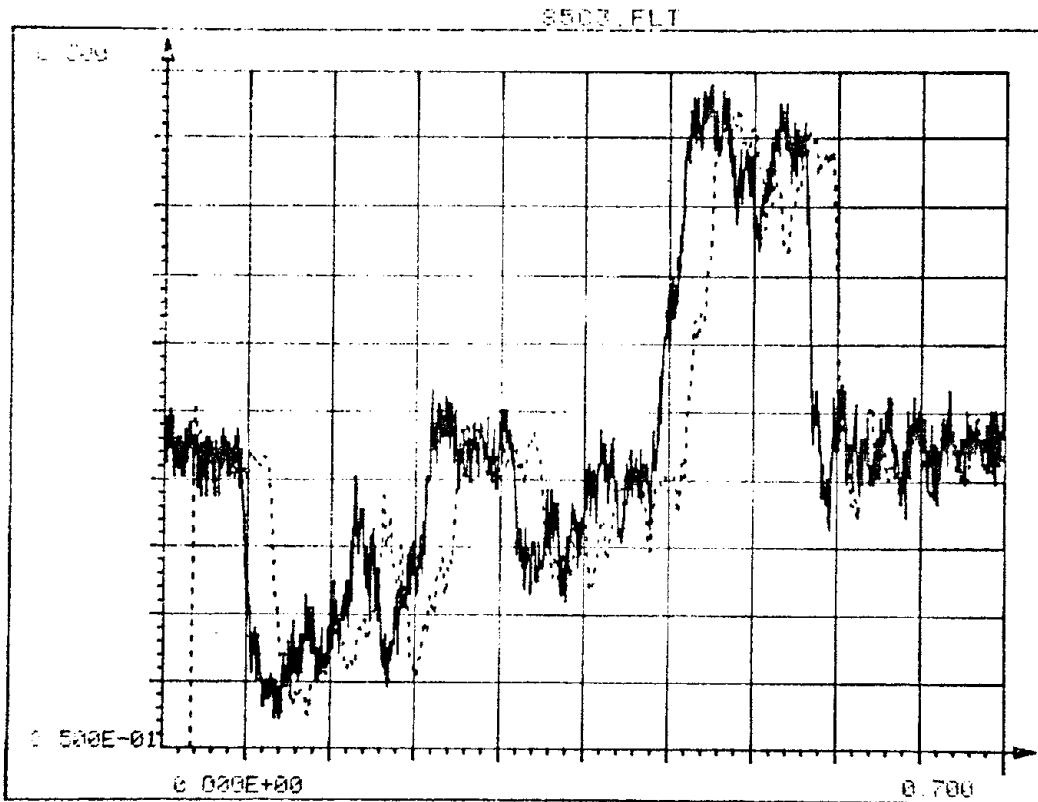


Sφ5.16

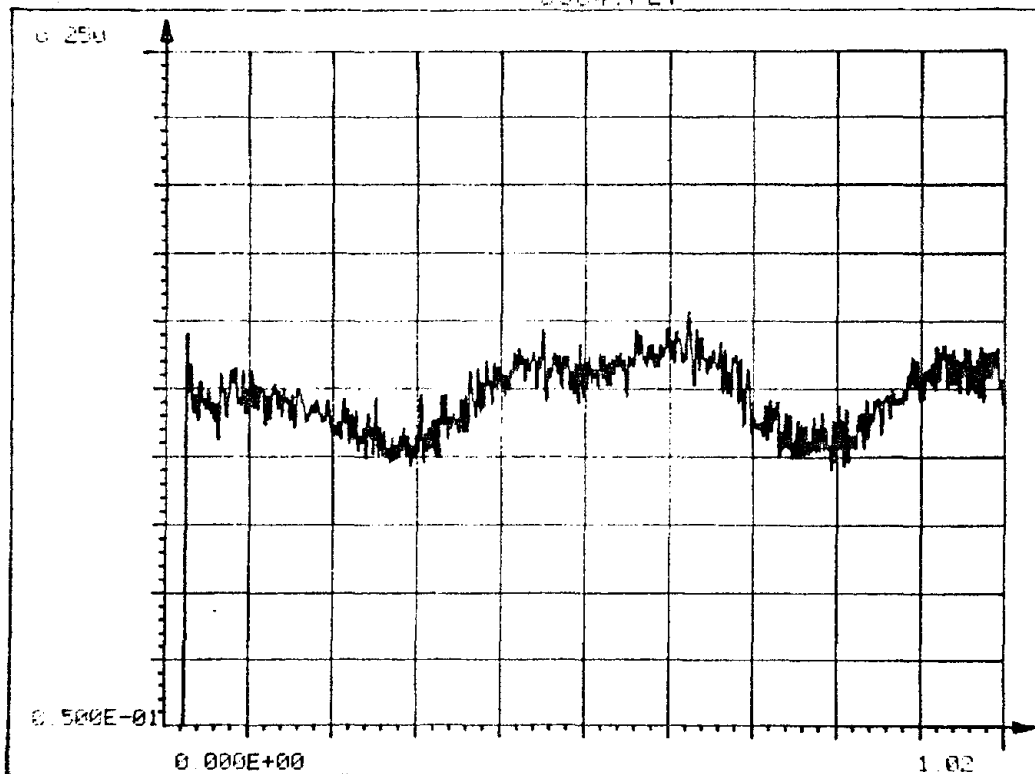
B-10



B-11

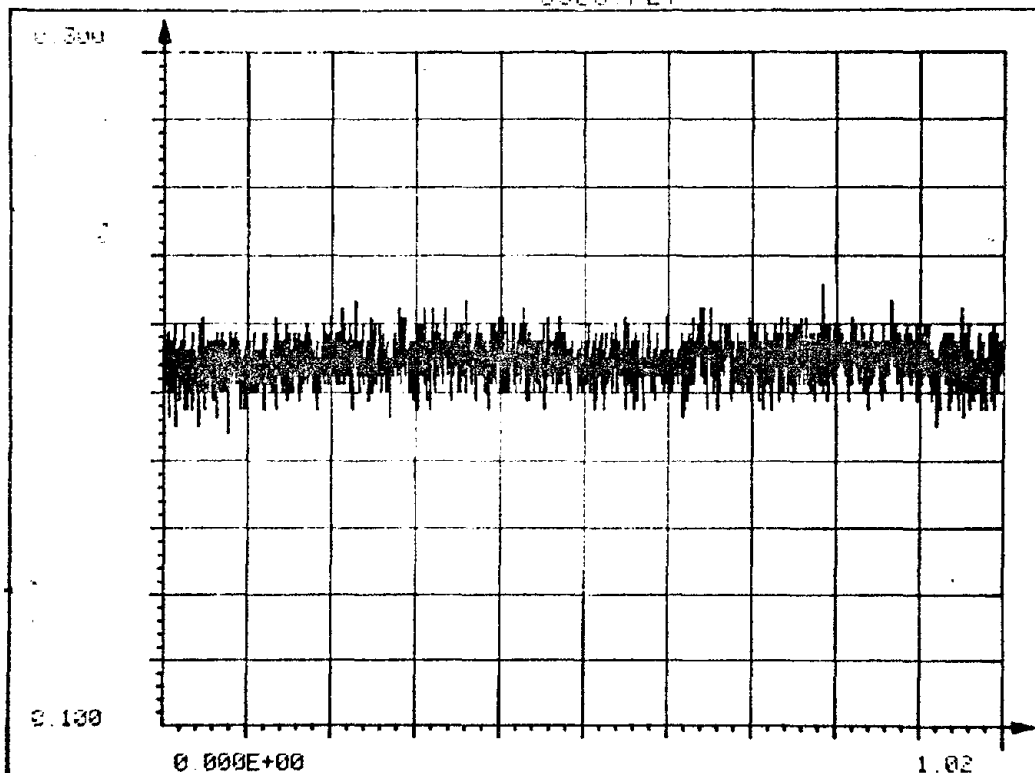


S504.FLT



Sφ5.21

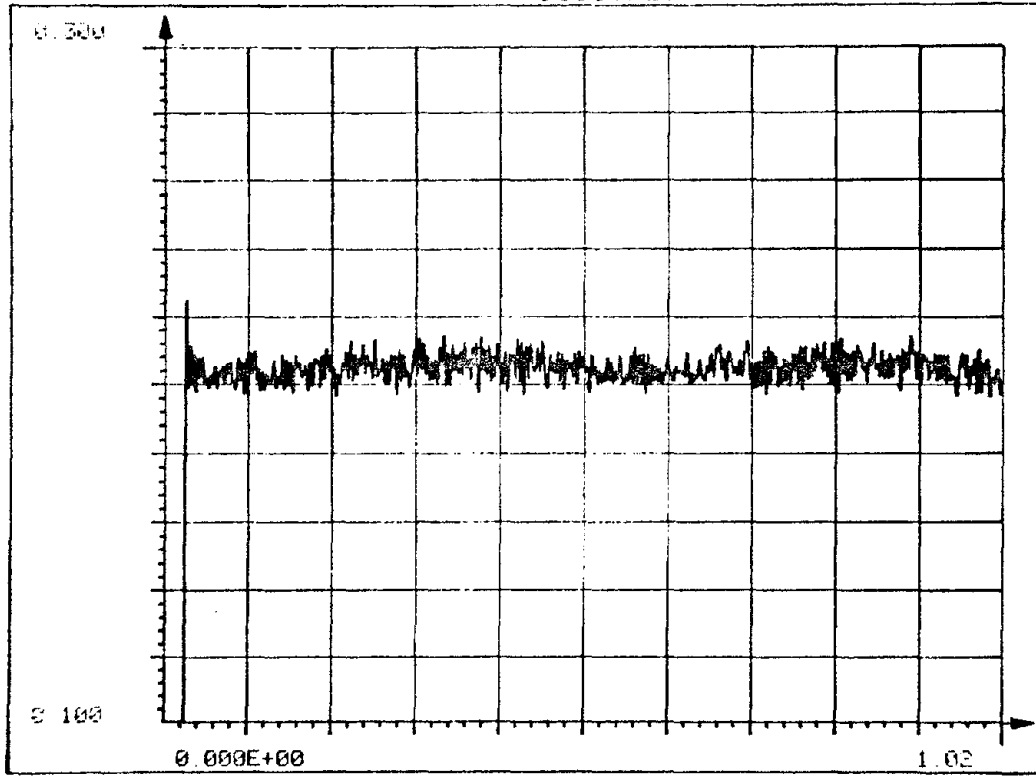
S505.FLT



Sφ5.22

B-13

S505.FLT



Sφ5.23

APPENDIX 3

Linear Dynamic (Group D)

D1373P5.10S 3500 SR D13C1.OAF Filtered from D1373P5.10S
 7 Ch D13C2.OAF 2048 pts
 D13C3.OAF 0 - 4s
 D13C4.OAF
 D13C6.OAF

Group D (Forced Linear Vibration)

Notation : D1-Base displacement (LVDT)

D2-Mass displacement (OPTRON)

A1-Base acceleration

A2-Mass acceleration

V -Function generator

(F)-Filtered data

For figures with 2 curves first curve

----- second curve

*Figures D13.6-D13.20 correspond to the first 4 sec of the original
 (unfiltered) data file.

Fig. no.	Caption
D13.1	D1
D13.2	A1
D13.3	D2
D13.4	A2

FRICITION

D13.5	V
D13.6	D1
D13.7	D1(F)
D13.8	1.D1
	2.D1(F)
D13.9	A1
D13.10	A1(F)
D13.11	1.A1
	2.A1(F)
D13.12	D2
D13.13	D2(F)
D13.14	1.D2
	2.D2(F)
D13.15	A2
D13.16	A2(F)
D13.17	1.A2
	2.A2(F)
D13.18	V
D13.19	V(F)
D13.20	1.V
	2.V(F)

*Figures D33.7-D33.25 Correspond to the first 8 sec of the original
(unfiltered) data file.

D3373P5.10S 3500SR D33C1.OAF Filtered from D3373P5.10S
7 ch D33C2.OAF 4096 pts
 D33C3.OAF 0 - 8 s
 D33C4.OAF
 D33C6.OAF

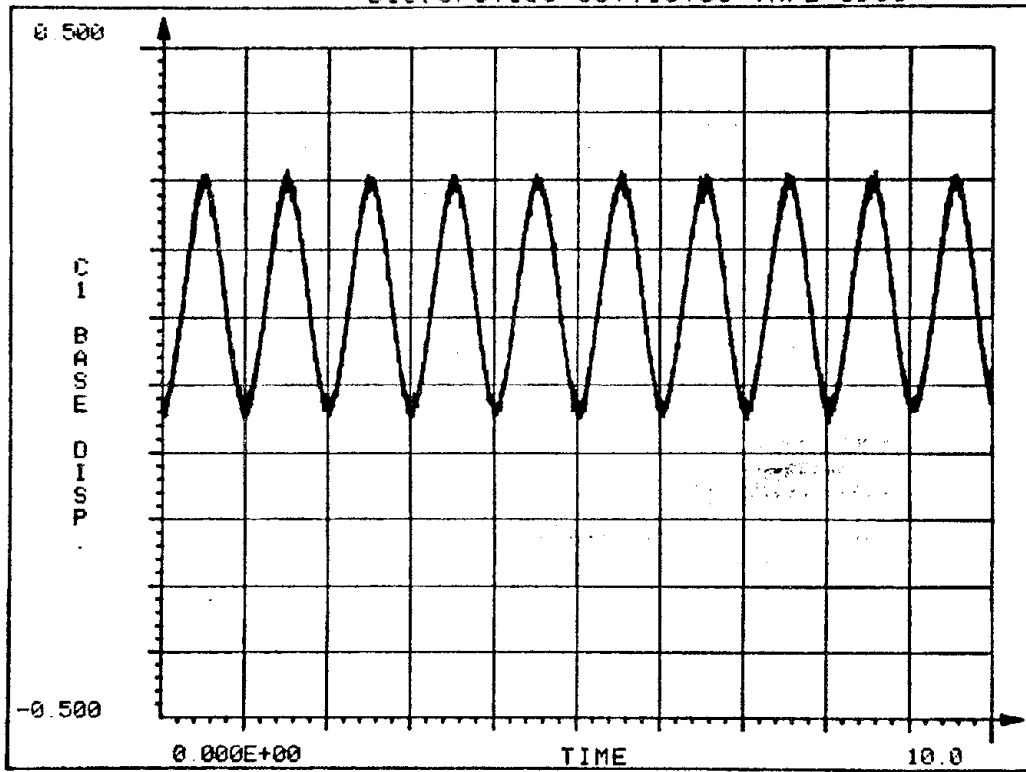
FRICITION

D33.1	D1	
D33.2	A1	
D33.3	D2	
D33.4	1.D1 PHASE RELATION	
	2.D2	
D33.5	A2	
D33.6	V	
D33.7	D1	
D33.8	D1(F)	
D33.9	1.D1	(blow-up)
	2.D1(F)	
D33.10	1.D1	(blow-up)
	2.D1(F)	
D33.11	1.D1	(blow-up)
	2.D1(F)	
D33.12	A1	
D33.13	A1(F)	
D33.14	1.A1	(blow-up)
	2.A1(F)	
D33.15	D2	
D33.16	D2(F)	
D33.17	1.D2	(blow-up)
	2.D2(F)	
D33.18	1.D2	(blow-up)
	2.D2(F)	
D33.19	A2	
D33.20	A2(F)	
D33.21	1.A2	(blow-up)

FRICION

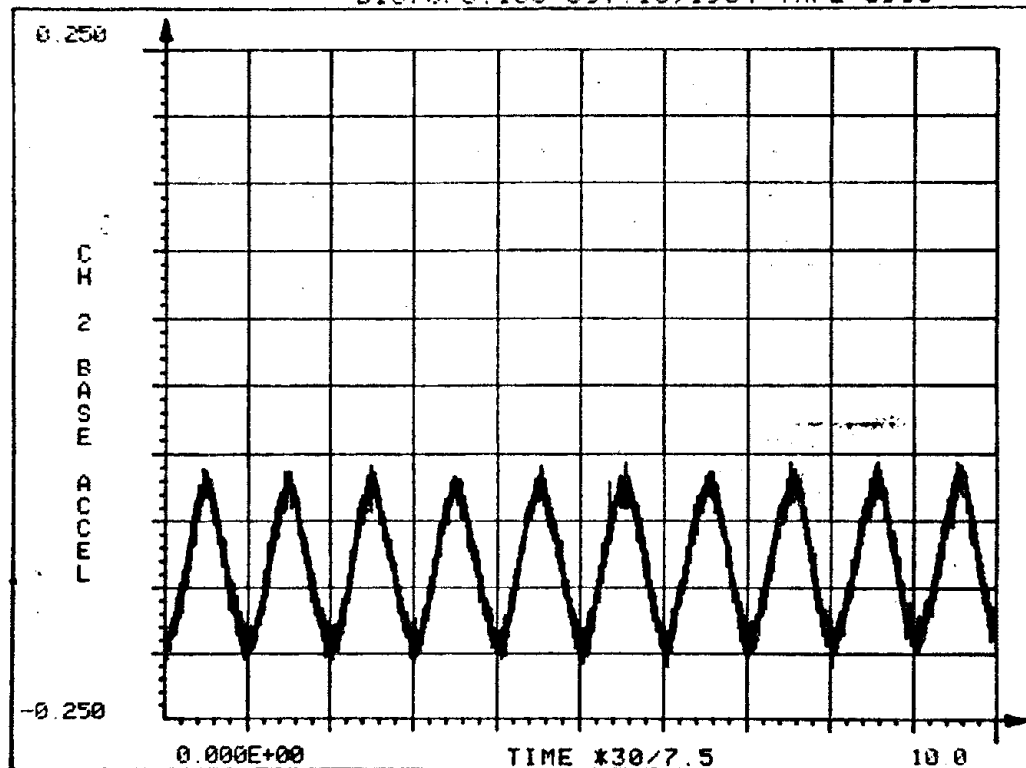
	2.A2(F)	
D33.22	1.A2	(blow-up)
	2.A2(F)	
D33.23	V	
D33.24	V(F)	
D33.25	1.V	(blow-up)
	2.V(F)	

D1373P5.10S OCT.15.85 TAPE:3980



D13.1

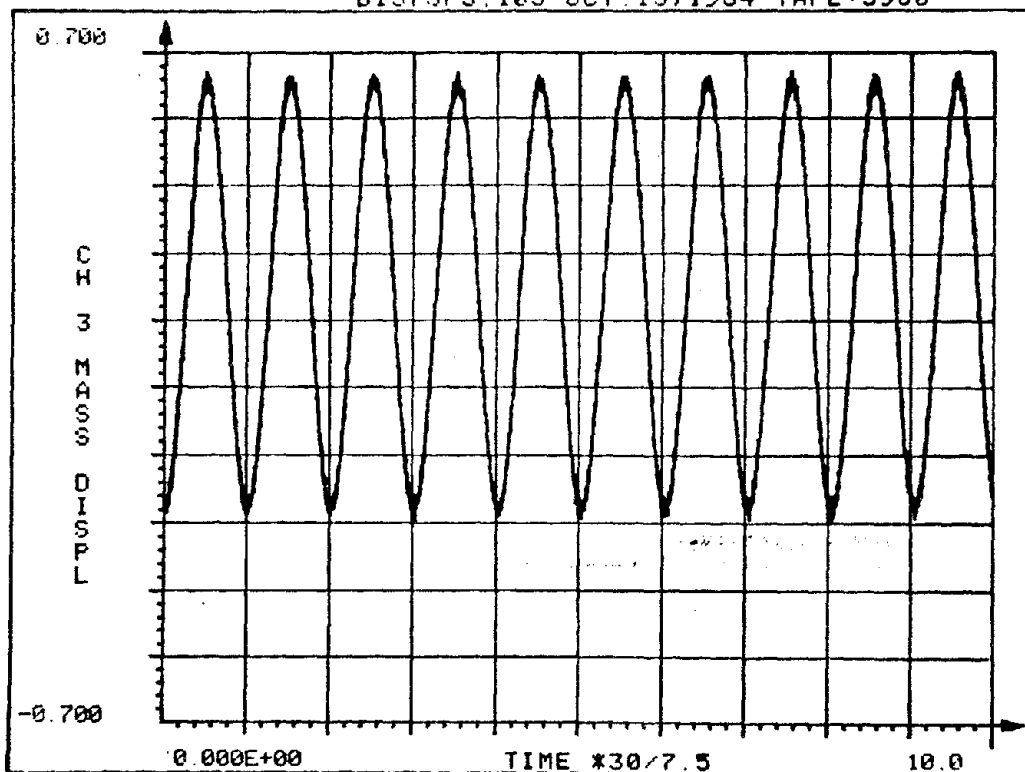
D1373P5.10S OCT.15,1984 TAPE:3980



D13.2

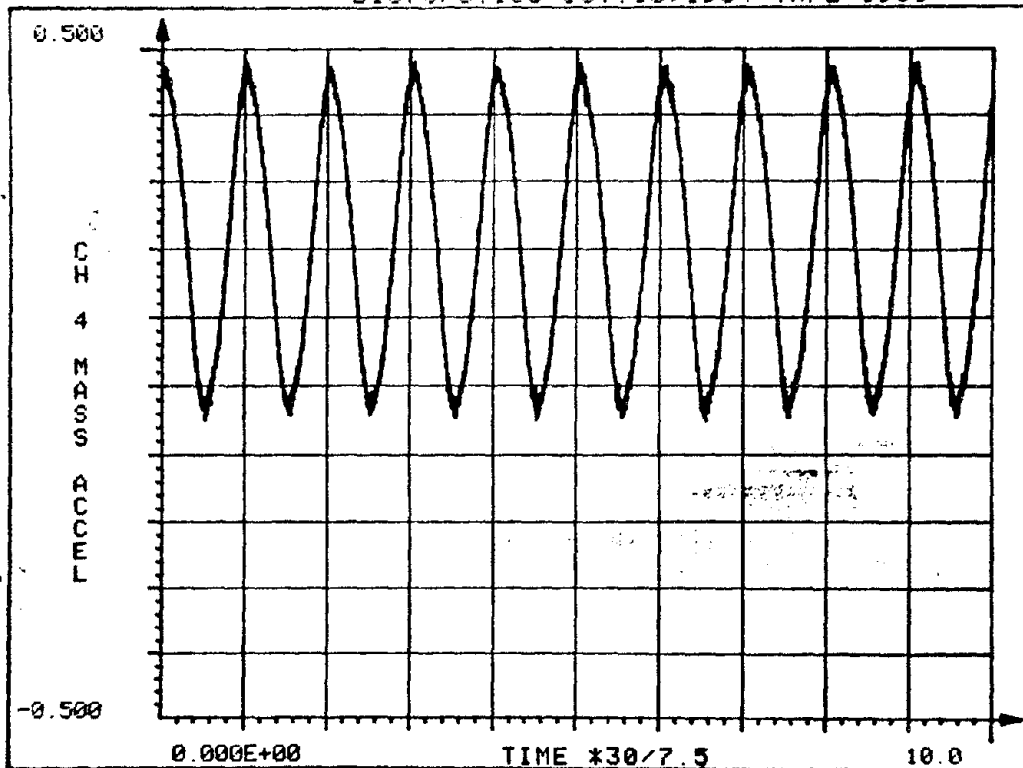
C-5

D1373P5.10S OCT. 15, 1984 TAPE: 3980

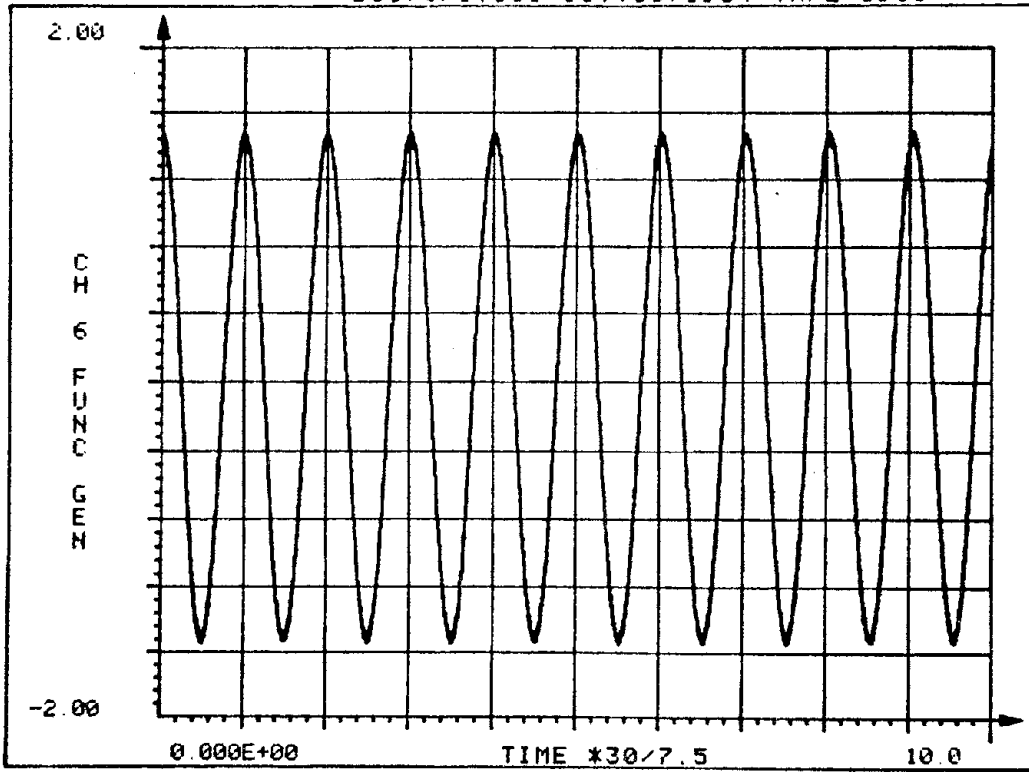


D13.3

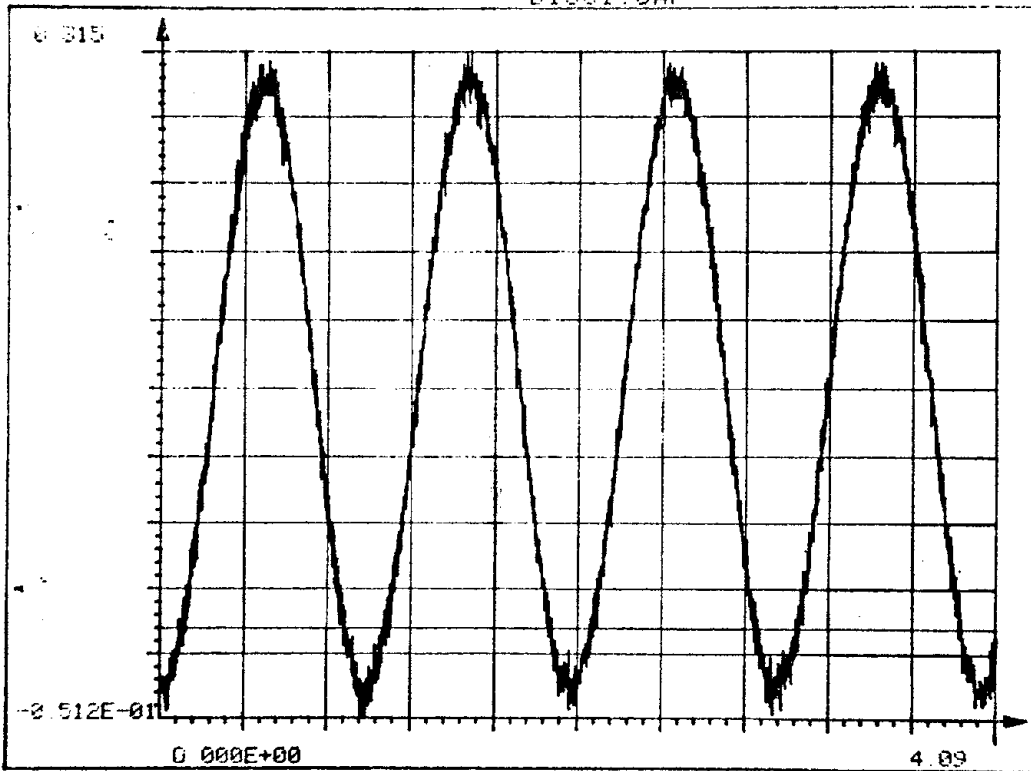
D1373P5.10S OCT. 15, 1984 TAPE: 3980



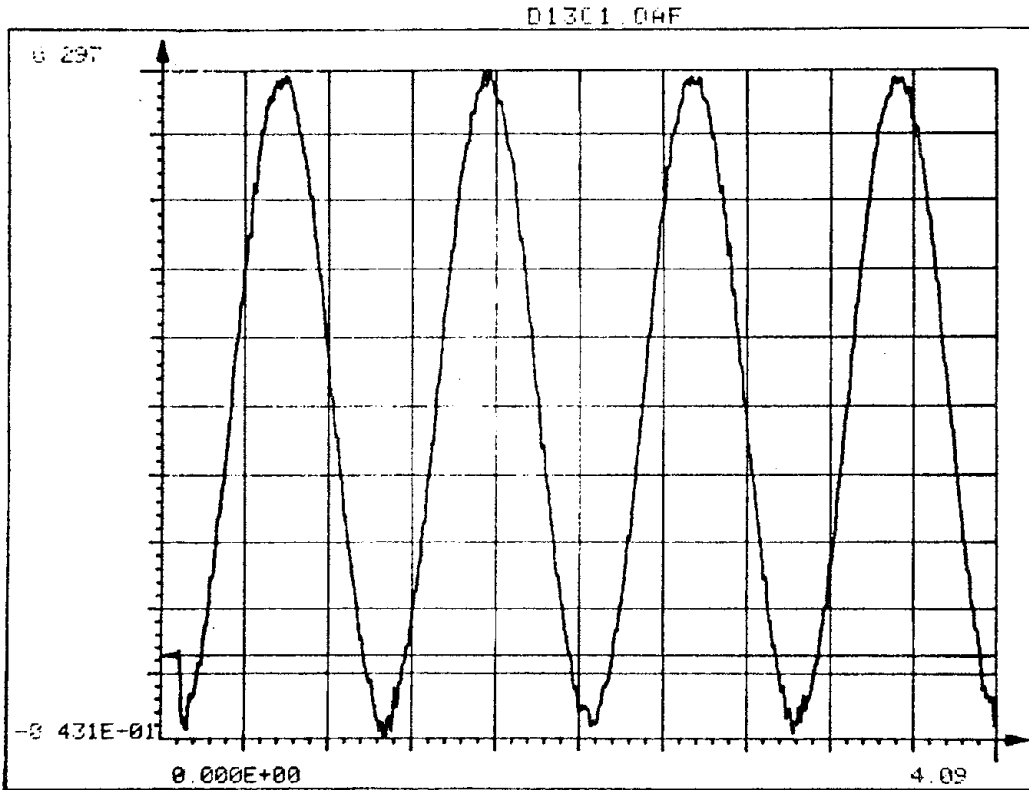
D13.4



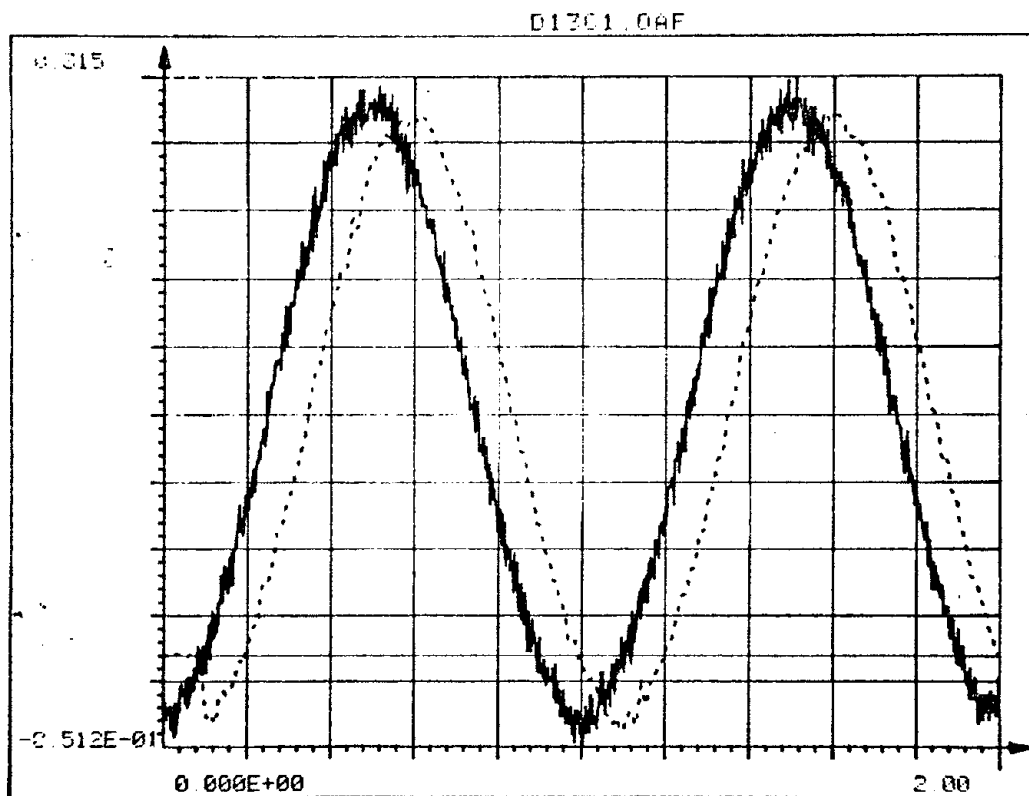
D13.5



D13.6



D13.7

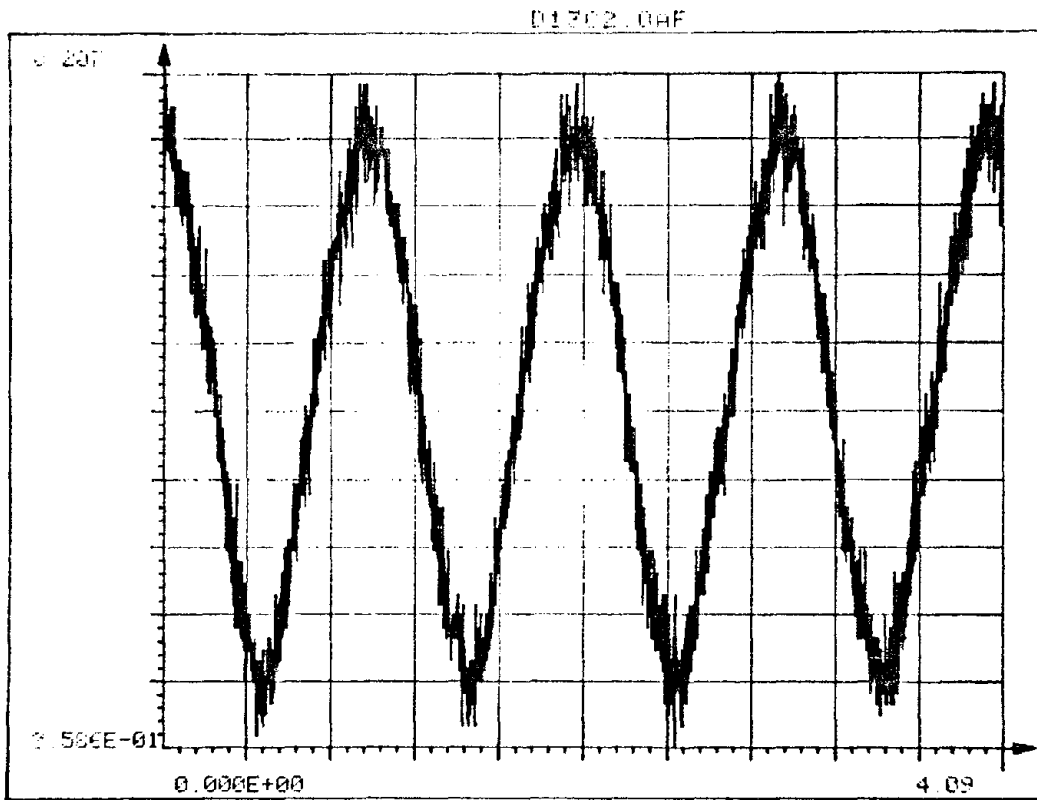


D13.8

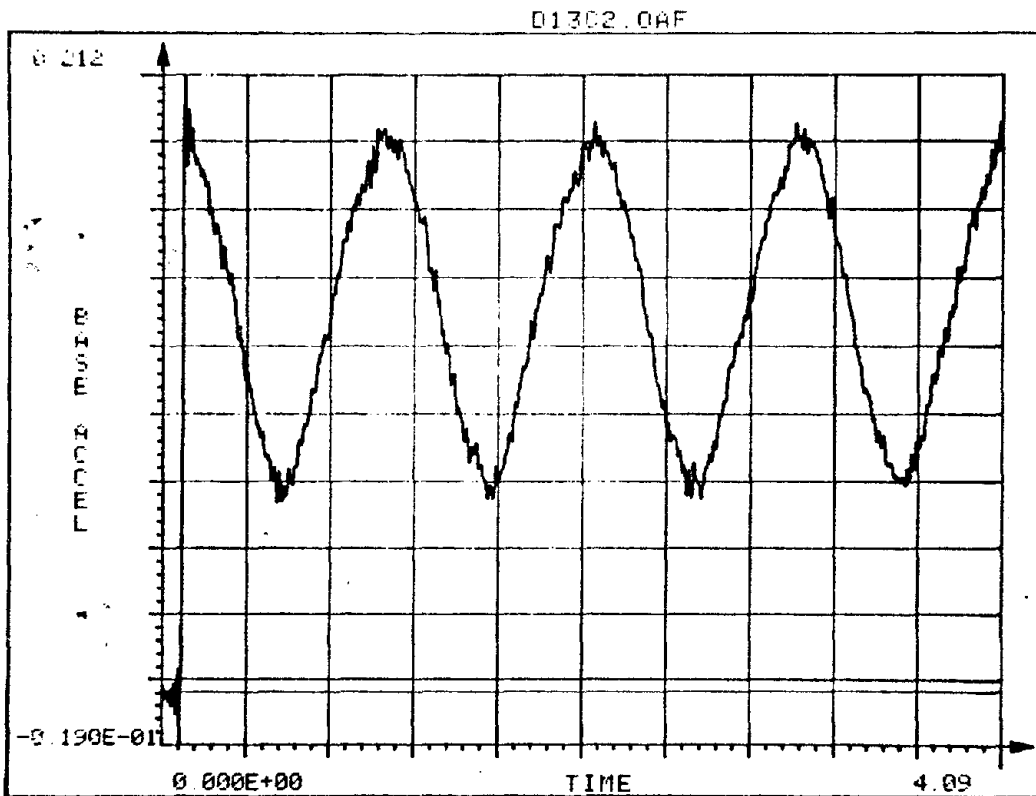
Reproduced from
best available copy.



C-8



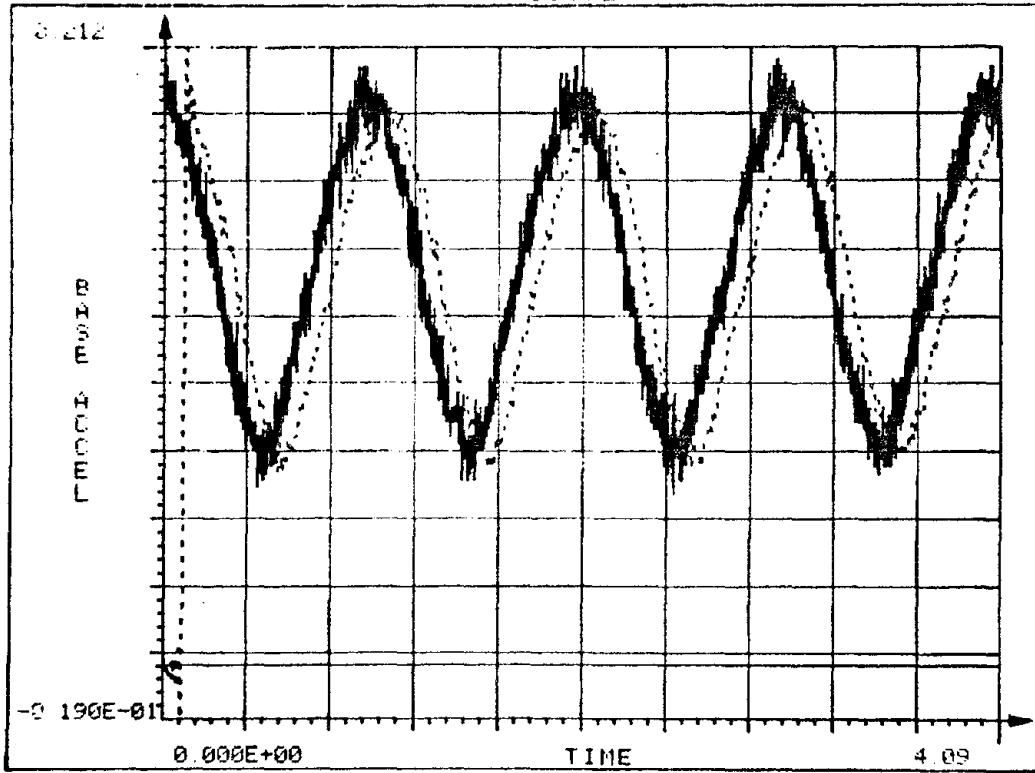
D13.9



D13.10

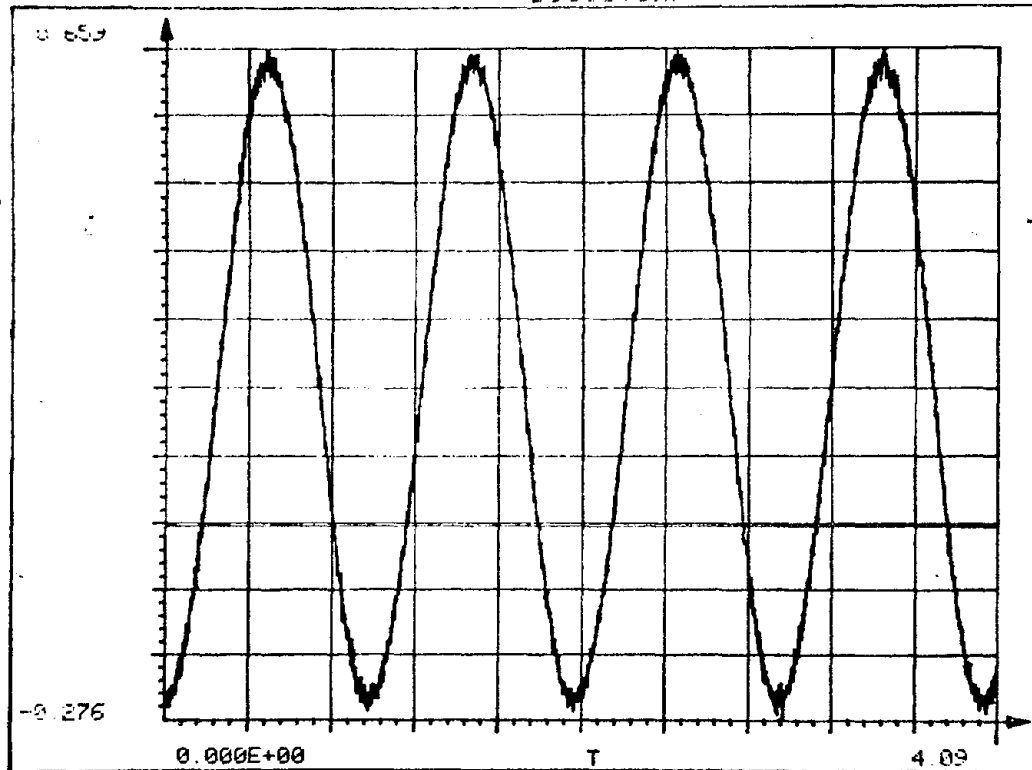
0-9

D1302.04F



D13.11

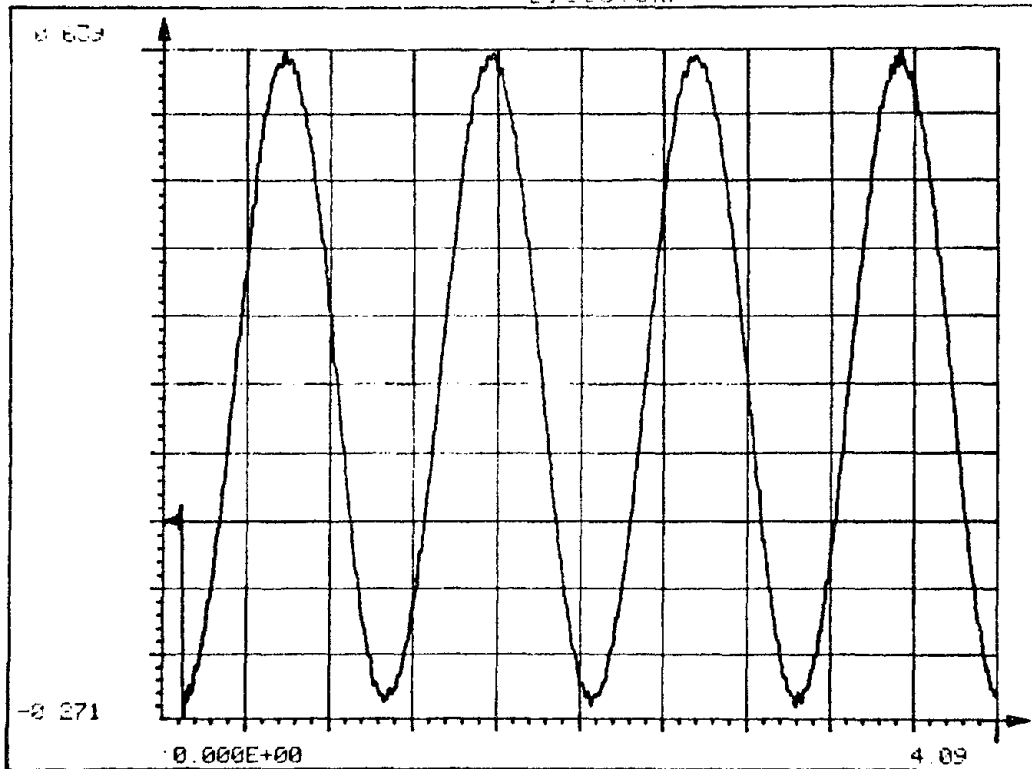
D1303.04F



D13.12

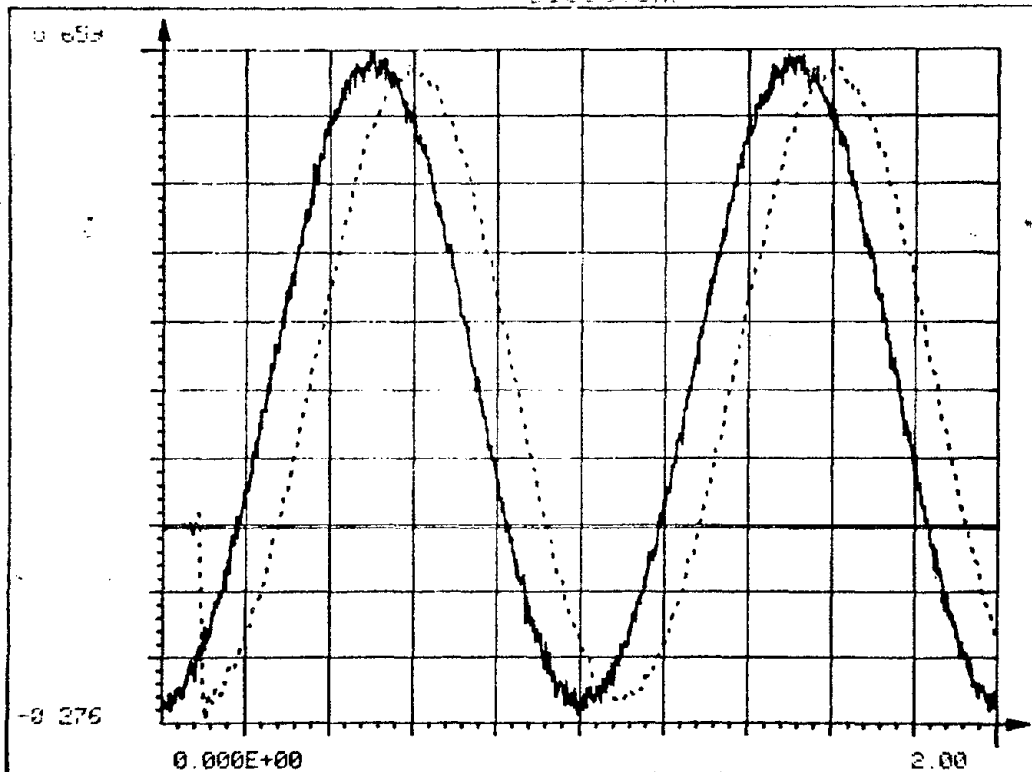
C-10

D1303.0AF



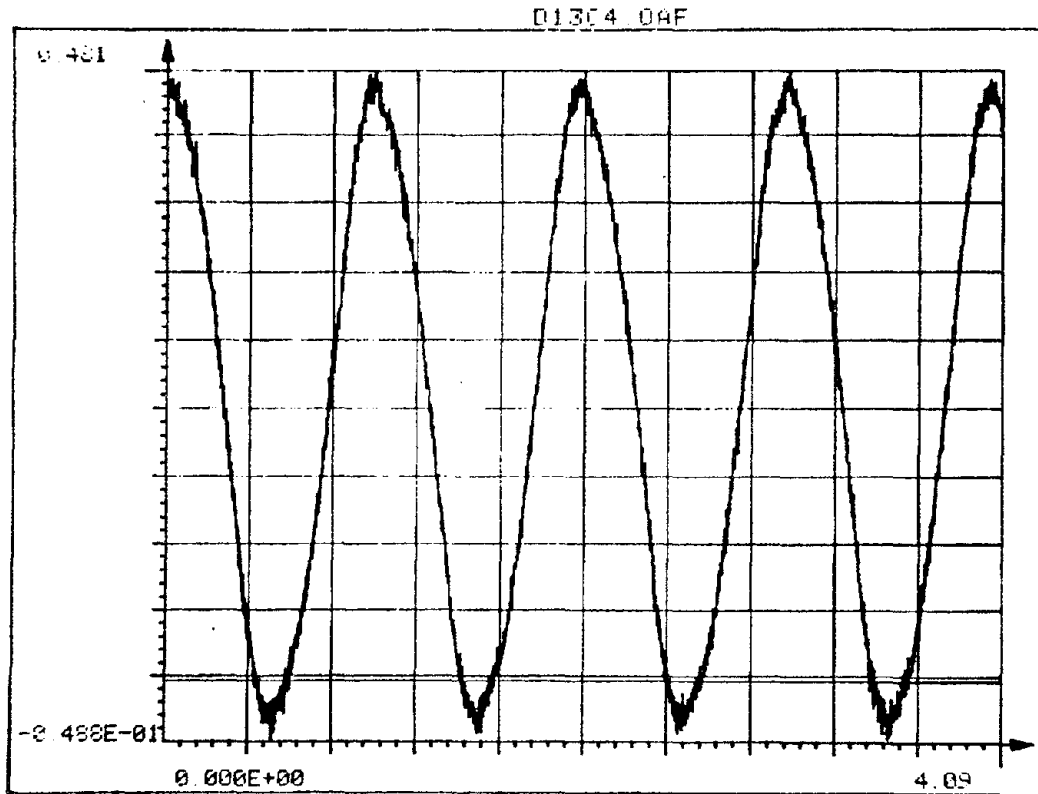
D13.13

D1303.0AF

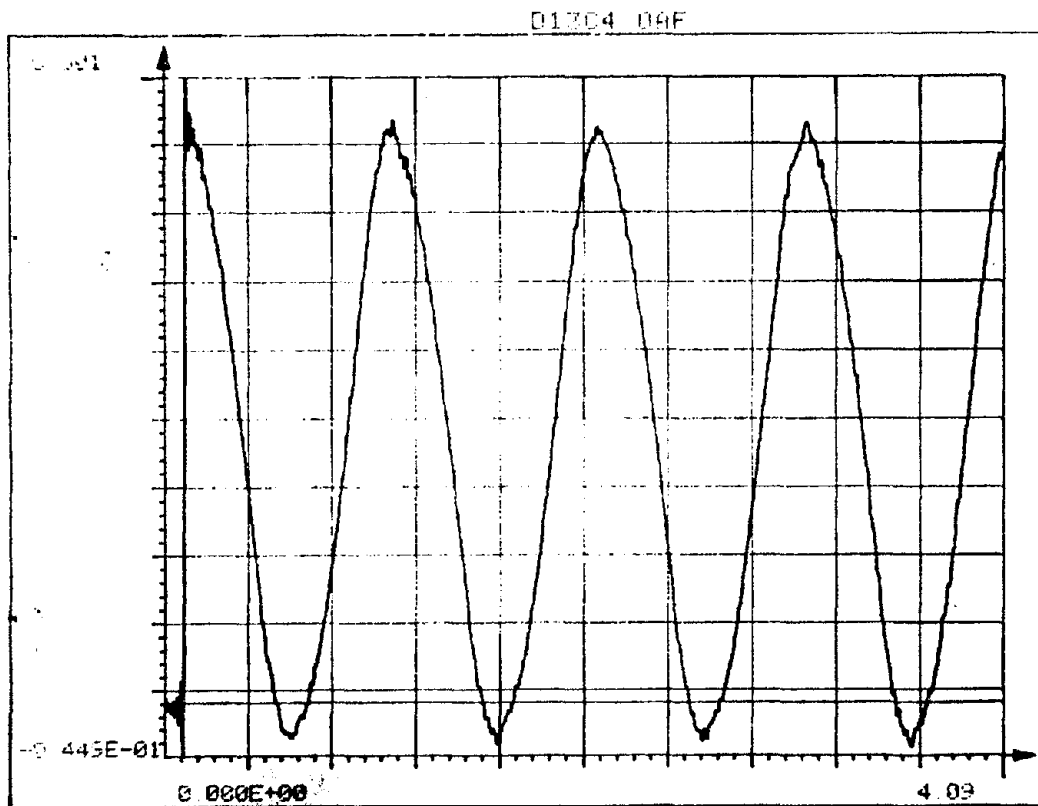


D13.14

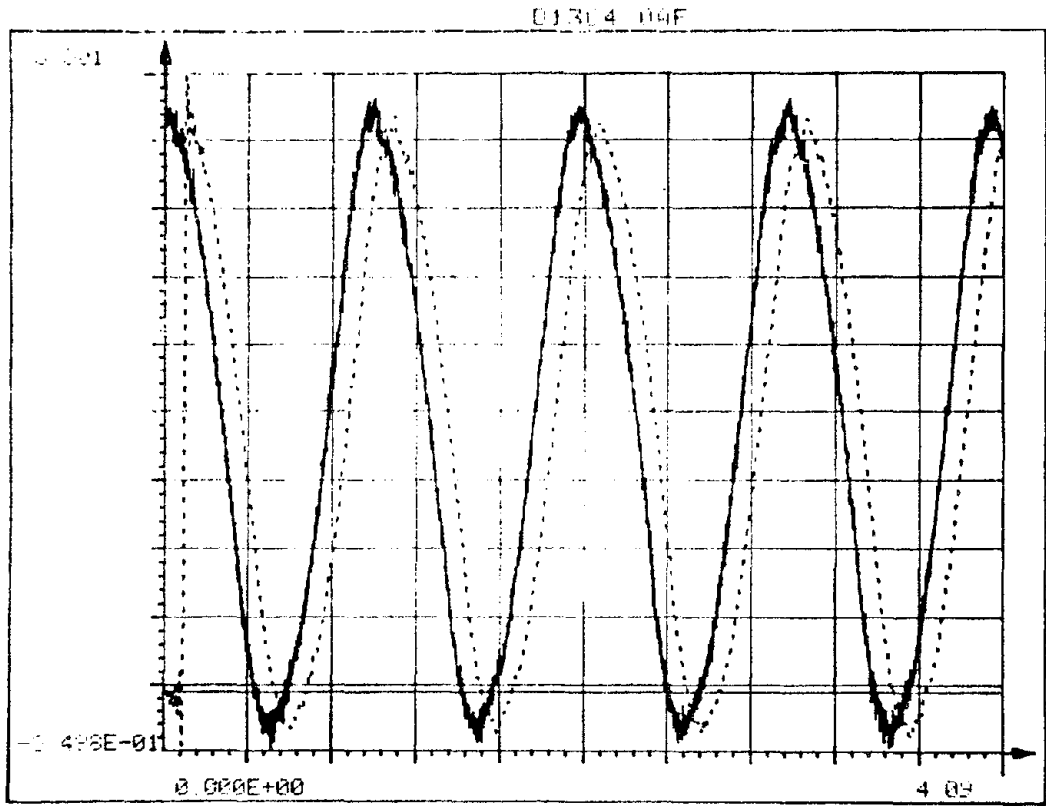
C-11



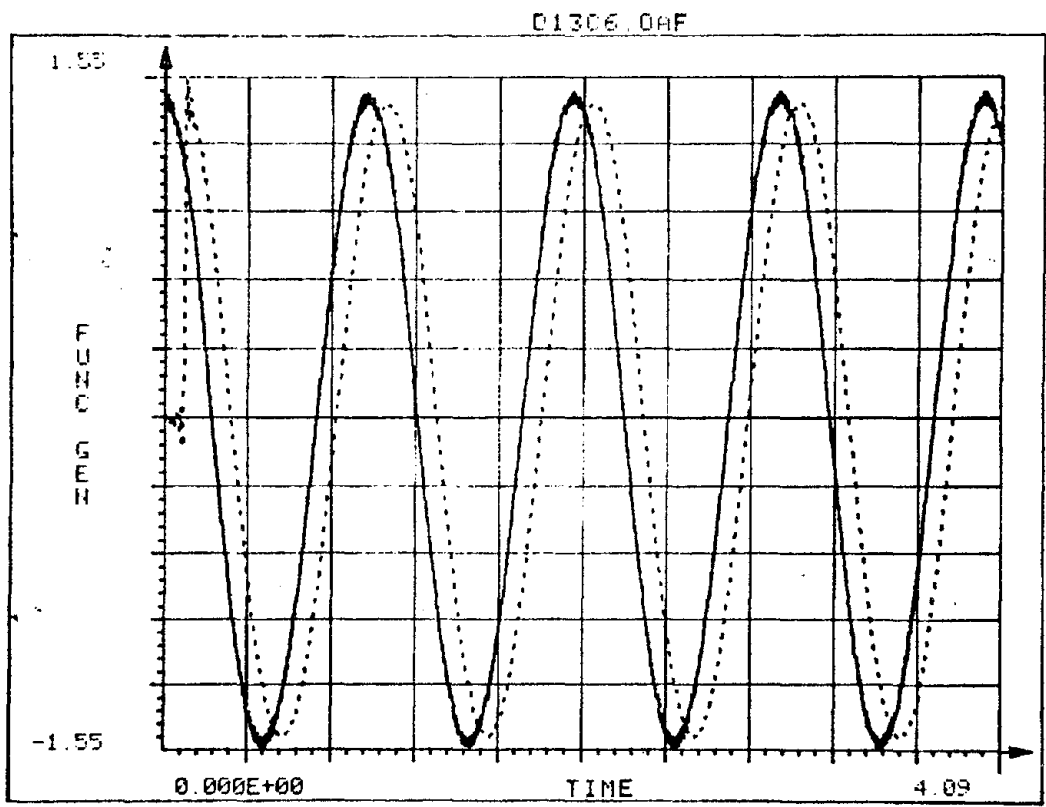
D13.15



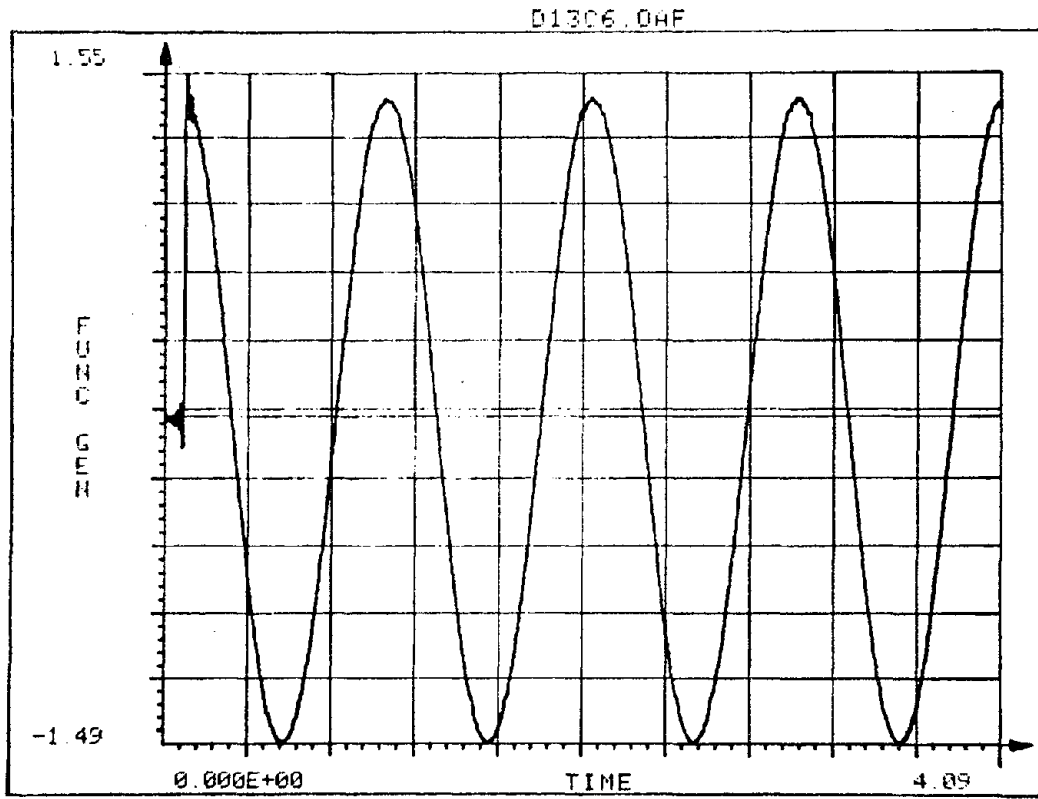
D13.16



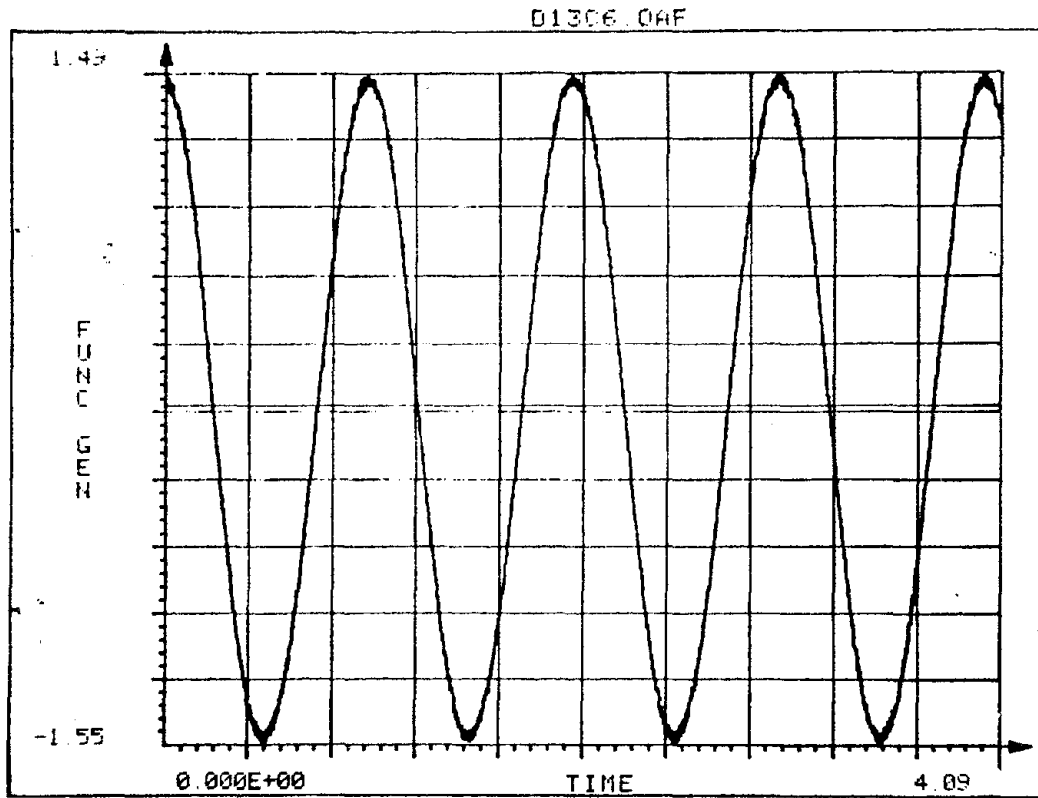
D13.17



D13.18

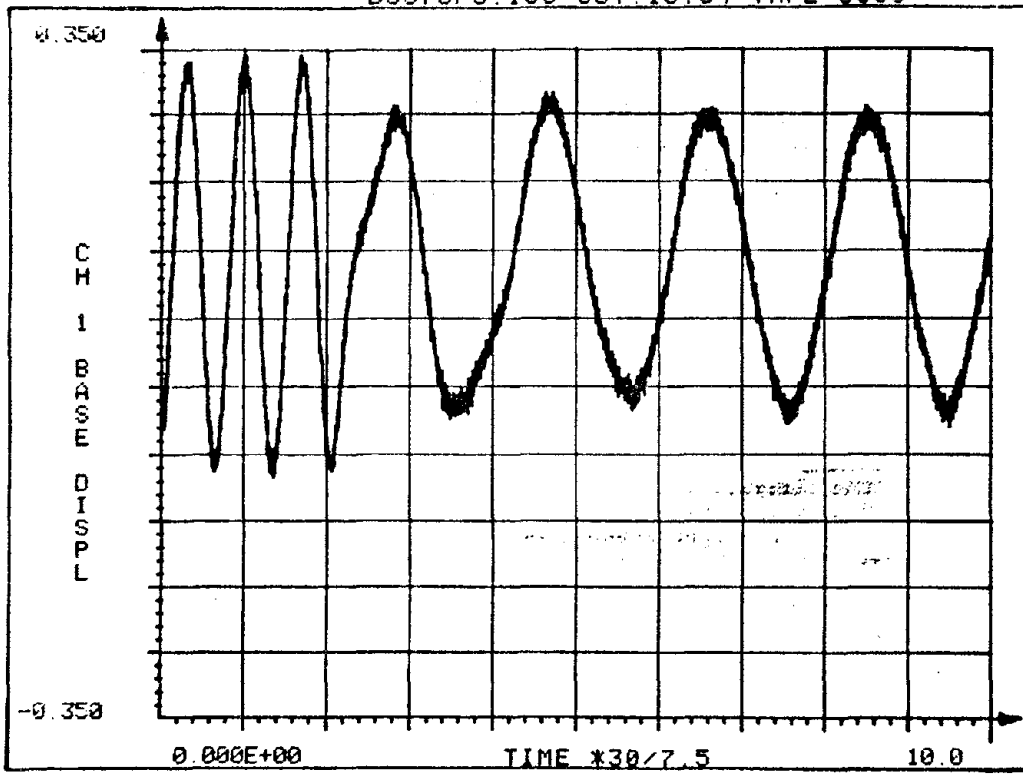


D13.19



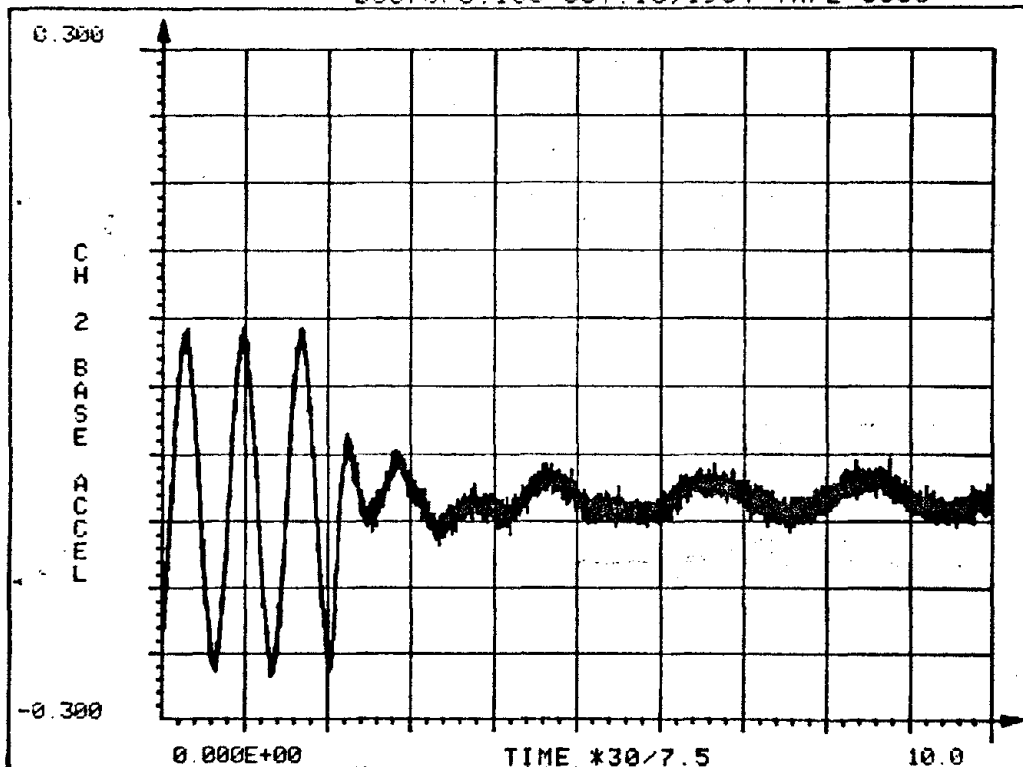
D13.20

D3373P5.10S OCT. 15.84 TAPE:5300

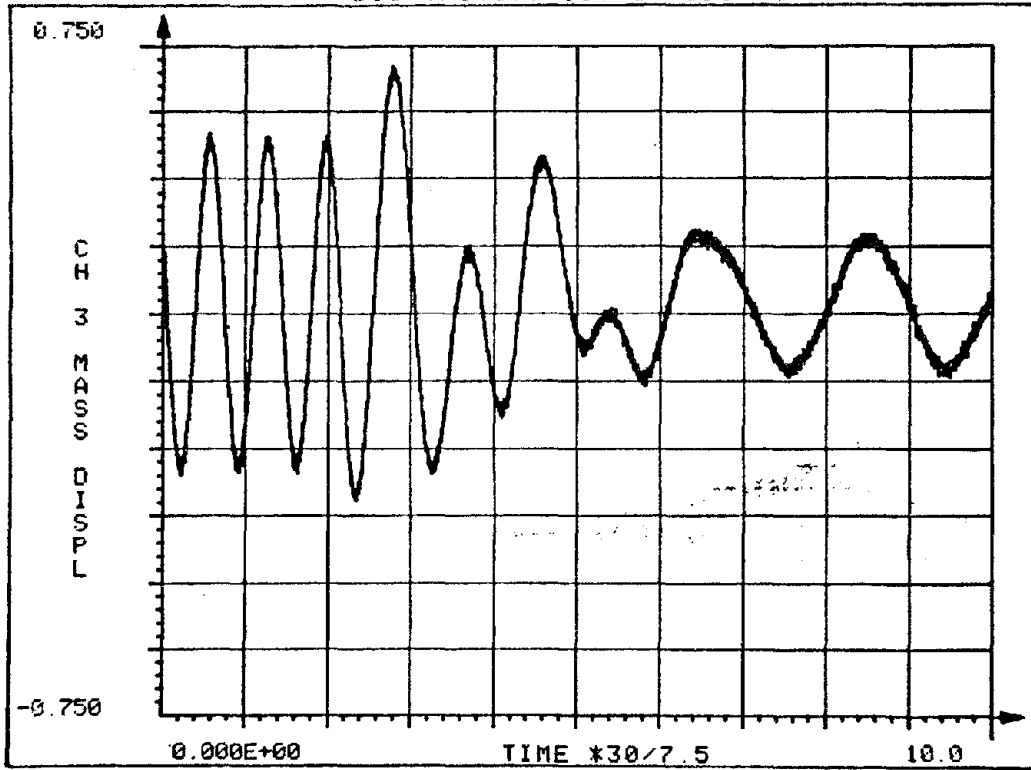


D33.1

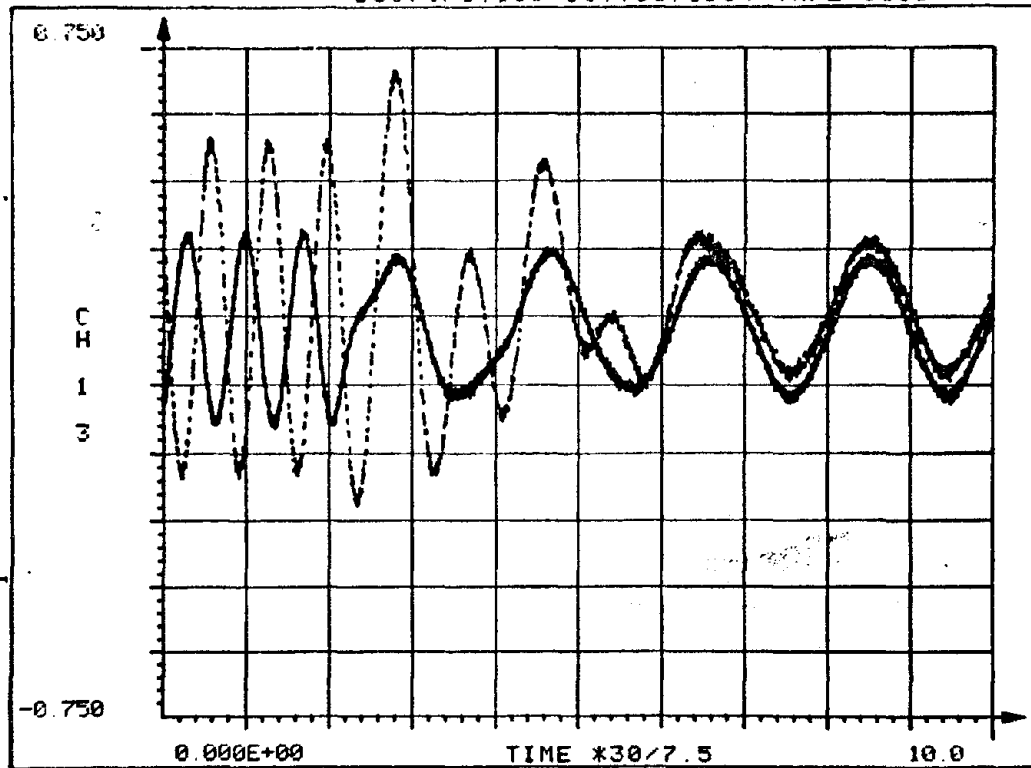
D3373P5.10S OCT. 15, 1984 TAPE:5300



D33.2

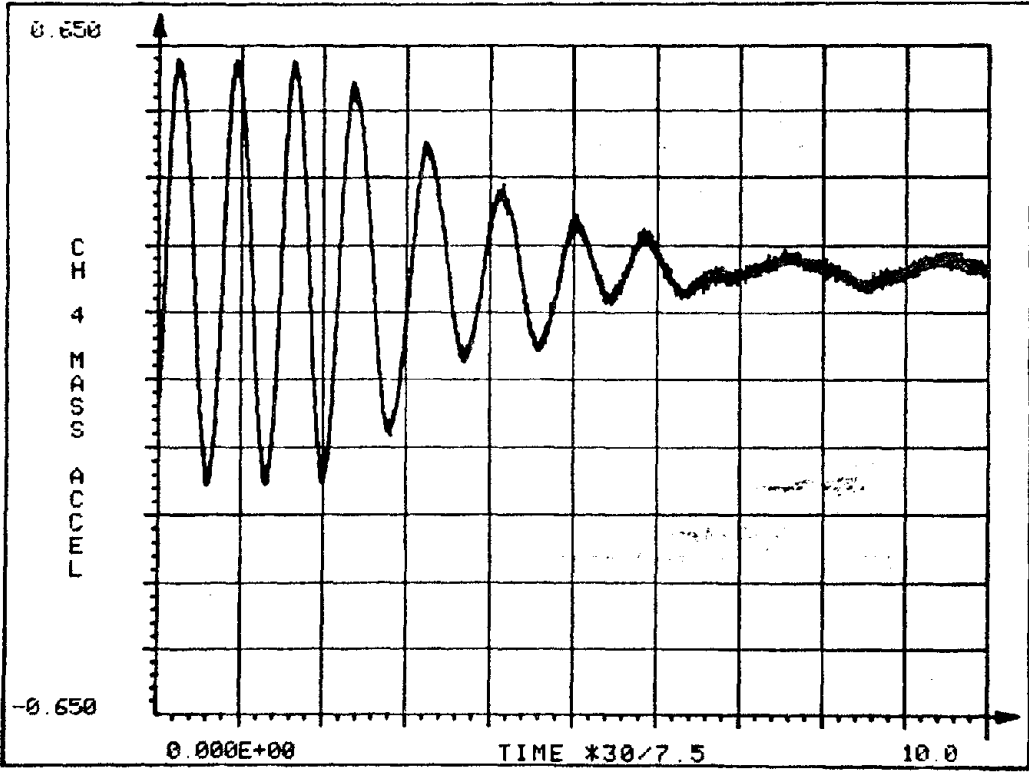


D33.3



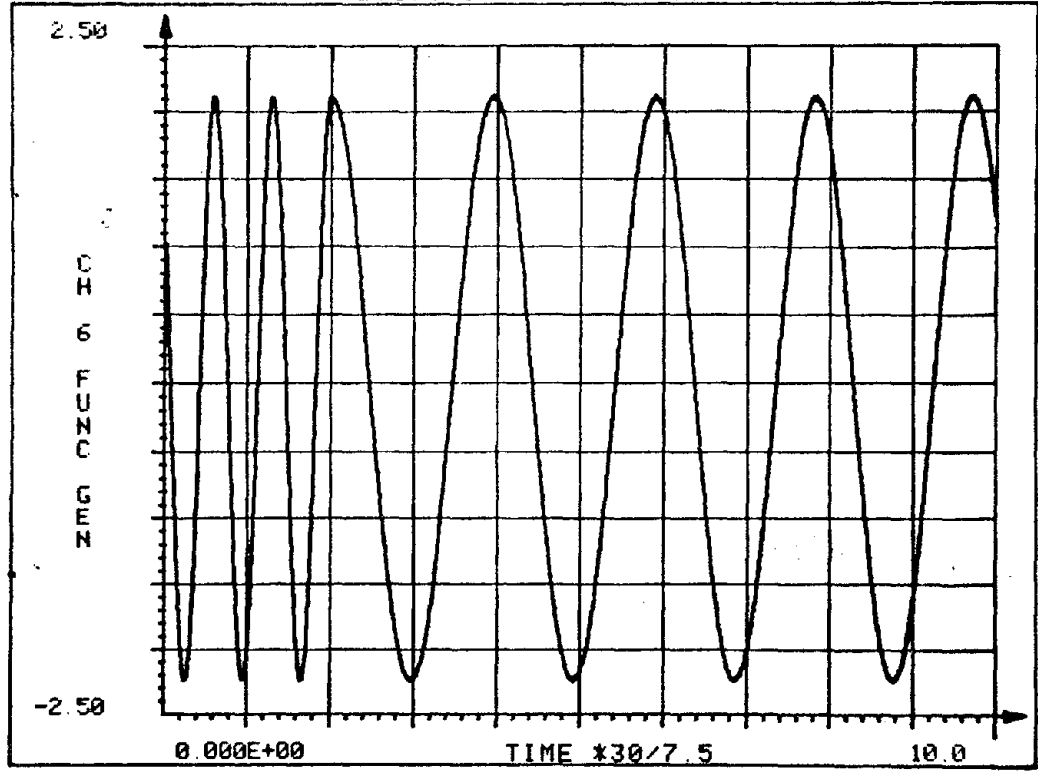
D33.4

D3373P5.10S OCT. 15, 1984 TAPE 5300

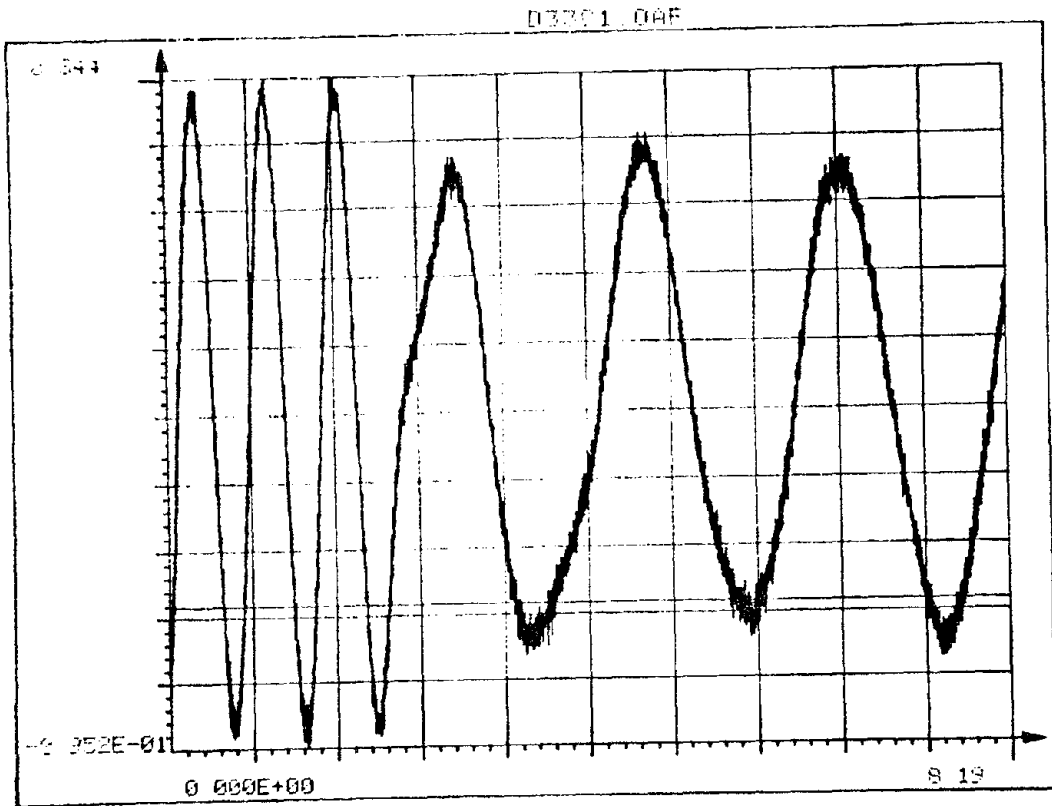


D33.5

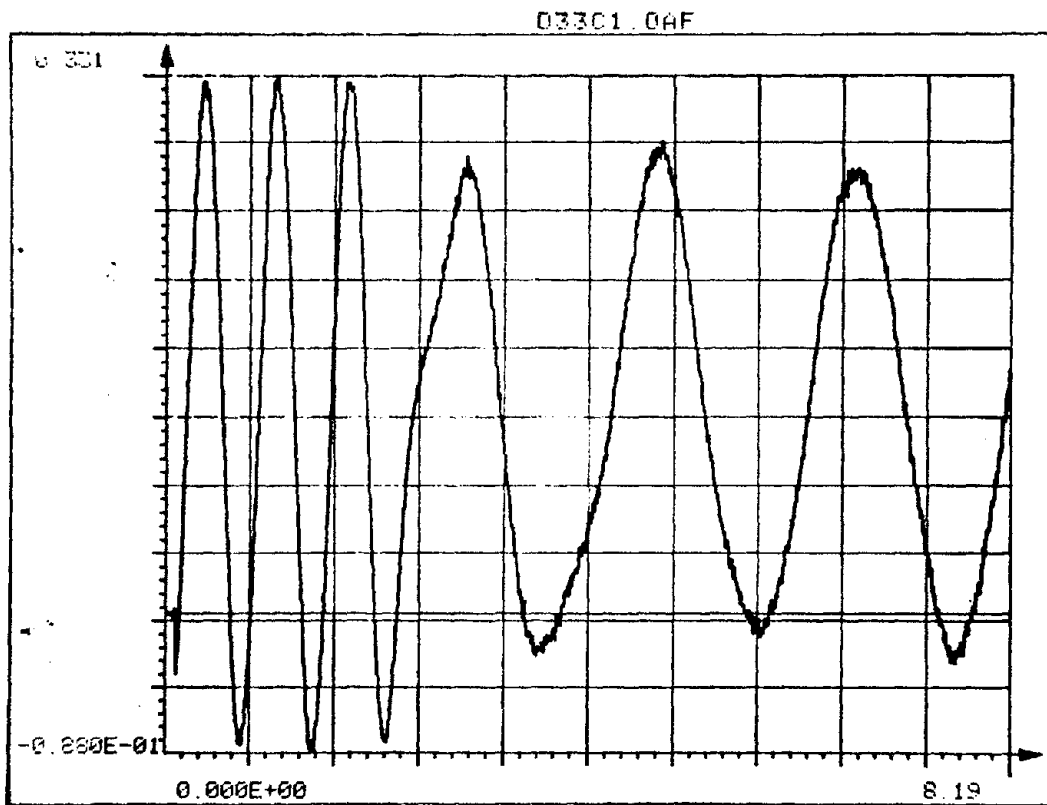
D3373P5.10S OCT. 15, 1984 TAPE 5300



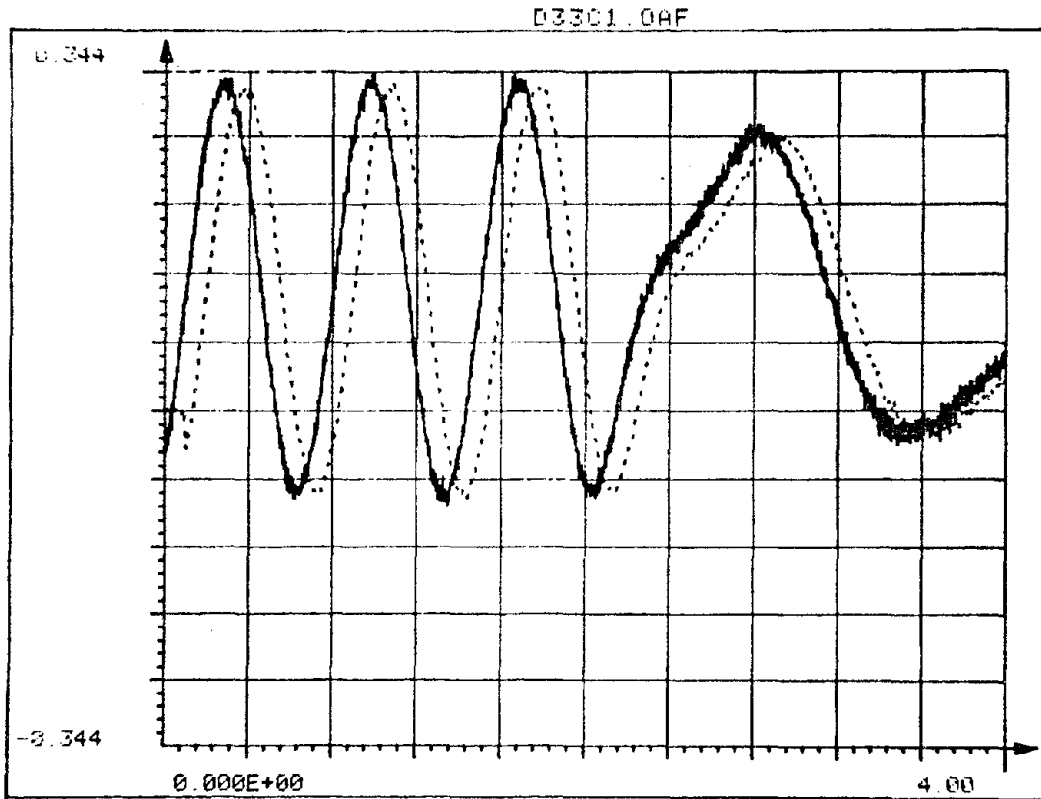
D33.6



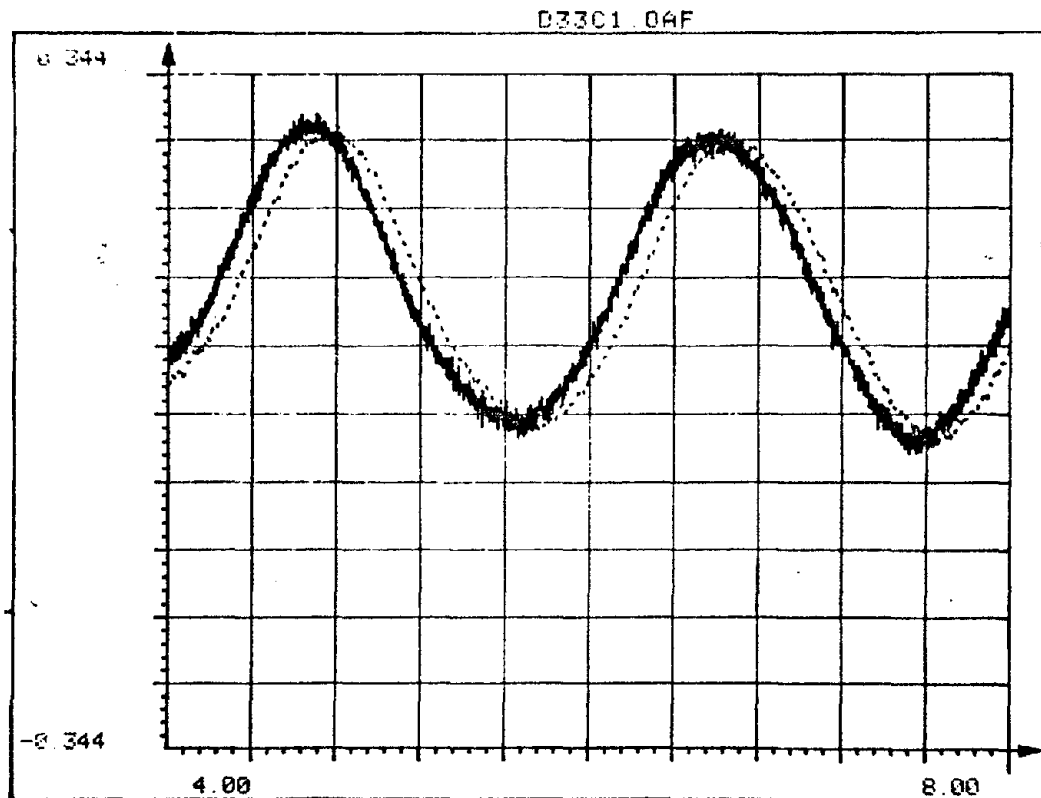
D33.7



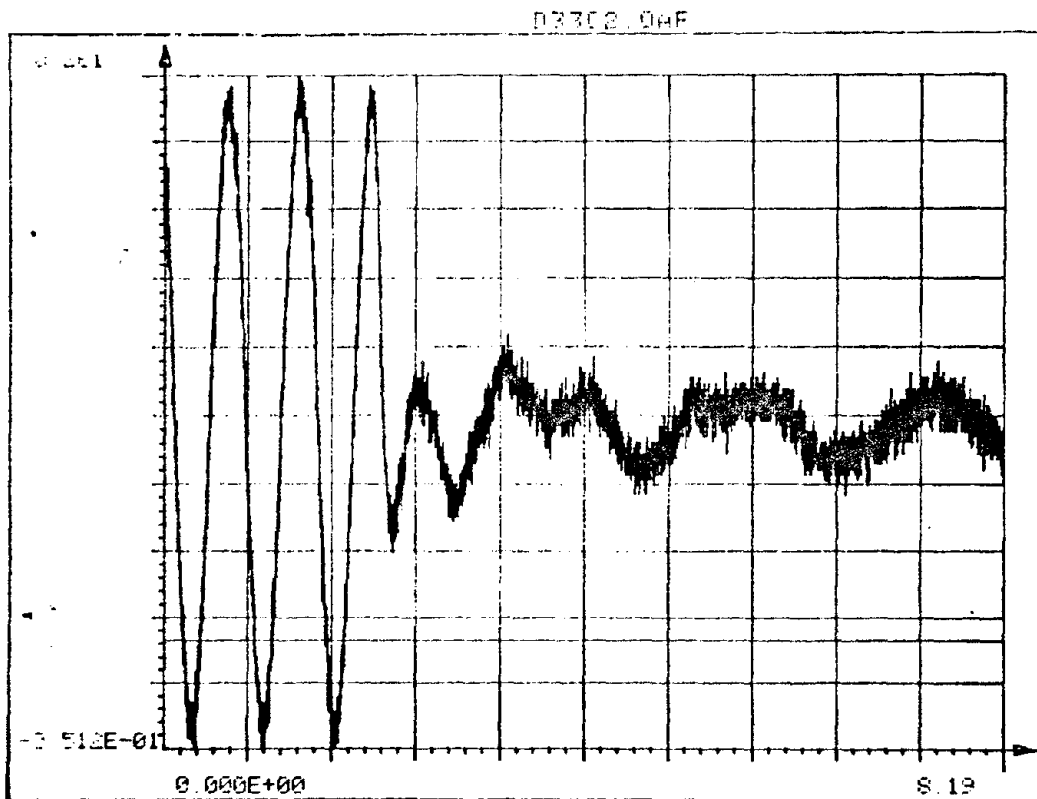
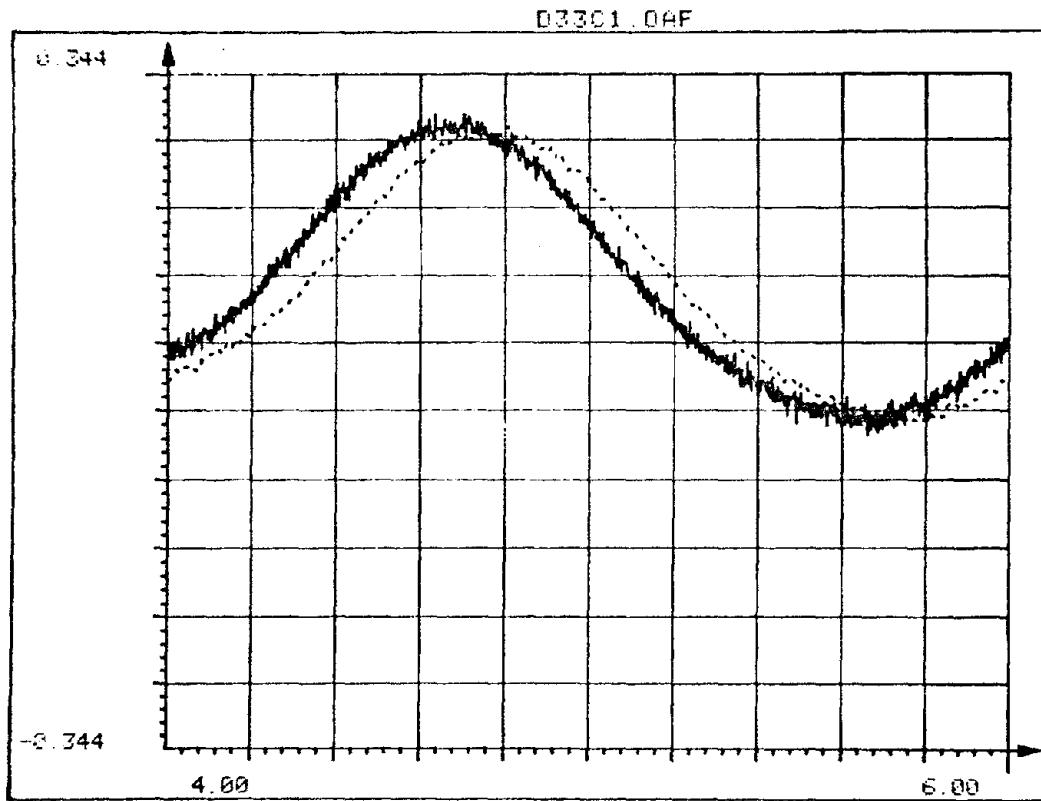
D33.8

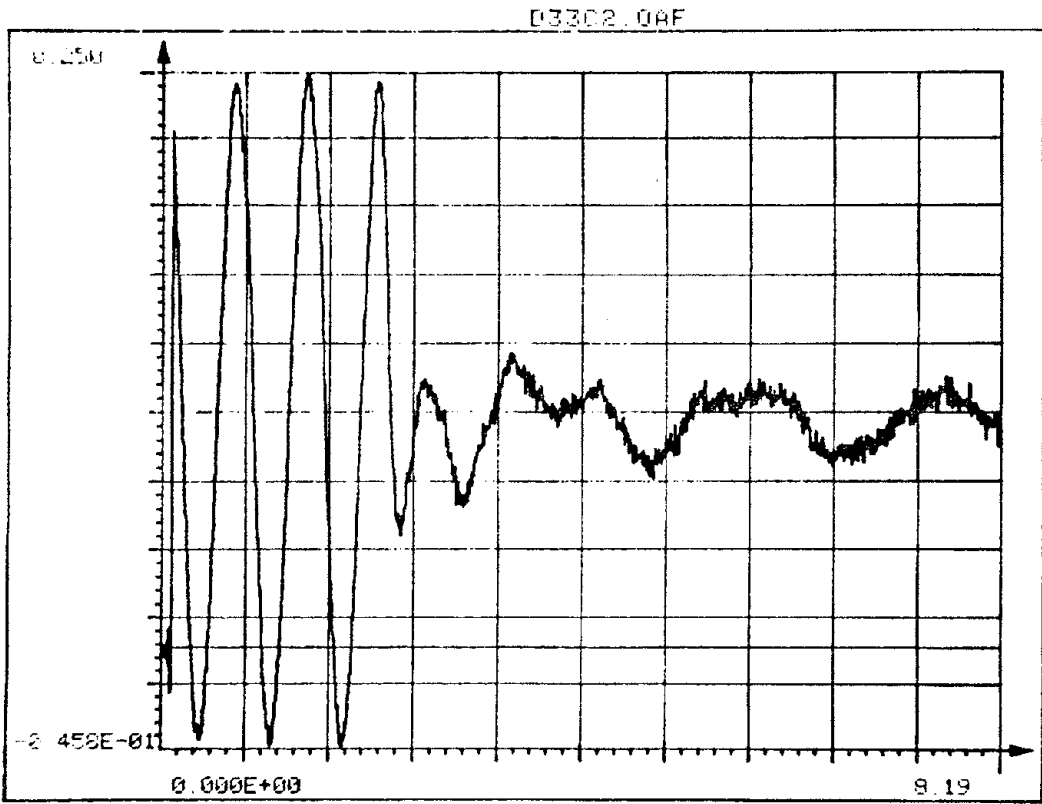


D33.9

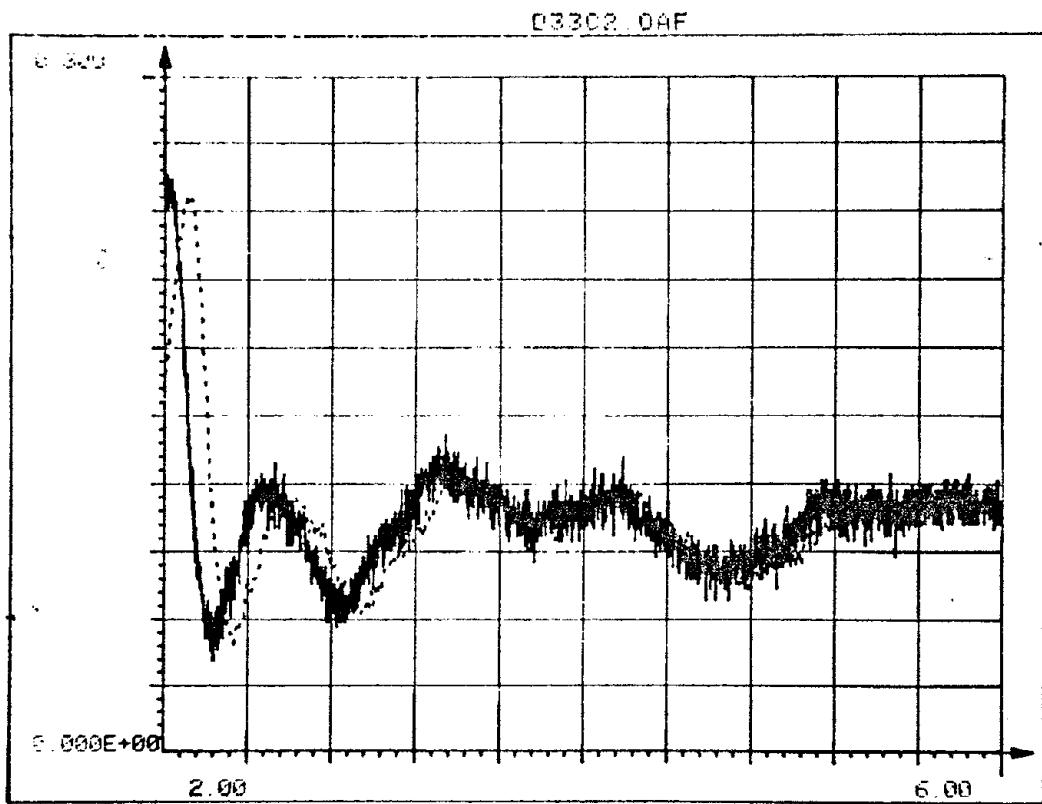


D33.10





D33.13

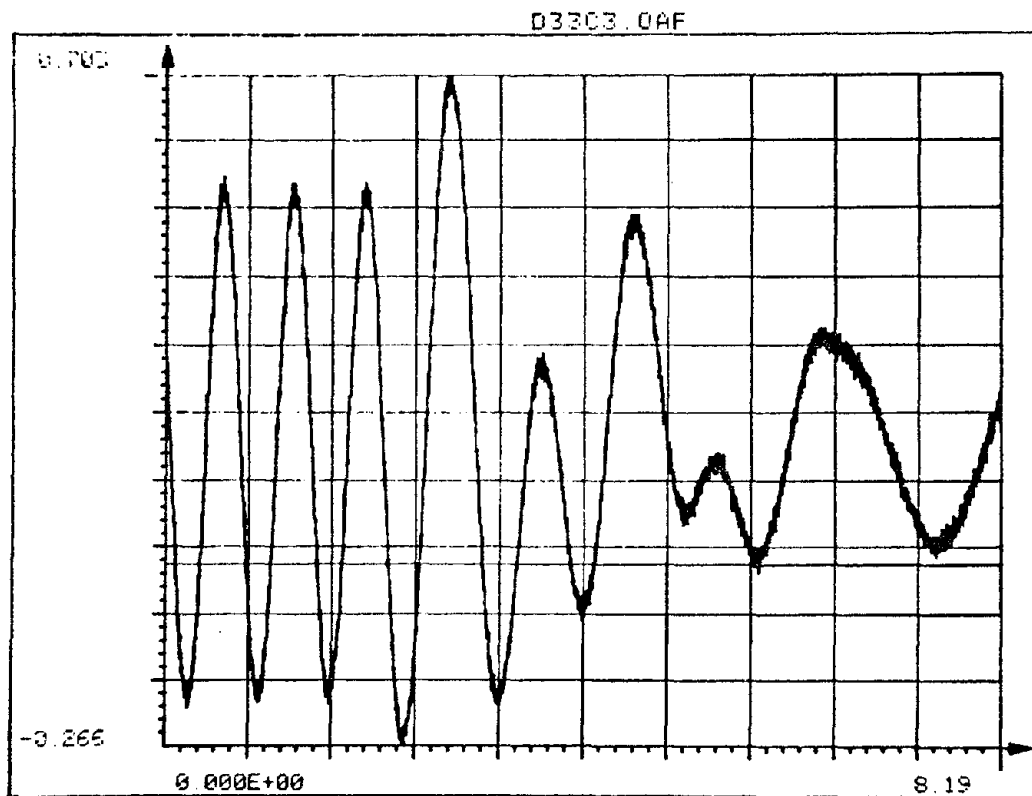


D33.14

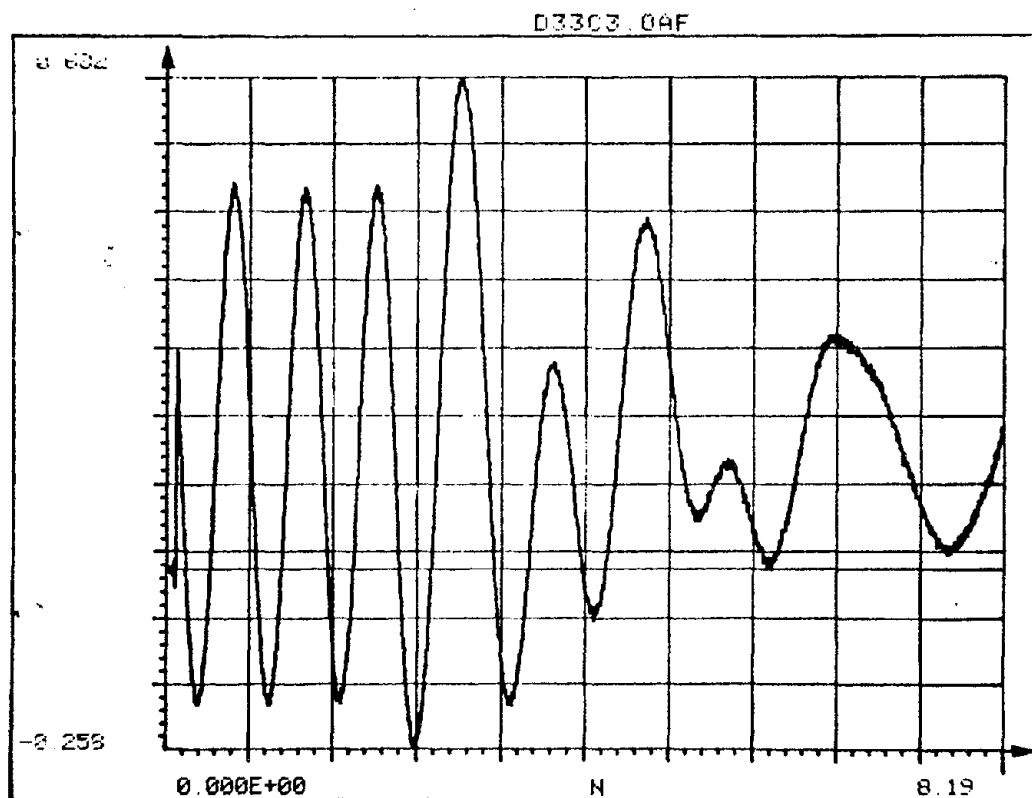
Reproduced from
best available copy.



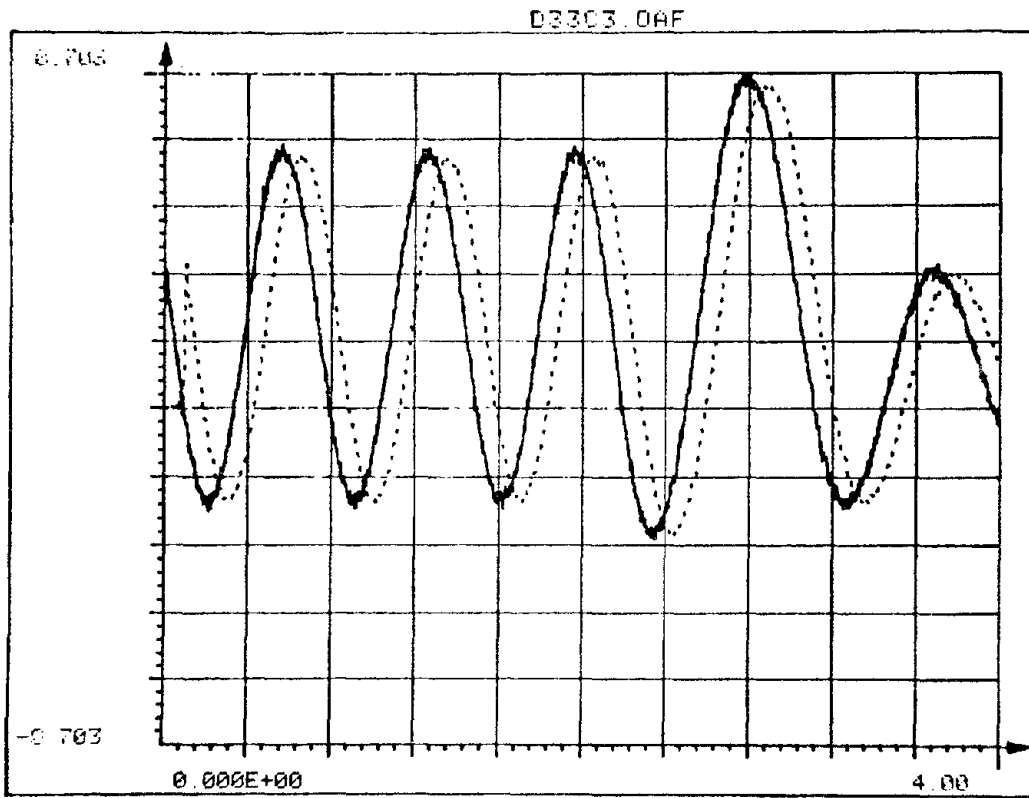
0-21



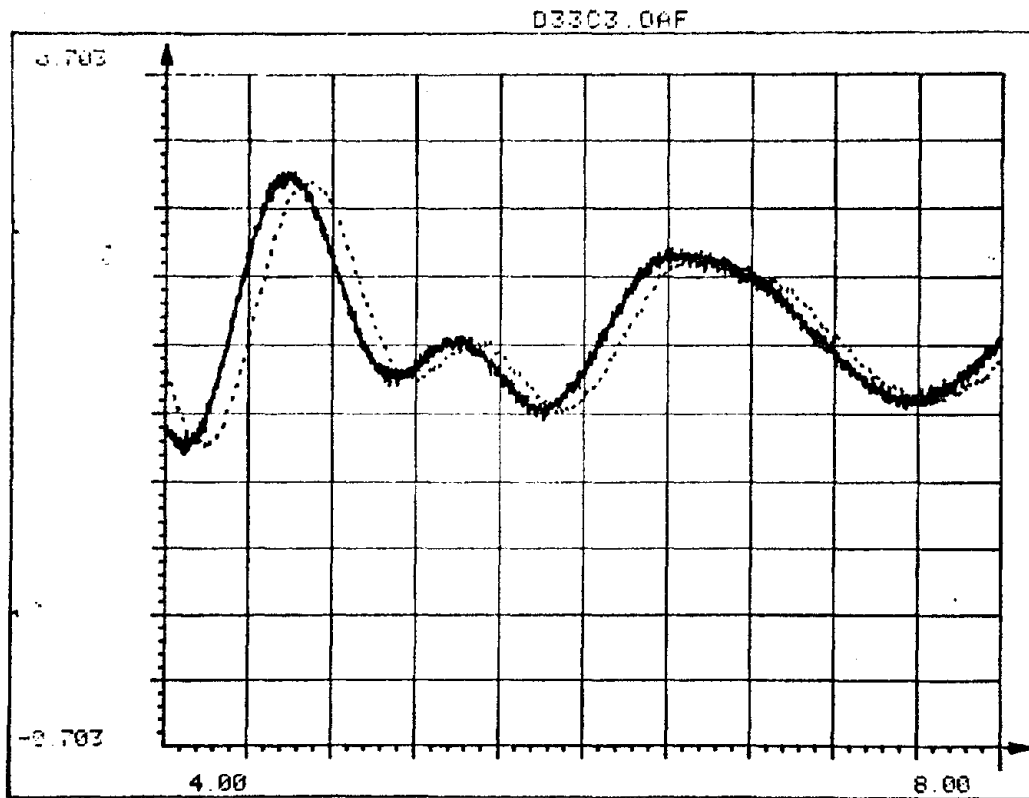
D33.15



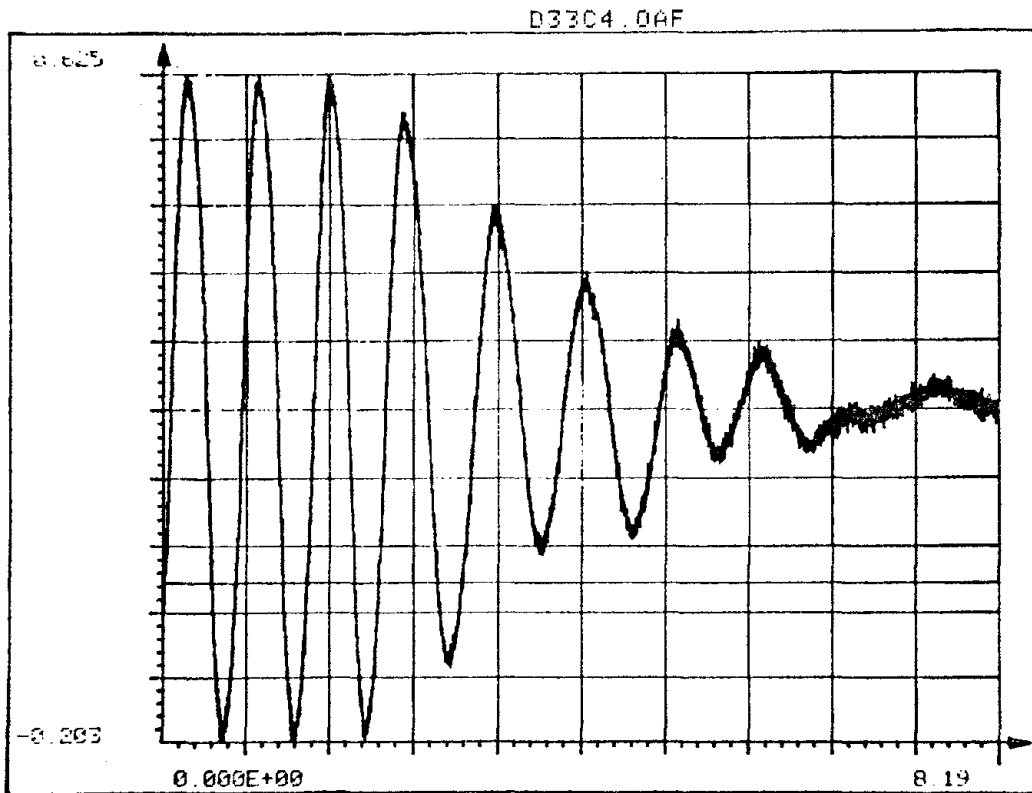
D33.16



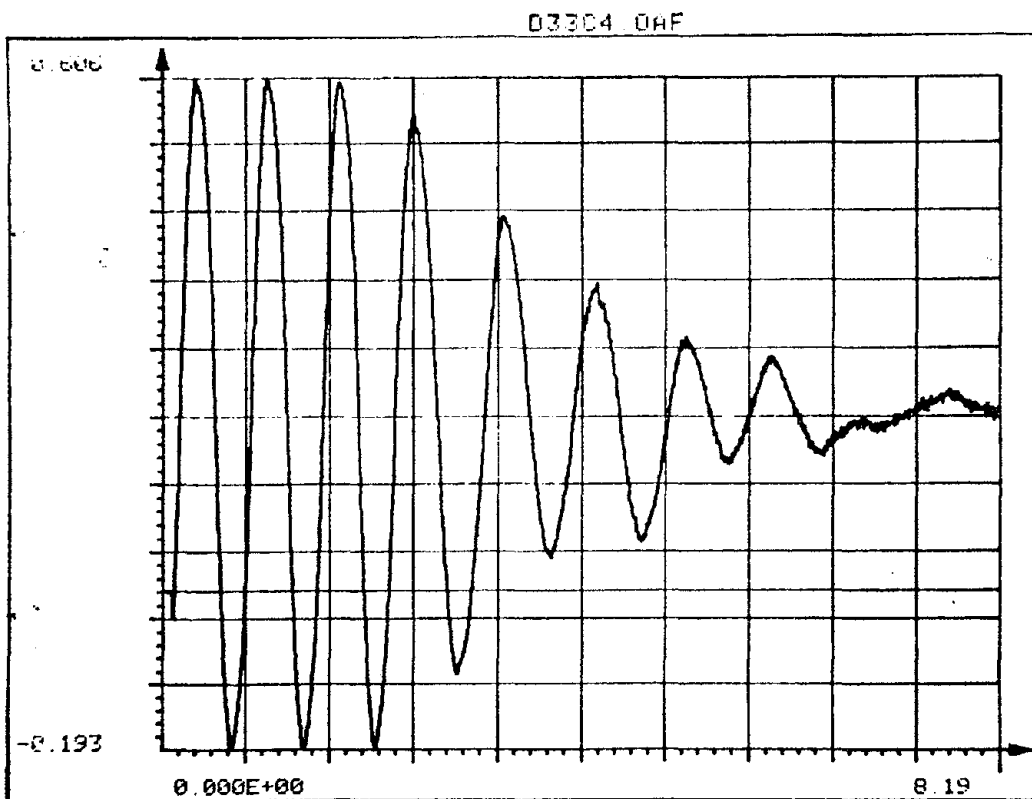
D33.17



D33.18

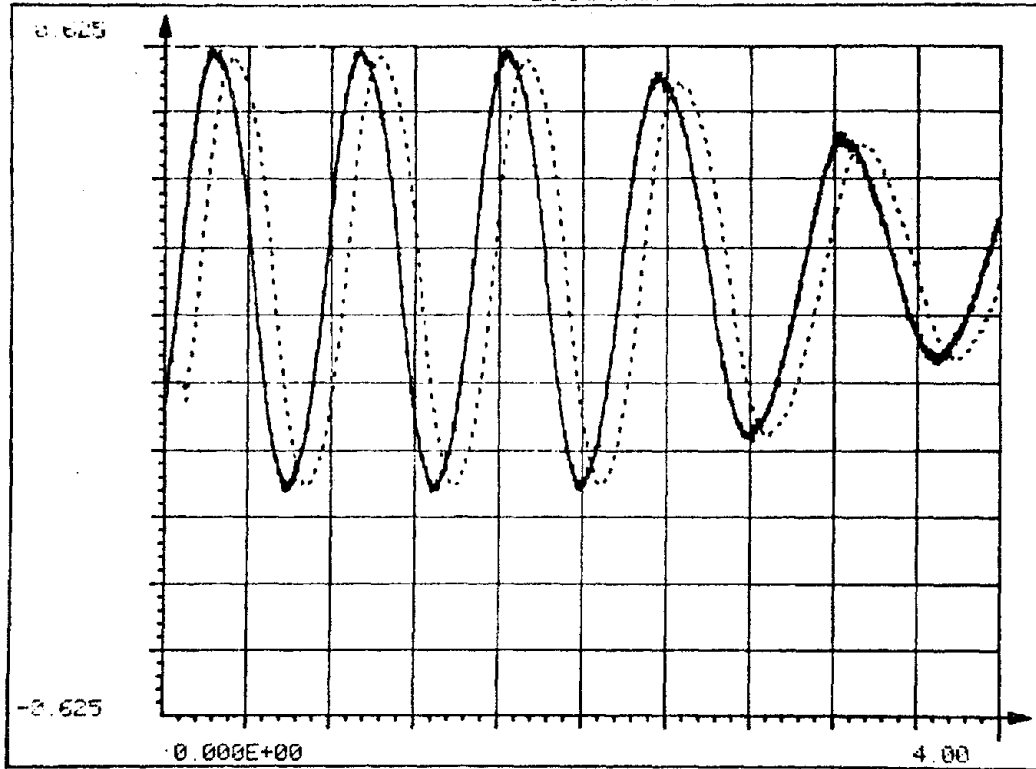


D33.19



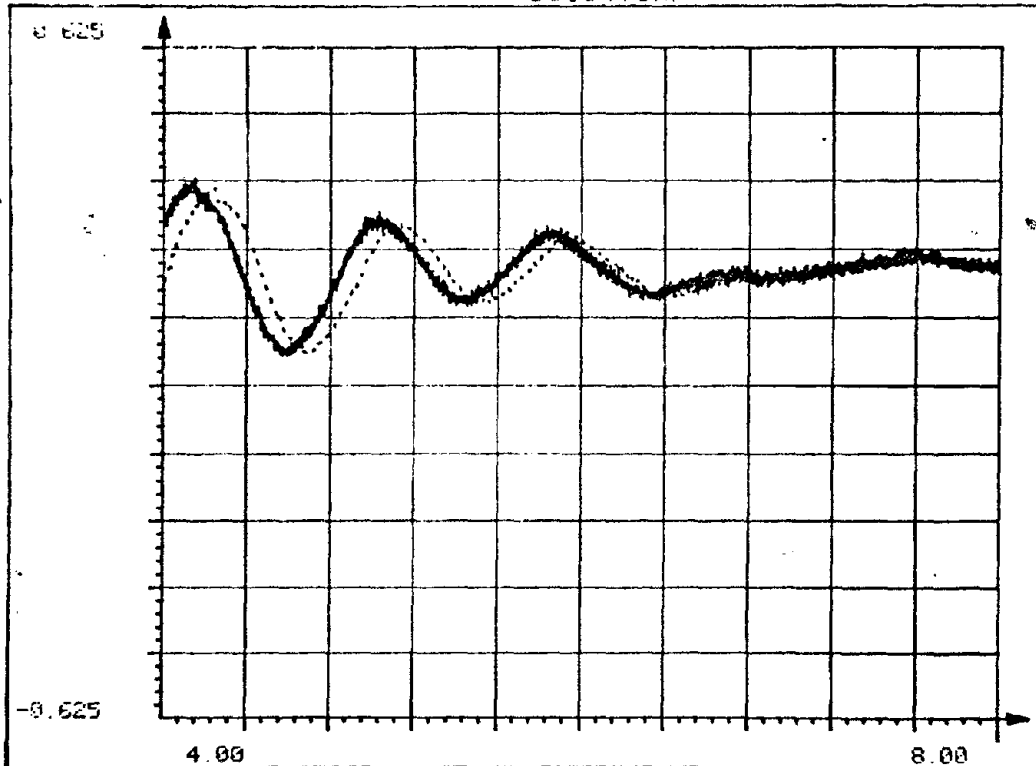
D33.24

D33D4.0AF



D33.21

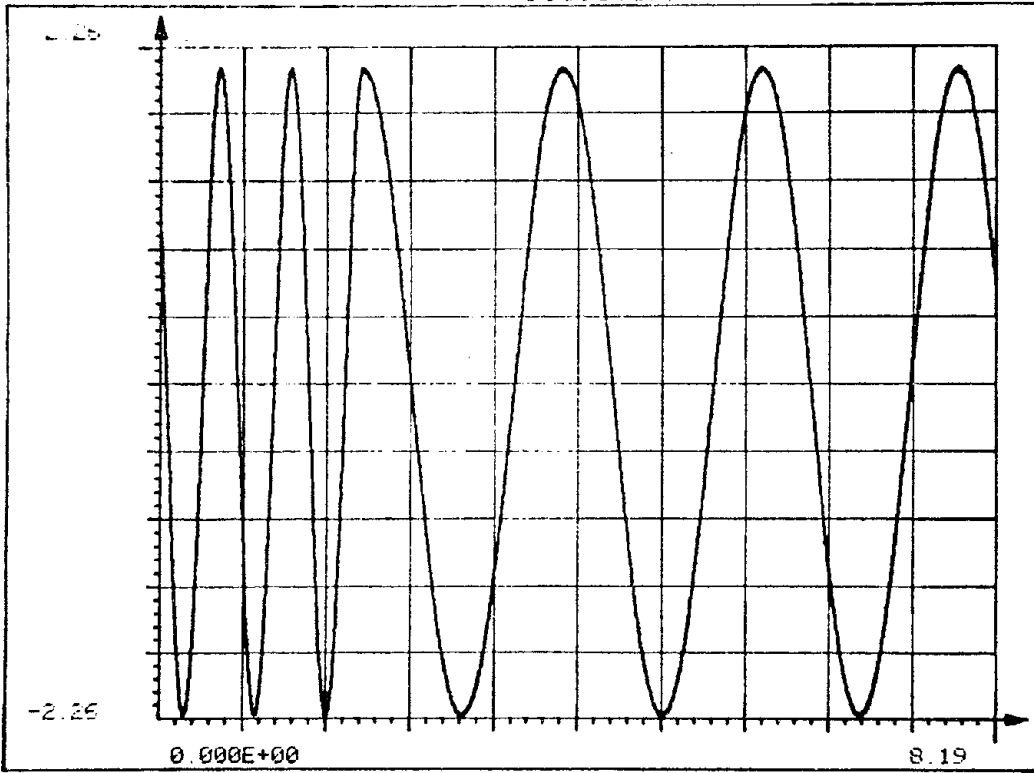
D33C4.0AF



D33.22

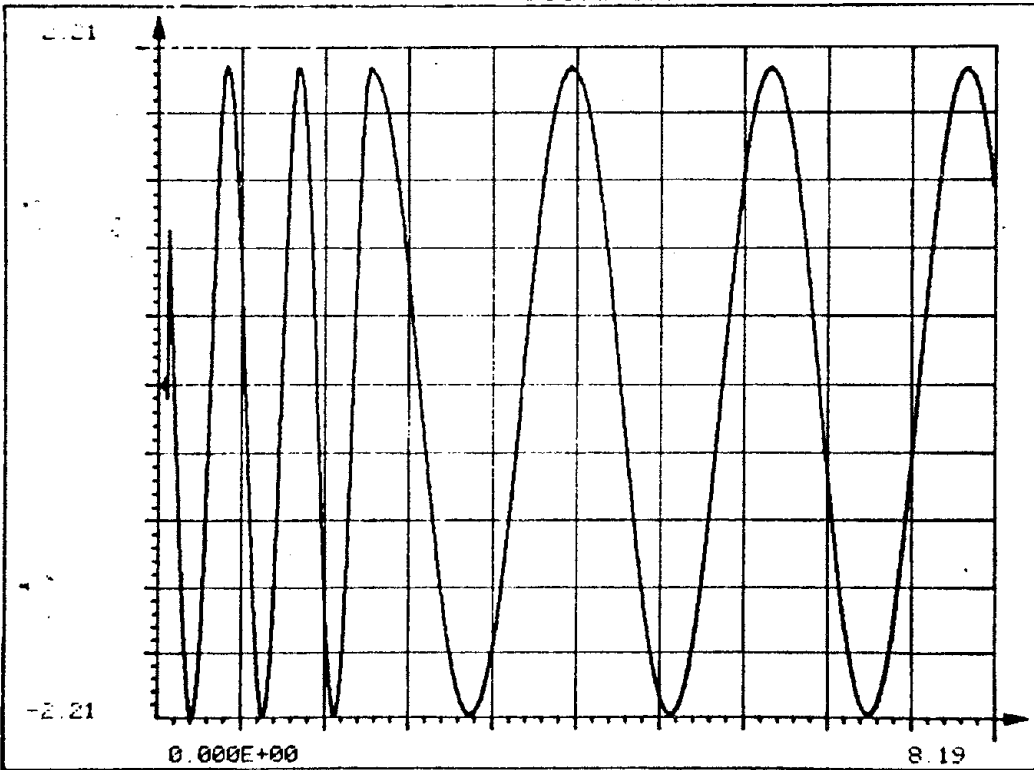
0-25

D3306.04F



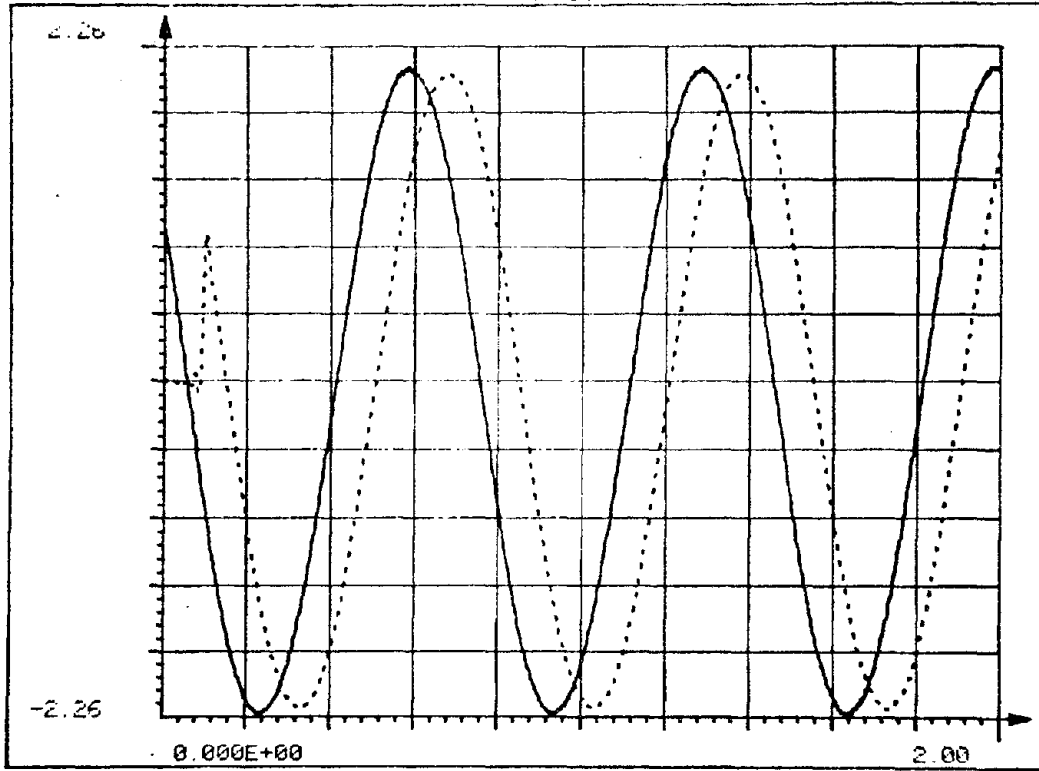
D33,23

D3306.04F



D33,24

03306 OAF



D33.25

APPENDIX 4

Nonlinear Dynamic (Group N)

N01714.110-1st 10,000p	14000sr	N01C1.OAF	N01C4.OAF filtered 2-4 sec
N01714.210 2nd	7ch	N01C2.OAF	N01C5.OAF from 4000-8098 pts
N01714.310 3rd	20 sec	N01C3.OAF	N01C6.OAF N01714.110

Group

Group N (Dynamic Nonlinear)

Notation: D1-Base displacement (LVDT)
 D2-Mass displacement (Optron)
 A1-Base acceleration
 A2-Mass acceleration
 F -Friction device
 V -Function generator
 (F)-Filtered data
 for figures containing 2 or 3 plots

Key: __ First curve
 - - second curve
 -.-. third curve

Note: Figure number interpretation, first field-test number
 second field-figure number
 third field-part number

Part number 1: 0-5 sec

FRICTION

2: 5-10 sec

3: 10-15 sec

Fig No	Caption
N01.1.1	1.D1 2.A1
N01.2.1	1.D2 2.A2
N01.3.1	1.D2 Blow-up ; Dynamic slip 2.A2
N01.4.1	1.D2 Blow-up ; Dynamic slip 2.A2
N01.5.1	1.D1 2.D2
N01.6.1	1.D1 Blow-up ; phase relation at dynamic slip 2.D2
N01.7.1	1,D1 Blow-up ; phase relation at dynamic slip 2.D2
N01.8.1	1.A1 2.A2
N01.9.1	1.D1 Blow-up ; phase relation and dynamic slip 2.D2 3.A2
N01.10.1	F
N01.11.1	V
N01.12.1	1.D1 2.A1
N01.13.2	1.D2 2.A2

FRICTION

N01.14.2	1.D1	
	2.D2	
N01.15.2	1.A1	
	2.A2	
N01.16.3	1.D1	
	2.A1	
N01.17.3	1.D2	
	2.A2	
N01.18.3	1.D2	Blow-up ; dynamic slip
	2.A2	
N01.19.3	1.D1	
	2.A2	
N01.20.3	1.D1	Blow-up ; phase relation at dynamic slip
	2.D2	
N01.21.3	1.D1	Blow-up ; phase relation at dynamic slip
	2.D2	
N01.22.3	1.A1	
	2.A2	
N01.23.3	1.D1	Blow-up ; phase relation and dynamic slip
	2.D2	
	3.A2	

Note Figures N01.24.1-N01.39.1 correspond to the time segment of 2-4 sec in the actual (unfiltered) data file

N01.24.1	D1	
N01.25.1	D1(F)	
N01.26.1	1.D1	
	2.D1(F)	
N01.27.1	A1	

FRICITION

NO1.28.1 A1(F)
NO1.29.1 1.A1
2.A1(F)
NO1.30.1 D2
NO1.31.1 D2(F)
NO1.32.1 1.D2
2.D2(F)
NO1.33.1 A2
NO1.34.1 A2(F)
NO1.35.1 1.A2
2.A2(F)
NO1.36.1 F(F)
NO1.37.1 V
NO1.38.1 V(F)
NO1.39.1 1.V
2.V(F)

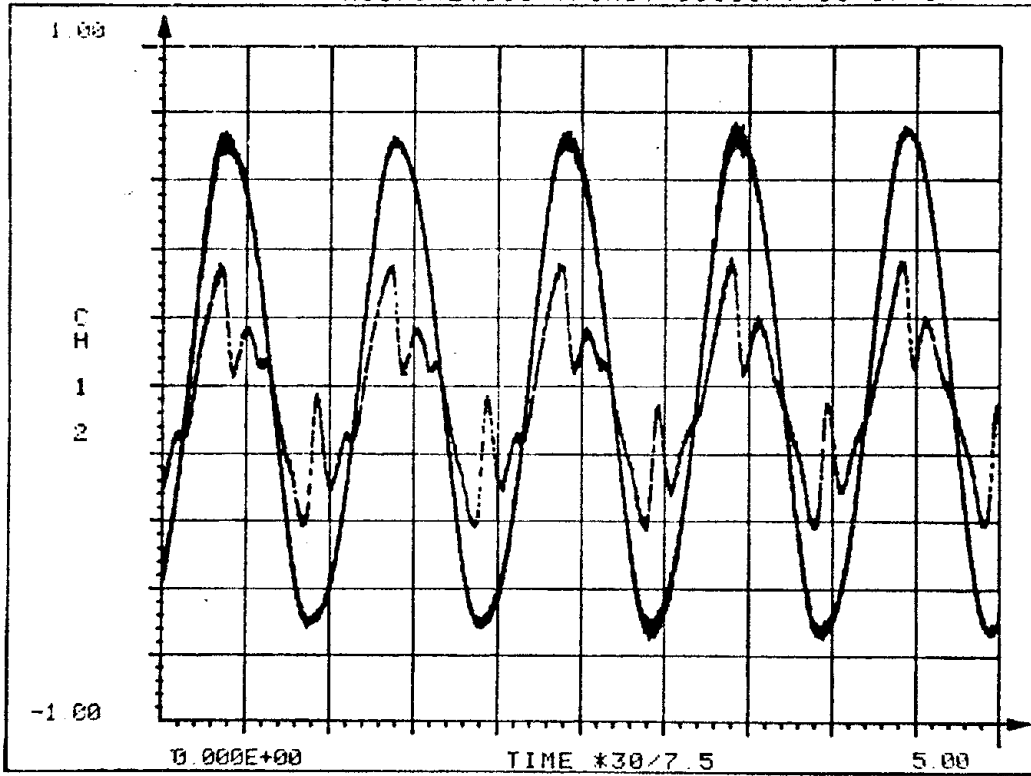
*Note figures NO1.40.3-NO1.54.3 correspond to the time segment of 11-13 sec in the actual (unfiltered) data file

NO1.40.3 D1
NO1.41.3 D1(F)
NO1.42.3 1.D1
2.D1(F)
NO1.43.3 A1
NO1.44.3 A1(F)
NO1.45.3 1.A1
2.A1(F)
NO1.46.3 D2
NO1.47.3 D2(F)

FRICITION

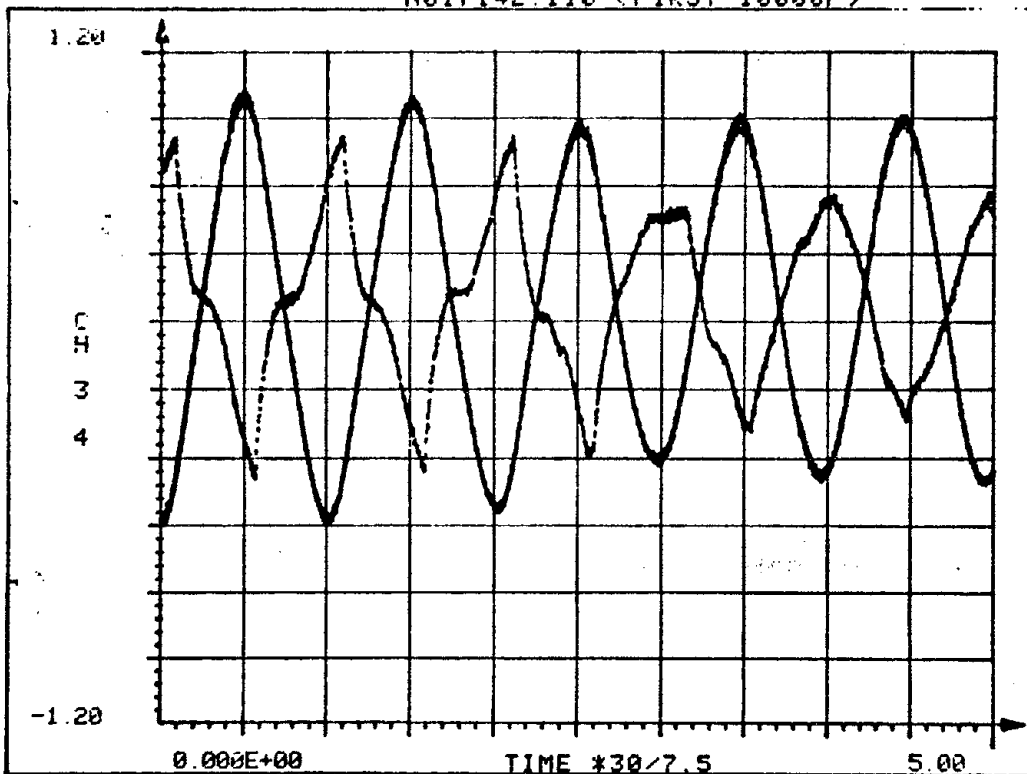
N01.48.3 1.D2
2.D2(F)
N01.49.3 A2
N01.50.3 A2(F)
N01.51.3 1.A2
2.A2(F)
N01.52.3 V
N01.53.3 V(F)
N01.54.3 1.V
2.V(F)

N017142.110 (FIRST 10000P) 10-17-84



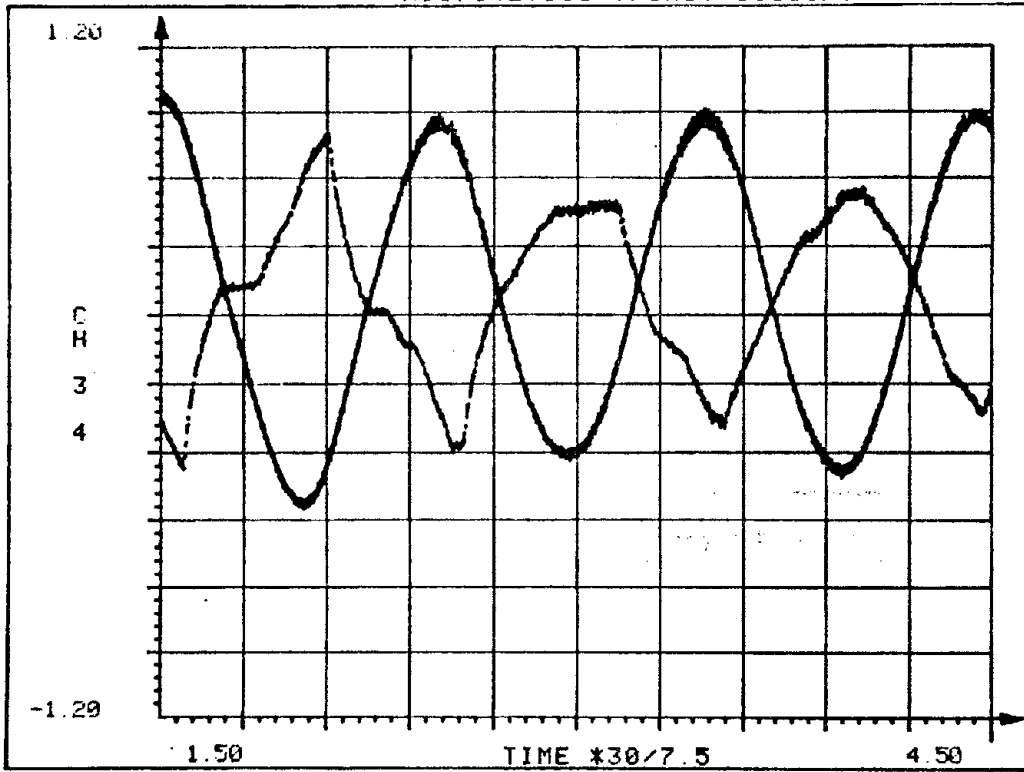
N01.1.1

N017142.110 (FIRST 10000P)



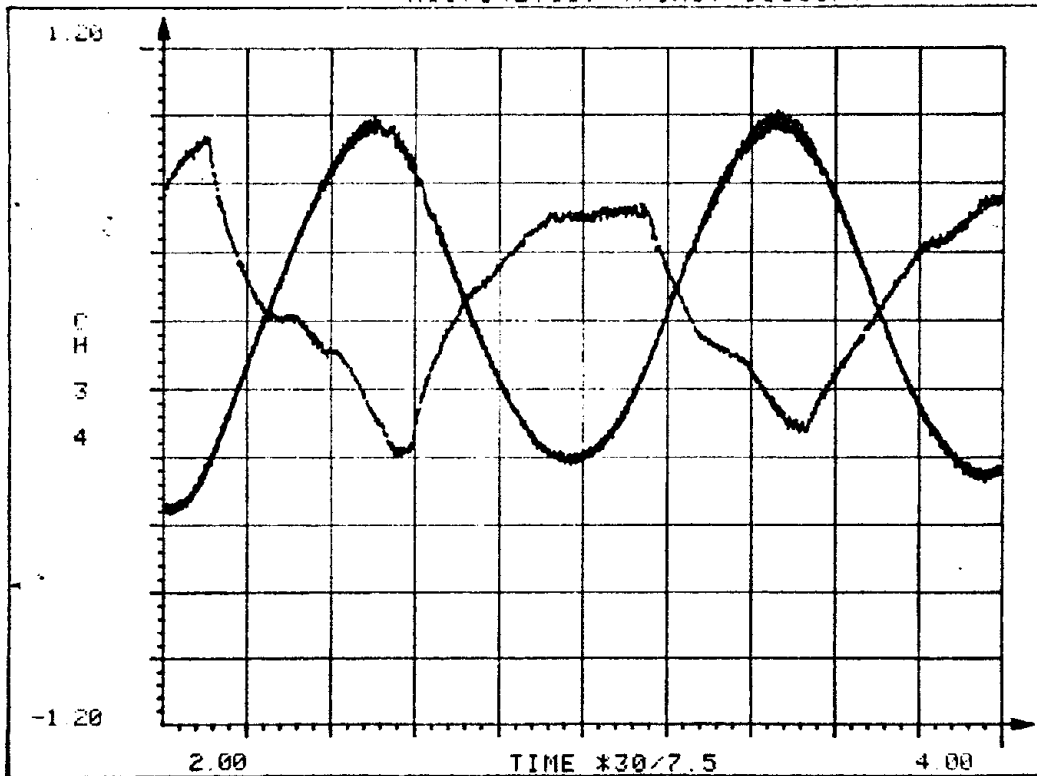
N01.2.1

N017142.110 (FIRST 10000P)



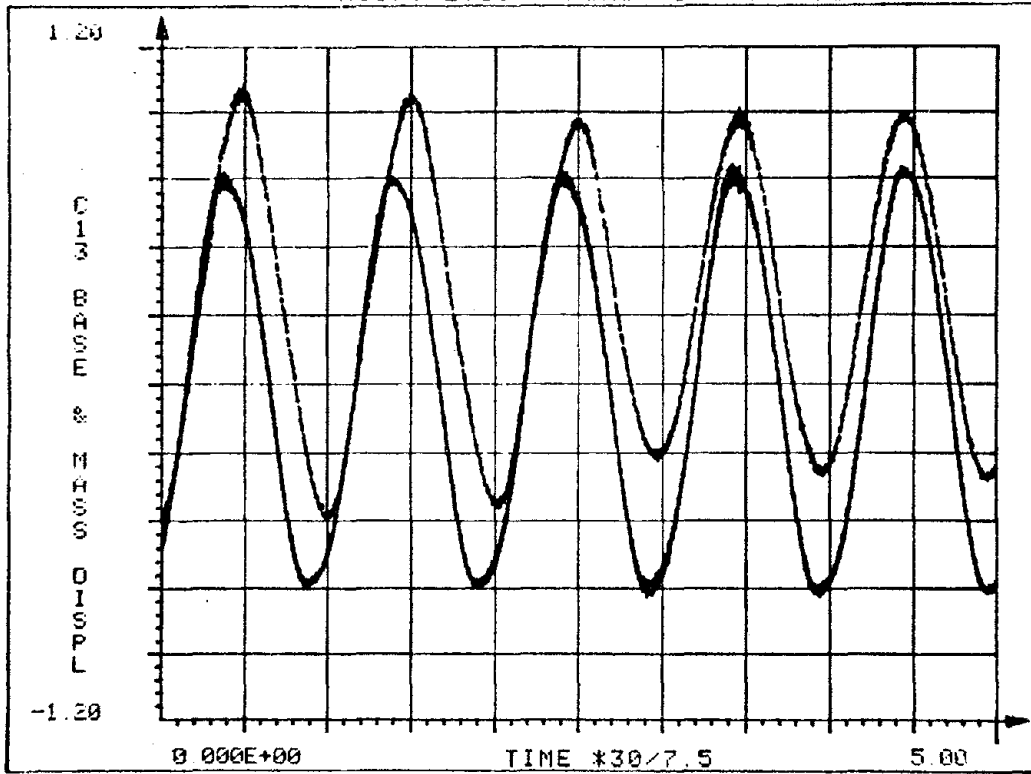
N01.3.1

N017142.110 (FIRST 10000P)



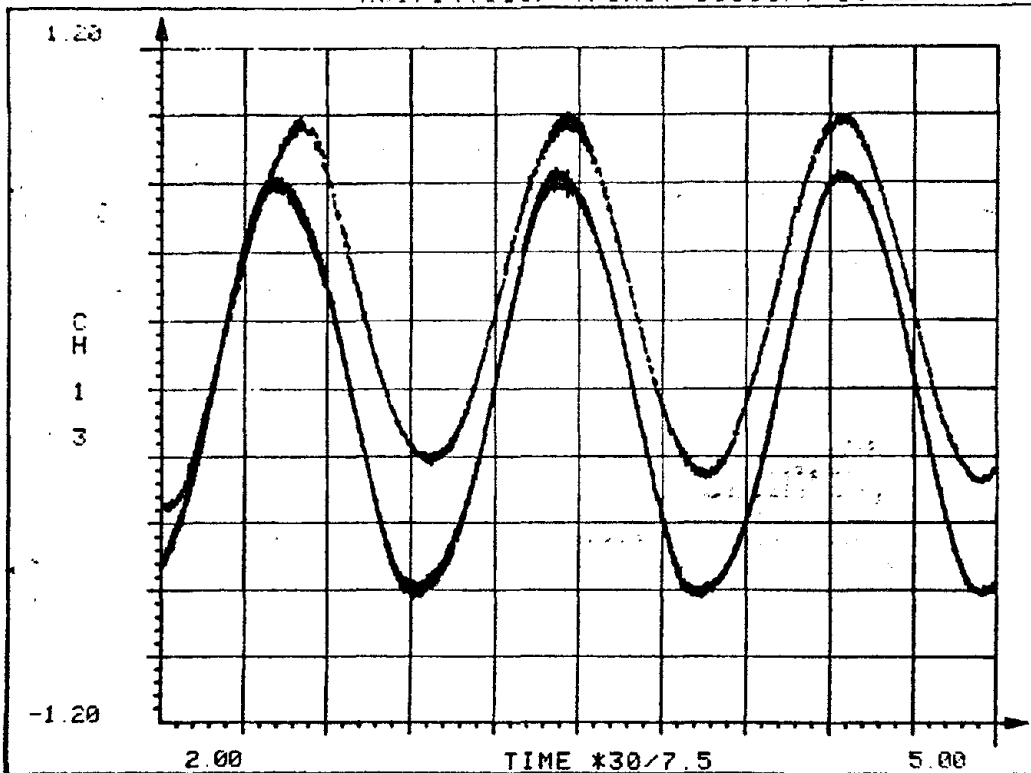
N01.4.1

N017142.110 (FIRST 10000P) 10-17-84



N01.5.1

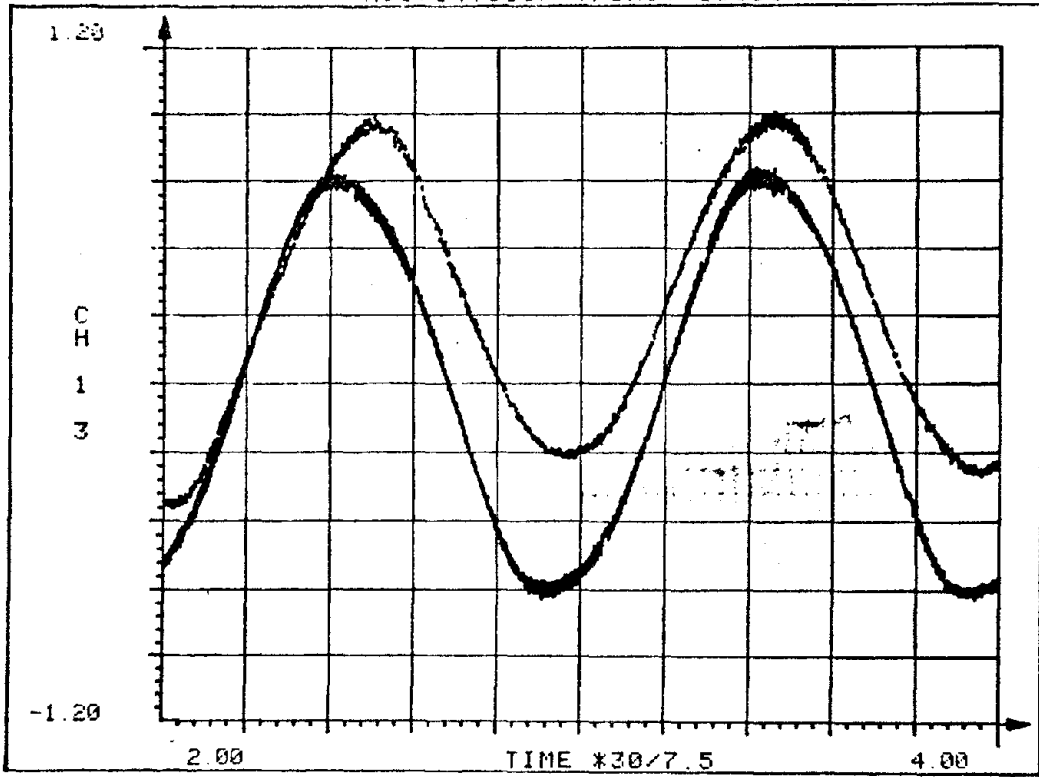
N01714.110F (FIRST 10000P) 10-26



N01.6.1

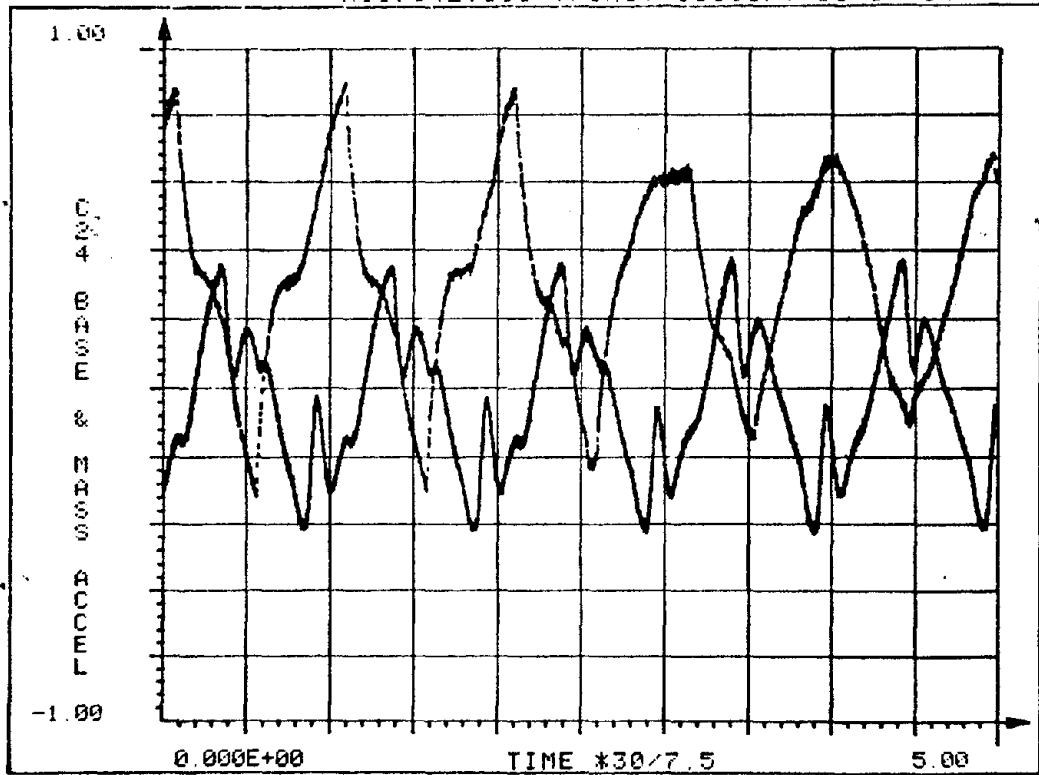
D-8

N01714.110F (FIRST 10000P) 10-26



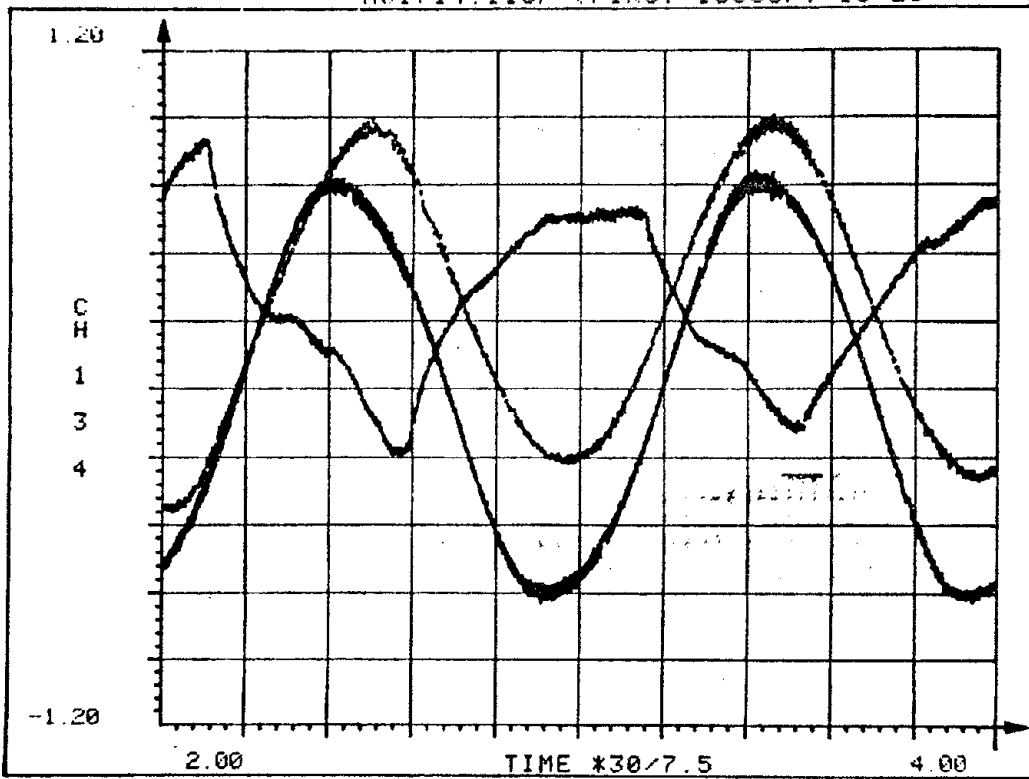
N01.7.1

N017142.110 (FIRST 10000P) 10-17-84



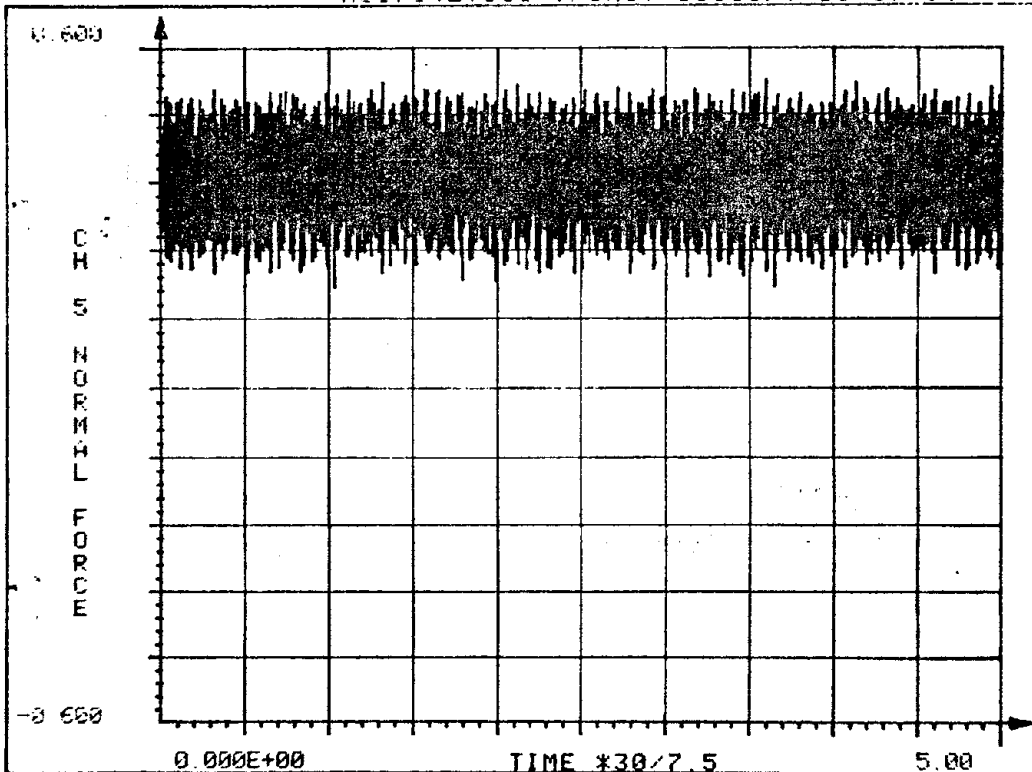
N01.8.1

N01714.110F (FIRST 10000P) 10-26



Nφ1.9.1

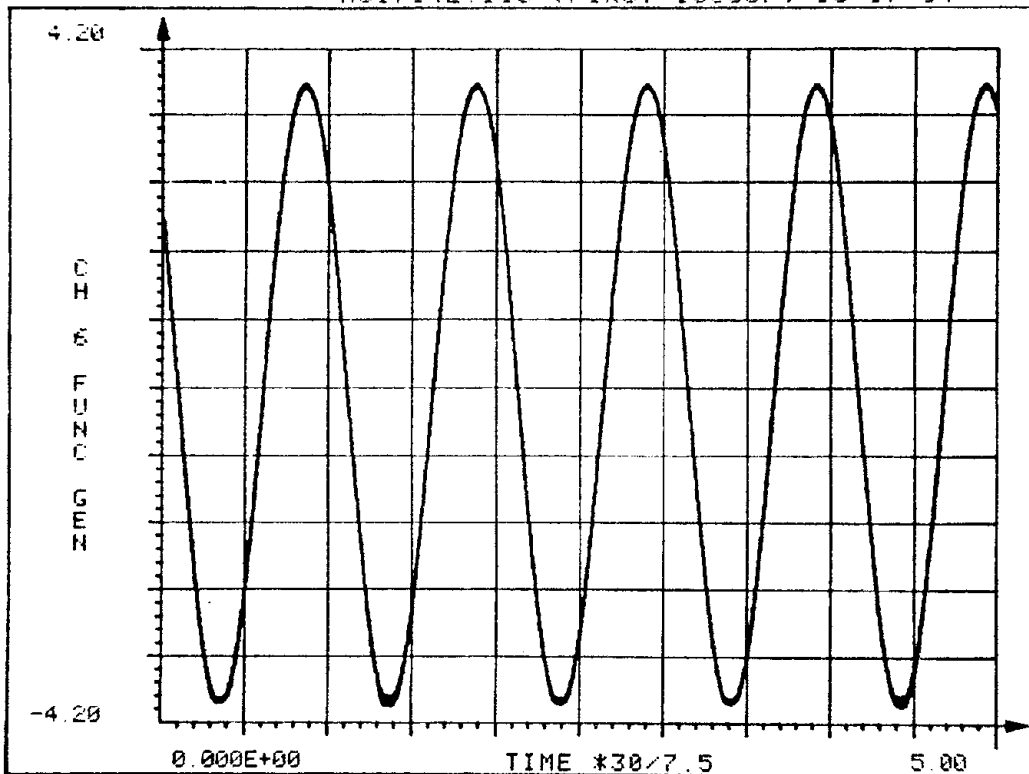
N017142.110 (FIRST 10000P) 10-17-84



Nφ1.1φ.1

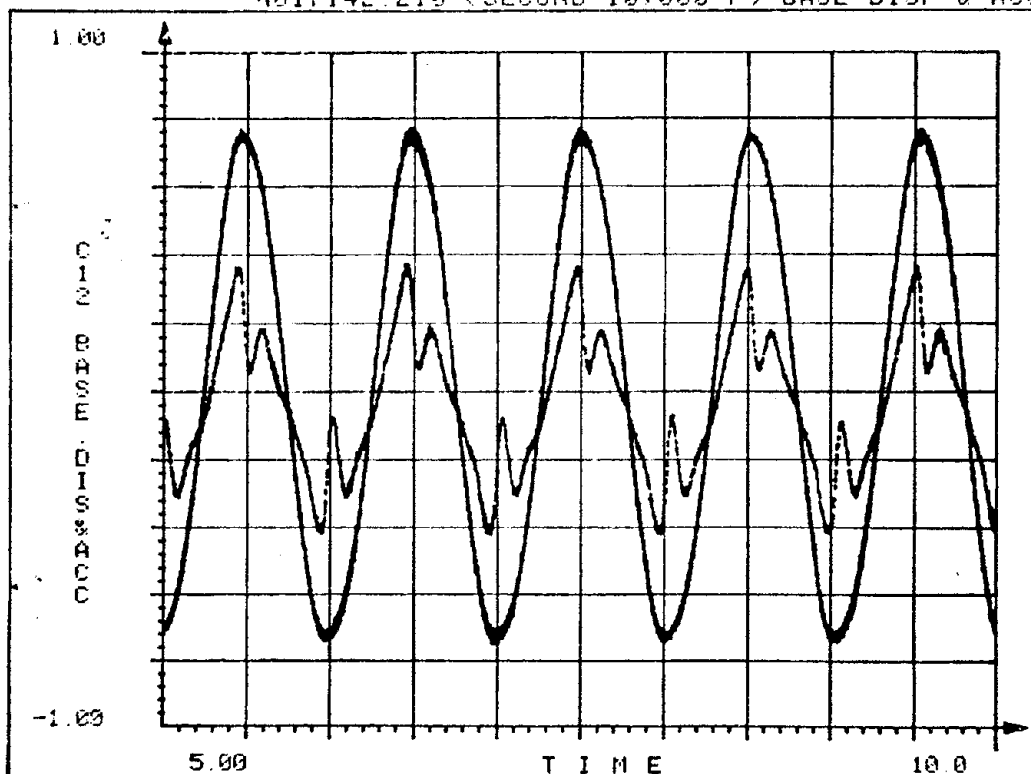
D-10

N017142.110 (FIRST 10000P) 10-17-84

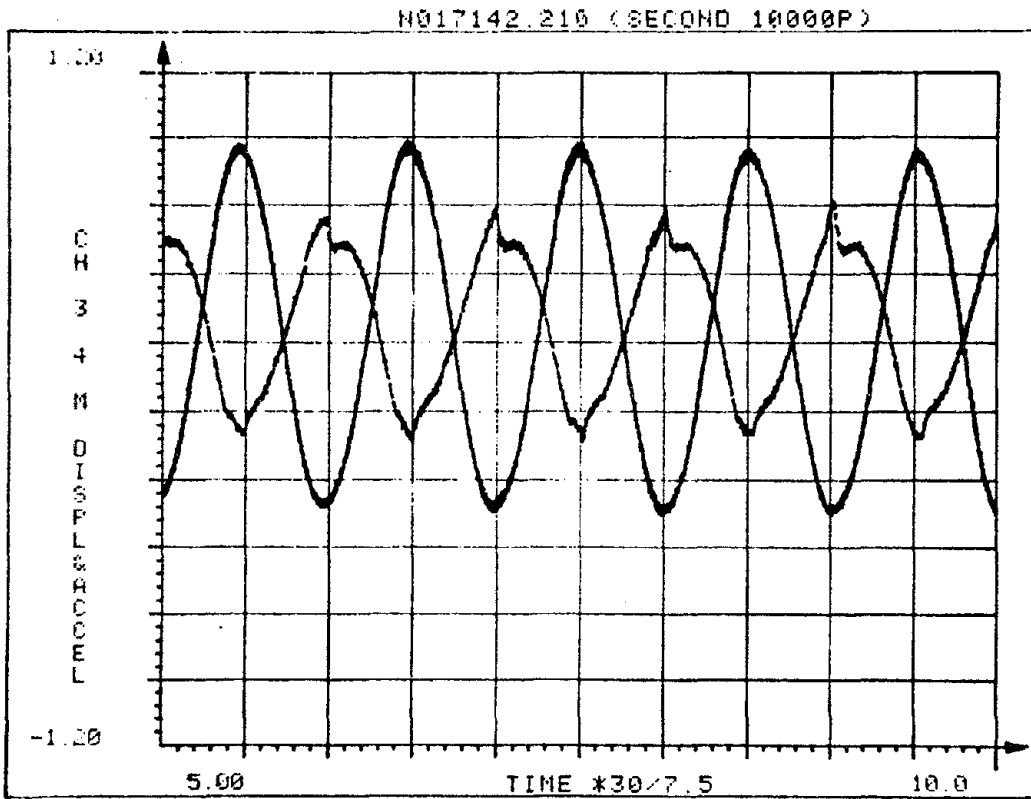


N01.11.1

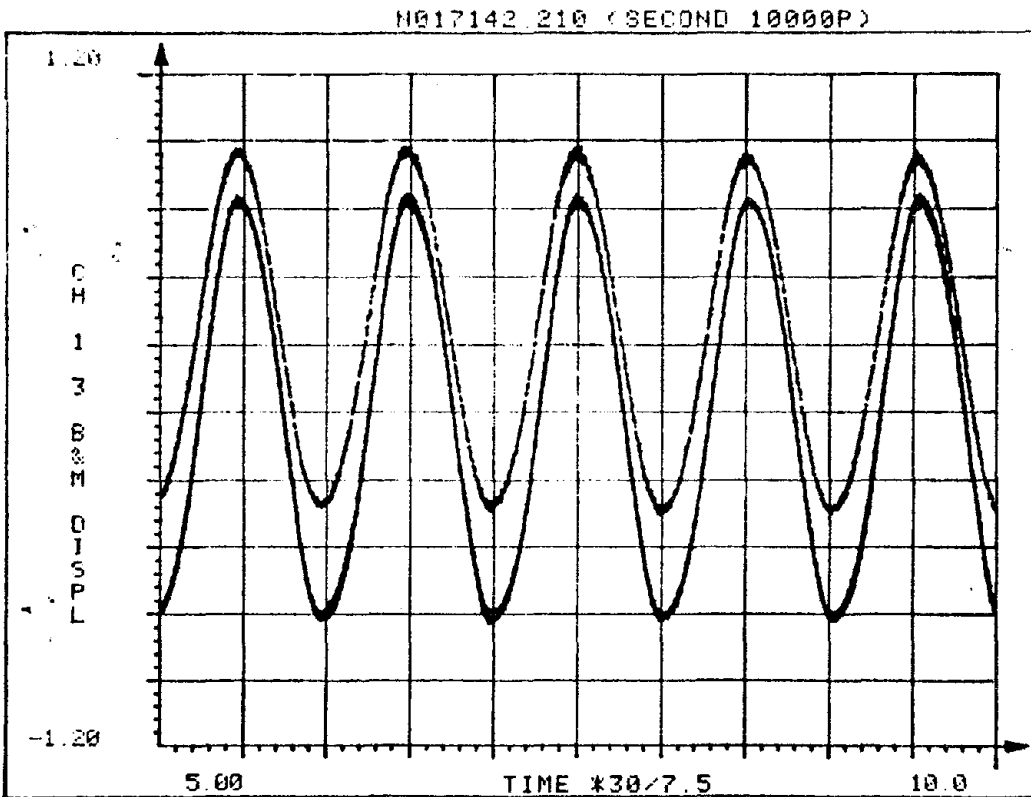
N017142.210 (SECOND 10.000 P) BASE DISP & ACCL



N01.12.2

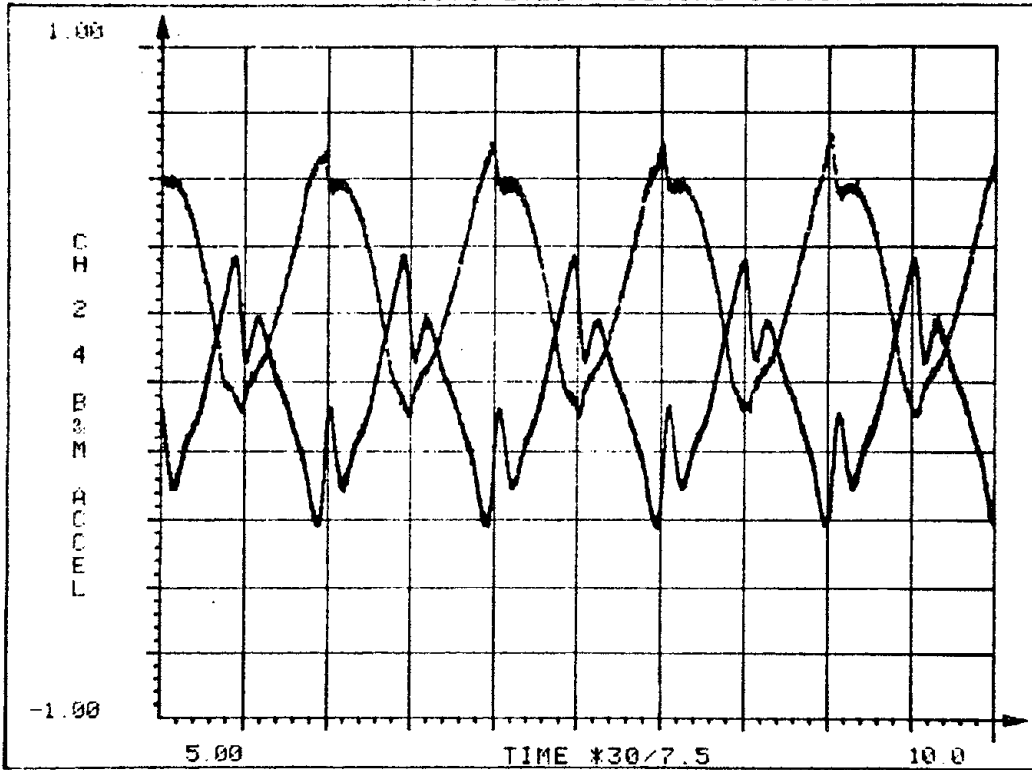


N01.13.2



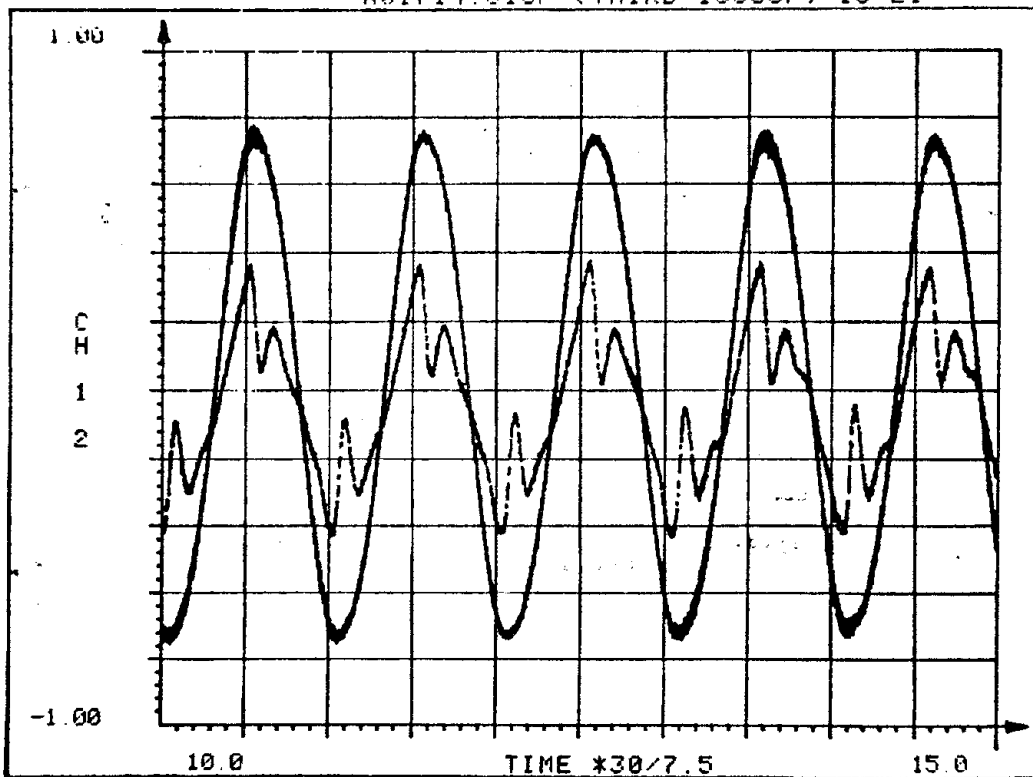
N01.14.2

N017142.210 (SECOND 10000P)



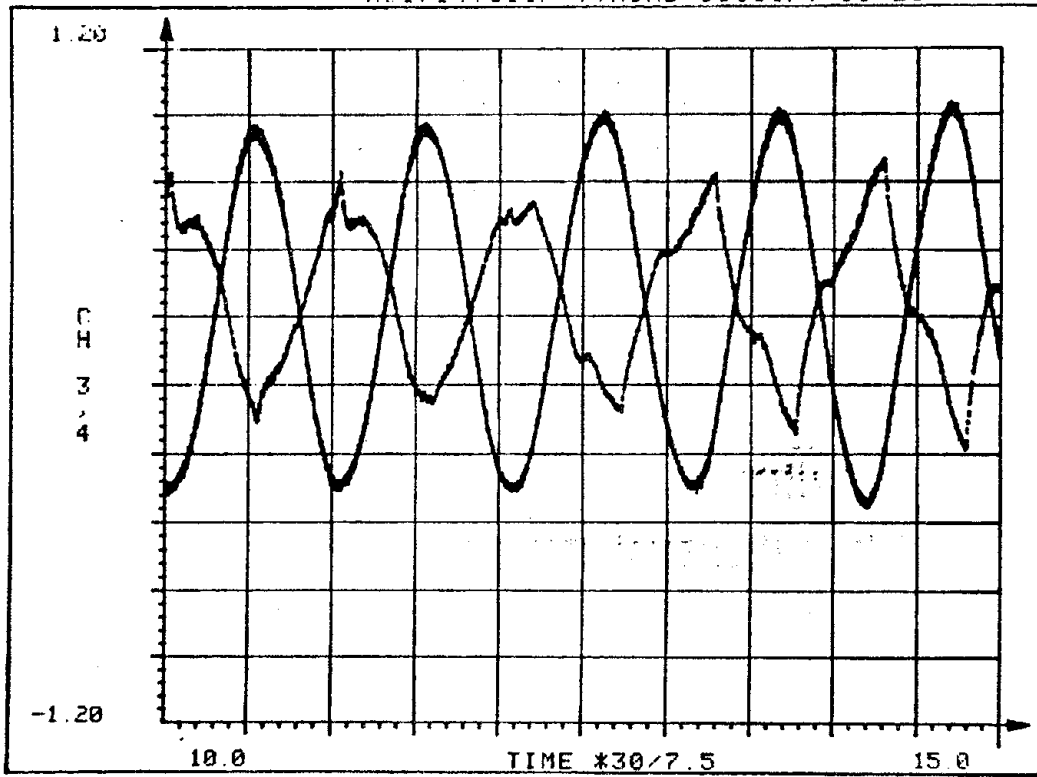
N01.15.2

N01714.310F (THIRD 10000P) 10-21



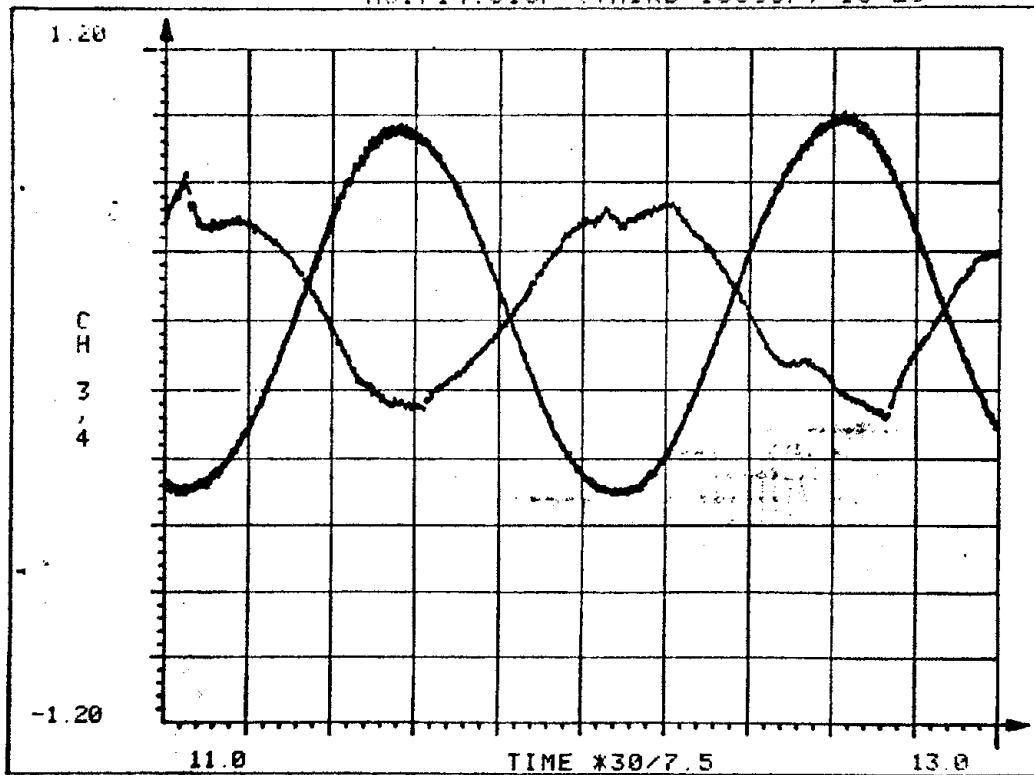
N01.16.3

N01714.310F (THIRD 10000P) 10-26



Nφ1.17.3

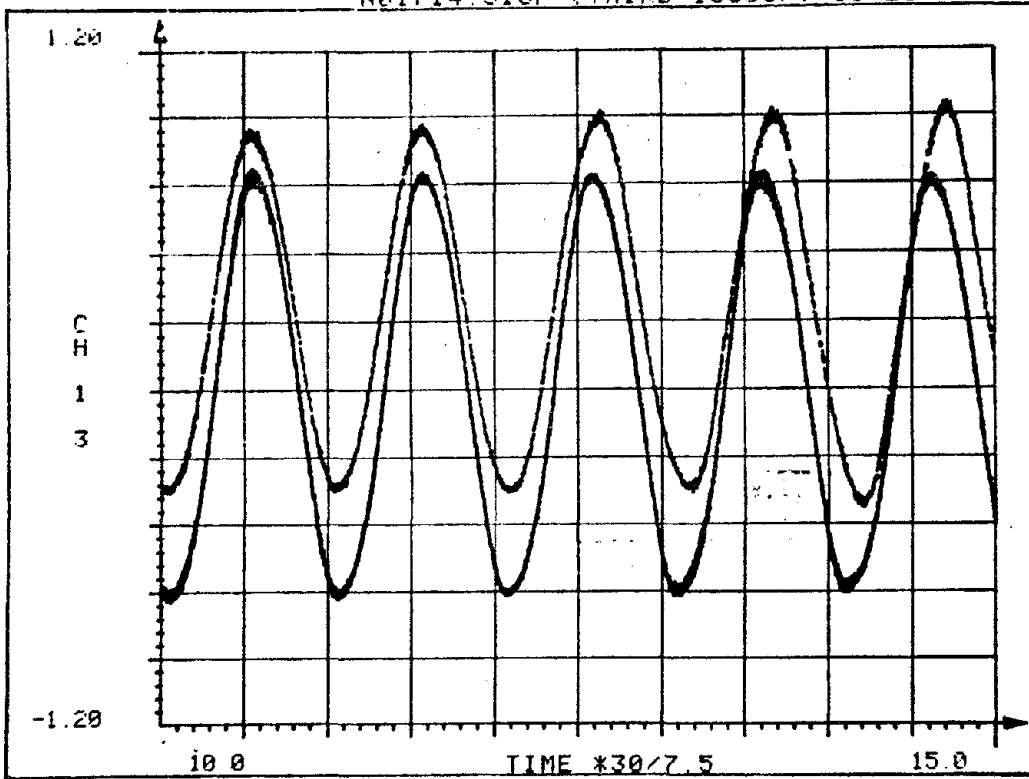
N01714.310F (THIRD 10000P) 10-26



Nφ1.18.3

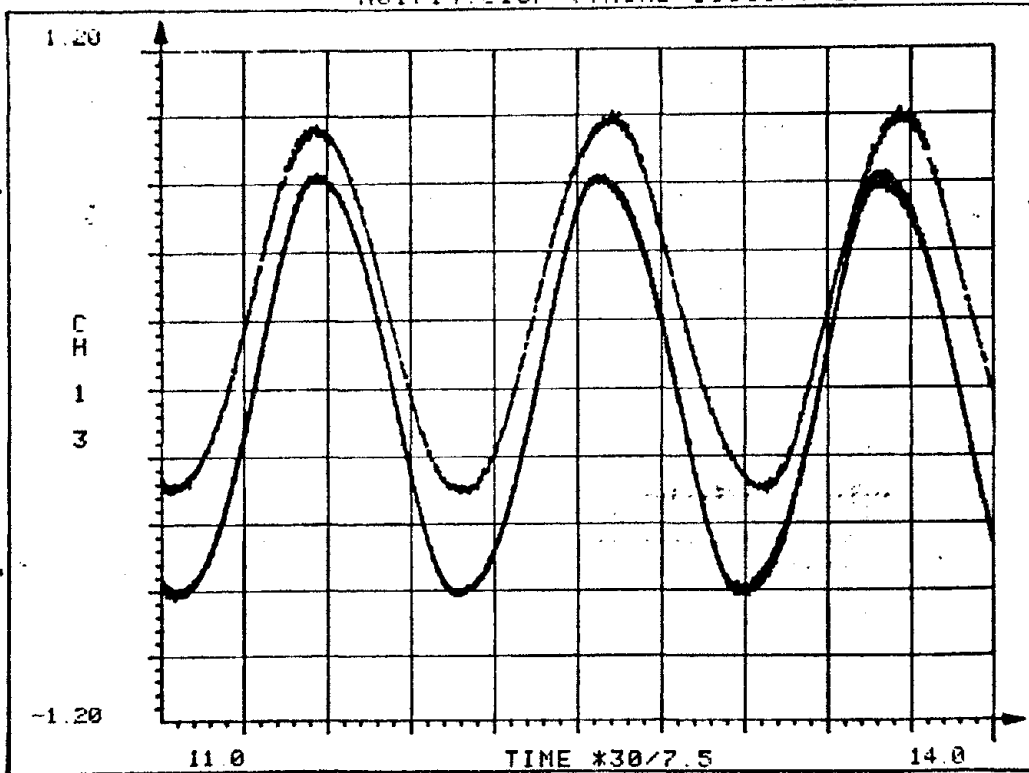
D-14

N01714.310F (THIRD 10000P) 10-26



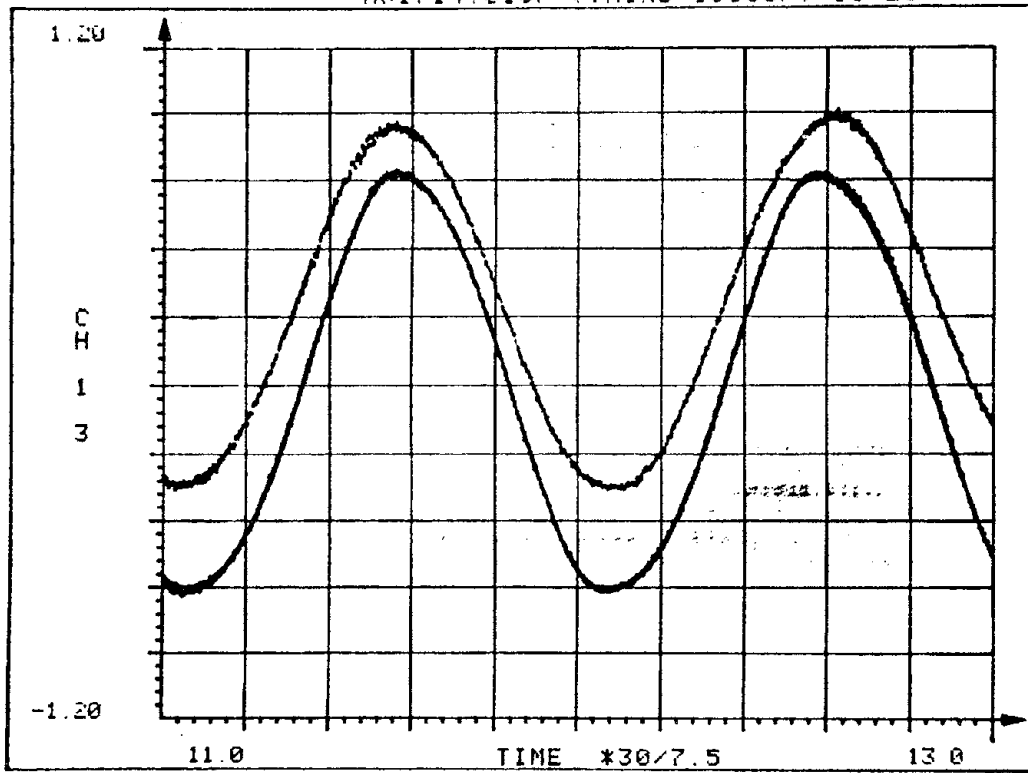
N01.19.3

N01714.310F (THIRD 10000P) 10-26



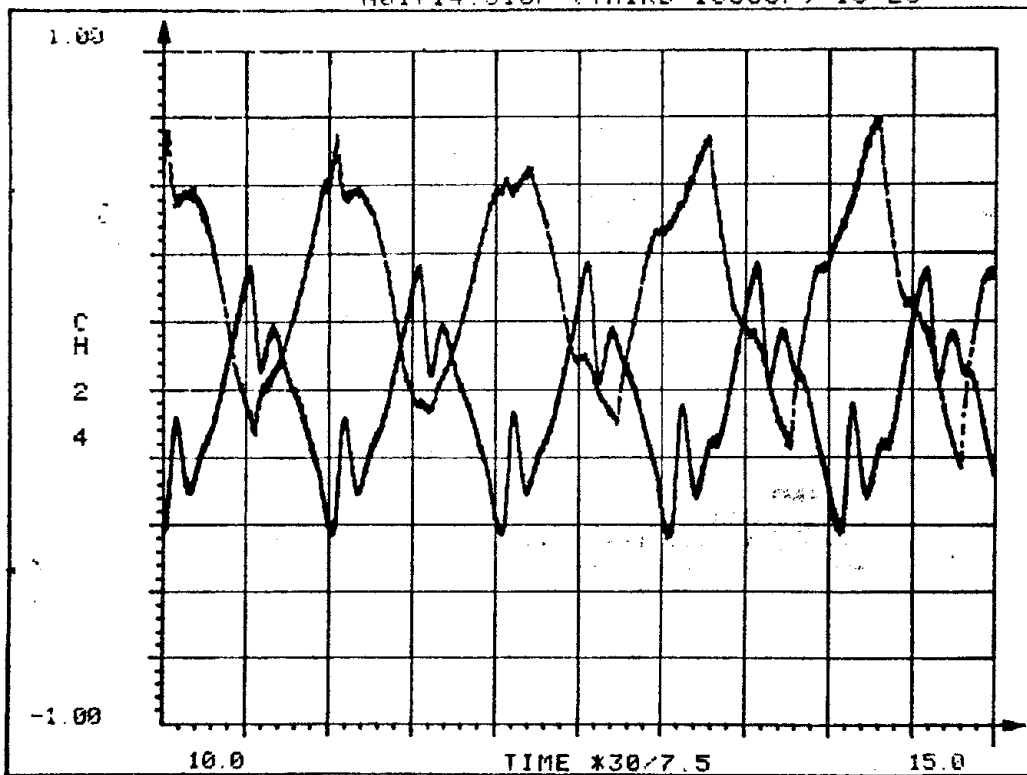
N01.20.3

N01714.310F (THIRD 10000P) 10-26



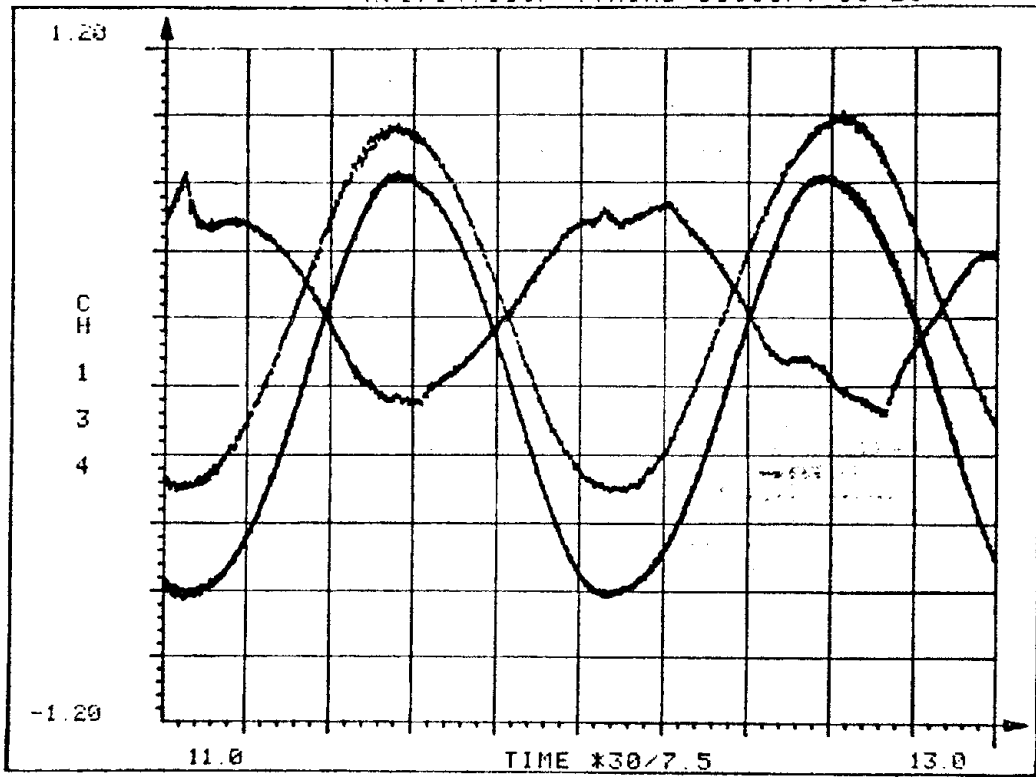
N01,21,3

N01714.310F (THIRD 10000P) 10-26



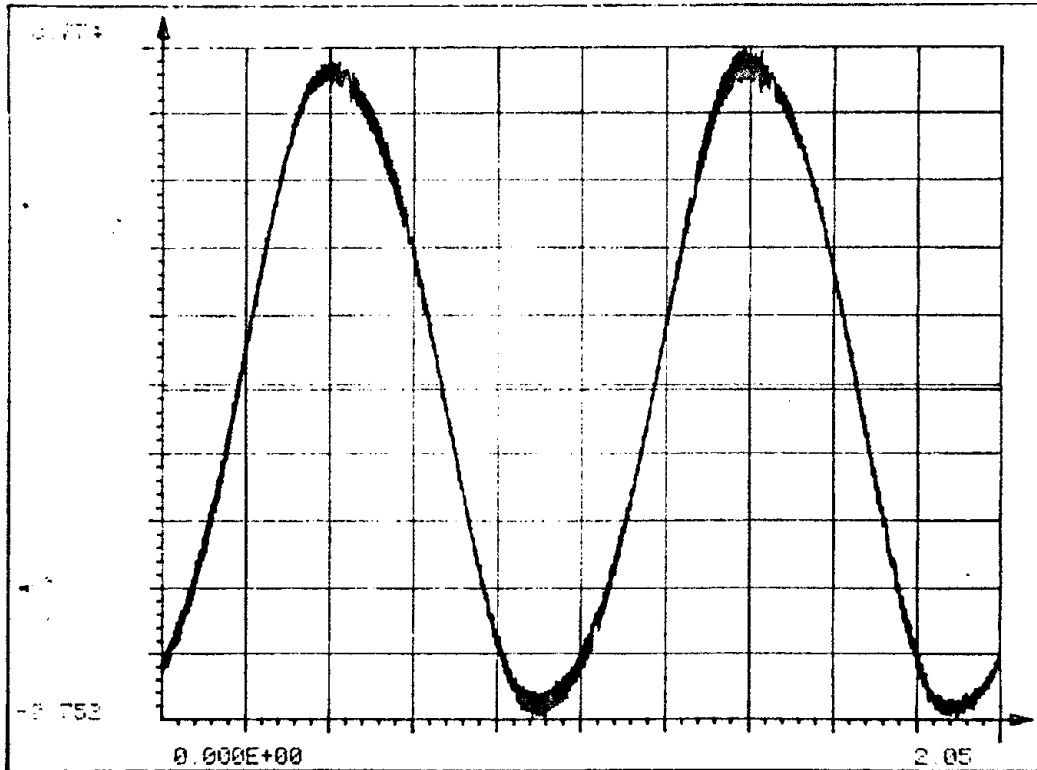
N01,22,3

N01714.310F (THIRD 10000P) 10-26



N01.23.3

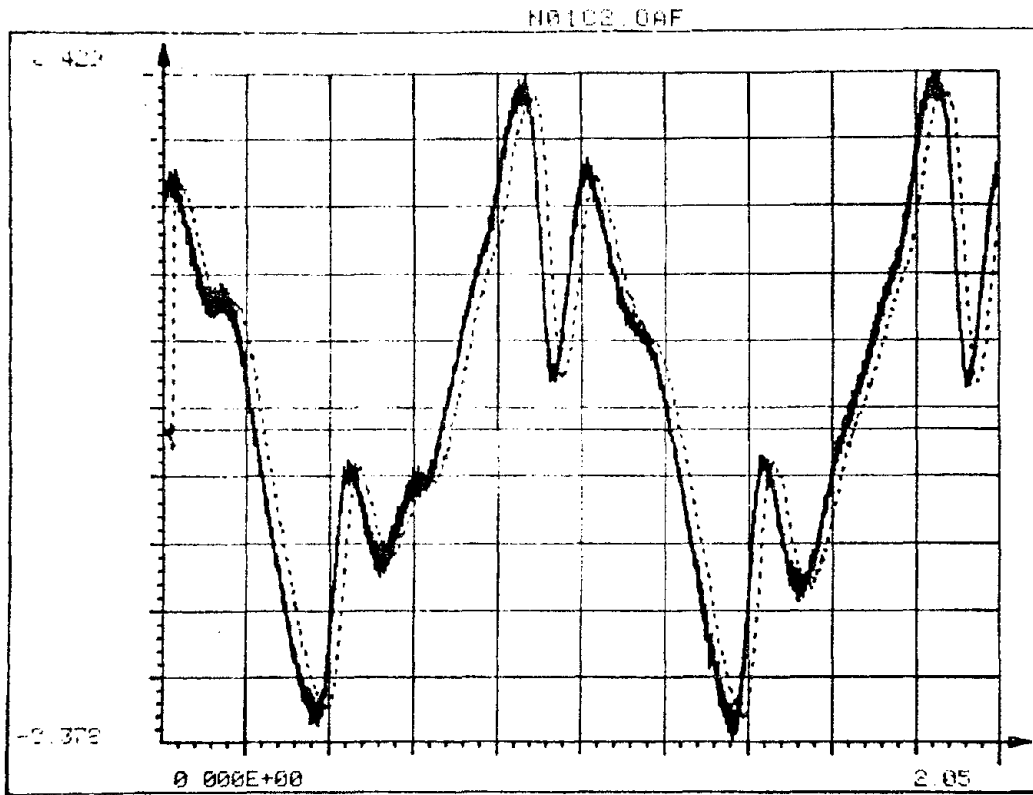
N0101.0AF



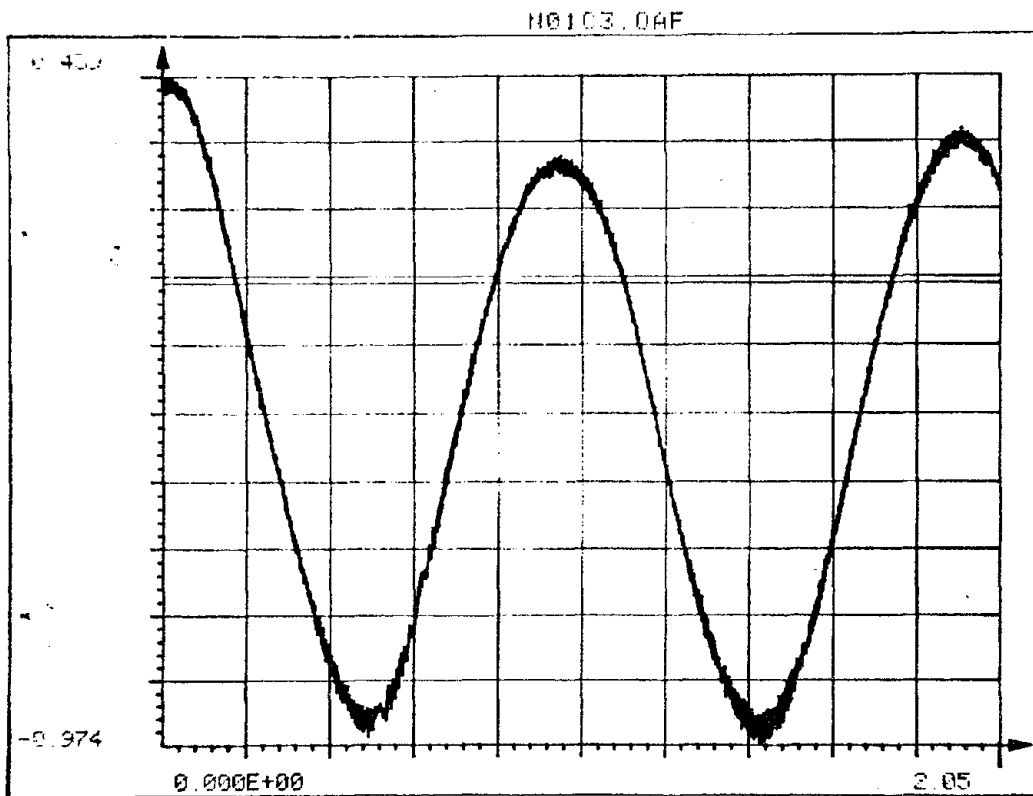
N01.24.1

Reproduced from
best available copy.

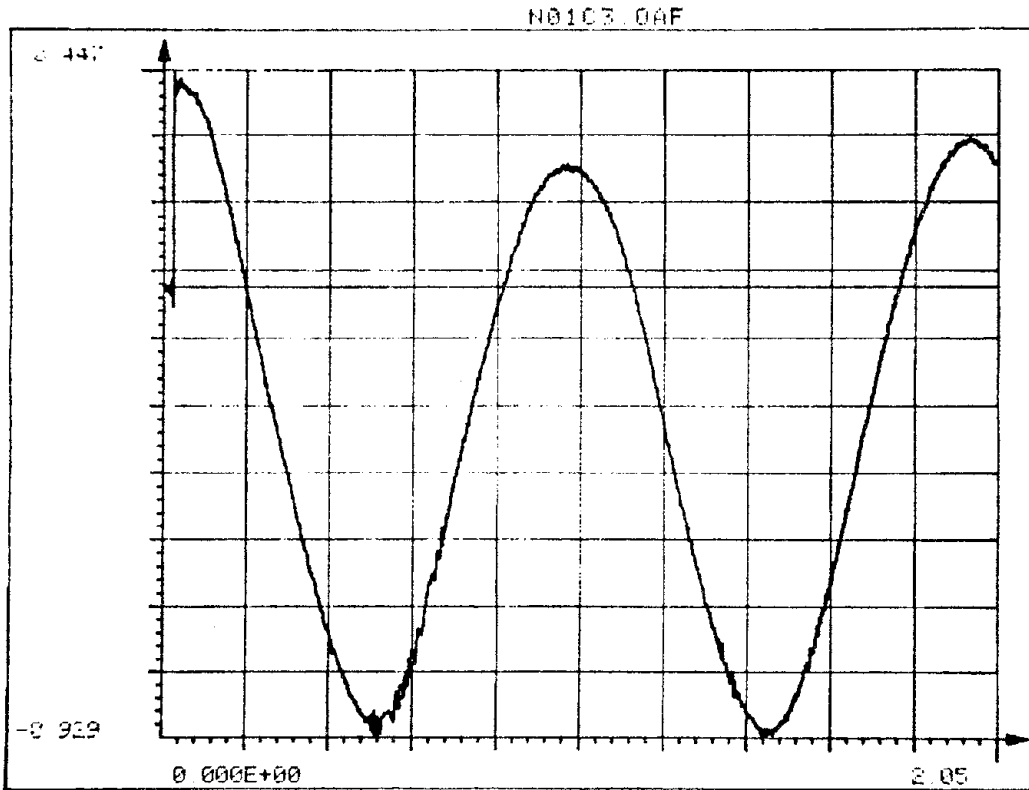




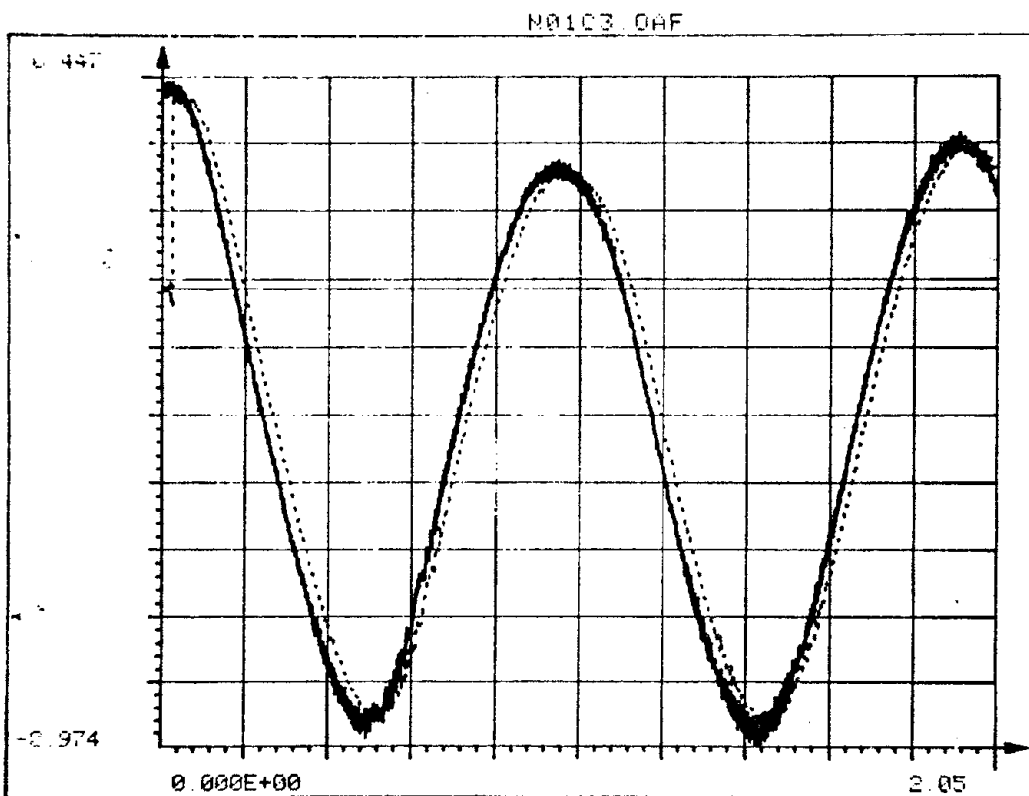
N01.29.1



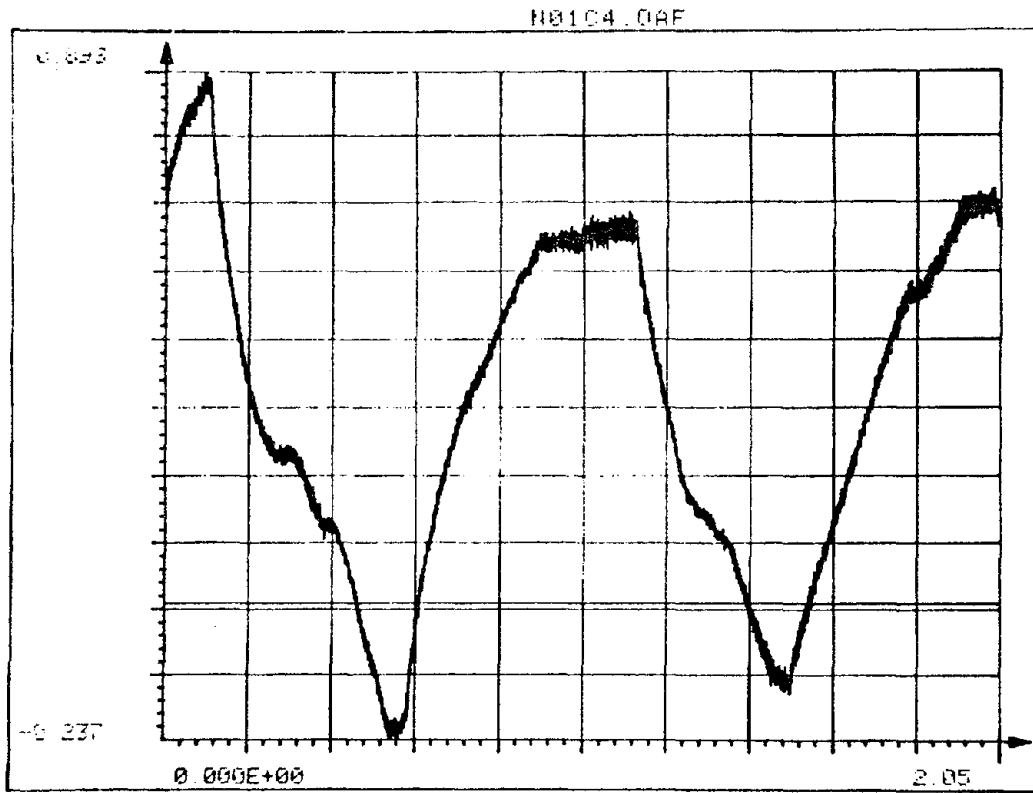
N01.30.1



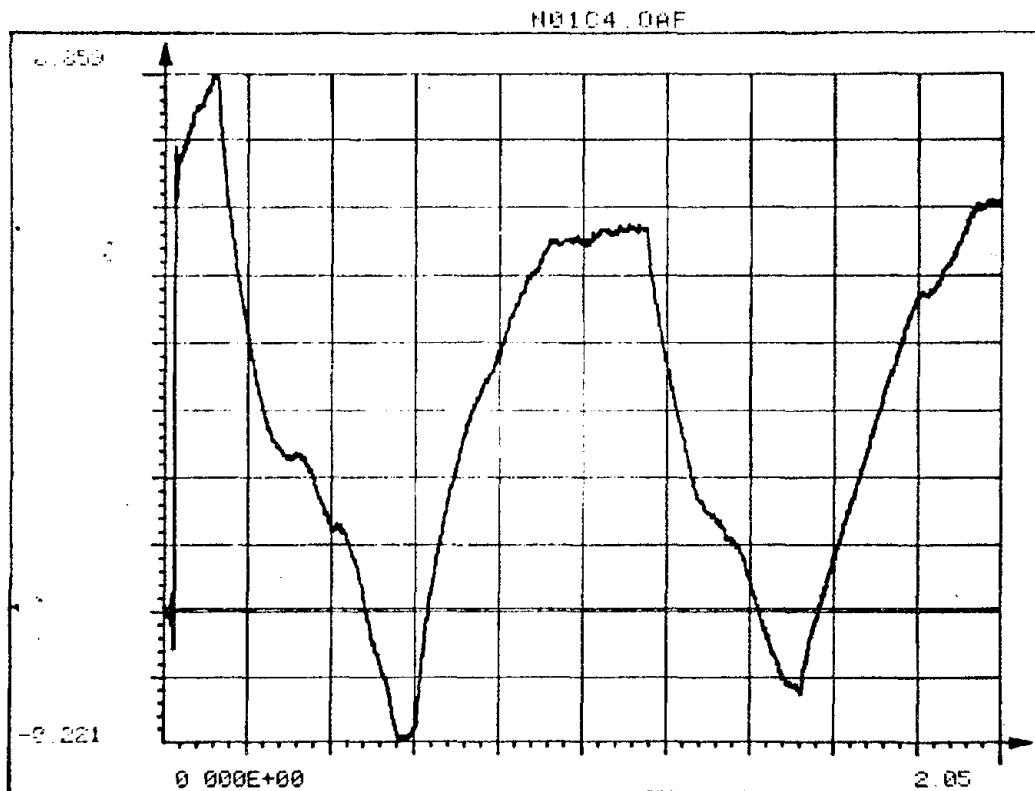
N01.31.1



N01.32.1



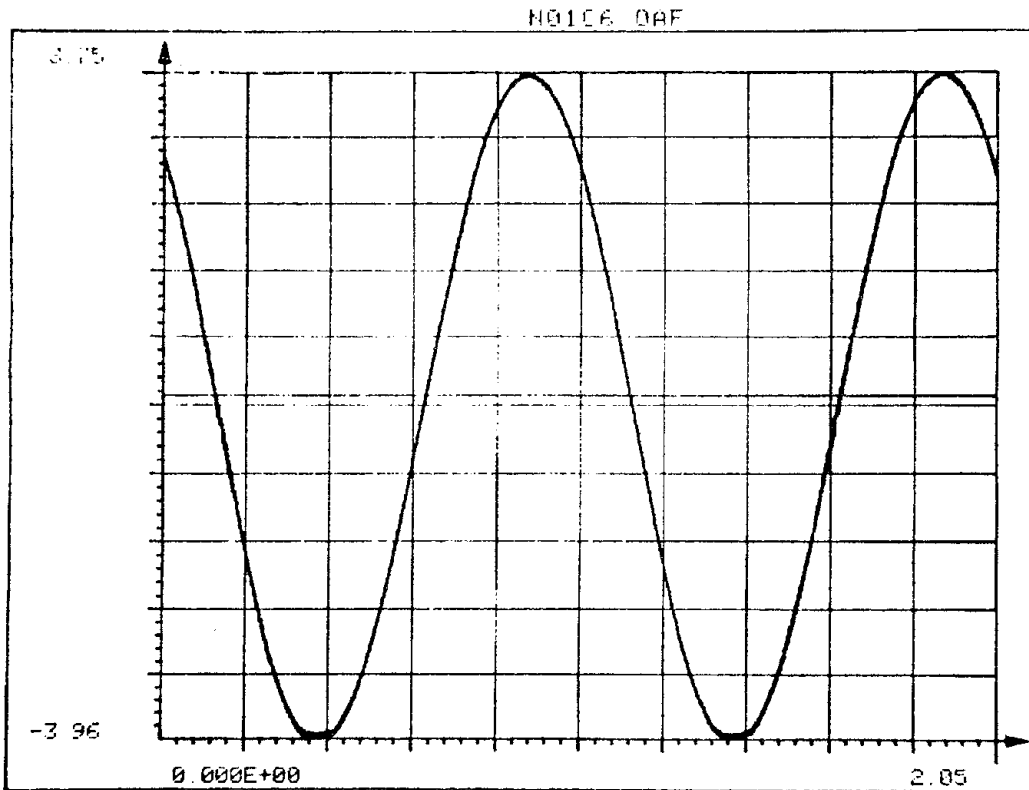
Nφ1.33.1



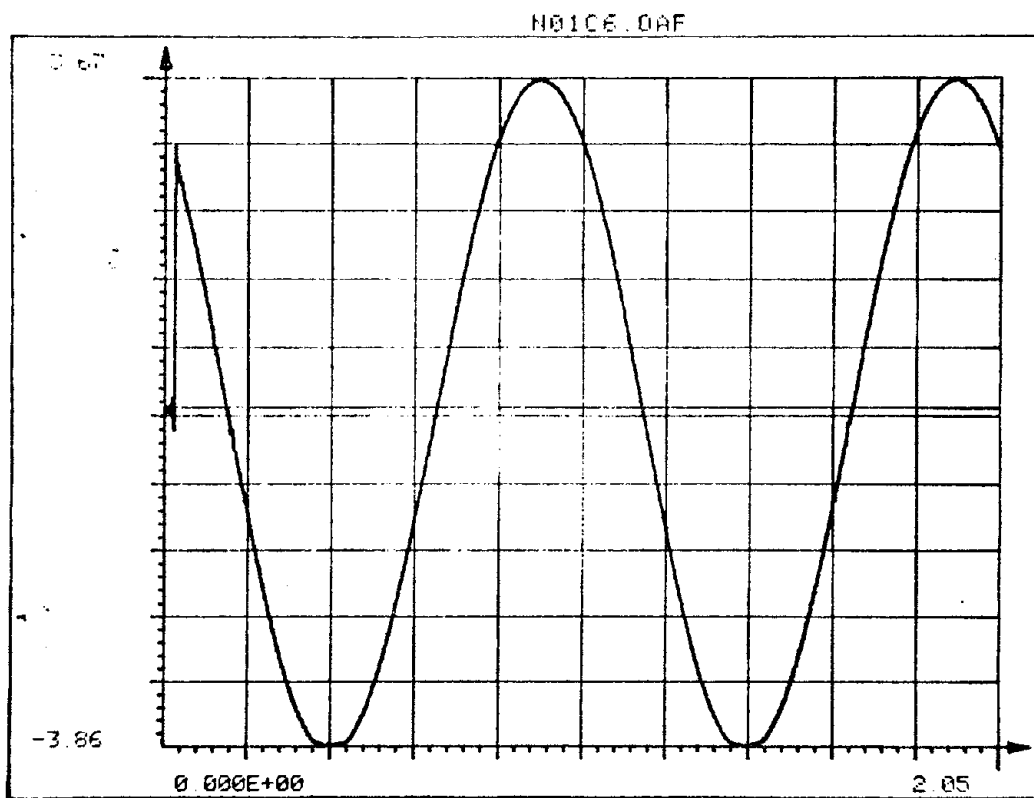
Nφ1.34.1

Reproduced from
best available copy.

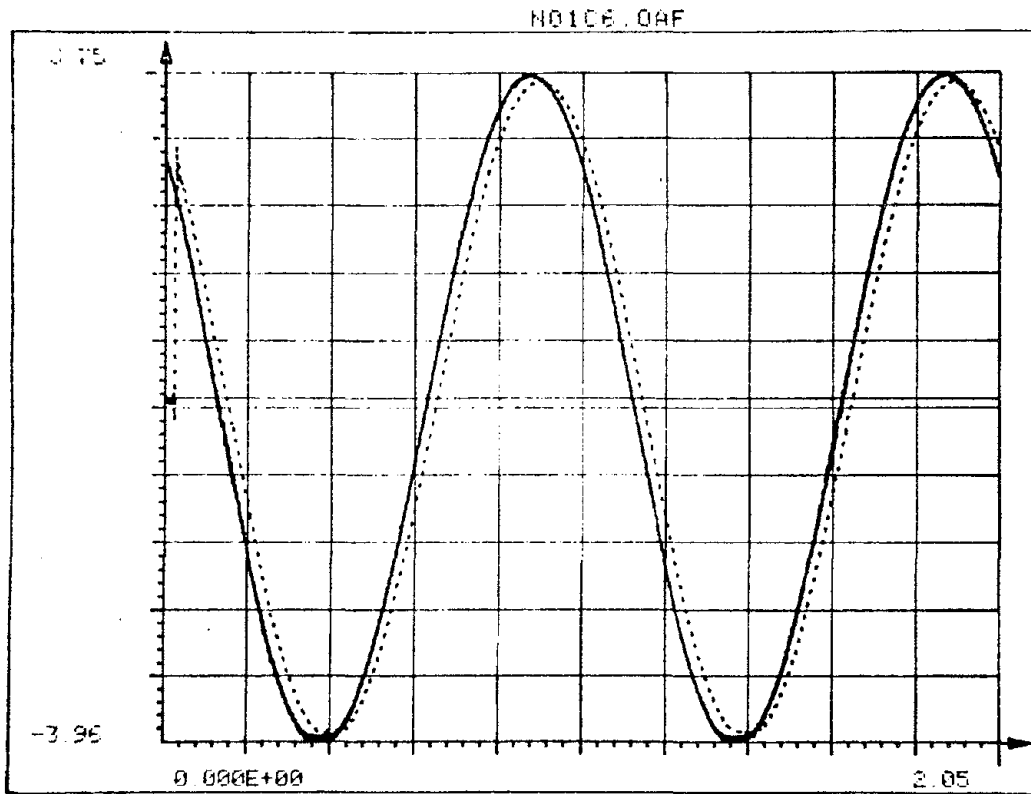




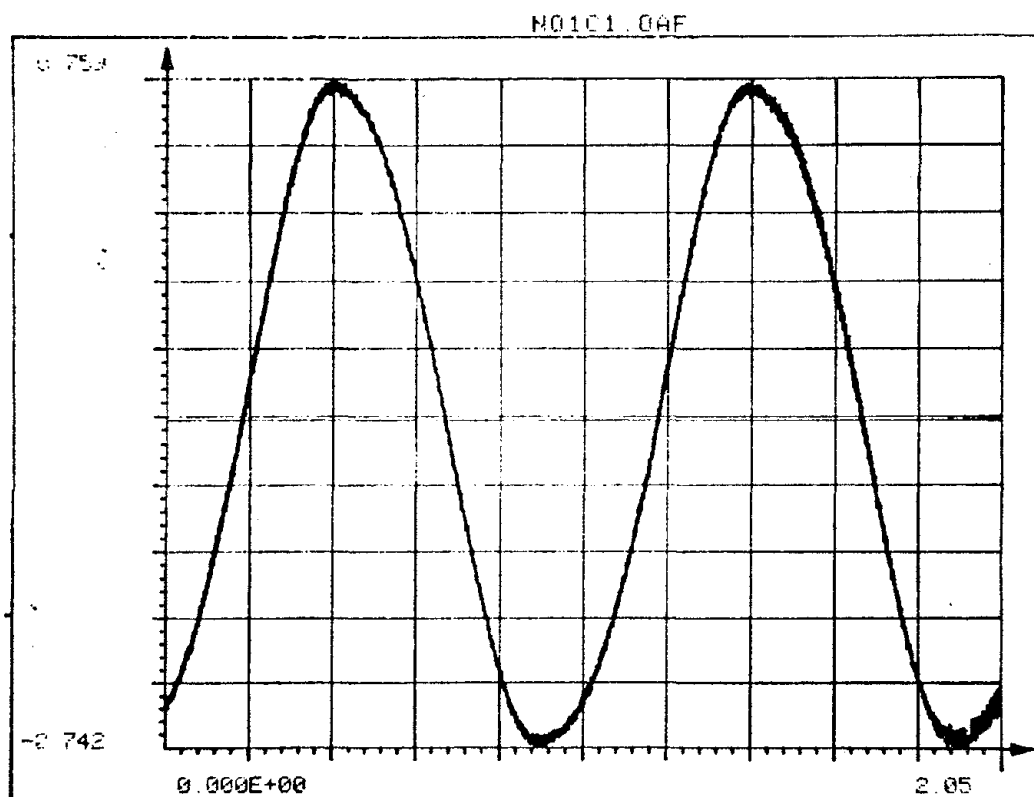
N01.37.1



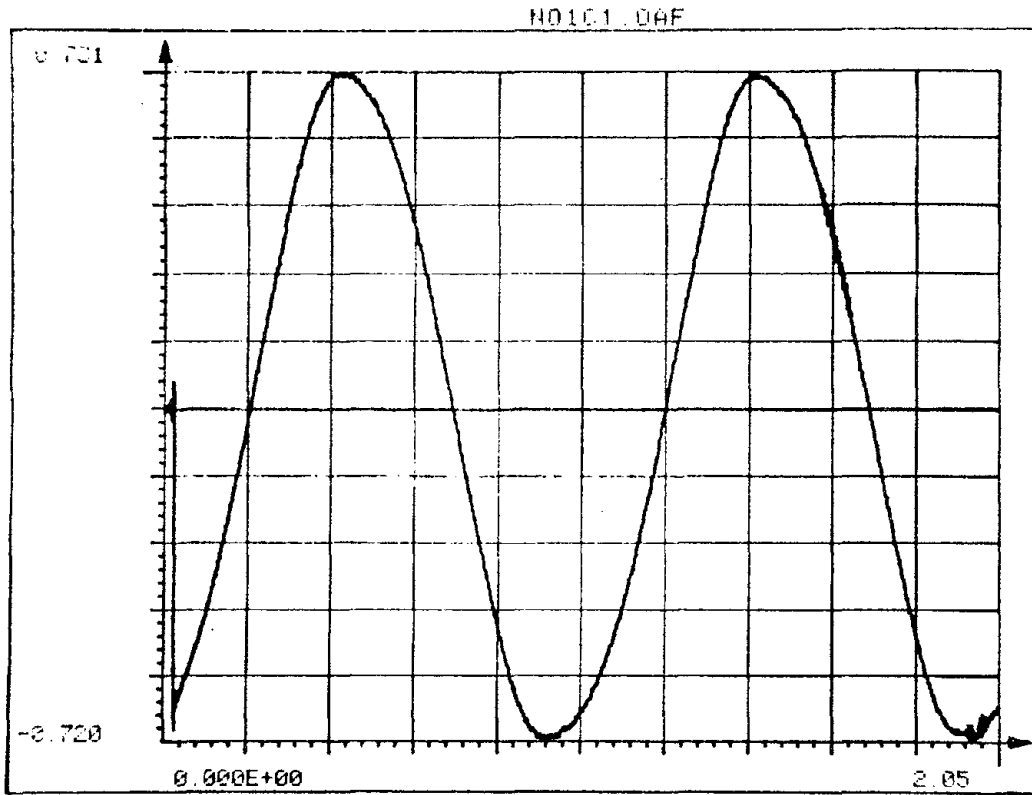
N01.38.1



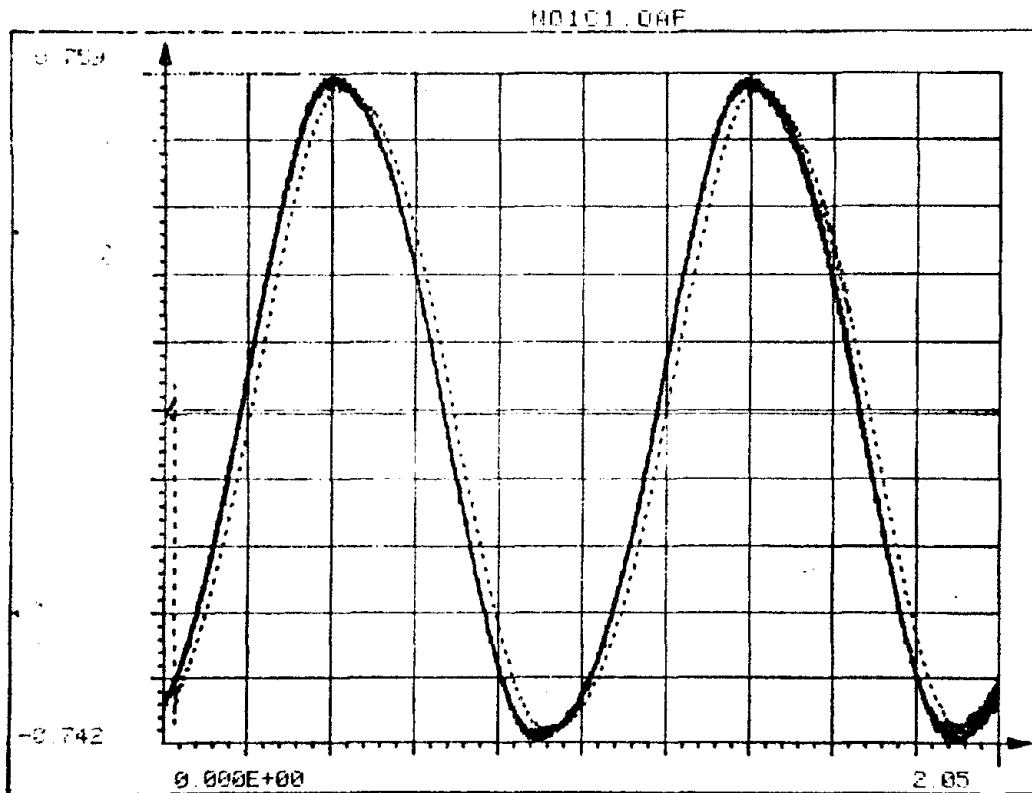
N41.39.1



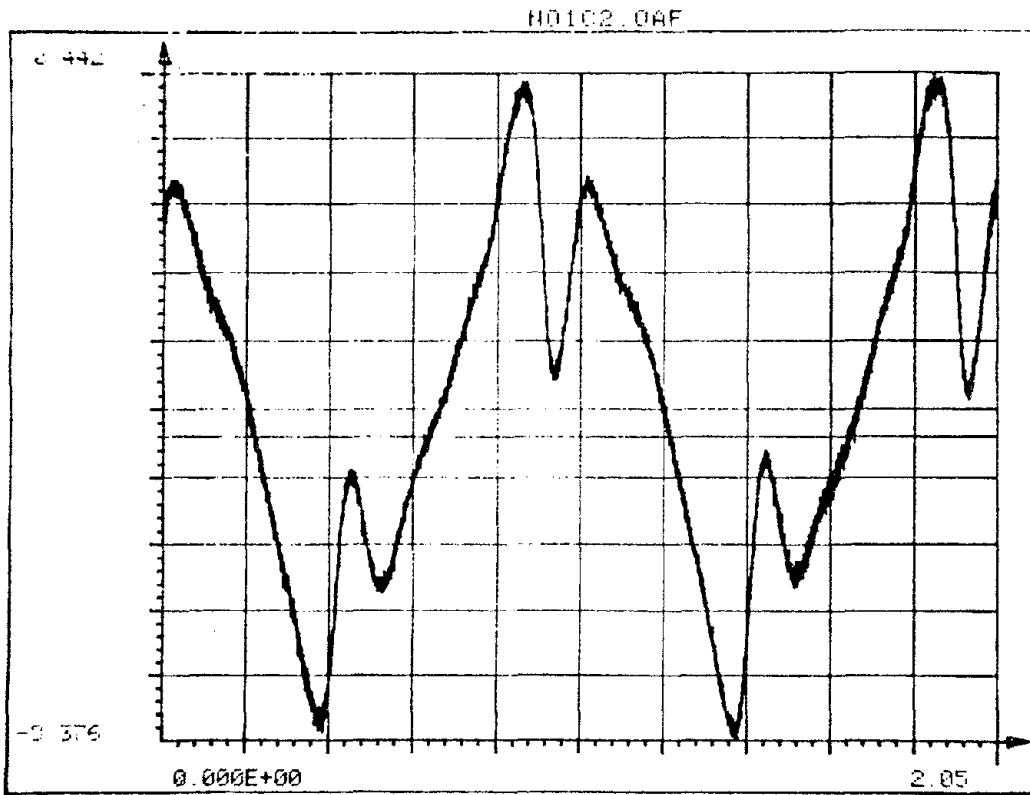
N41.40.3



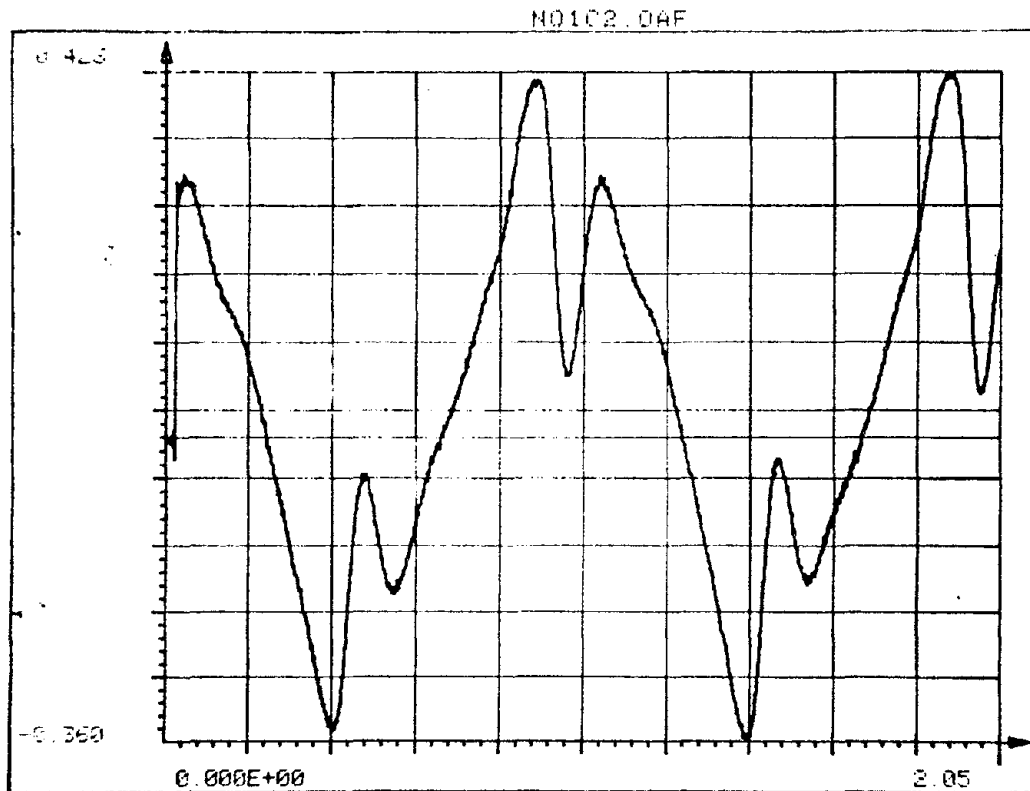
N01.4L.3



N01.42.3

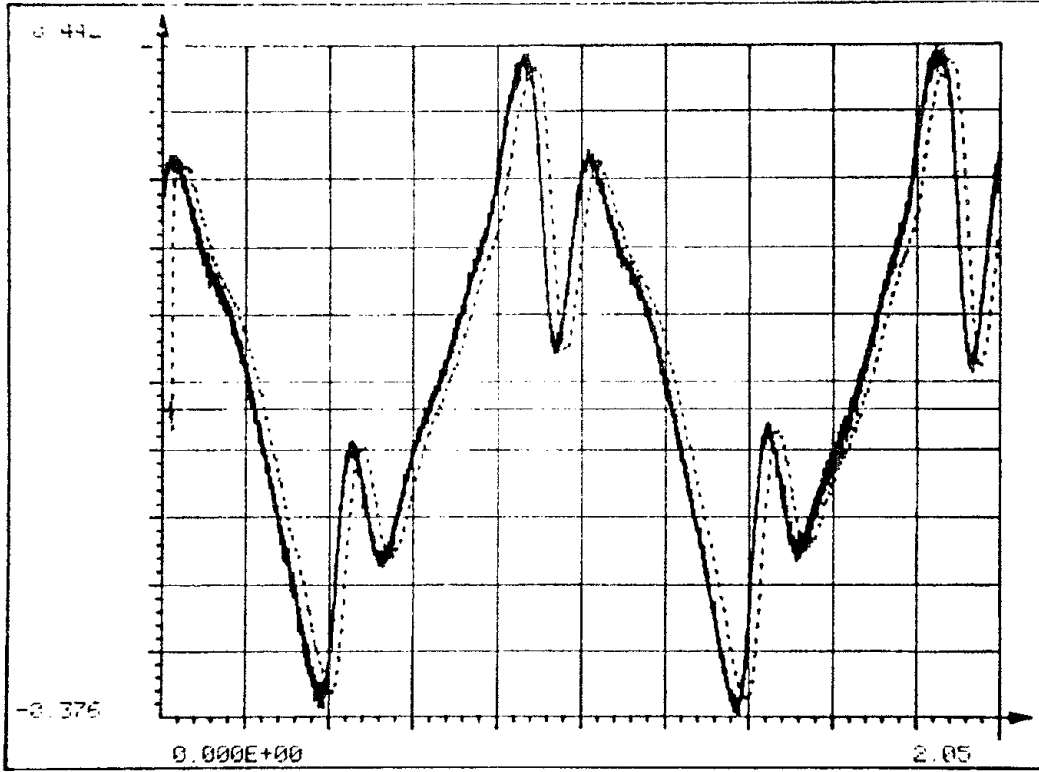


N01.43,3



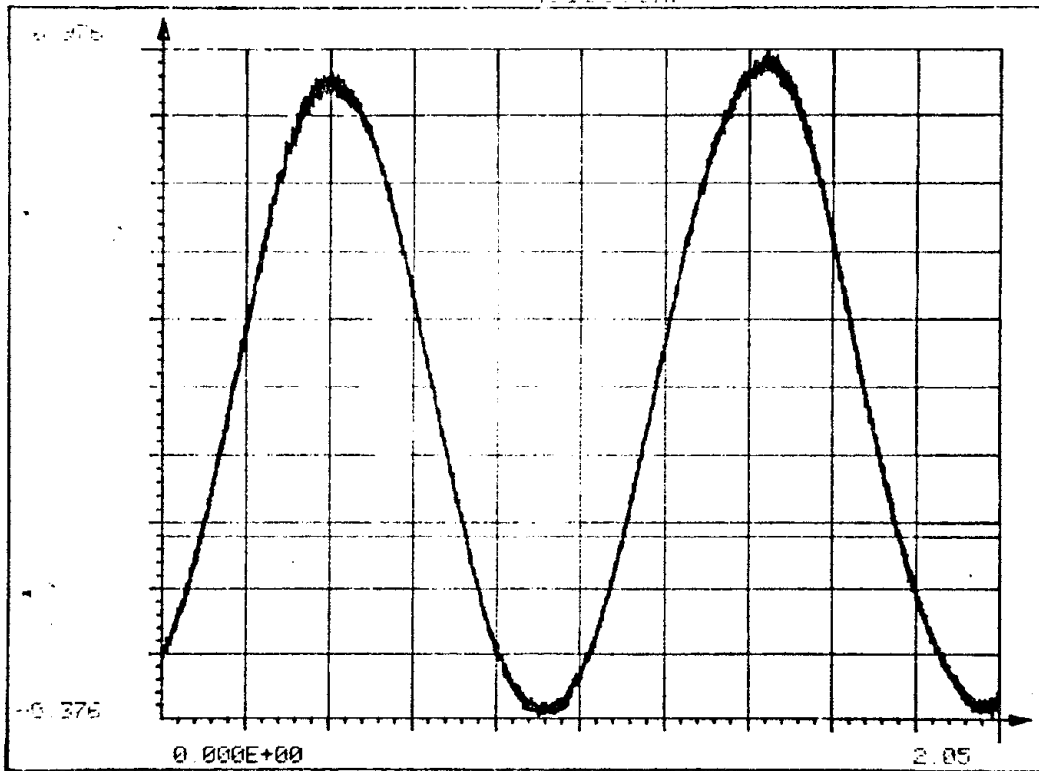
N01.44,3

N0102.00F



N01.45.3

N0103.00F

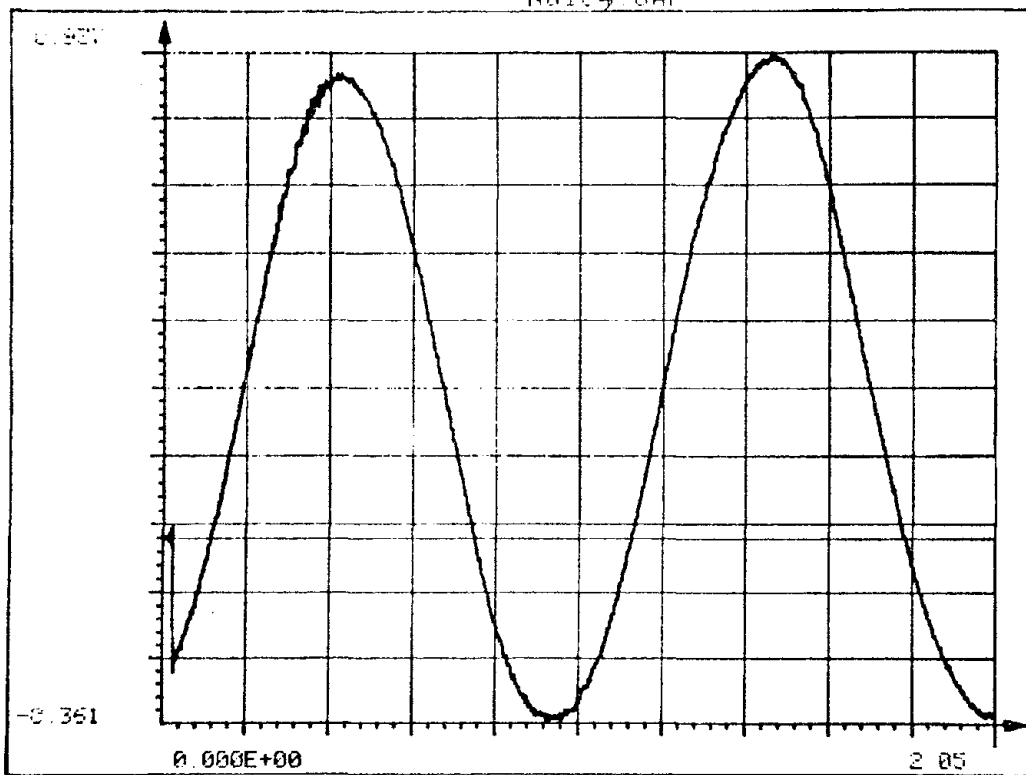


N01.46.3

Reproduced from
best available copy.

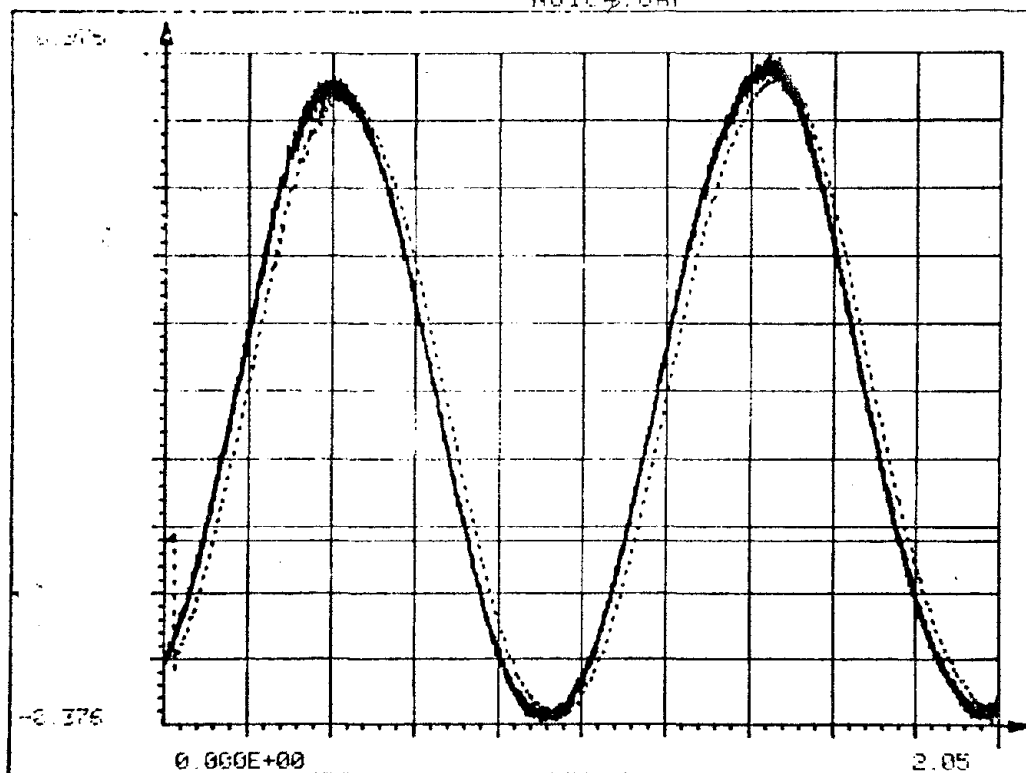


3
NO104 DAF

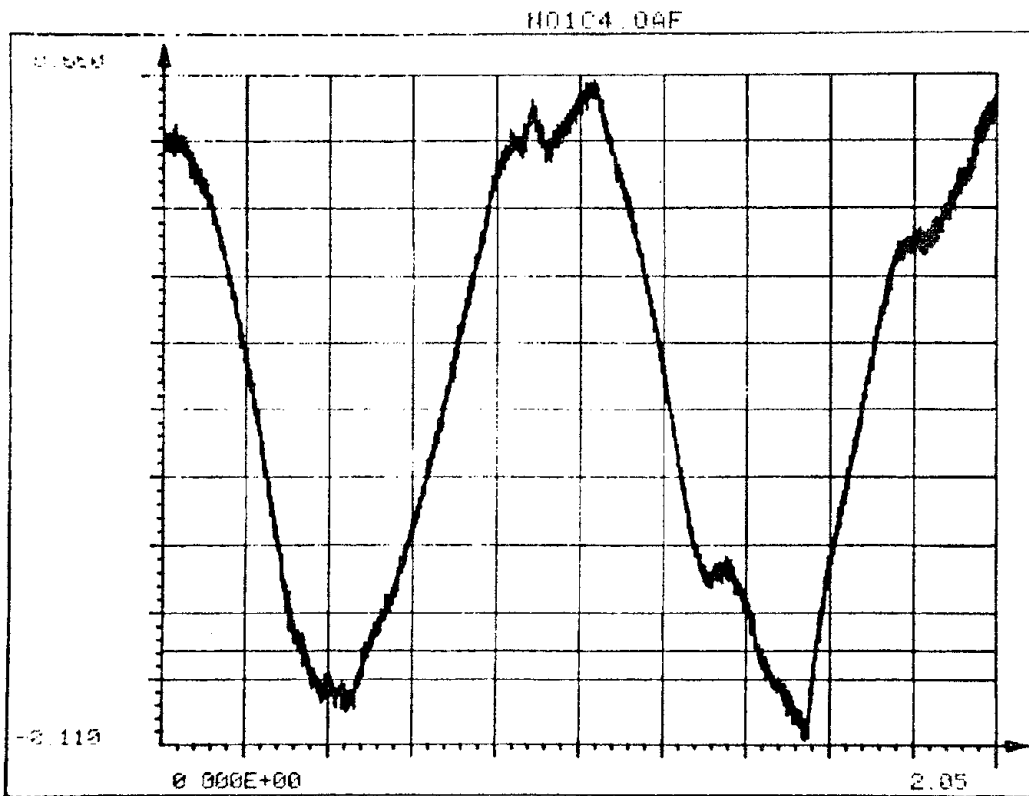


N01.47.3

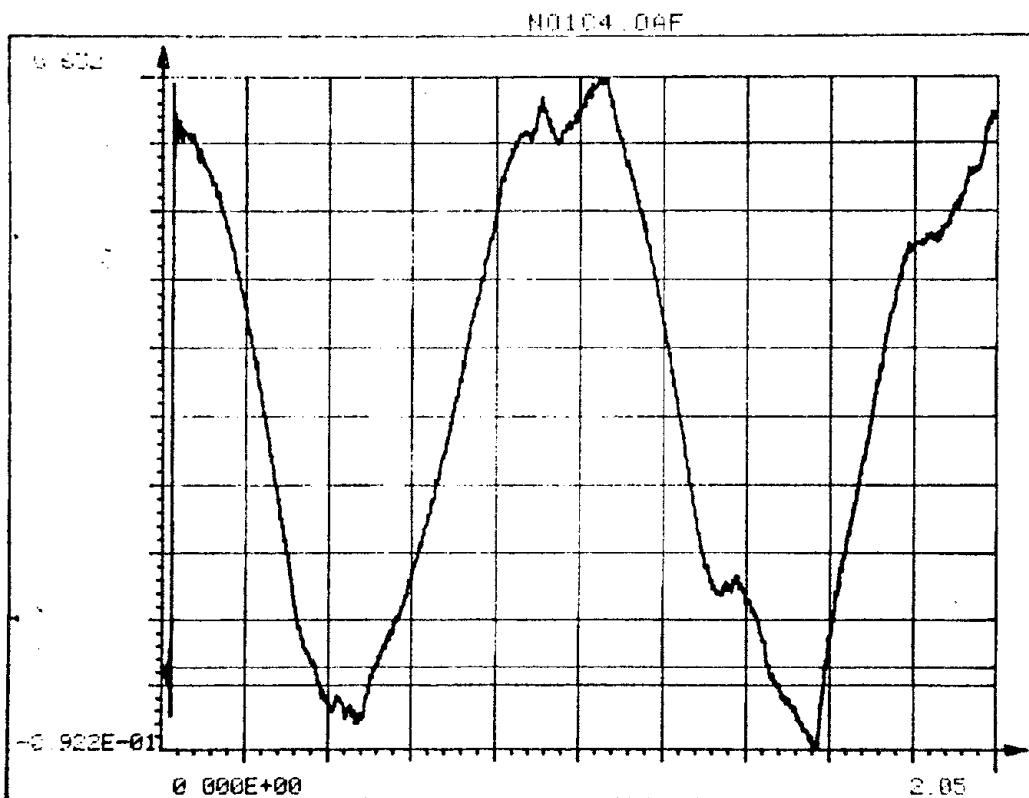
3
NO105 DAF



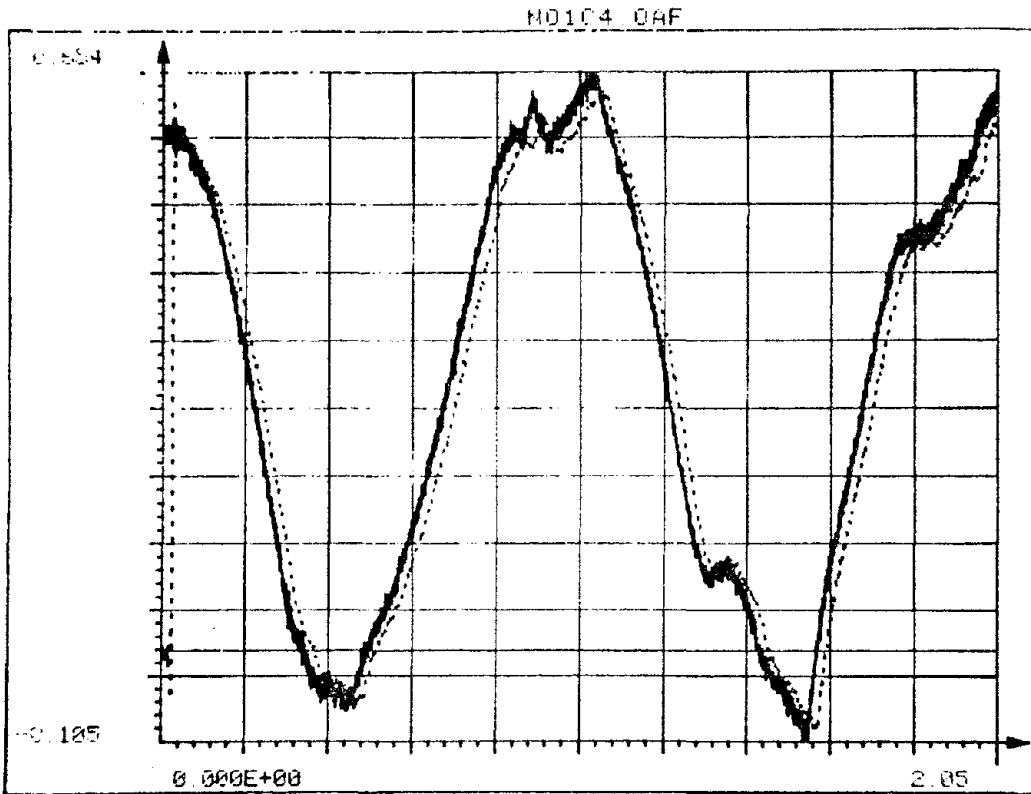
N01.48.3



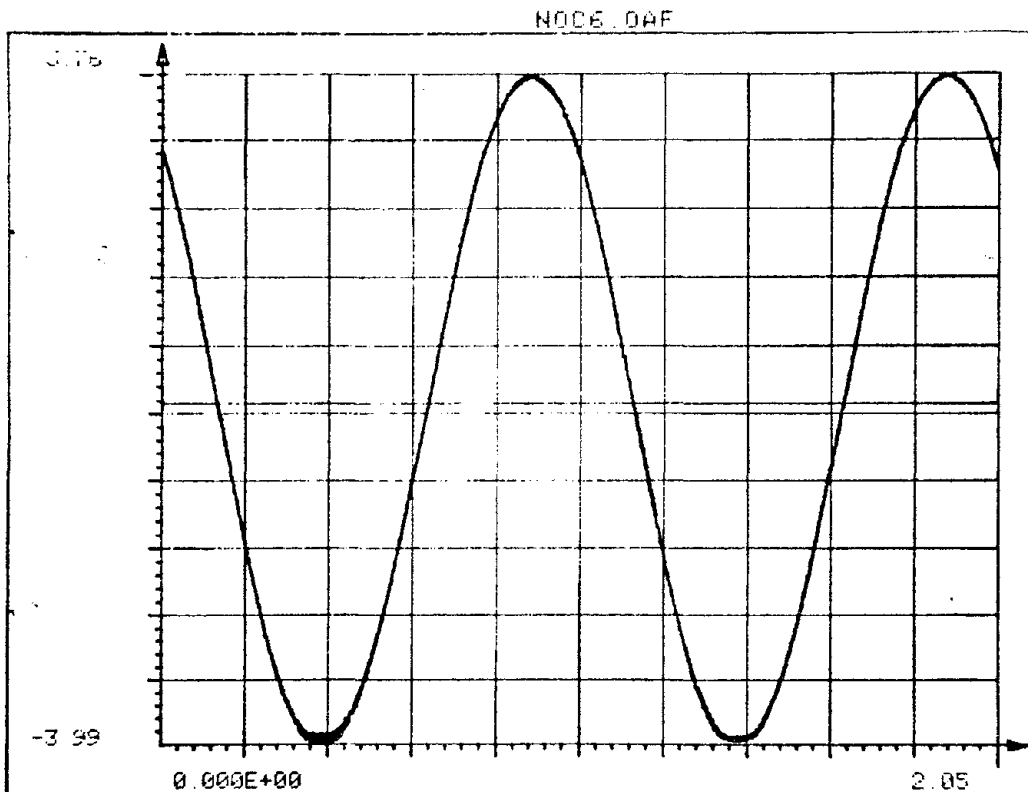
Nφ1.49.3



Nφ1.50.3



N01.51.3



N01.52.3



FRICTION

APPENDIX 5

XY PLOTS

Nonlinear Dynamic 3rd 10,000 pts

Blow-up 1st slip NO1C03.013 Fig NO1.47.3

Blow-up 2nd slip NO1C04.014 No1.50.3

FXY1.NO1 201-4096

FXY2.No1 201-2148

FXY3.NO1 2148-4096

FXY4.NO1 350-1200

FXY5.NO1 1550-2400

Nonlinear Dynamic 1st 10,000pts

Blow-up 1st slip NO1C03.013 Fig NO1.31.1

NO1C04.014 NO1.34.1

FXY1.NO1 201-4096

FXY2.NO1 201-2148

FXY3.NO1 2048-4096

FXY4.NO1 1600-2450

Free Vibration

Blow-up 1st period F03C02.012 F03.11

F03C03.013 F03.14

FRICTION

FXY1.F03 201-2048

FXY2.F03 550-1000

Linear Dynamic

D33C03.333 D33.16

D22C04.334 D33.20

FXY1.D33 201-4096

FXY1.D33 201-1000

FXY3.D33 1000-2400

FXY4.D33 2400-4096

Dynamic Linear

D13C03.133 D13.13

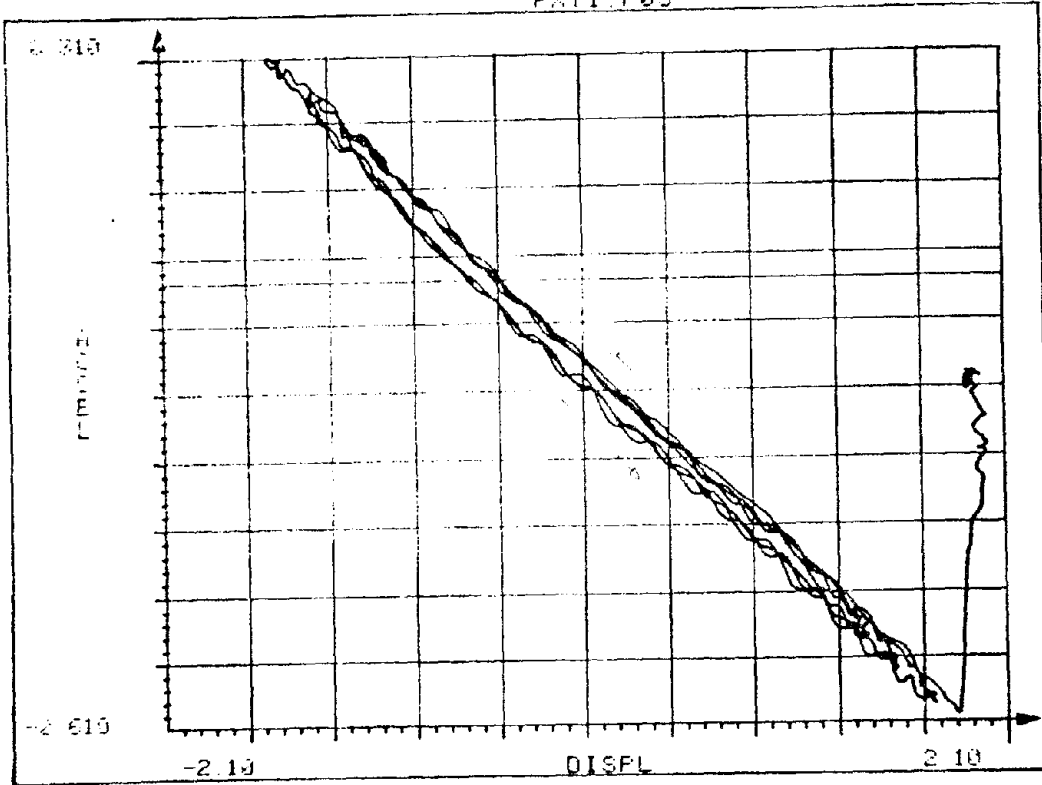
D13C04.134 D13.16

Static Nonlinear

S05C01.051 505.9

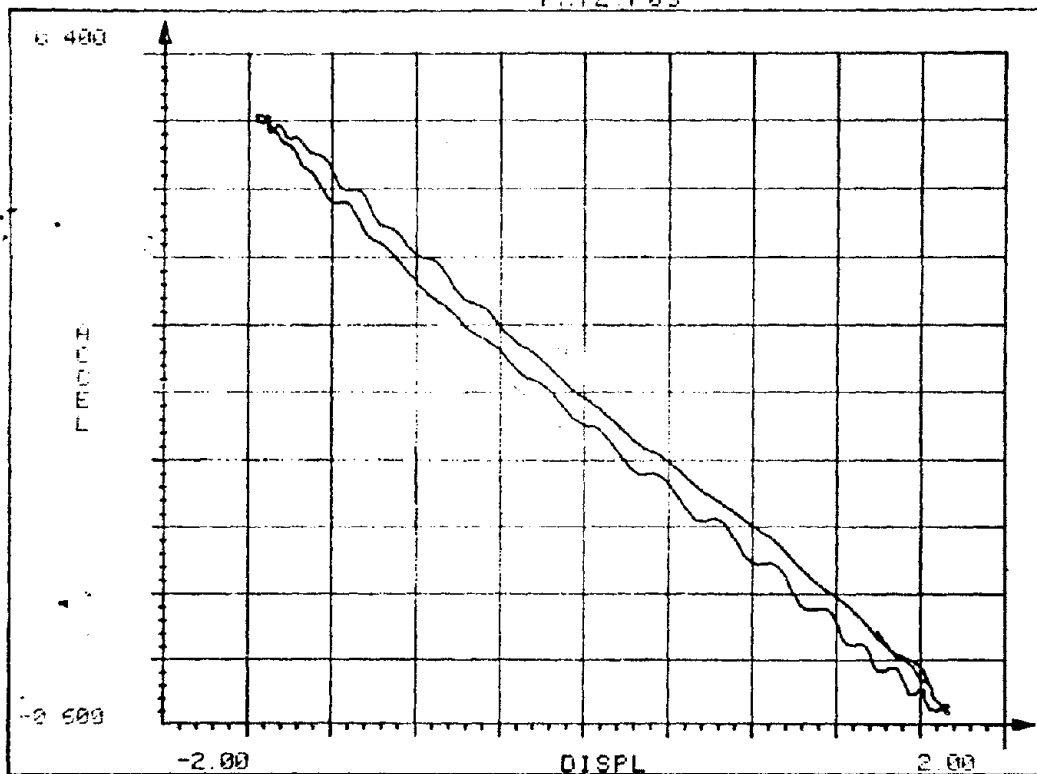
S05C04.054 505.15

FXY1.F03



F03XY.1

FXY2.F03

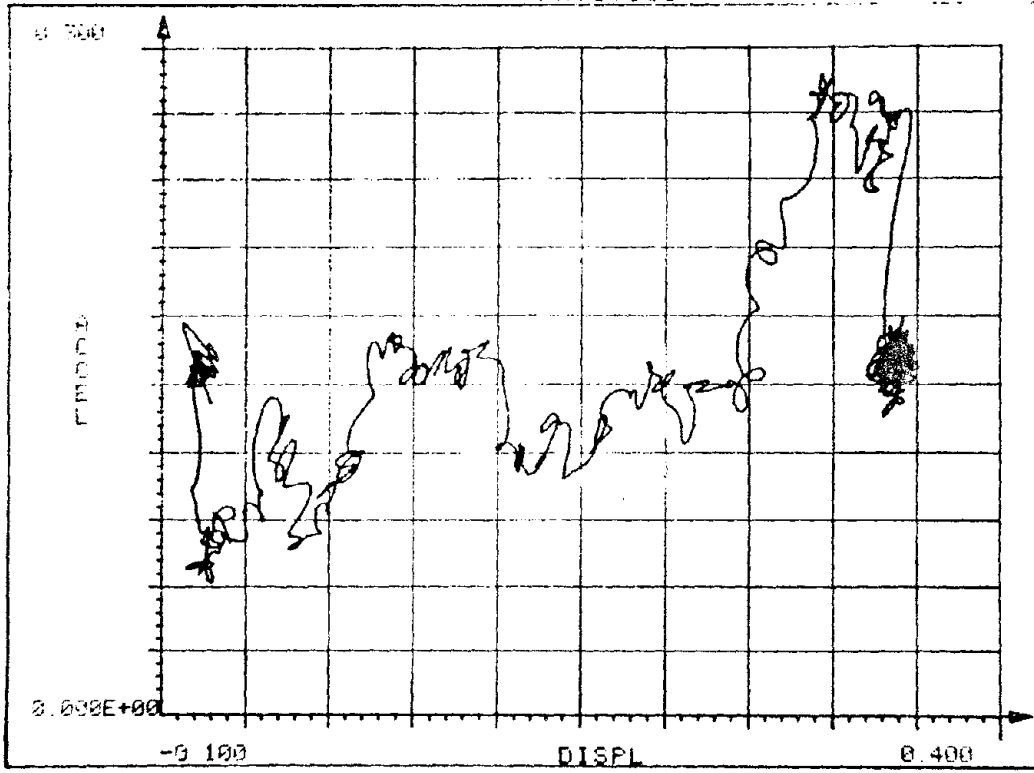


Reproduced from
best available copy.



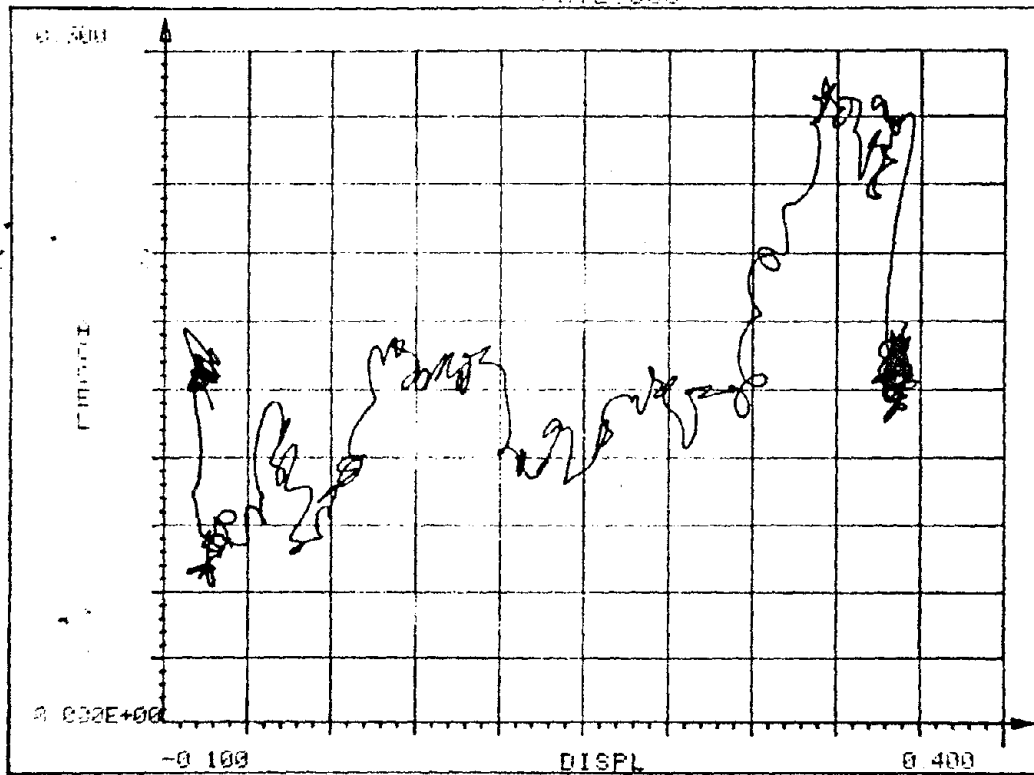
F03XY.2

FKY1.S05



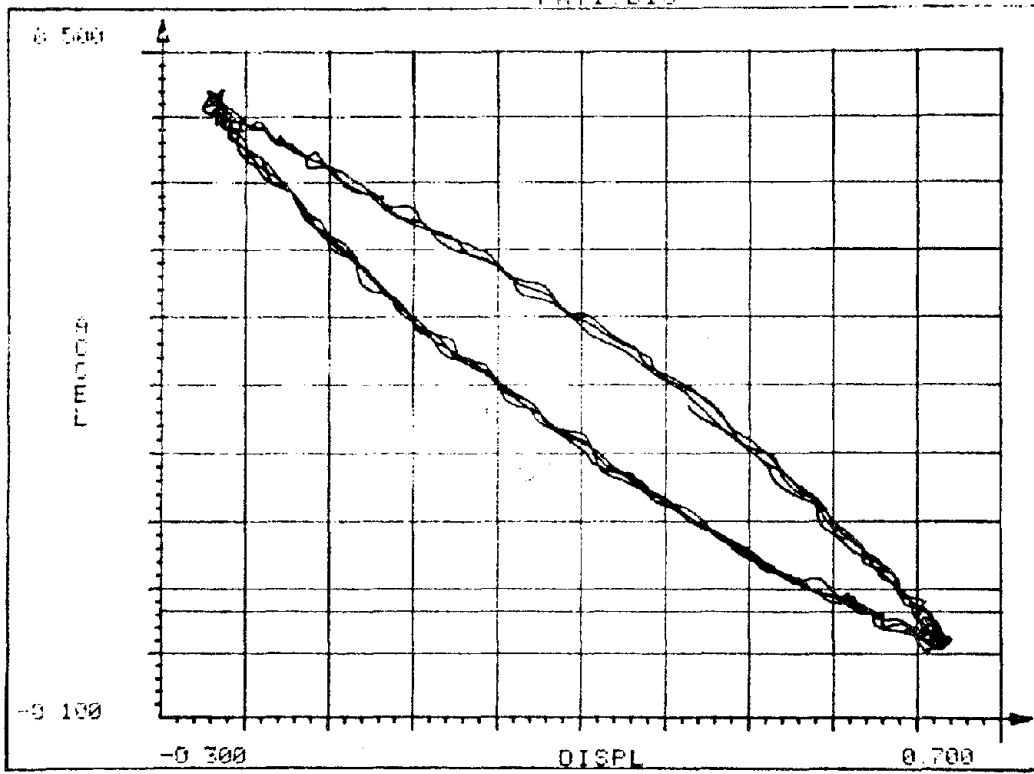
S05XY.1

FKY2.S05



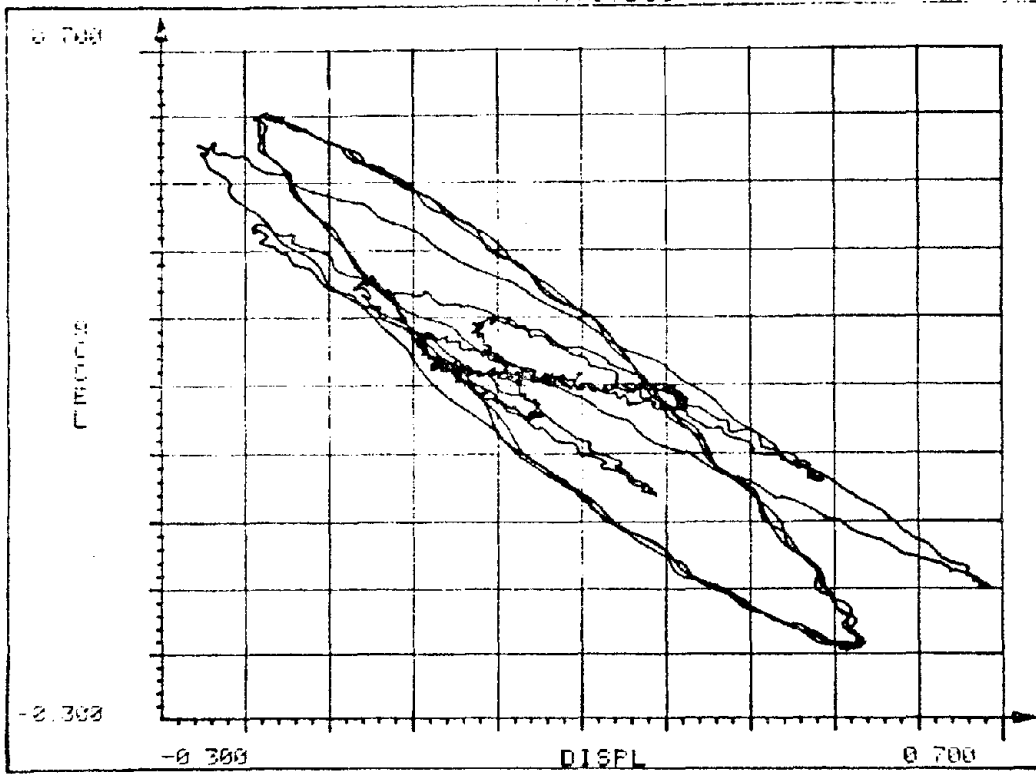
S05XY.2

FXY1 013



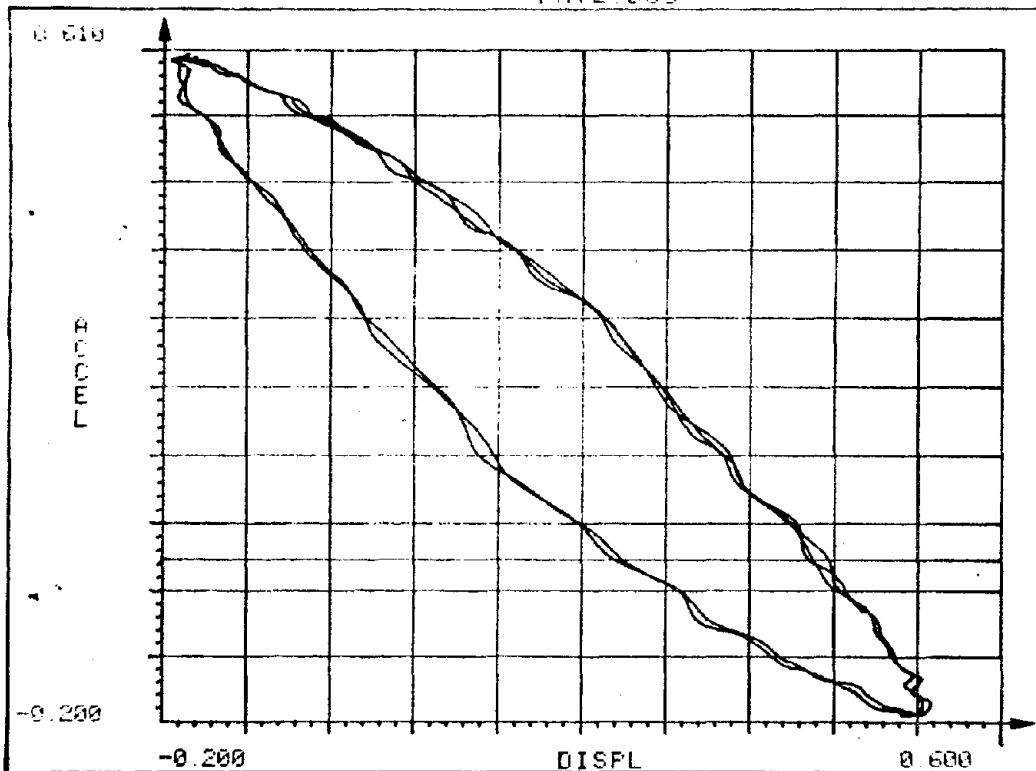
DI3XY.1

FXY1 D33



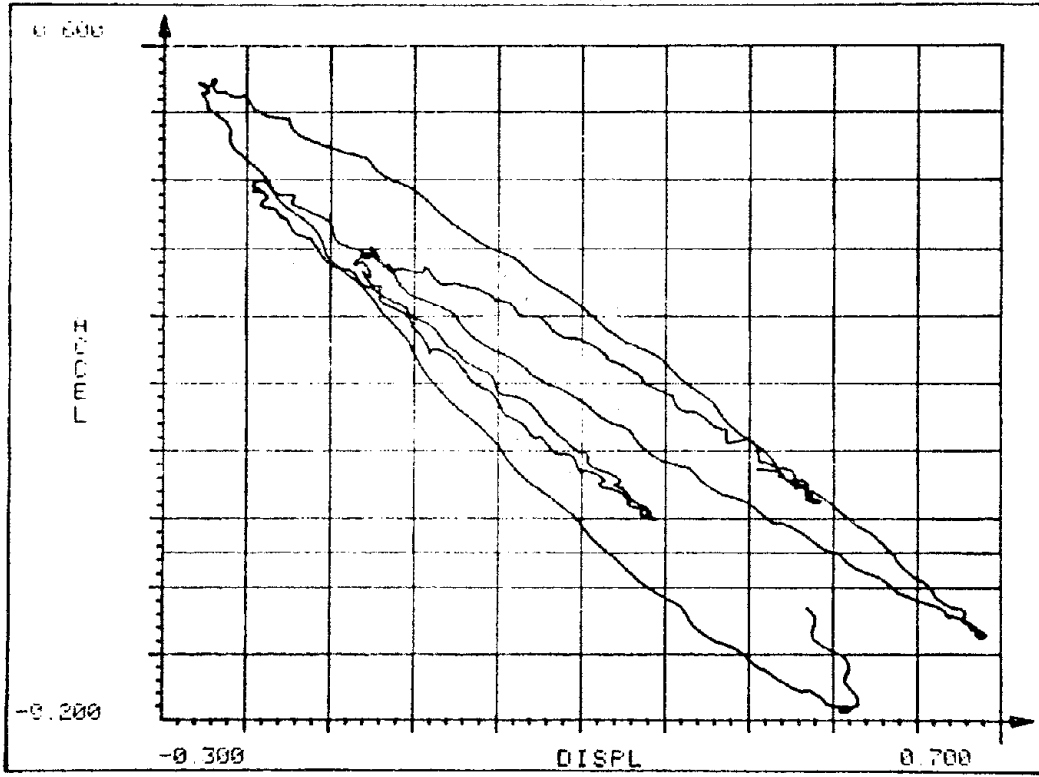
D33XY.1

FXY2 D33



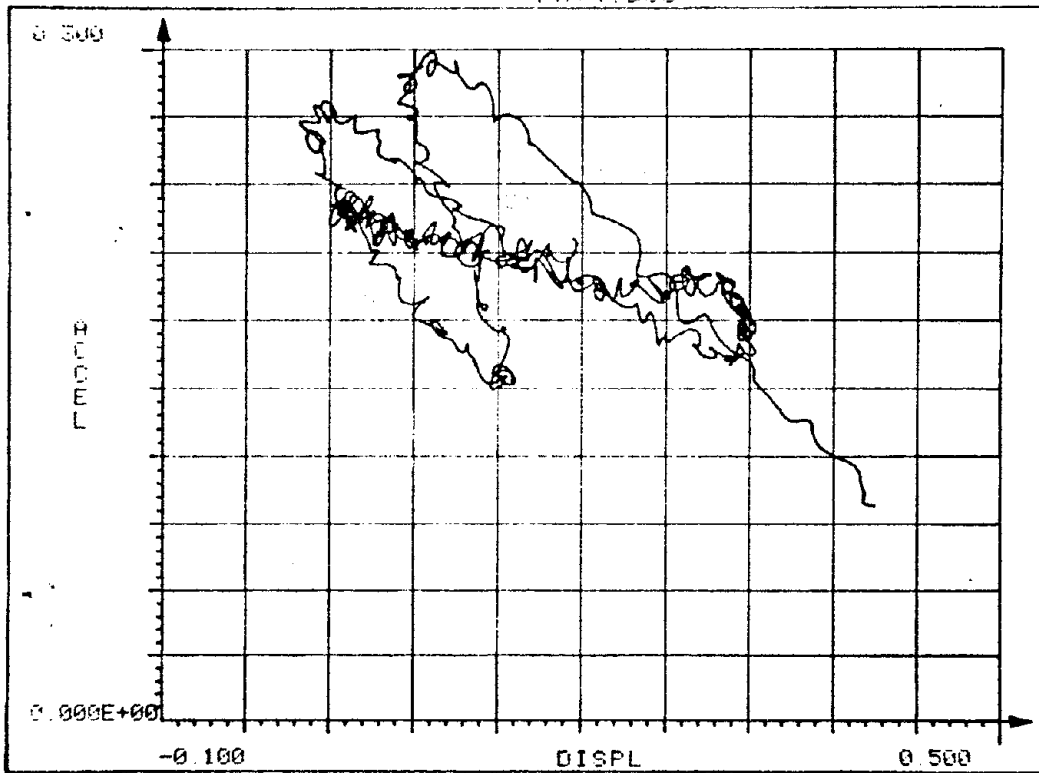
D33XY.2

FWY3.D33

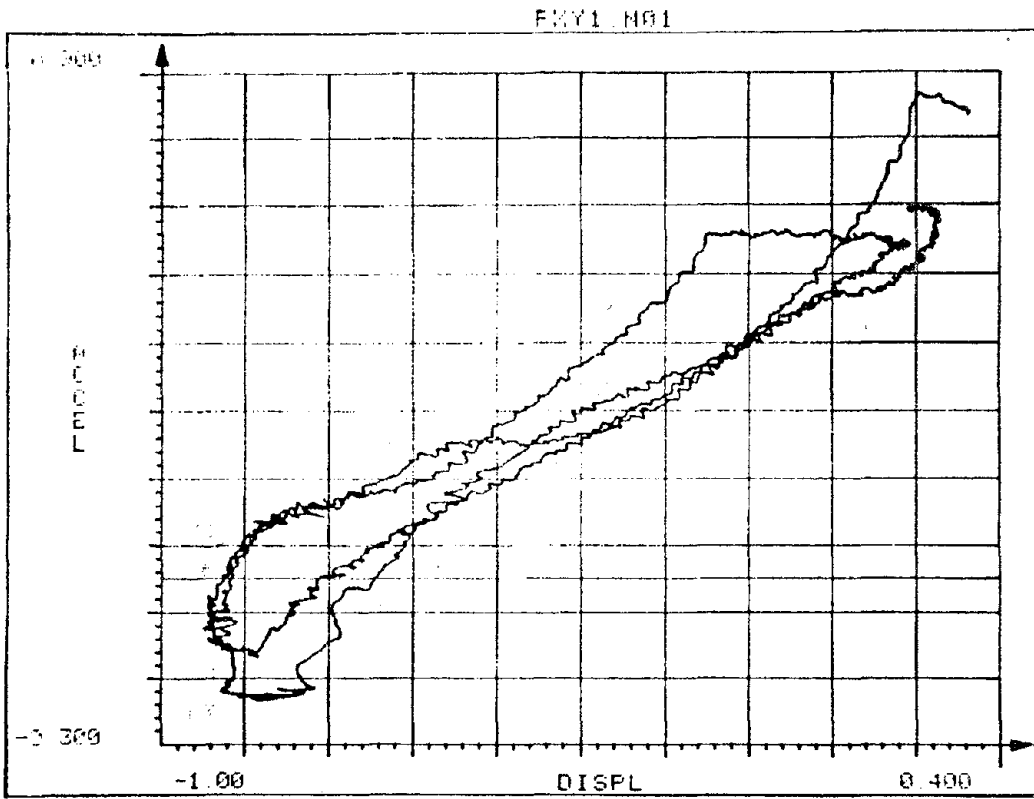


D33XY.3

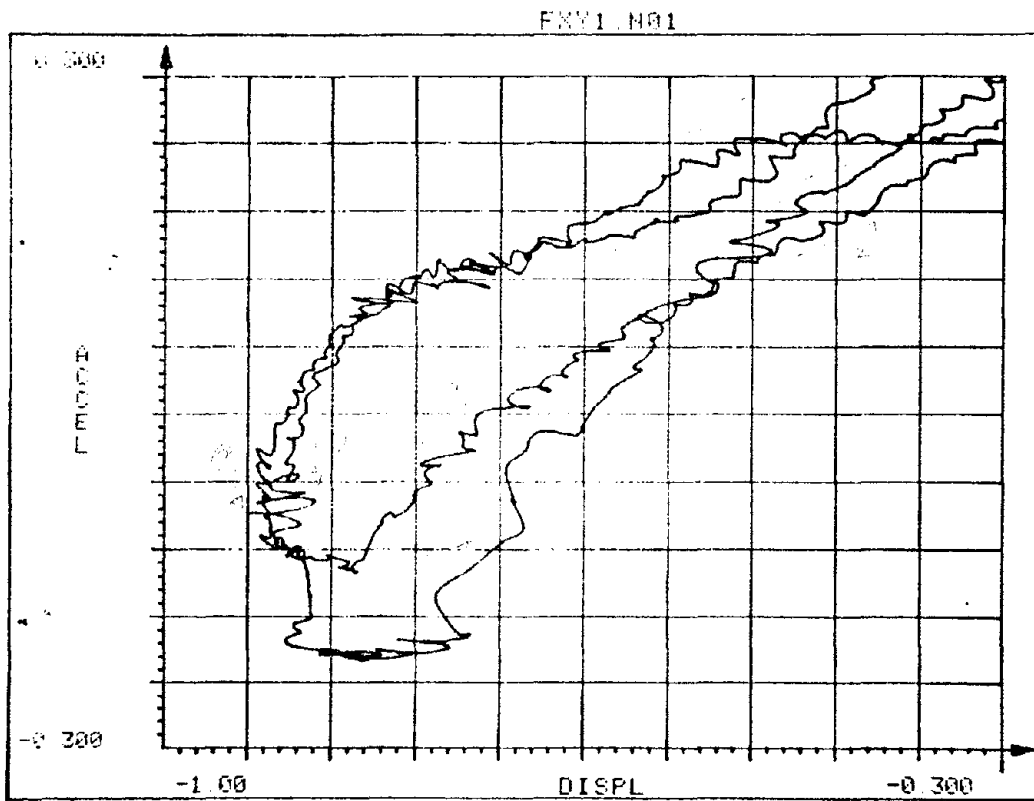
FWY4.D33




D33XY.4



NΦIXY.1

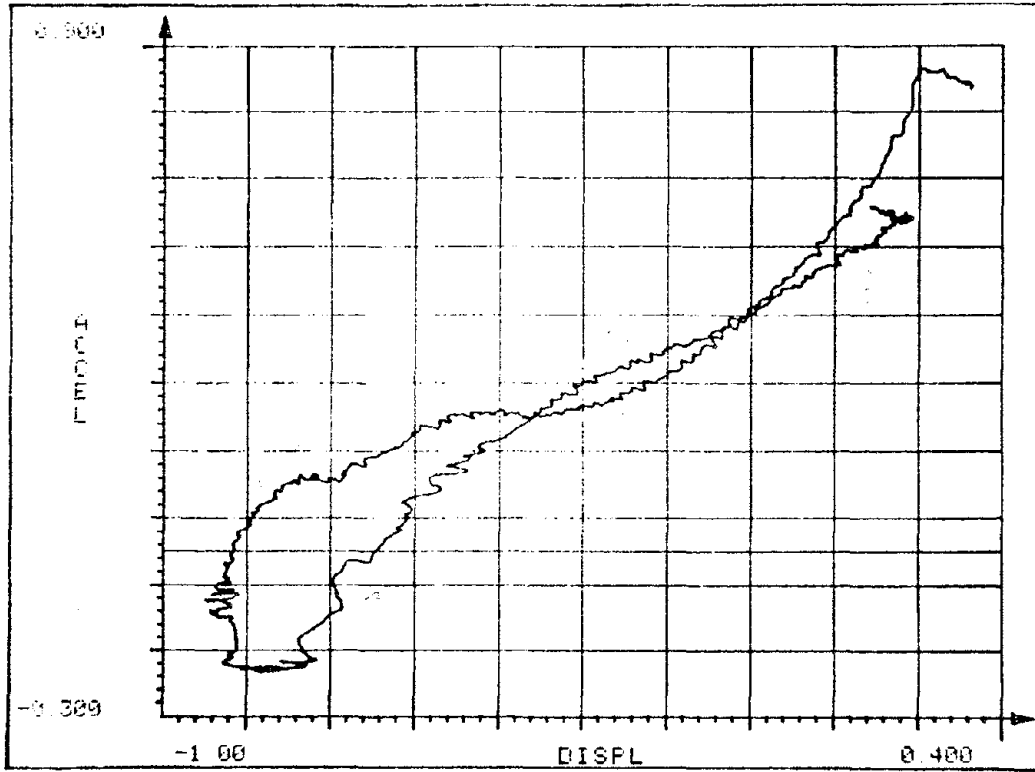


NΦIXY.2

Reproduced from
best available copy. 

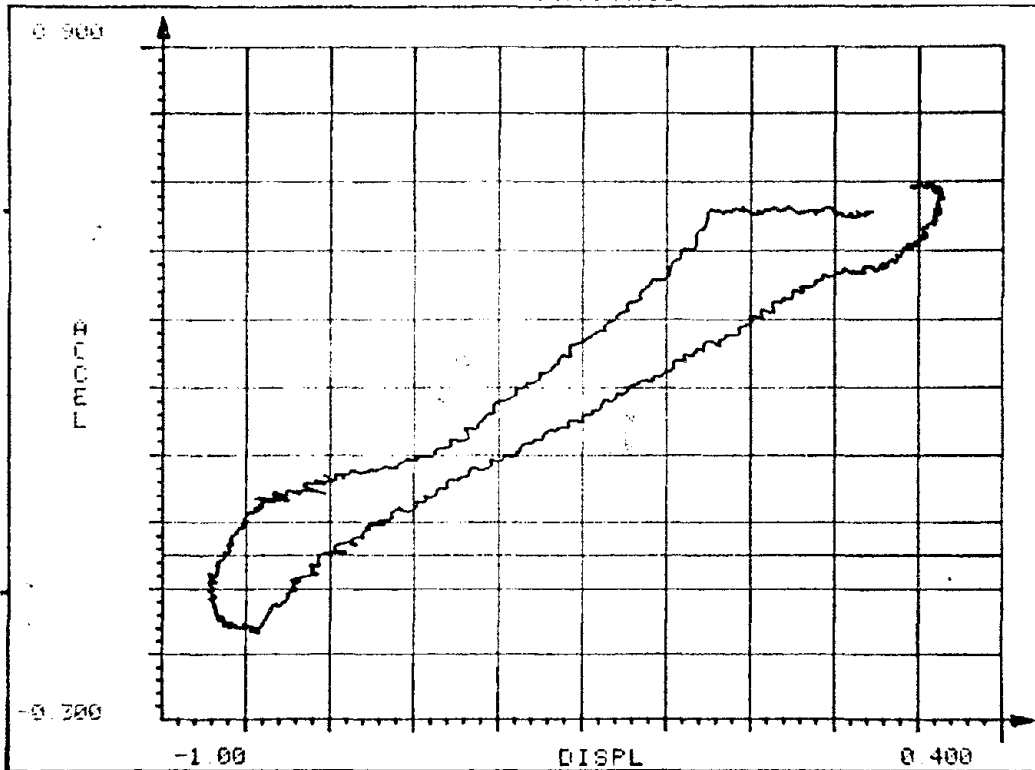
88

EXY2.N01



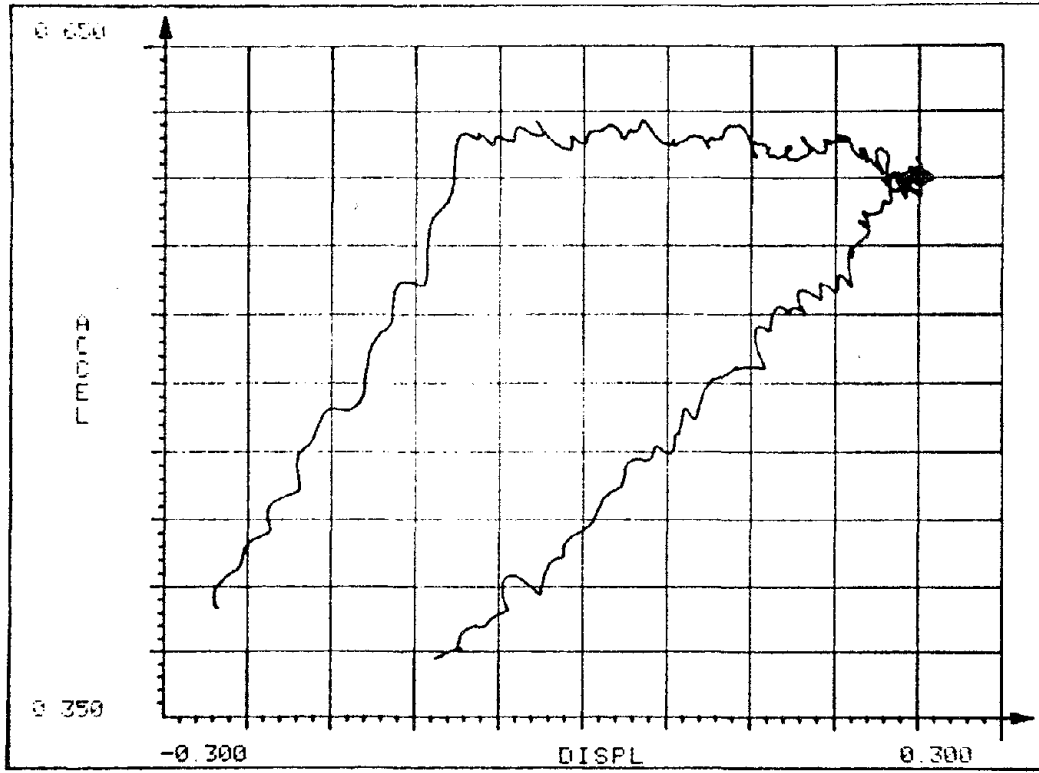
NΦIXY.3

EXY3.N01



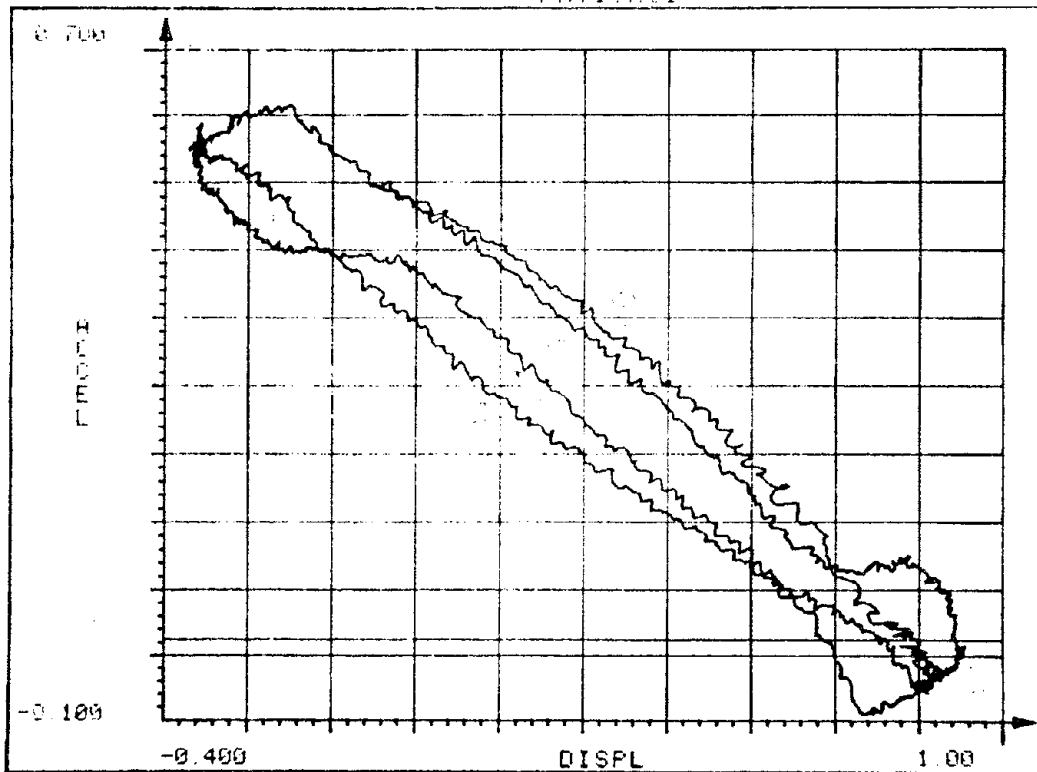
NΦIXY.4

F2Y4.H01



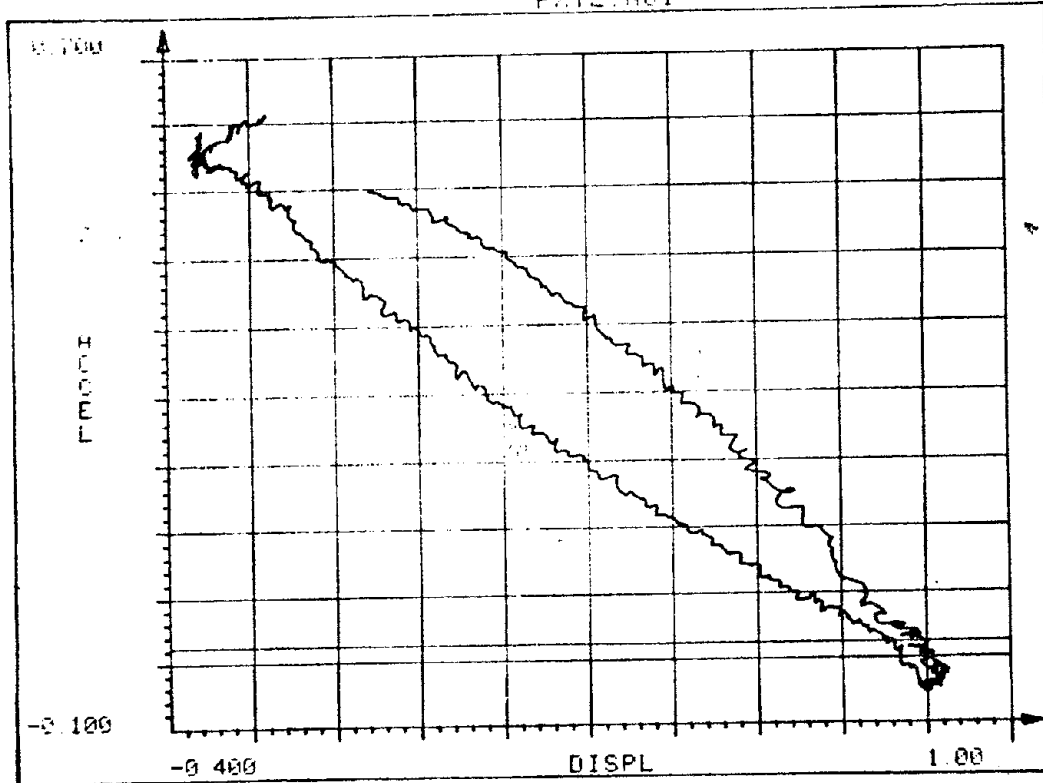
N01XY.5

FXY1.H01

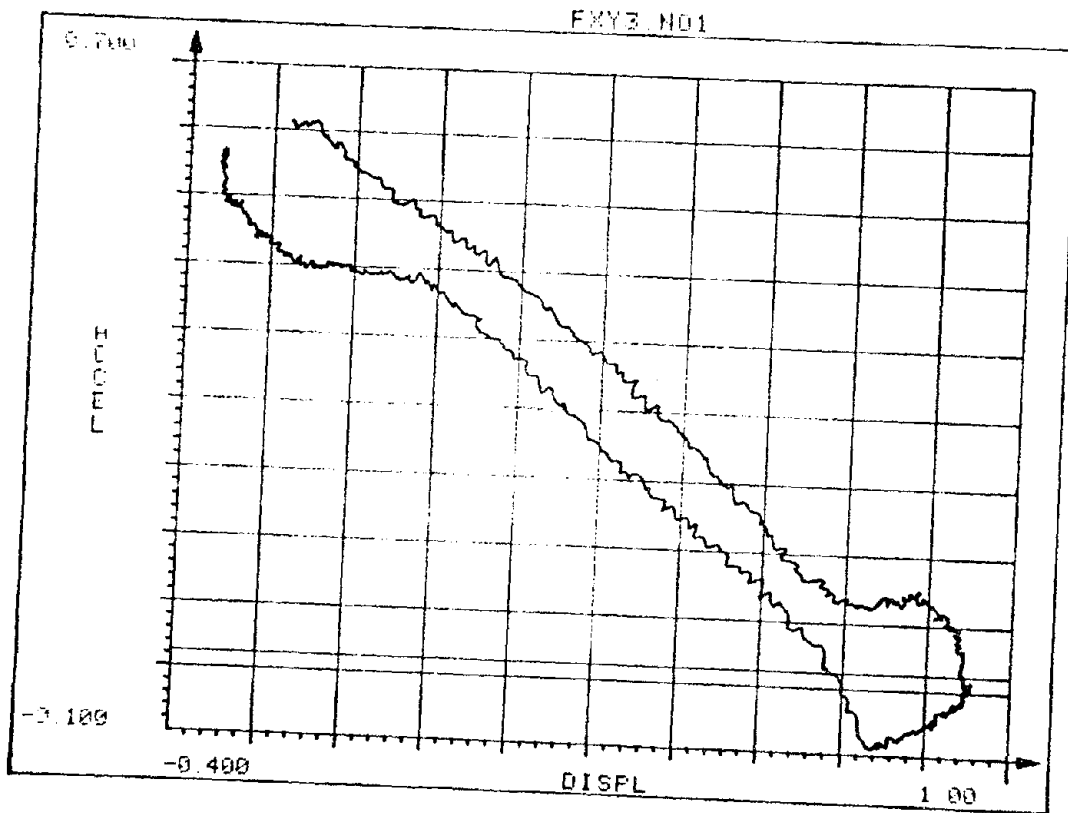


NOIXY.1

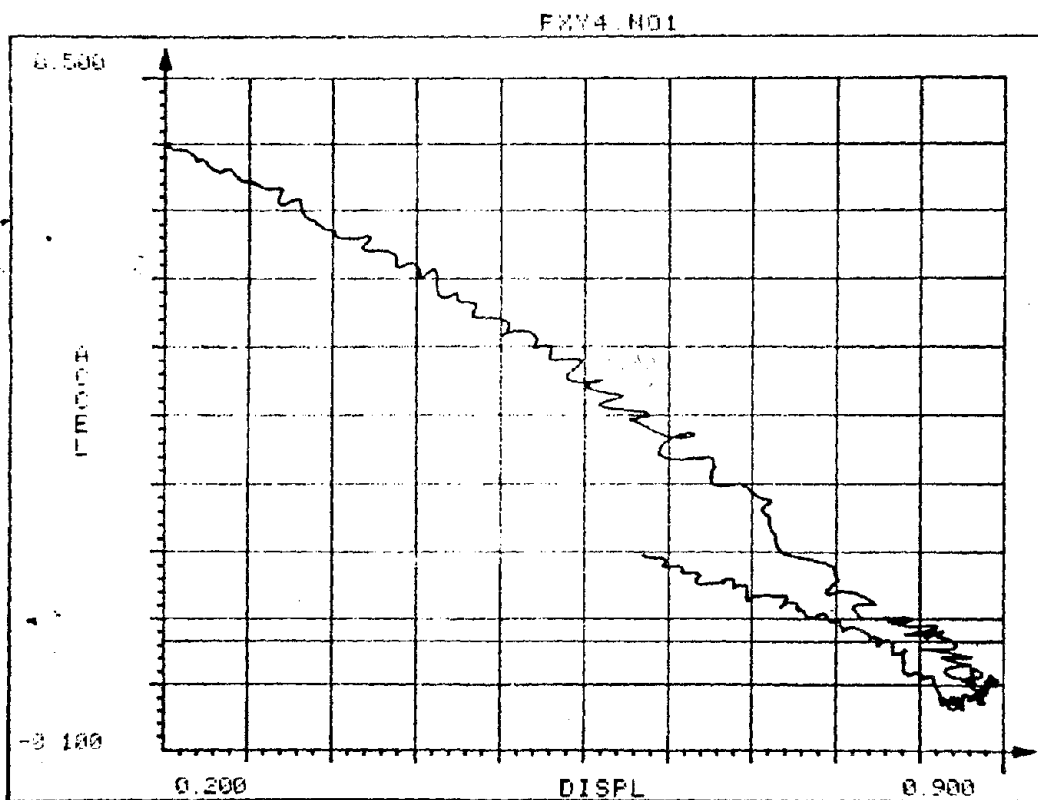
FXY2.H01



NOIXY.2

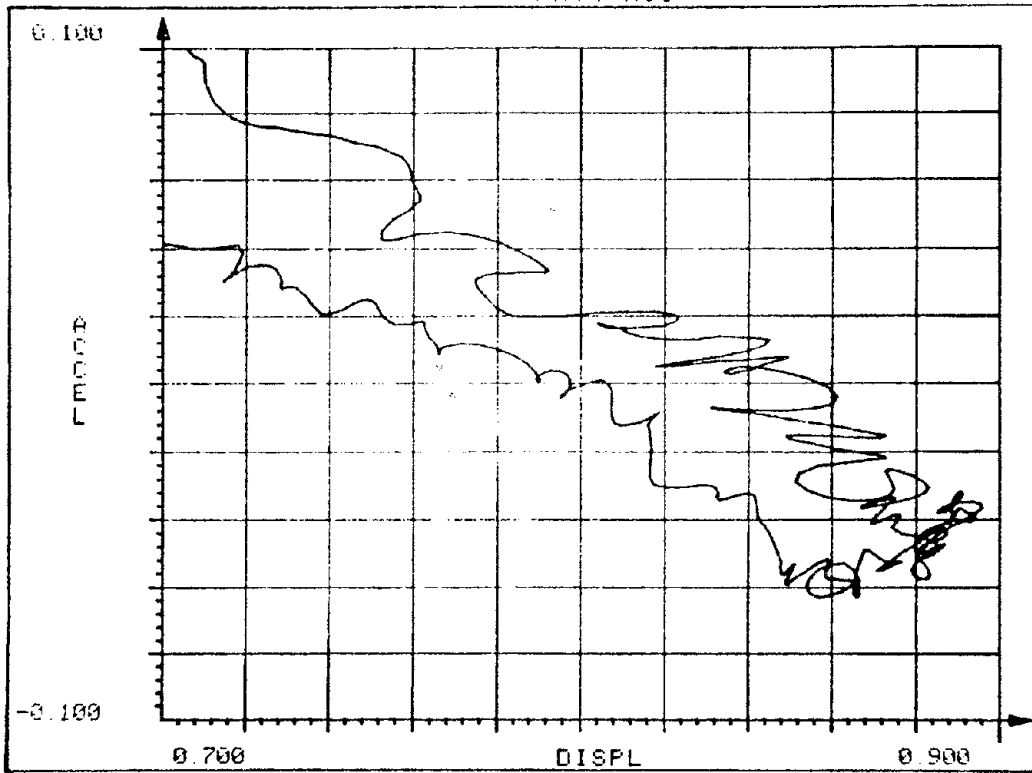


NOIXY.3



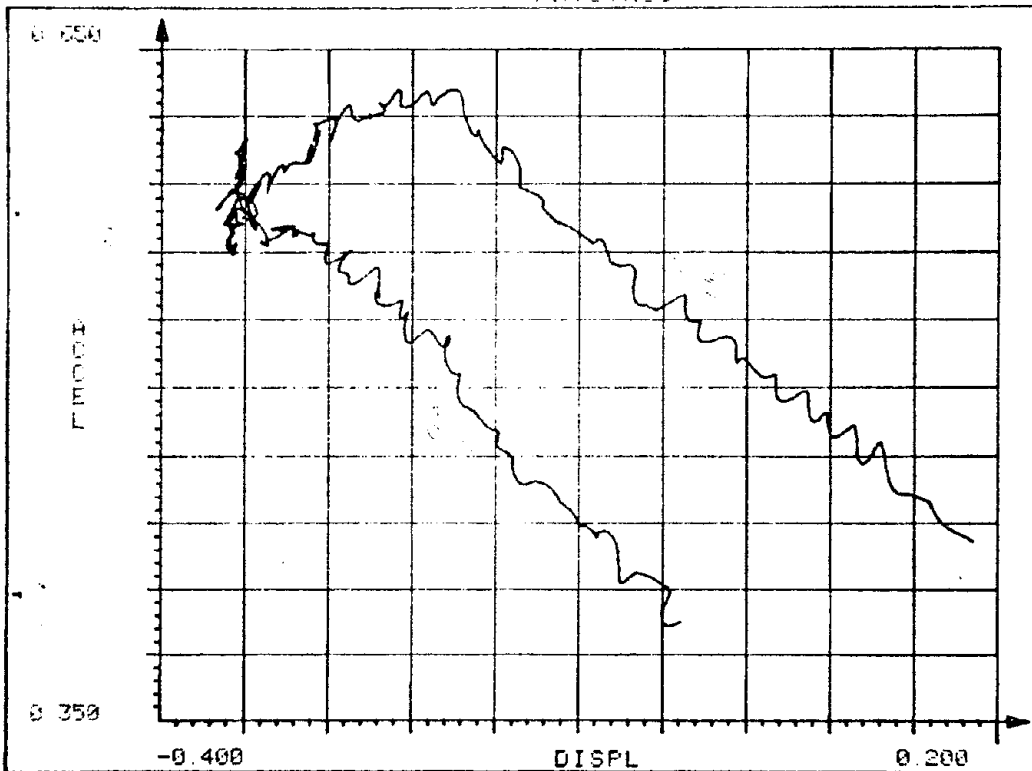
NOIXY.4

FX74.N01




NOIXY.5

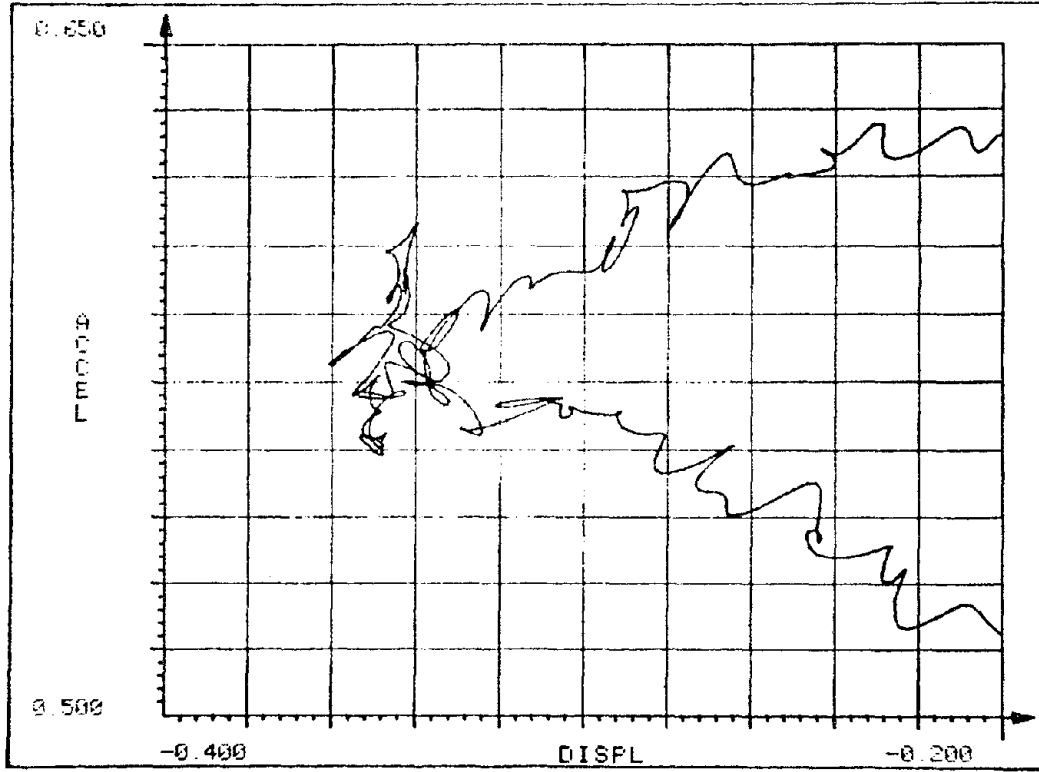
FX75.N01



NOIXY.6

Reproduced from best available copy. 

FRY5.N01



NOIXY.7